Middle Atmosphere Program

HANDBOOK FOR MAP VOLUME 15

Edited by
D.G. Murcray

M I D D L E

A T M O S P H E R E

P R O G R A M

HANDBOOK FOR MAP

Volume 15

Balloon Techniques

Edited by

D. G. Murcray

June 1985

Published for the ICSU Scientific Committee on Solar-Terrestrial Physics (SCOSTEP) with financial assistance from the National Aeronautics and Space Administration Contract NASW 3805 and Unesco Subvention 1983-1984

Copies available from SCOSTEP Secretariat, University of Illinois, 1406 W. Green Street, Urbana, Illinois 61801

FOREWORD

The balloon has a long history of use as a platform for upper atmospheric research. In fact for many years it was the only vehicle capable of obtaining in situ data on the lower stratosphere. The development of the various polymers which could be extruded into uniform thin films dramatically increased the capability of the balloon as a lower stratospheric research vehicle. The materials not only made it possible to fabricate much larger balloons at low cost but also to construct the units so that rather than bursting they remained at float altitude for extended periods of time. Initially the units were designed with modest capabilities (100 kgs to 30 km). The existence of this capability increased the number of investigators and the range of research being performed with them. This, in turn, led to interest in increasing the altitude and load capability of the vehicle. The size of the balloons available increased and thickness of the material required to fabricate the balloon decreased rather rapidly so it became possible to get light (<1000 kgs) payloads to 35 km. Heavy payloads (>1000 kgs) were a problem and most heavy payloads were flown on balloons constructed of a mylar scrim. Since these were very expensive their use was limited. Another problem occurred as the larger units were used at low latitudes and this was the failure of the units at the tropopause. It was recognized that the failure was due to the material becoming brittle at the cold temperatures associated with the low latitude tropopause. This led to the development of a material designed with better cold brittleness characteristics for fabricating balloons. With the additional development of load tapes and caps to handle heavy loads, both problems were overcome, and the balloon has become a reliable heavy load platform. It is interesting to note the recent records achieved with large balloons. These include carrying a 4536 kg payload to 34 km and a 232 kg payload to 51.8 km. This capability has been used by many investigators to obtain data on the middle atmosphere.

In this volume we discuss some of the techniques employed by investigators using balloons to obtain data on the properties of the middle atmosphere. The balloon provides an excellent platform for obtaining such data and the number of investigators using it is large. As a result it is difficult for a volume such as this to be complete and several techniques are not included. This lack of completeness is also partially because manuscripts from several authors were not received in time for inclusion in this volume. The editor apologizes for the omissions and emphasizes that their omission does not imply that the techniques are unimportant.

The first stratospheric parameter to be measured with balloon-borne instruments was temperature. Temperature continues to be an important parameter and most of the data concerning the temperature and dynamics of the lower stratosphere continue to be obtained by means of balloon-borne sensors. This is due to the development of the small radiosondes which can be flown to 30 km on small inexpensive balloons. The importance of measurements of the variable minor species (O_3 and H_2O) has long been recognized. A great deal of effort has gone into developing instruments which could be used on small balloons to measure these constituents. These are discussed in detail in the first chapter.

The question of whether man's activities could affect the composition of the lower stratosphere (particularly the ozone layer), which arose during the controversy over the building of the Supersonic Transport aircraft, increased the interest in the measurement of stratospheric composition. This interest carried over into the study of other possible sources of pollution including the possible effects of chlorofluormethanes on the ozone layer. This in turn added to the list of compounds for which measurements of the stratospheric concentration were badly needed. Many of these compounds were predicted to be present in the ppt to ppb range and instruments were required that could measure these

compounds from a balloon platform. Several different techniques have been used to obtain such information and rather than arranging the chapters according to compounds, they have been arranged according to the measuring technique. In chapters 2 through 4 various remote sensing techniques used to obtain data on atmospheric composition are described. These are arranged according to the wavelength regions used to make the measurement.

Several in situ techniques have been developed for use on balloon platforms. In addition to the measurements of neutral constituents, a number of groups have developed instrumentation required for measurement of the ion composition from balloon platforms. In many respects, the balloon measurement has proven to be much more difficult than measurements at the higher altitudes. These are discussed in chapter 5.

Interest in the stratospheric aerosol seems to wax and wane with volcanic activity and the last few years has seen a tremendous increase in this interest. The balloon has proven to be an excellent vehicle for studying both the physical and chemical properties of the aerosol. The final chapter in this volume reviews the balloon measurements in this area.

D. G. Murcray
Editor

BALLOON TECHNIQUES

TABLE OF CONTENTS

1. THE MEASUREMENT OF TEMPERATURE, OZONE AND WATER VAPOUR

T. McElroy
Atmospheric Environment Services
Downsview, Ontario, Canada M3H 574

INTRODUCTION

In 1904 Teisserenc de Bort published the results of 581 unmanned balloon ascents during which recording instruments measured temperature and pressure. As a number of these flights reached 14 kilometers or more, de Bort was able to observe the change from the normal tropospheric adiabatic lapse rate to the near isothermal conditions of the stratosphere. In fact, de Bort named the stratosphere and troposphere to indicate the difference in static stability which is typical of these two regions of the atmosphere. The determination of the vertical, temperature and pressure profiles of the atmosphere is an important task of every stratospheric research flight.

Ozone was clearly identified in the atmosphere when FABRY and BUISSON (1921) found characteristic absorption features in spectrographic measurements of the sun. DOBSON (1930) reported the development of a spectrophotometer designed specifically for the ground-based measurement of ozone. The instrument measures the differential absorption of light, by ozone, at two wavelengths in the near ultraviolet. The observed absorption is converted to an amount of ozone based on laboratory measurements of the absorption coefficients of ozone. The Dobson spectrophotometer still serves as the primary standard of measurement for the amount of ozone in the atmosphere.

Because of the importance of knowing the temperature and humidity structure in the troposphere for the purpose of forecasting the weather, temperature and humidity measurements as a function of pressure have been made operationally for many decades. It is only recently, however, that studies of the structure of the upper atmosphere has become of general interest.

During the second world war the British Ministry of Defense began to measure the humidity structure at high altitude (20,000 - 40,000 feet). DOBSON (1946) and BREWER (1949) undertook the measurement of the very low values of stratospheric humidity using an airborne, manually operated frost point hygrometer. The results of a recent program of water vapour measurements which grew out of the wartime effort are reported by CLULEY (1978).

Since these early observations, many methods have been employed to make measurements of these three important atmospheric parameters. Some of these were developed, or conducted through the use of the stratospheric research balloon, or high altitude sounding balloon. A sampling of these measurement techniques will be presented in more detail in the pages to follow.

PRESSURE, TEMPERATURE AND HUMIDITY

In order for an operational weather forecast to be prepared, it is necessary to have a continually updated knowledge of the curent state of the atmosphere. This current "picture" or analysis of the atmosphere includes as one of its fundamental elements a measure, over the surface of the earth, of the height of standard pressure levels. The determination of these constant pressure surfaces is accomplished by the release of radiosonde sounding instruments to determine the pressure, temperature and humidity of the atmosphere. The interrelation of these three atmospheric variables with height and air density is governed by two important physical relations. One of these is the perfect gas law, which may be expressed as:

$$p = \rho KT \tag{1}$$

where p is pressure (in Pa), ρ density (molecules/m^3), T temperature (°K), and K is Boltzmann's constant (1.3806 E -23 J/°K/molecule).

This relation will apply instantaneously at each point in the atmosphere over the range of pressures and temperatures encountered there. The second relation is the equation of hydrostatic balance for a parcel of air in the atmosphere, which expresses the fact that the pressure difference across the parcel must support its weight due to the local gravitational attraction. The relation may be written as:

$$dp = -g\rho M dz \tag{2}$$

where dp is pressure difference across parcel, dz the thickness of the parcel, g the acceleration due to gravity (9.8 m/s^2), and M the mass of one air molecule (4.81 E -26 kg).

Combining equation 1 and 2 to eliminate density yields the usual form of the equation of hydrostatic balance:

$$\frac{dp}{p} = -\frac{gM}{KT}\, dz \tag{3}$$

The logarithmic change of atmospheric pressure with height is immediately obvious with equation (3) integrating to:

$$\ln \frac{PL}{PU} = \frac{M}{K} \int_{Z_L}^{Z_U} \frac{g}{t}\, dz \tag{4}$$

where subscripts L,U represent the lower and upper limits in altitude of the range of integration.

The variables g,T are left inside the integral since they may in general both be functions of height, that is g(z), T(z). One useful simplification is to take g as a standard, surface value g_o, and remove it from inside the integral. If this simplification is made, the resulting heights, which will not quite agree with the actual physical height of a given pressure surface, will be expressed in geopotential meters. Since g(z) falls as the inverse square of the distance from the center of the earth, and heights within the stratosphere are small compared with the earth's radius, the difference is not great. It may be important, however, if measurements from radar heights are to be compared to measurements which have been plotted as a function of geopotential height. The relation between geopotential and geometric height is tabulated in standard atmospheres for particular atmospheric temperature profiles. (e.g.: US Standard Atmosphere; ICAO Standard Atmosphere; COSPAR International Reference Atmosphere.)

If the temperature is also taken to be constant, which can be true for reasonable distances in the stratosphere, equation 4 becomes particularly simple:

$$\ln \frac{P_L}{P_U} = \frac{gM}{KT} (Z_U - Z_L) \tag{5}$$

or

$$P_U = P_L \exp[-\frac{Z_U - Z_L}{H}]$$

where $H = \frac{KT}{gM}$ is the scale height of the atmosphere (8.3 km for 300°K).

The scale height of the atmosphere is the pressure e - folding distance in the vertical. It is an approximate measure of the expected vertical resolution of several remote sensing techniques. Equation 5 also has a simple solution for a linear rate of change of temperature with height:

$$\frac{P_U}{P_L} = [T(z_L)/T(z_u)]^{-b} \tag{6}$$

where b is $(gM)/(K\alpha)$. α is the temperature lapse rate with respect to height.

When an atmospheric sounding is made, the variables actually measured are pressure, temperature, and humidity. In order to determine the height at which a pressure and temperature measurement was made, the whole sounding from the surface pressure up to the pressure of the observation must be numerically integrated according to equation 3 to yield the height corresponding to each pressure. The perfect gas law, equation 1, may be used to calculate the local air density at any point from the corresponding pressure and temperature.

A useful re-expression of these equations may be developed by noting that the pressure difference across a macroscopic layer:

$$\Delta p = p_L - p_U \tag{7}$$

must be sufficient to support the weight of molecules between those pressure levels. This relation yields an accurate mean number density for a particular layer since:

$$\Delta p = g\bar{\rho} M\Delta z \tag{8}$$

where $\Delta z(=Z_U - Z_L)$ is the layer thickness and $\bar{\rho}$ is the mean number density in the layer.

The use of this relation prevents the "loss" of molecules which will result from the imprecision of numerically integrating the density function through the layer.

Since temperature errors of a few degrees K can result in a height error of more than 1000 meters at a float height of 30 km, it is important that accurate pressure and temperature data be available for a particular balloon flight analysis. It may not be acceptable, in relation to the accuracy of other measurements made, to rely on a standard atmosphere in the reduction of data. This is particularly so in the case of solar occultation data, and long path length data at near horizontal angles of view. For example, LOUISNARD (1983) calculates that the air mass traversed by the incident solar beam may be in error by as much as 5% from an error in calculated balloon height of 0.5 km when a layer at 20 km is observed from a balloon height of 40 km.

The measurement of temperature then has two important contributions to the analysis of a research balloon flight. One of these is the calculation of the air density as a function of height for the ambient atmosphere, and the other is the provision of local temperature measurements for those instruments, principally emission radiometers, which require it for the evaluation of their data.

THE MEASUREMENT OF TEMPERATURE

A considerable number of atmospheric sounding devices have been built over the years. They all have incorporated some relatively simple device for converting the local air temperature into an electrical signal, which is then transmitted via a radio link to the ground. While some unusual devices such as magnetic flux modulating thermometers have been used, (British Kew radiosonde) the majority of radiosondes have employed a simple thermistor, which is a temperature variable resistance.

Since the VIZ radiosonde has been reported as being used in 20 countries around the world (RICHNER, 1981), and it is also the most likely choice to be used in support of a large balloon payload, it is the only device which will be described here. Similar comments to those made here would be, in a large part, appropriate in the case of most radiosondes currently in use around the world. The global temperature data obtained by radiosondes forms the standard of evaluation of performance for other techniques, such as temperatures deduced from satellite atmospheric radiance measurements.

The standard VIZ radiosonde, of United States manufacture, is a very simple instrument. It has an aneroid driven pressure contact switch which selects between the output of the humidity sensor, the thermistor output, and internal reference signals. Each time a pressure contact changes from one signal source to another it indicates that the instrument has passed through the corresponding pressure level. Each baroswitch is calibrated after construction and the calibration data are supplied along with the instrument.

Many details must be properly looked after if the instrument is to provide optimum performance. To list just a few of these: (1) The temperature and humidity sensors must be properly checked on the ground with a baseline testing unit; (2) The pressure aneroid must be adjusted to reflect the surface pressure at launch; (3) The humidity sensor must be handled carefully to avoid contamination; (4) The thermistor must be clean and properly rigged to avoid a large radiation correction. In short the radiosonde must be carefully used by knowledgeable operators.

A number of studies of the performance of the radiosonde system have been conducted. The most useful of these are the two-sonde balloon tests, since these demonstrate random errors in the sondes of the absence of a highly accurate knowledge of the atmospheric state when the tests are done. Notable examples of this type of intercomparison can be found in the work of RICHNER (1981), LENHARD (1970, 1973), PHILLIPS (1983), SCHMIDLIN (1982) and ANTIKAINEN (1983). Generally the results suggest a random error of approximately 1 to 2 mb in pressure and 0.4 to 0.5 °K in temperature.

The most recent work, that of Phillips, suggests an expected error of approximately 1 mb in pressure. With the exception of Schmidlin, no attempt is made to discuss absolute accuracy in the determination of atmospheric temperature and pressure. Rather the random differences between particular instruments is measured, and the instrumental bias is taken to be zero.

An important point is made by Richner, who suggests a radiational heating correction of 1 - 2°K should be applied to the temperatures measuring during the day by the VIZ radiosonde. It should be noted that the correction is pressure dependent, and is quite important above an altitude of approximately 20 km. This effect is also noted by PHILLIPS (1983) who has used the correction cited by Richner in compiling his tables of relative performance among a group of radiosondes of diverse manufacture.

Schmidlin's paper asserts that radar is the only solution to the height accuracy problem in the use of a radiosonde. He suggests that the error of ±2 mb quoted from the results of the study will cause an uncertainty of close to 1 km in geopotential height calculated using radiosonde ascent data. As with the other authors mentioned the study reported showed rather small random temperature effects compared to the influence of pressure errors. It is not clear from the paper, however, whether a radiation correction was applied to the measured temperatures, and whether that would have influenced the final conclusion.

In addition, Schmidlin's paper does not include the analysis of another option open to the stratospheric investigator. When using a radiosonde to the maximum limit involving altitudes near 40 km, the inclusion of a hypsometer is a sensible alternative to the acquisition of a radar set. Performance data for the hypsometer sondes reported by LENHARD (1970, 1973) clearly indicates the potential for the radiosonde to provide useful pressure data. and geopotential heights to more than 35 km.

It would appear that the radiosonde instrument, properly handled, with either a hypsometer or radar height recording, will provide adequate vertical temperature, pressure, and density information for the support of research balloons. A factor which influences the accuracy of a constituent profile is the quality of the balloon position data. If the radiosonde is supplying direct support to an in situ sensor, then there is no dislocation between the position of the experiment and that of the radiosonde. If, however, the sonde is supporting a payload with solar absorption instrumentation, then the actual position of the payload in latitude and longitude is required. In addition, if the height of the payload is needed and the radar is not available, small errors may develop in the height determined by the pressure data, since the payload may not be contained in the same region of the atmosphere through which the radiosonde climbed to determine the temperature-pressure profile. Errors of this type are harder to quantify, although some discussion of closely spaced balloon launches is presented by LENHARD (1970, 1973).

A useful guide to the general reliability of the atmospheric profile estimate for a given balloon flight may be made by the release of a series of radiosondes. If several ascents can be made within ±6 hours of the period of interest, the data set may be considered as a whole, and a better assessment of the state of the atmosphere at a particular time and place may be made. In addition the magnitude of the random component in the error in determining the atmospheric variables may be estimated by the judicious comparison of profile differences observed in the time series.

For example, a series of atmospheric soundings taken with VIZ radiosondes in support of the Canadian Stratoprobe program were published by BAIN (1976).

Radiosondes are not the only method by which the atmospheric temperature profile may be measured using a balloon. The emission of radiation by the molecules which make up the atmosphere may be detected by a spectro-radiometer and the temperature profile derived therefrom. SHAW (1970) and McCLATCHEY (1969) report the successful determination of a vertical temperature profile in this way.

WATER VAPOUR

ELLSAESSER (1983), in a recent review article, has observed that in the 20 years or so which have elapsed since GUTNICK's (1961) review of water vapour measurements, the variability of the measurements has not significantly decreased. Both the variability among the various measurement techniques and the variability from occasion to occasion for the use of one technique, have

provided such a range of values as to leave some fundamental questions unanswered.

NEWELL (1981) also has made a similar point, although has gone on to assume that the largest bodies of data available, the flights of MASTENBROOK (1974a) and the Meteorological Research Flights of the British Meteorological Office are substantially correct. This is to assume that the mixing ratio values at the extreme low end of the scale are closest to the correct values. The extreme dryness which this implies for the stratosphere is then extremely difficult to explain from a theoretical standpoint (NEWELL, 1981; ELLSAESSER, 1983; DANIELSON, 1982).

Another unsolved problem in the stratosphere is the reconciliation of the mixing ratio behaviour with height, with the expected H_2O source from methane oxidation in the stratosphere. ELLSAESSER (1983) suggests that methane oxidation should provide a source of water vapour of up to 2 ppmm at heights of 30-40 km. The Mastenbrook results are substantially constant with height in the stratosphere, but some Murcray results show an increase with height which is greater than that expected if it were due entirely to the oxidation of methane. It is instructive to consider the methods and instruments with which these conflicting data have been gathered over the years.

In the following short descriptions of instruments and techniques, no particular attempt has been made to create a chronological review. Rather the techniques selected for elaboration have been chosen according to the following rather loose criteria. The selected techniques are usually the best known and most recently used of their type. Furthermore any researcher whose results are, in the light of current knowledge, rather extreme when considered as a part of the extant data set, are not used as examples of measurement technique, even though their method has been successfully employed since.

The current concept of the stratosphere as a dry region of the atmosphere with mixing ratios on the order of 1 to 2 ppm by mass, owes its existence to the work of Dobson and Brewer. Many measurement flights on aircraft using manually operated frost point hygrometers were conducted both during and after the second world war by the British Meteorological Office. Data from these flights are reported by DOBSON (1946) and by BREWER (1949), and for the later Meteorological Research Flights by CLULEY (1978). While these flights produced the first large data set which accurately represented the humidity conditions in the stratosphere, they were limited, even with the use of higher flying aircraft in later years, to the lower stratosphere.

An obvious solution to the altitude limitation was the use of stratospheric balloons for sampling the water vapour content of the stratosphere. The many and varied techniques for the measurement of water vapour form the basis of the following section of this chapter.

THE FROST POINT HYGROMETER

The principle of the frost point hygrometer has been employed by a number of investigators over the years to make measurements in the stratosphere. Indeed, as mentioned in the introduction to this section, the first measurements indicating the existence of a "dry" stratosphere were made on board aircraft by DOBSON (1946), using a manually operated frost point hygrometer. The most extensive set of balloon-based observations of water vapour using frost point hygrometers has been contributed to the literature by MASTENBROOK (1961, 1965, 1968, 1971, 1974a, 1974b, 1979).

The Mastenbrook frost point hygrometer was described in a review delivered by MASTENBROOK (1974b) at the Australian conference on the structure and

composition of the stratosphere, and in more detail in MASTENBROOK and DINGER (1961).

The instrument consists of a condensing mirror surface on which frost is allowed to form. Air is drawn into the measurement cavity of the instrument by a blower and passed over the mirror surface. The mirror is connected to a heat sink which consists of freely boiling Freon 13, and induction heated, so that its surface may be maintained at any temperature above the boiling point of the Freon 13 by adjusting the heating rate.

In order to detect the formation of frost, an optical sensing element views light scattered from frost which has condensed on the cold mirror. The optical signal is detected and used to control a servo loop through the induction heater. The system may be balanced with a small, equilibrium amount of frost on the reflecting surface. The temperature of the surface is detected with a thermistor, and the measured temperature is taken to be the frost point temperature of the air sampled.

In order to avoid contamination problems from the presence of entrained water in the vicinity of the balloon and payload, measurements of stratospheric water vapour amounts are made only in the descent phase of the balloon flights. In addition the mirror is temporarily heated at the top of the flight profile to ensure good sensitivity to the small vapour pressures observed in the stratosphere.

MASTENBROOK (1974a) has conducted a large number of balloon ascents since the beginning of his measurement program at the National Research Laboratory in the early sixties and has discussed them, and their associated error analysis in considerable detail. It would seem appropriate, however, to mention briefly some of the systematic error sources which he has identified in the course of his research.

The problem of contamination, which has been discussed by other authors as well, (ZANDER, 1966) is probably the single biggest difficulty encountered in the in situ measurement of the low water vapour mixing ratios observed in the stratosphere. Mastenbrook's early work identifies two related, but distinct methods by which some of the early ascents were contaminated. The first of these is the balloon/payload water vapour cloud, which is carried aloft into the stratosphere in the form of water vapour absorbed onto the balloon and payload surfaces during the ascent through the wet troposphere. Water may also be evolved from the interior of the materials used in the payload construction at the lower pressures encountered in the stratosphere. This effect was eliminated by the use of a descent measurement so that the vertical velocity of the instrument package presented uncontaminated air to the instrument, without allowing water vapour from the balloon or instrument package to mix into the air sample, and contaminate the measurement.

The second problem encountered was internal contamination in the hygrometer sampling system itself, which was caused by an inadequate airflow through the instrument. The inadequate airflow resulted from a malfunctioning sampling blower; a problem which was not encountered during the later flights on which Mastenbrook placed his greatest emphasis.

The final conclusions drawn from the series of measurements reported by Mastenbrook are: (1) The stratosphere is dry with a mixing ratio of 2.3 ppmm in the low stratosphere; and (2) That there is no substantial gradient in water vapour mixing ratio between this level and 25-30 km altitude.

It is tempting to accept the study of Mastenbrook as the final assessment of water vapour in the stratosphere for two reasons. First, the low altitude

measurements are in reasonable agreement with extensive sets of data collected by the Meteorological Research Flight of the Meteorological Office in Bracknell, England. (When a correction for frost point temperature measurement is made (OLIVER, 1978).) The aircraft measurements are unlikely to be contaminated with water vapour since the air collection is done at very high ventilation rates, and the aircraft continuously moves at high speed into new stratospheric air. Second, Mastenbrook has achieved these results after grappling extensively with the problem of balloon contamination, and has assembled a large enough data set that temporal variations are not likely to bias his mean results to a great extent. It must be remembered, however, that at least one flight represents a reliable measurement of water vapour in the stratosphere substantially higher than the average value which Mastenbrook reports.

It is probably safe to conclude as Mastenbrook has done, that other reported frost point hygrometer flights with mixing ratios an order of magnitude or more larger (BARCLAY, 1960; BARRETT, 1950) were in fact the result of the local contamination. Even more recent flights (BROWN, 1964) have also been the victim of contamination. As has been expressed elsewhere (ELLSAESSER, 1983; GUTNICK, 1961) it is extremely difficult to sort the "good" results from the "bad" with high reliability.

AN ALUMINUM OXIDE HUMIDITY SENSOR

The useful range of conventional radiosonde humidity sensors is such that they are not of any use in measuring the water vapour content of the stratosphere. For example, the Canadian radiosonde network does not regard results obtained in ambient temperatures below -40°C as useful. In order to provide an inexpensive and easily employed detector for stratospheric humidity sensing, it would be desirable to have a simple device like that of the standard radiosonde hygristor, available for use on small and simple radiosonde-type instrument packages. Parametrics Corporation has attempted to develop such a sensor, and some results from its use are available in the literature (HOFMANN, 1972; CHLECK, 1979).

CHLECK (1979, 1966) describes the development and use of an aluminum oxide water vapour sensor (Parametrics Aquamax II) capable of the measurement of very low levels of humidity in the atmosphere. The sensor is a thin film fabrication incorporating an integral heater, temperature monitor and humidity sensor. The sensor element is a porous dielectric layer formed on a layer of aluminum, which is deposited on a silicon substrate. The dielectric layer is overcoated with a layer of porous gold which forms one electrode of the sensor. The aluminum beneath the dielectric forms the other. The water vapour pressure in the vicinity of the sensor alters the impedance measured between the electrodes as water is taken up or released from the dielectric layer. The complete sensor occupies a 5 mm square area on the thin film substrate, with a 1 mm total thickness. While measuring, the temperature of the sensor is stabilized by ohmic heating with the integral heater, to which current is supplied by an external control circuit. The control circuit monitors the temperature of the substrate with the integral diode temperature monitor.

The temperature of the device is stabilized in order to eliminate the temperature corrections which were required in earlier forms of the device (CHLECK, 1966). During radiosonde flights the temperature of the sensor is telemetered to the ground to verify the correct operation of the heater, and to ensure that the temperature remains within acceptable limits.

The sensor was tested in a series of flights reported by CHLECK (1979) and HOFMANN (1972) in which they describe both the calibration procedures used with the sensor, and the results obtained in atmospheric tests. The sensors were individually calibrated before flying, since the sensor does not have an

absolute physical response to water vapour pressure.

Two calibration procedures were employed. One used the humidification of a variable stream of dry, cold nitrogen by a fixed rate of evolution of water vapour from a temperature stabilized permeation tube. The total mass of water evolved from the tube was determined by the weight loss experienced throughout the calibration procedure. Various flow rates of nitrogen were humidified by the fixed water vapour evolution rate to yield the varying humidity levels to which the sensor was exposed.

In addition to the permeation tube calibration a more conventional humidity source, a bubbler, was used to produce air at various humidity levels. The gas thus produced as passed over the sensor, and measured by a frost point hygrometer which was used to measure the humidity down to a frost point temperature of -89°C.

The observations made with these methods were intercompared to yield an empirical relation for the sensor response. This relation may be used to extrapolate the sensor response down to a frost point of -100°C. The final accuracy of the calibrated sensor is estimated to be ±3°C at a frost point of -65°C.

In addition to the humidity calibration, the response of the sensor to step changes in the humidity was determined. As an example the sensor responded to a frost point change from -90°C to -75°C in 70 seconds, and to the opposite change in 30 seconds.

The sensor was tested on a series of balloon flights while connected to a standard radiosonde by a 7.6 m cable hanging below the radiosonde. Measurements were made both on the ascent and descent legs of the flight. A clear difference in the profiles, presumably due to water vapour outgassed by the balloon, is seen in the profiles. The true response of the detector can be seen in the low water vapour amounts recorded in the descent phase of the flight. The measurements made included some as low as 1 ppmm, and are in good agreement with those of other investigators as stated in the paper (CHLECK, 1979).

CRYOGENIC SAMPLING

Several investigators have employed cryogenic sampling instruments to collect samples of stratospheric air for subsequent analysis in the laboratory. An early attempt was made by BARCLAY (1960) but the large amounts of water vapour measured (on the order of 37 ppmm) suggests that the measurement was contaminated by water carried into the stratosphere by the sampling system.

More recent papers by POLLOCK (1980) and LUEB (1975) describe a cryogenic sampling system for the collection of stratospheric air samples, which will be described in some detail here.

The collection system consists of a set of stainless steel cylinders 70 cm long by 3.8 cm diameter designed to collect cryogenically cooled samples of 10 litres STP volume at all flight levels in the stratosphere. The collected gasses, which include all atmospheric constituents except molecular hydrogen, neon and helium are collected in the cylinders, which are partially immersed in liquid neon which maintains the collecting surface of the cylinder at approximately 30°K.

Up to sixteen cylinders are connected together to form the sampling system which is illustrated in Figure 1, taken from LUEB (1975). The individual cylinders each have motor operated valves which can be opened or closed in flight by command. These valves lead out to a common manifold, which in turn connects to the sampling inlet tube. The gas samples are taken at a position

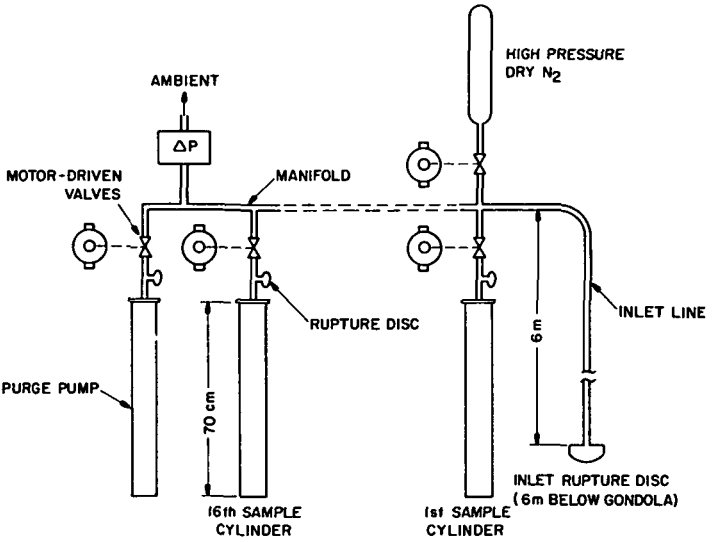

Figure 1. Schematic diagram of the balloon-borne low temperature sampler. Sample cylinders are arranged in concentric circles of eight cylinders with the purge pump in the centre. The sample cylinders are submerged in liquid neon. Reprinted from *LUEB* (1975).

6 m below the gondola which is slung 75 to 150 m below the balloon. These precautions are intended to reduce the risk of contaminating the samples collected.

The whole system is baked out at 350°C to 400°C at high vacuum to remove water which might be absorbed onto any of the surfaces with which the sample gases might come in contact. The stainless steel is exposed at moderate pressure to a source of O_2 to passivate it and the system re-evacuated. The inlet tube is sealed with a rupture diaphragm. which is blown out in flight by a high pressure supply of gaseous nitrogen. The rupture of the disc allows an extension, which had been sealed inside the collection tube, to add 0.7 meters to the length of the collection tube. In addition to extending the distance which the collection inlet is below the gondola, it also ensures that the sample taken is always at least 0.7 m away from any unprepared surface.

Before the start of each sample collection the inlet tube and manifold is purged by collecting gas in an extra sample cylinder which is provided for that purpose.

The flight profile is arranged so that the sampling system is held at float altitude for approximately two hours before sampling is started. After the purge has been done, a sample taken at float altitude, to be analyzed for the amount of contamination which collection in the balloon environment has produced. The payload is then allowed to descend while the main collection procedure is carried out. With a slow descent in the early phases of the process and a more rapid one later on, all samples may be easily collected within a vertical range of 0.5 km each. This allows good height resolution in

the final distributions of gases which are analyzed. The collection procedure is carried out from a float altitude of 35 km down to about 12 km, where the balloon is normally cut down.

The water vapour contamination problem is illustrated by the comparison of the mass mixing ratio observed in the float altitude sample and the first descent sample. On the flight reported by LUEB (1975) the float sample exhibited a mixing ratio of 21 ppmm, while on the first descent sample a mixing ratio of only 5.7 ppmm was found.

When the samples are returned to the laboratory they are in the form of high pressure gas samples. The water vapour is separated in a cryogenic trap, converted to hydrogen gas, and the volume of the hydrogen is measured.

It is immediately obvious that the operational procedures and design elements described by Pollock and Lueb are thoughtfully aimed at controlling those uncertainties which have caused errors in measurements of trace gases by other methods. The procedures for handling the equipment in the laboratory control the internal contamination problem, while the balloon contamination problem is addressed by the use of an appropriate flight profile. Also, the large volume of the sample reduces the contamination problem.

The authors point out a number of significant, advantageous features of their collection technique. These include the fact that the method allows the simultaneous sampling of a large number of interesting stratospheric trace gases (CH_4, H_2, CO, N_2O, $CFCl_3$, CF_2Cl_2) in addition to water vapour. Because of the large volume of gas collected, the measurement of HDO and HTO is also possible.

The technique is expensive, the equipment is complicated and cumbersome, and the samples require laboratory analysis after the flight; however, for the simultaneous collection of many stratospheric species it is a very effective technique.

ULTRA VIOLET FLUORESCENCE MEASUREMENTS

BERTAUX (1978) and KLEY (1978, 1979) describe two independently developed instruments for the in situ measurement of water vapour in the atmosphere. These instruments are similar in operation; and that of Kley will be presented here in detail. The method is based on the detection of fluorescent radiation from the decay of $OH(A^2\Sigma^+)$ to $OH(X^2\Sigma^+)$. The excited form of OH is produced in the photodissociation reaction:

$$H_2O + h\nu \rightarrow OH(A^2\Sigma^+) + H \qquad (9)$$

where the radiation involved is in the vacuum ultraviolet.

In the instrument, shown schematically in Figure 2, taken from KLEY (1978), light from lamp L which emits Lyman alpha radiation at wavelength 121.6 nm, is incident on an air sample. The fluorescence of OH as a result of the aforementioned reaction is observed by a photomultiplier detector oriented at right angles to the path of the dissociating radiation at a distance L_B from the lamp. The intensity of the beam at a distance L_A is monitored by an NO cell (NOC_A) and the intensity of the beam at the point where the fluorescence is detected, is monitored by an NO cell (NOC_B) at distance B' + B" ($=L_B$) from the lamp.

The presence of two detectors, NOC_A and NOC_B, allows the development of relations for the water vapour mixing ratio which are independent of the absolute light intensity supplied by the source lamp.

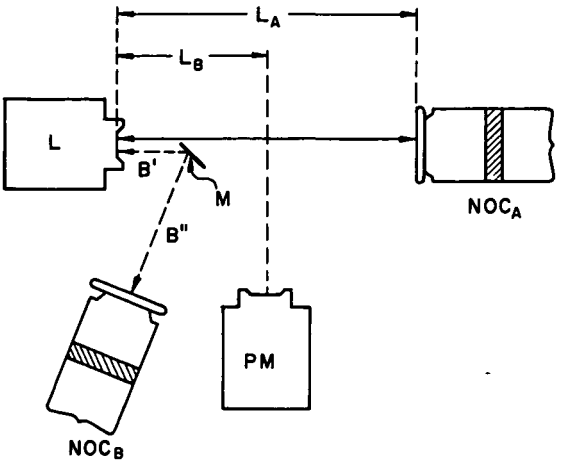

Figure 2. Schematic of the OH fluorescence flight instrument. L - Lyman-alpha lamp; NOC_A, NOC_B - NO ionization cell detectors; PM - photomultiplier; M - mirror. L_A = 18.5 cm; L_B = 9.4 cm. The distance B' + B" is equal to L_B. After KLEY (1979).

In the troposphere where water vapour concentrations are large, the instrument provides a measure of the amount of water in an absorption mode. The depletion of the beam along a path equivalent to $L_A - L_B$ is used to calculate the number of water vapour molecules in the path of the beam. A correction to the observed absorption is made for the influence of oxygen molecules, the density of which is determined from the measured ambient air pressure. At an intermediate height in the atmosphere (8-14 km) where the water vapour mixing ratio is beginning to fall toward the low values observed in the stratosphere, the fluorescence detector output is compared to the absorption measurement, to provide an in-flight calibration for the detector sensitivity and geometry, for the fluorescence measurement. The fluorescence technique is used to provide the measurement of water vapour in the stratosphere since the remaining absorption in the light path of the instrument at those altitudes is not large enough to detect.

A microprocessor in the instrument provides control and data collection functions. The system can make a useful measurement in 1 to 5 seconds, which provides good height resolution for both ascents, at approximately 5 m/s, and descents, at speeds up to 50 m/s.

A number of possible sources of instrumental error have been addressed by the authors. Because the instrument is mounted with a minimum of obstructions between the outside air and the fluorescence area, there is the possibility of starlight entering the detector. In addition there will be a small Rayleigh scattering signal from the light source. These two effects are measured in flight and corrected. By observing the fluorescence region periodically with the light source turned off, the stray light from outside may be measured by the detector. For another interval a quartz shutter is moved in front of the light source to ensure that light from longer wavelengths is not making a significant contribution to the detected light level by scattering from the air in the fluorescence region. The quartz is transparent in the near ultra violet region but does not transmit the dissociating radiation which causes the hydroxyl fluorescence signal.

Observations have been made on both the ascent and descent phases of balloon flights. Analysis of the results have lead the authors to an understanding of both the sample contamination problem, and the problem of outgassing from the instrument itself. Suitable strategies have been devised to overcome these problems, and the later results provide useful measurements of the stratospheric water vapour content. The flight the authors refer to as MW-5 (KLEY, 1979) made from Laramie, Wyoming, shows a water vapour maximum of 2.4 ppmm at 18 km, which is approximately 2 km above the tropopause, rising to 4.8 ppmm at 30 km.

In summarizing the features of this instrument, it may be stated that it has a major advantage compared to those instruments which have nonlinear properties at low vapour pressures of water. The absorption cell mode of operation will clearly operate well for large water vapour mixing ratios, and the transition region to low amounts of water provides a calibration for the fluorescence cell mode. This in-flight calibration removes the uncertainties that can develop in the use of instruments which must be pre-flight calibrated in the laboratory.

While the researchers have made a thorough attempt to reduce or eliminate the effects of contamination, the possibility still remains that the measurements at higher levels in the stratosphere may still contain the effects of contamination, as indicated in their paper.

The good vertical profile resolution of which the instrument is capable, is one of its most useful characteristics. Obviously the fundamental accuracy of the results is tied to the data used to calculate the absorption by water vapour and molecular oxygen, and the radiative lifetime and quenching rate for the $OH(A^2\Sigma^+)$ produced in the photodissociation. The authors estimate the overall accuracy in their final results to be about 20%, and the precision to be 10%.

LONGPATH SOLAR INFRARED ABSORPTION MEASUREMENTS BY SPECTROMETER

Many investigators have chosen to determine the humidity of the stratosphere through the application of the solar occultation technique in the infrared region of the spectrum. For example, MURCRAY (1966, 1969a) has measured water vapour in solar absorption in the 2.6, 6.3 μm region of the spectrum. ZANDER (1973) also measured in the 2.6 μm region, though at higher resolution. GIRARD (1963) and LOUISNARD (1980, 1983) have made measurements of water vapour using their Grille spectrometer. All three instruments measure the presence of water vapour through its absorption of solar radiation. Profile information is devised by consideration of the solar occultation geometry, and the growth of the observed absorption with solar zenith angle. The column amount of water vapour above the balloon may also be determined in regions of the spectrum where the water vapour features are not confused with solar lines, and the exoatmospheric spectrum may be inferred from the observations.

While MURCRAY (1962) has reported results of solar observations in the 1-15 μm region from balloon platforms using a relatively low resolution (5-10 cm^{-1}) prism spectrometer, the instrument described here is a later development of the Denver group (1963-1964) as described by MURCRAY (1967) in Applied Optics.

The design target of the spectrometer was a resolution on the order of 1 cm^{-1} in the 2.7 μm region of the spectrum. The instrument is a double pass 0.5 m Czerny-Turner grating spectrometer with a prism predisperser to provide order selection. The dispersion element is a 10.2 cm square Bausch and Lomb replica grating with 75 lines/mm, blazed at 12 μm. The instrument has short, straight slits. A signal chopper is mounted to chop the light path between the two passes through the instrument, as shown in the diagram in Figure 3. The

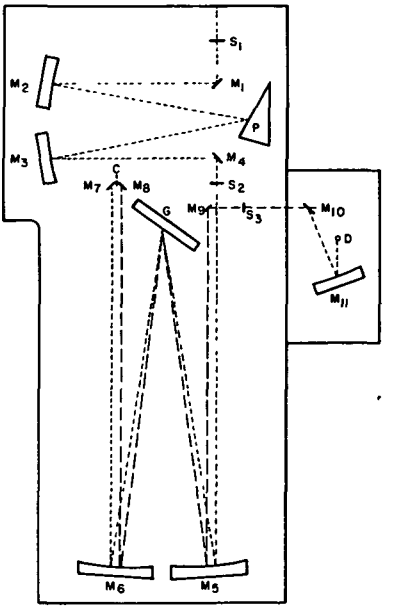

Figure 3. Optical diagram of the Czerny-Turner grating spectrometer and prism predisperser. The mirrors (M) are numbered sequentially. The incident radiation enters the spectrometer at slit S_1, is predispersed with a Littrow prism (P) with an aluminized rear surface and passes into the grating spectrometer at S_2. The grating is double passed using a corner reflector (M_7, M_8) at the focal point of the first pass. The radiation is mechanically chopped with a tuning fork (C) between the two mirrors of the corner reflector. The radiation is then focused onto the detector (D) behind the exit slit (S_3). From MURCRAY (1967).

signal resulting from the detection of radiation at the output of the monochromator is phase detected to separate the thermal background from incident radiation.

With a choice of predisperser prisms and orders of the grating in the main spectrometer, a variety of spectral regions may be studied. The instrument's optical properties were explored in the laboratory, and then the spectrometer was equipped with a sun tracking system and flown on a balloon (MURCRAY, 1966, 1969a,b). The instrument has flown successfully many times and has been used to determine water vapour profiles using lines in the 2.7 μm region and the 6.3 μm region of the spectrum.

The analysis procedures used to convert the spectra gathered, to a vertical profile of water vapour, are outlined by MURCRAY (1973, 1974). The method used involves fitting a model atmosphere to the observed data using a line by line calculation, using published line positions, line strengths and line width data. The profile is adjusted to make the model spectra fit the observed spectra, and then the model profile is assumed to be representative of the atmospheric profile at flight time.

Since the solar occultation process weights very heavily to the altitude where the beam is instantaneously tangent during sunset, a considerable amount of information may be obtained about the vertical distribution of the absorber in the atmosphere. SNIDER (1975a,b) reports the atmospheric model used for these calculations. The path lengths are calculated for the U.S. standard atmosphere in the program, and the mixing ratio of water vapour found from the fitting process. Line parameters are taken from the AFCRL (1973) summary as reported by MURCRAY (1974).

ZANDER (1973) reported measurements of water vapour obtained by long path length absorption, using a large Ebert-Fastie spectrometer illustrated in Figure 4. The instrument is a 2.5 m focal length monochromator operated in the double pass mode, with a narrow intermediate slit. The resolution of the spectrometer is reported at 0.04 cm^{-1}, and the data gathered for the above paper were taken in the 1.81 to 1.89 μm and 2.46 to 2.83 μm regions of the spectrum. A lead sulphide detector was employed for the measurement set reported in that paper (ZANDER, 1973).

The instrument is pointed at the sun to an accuracy of ±2 min of arc with a 40 cm Ritchey-Chretian telescope with a servo controlled mirror. The whole payload is roughly oriented in azimuth. Because of the high resolution capability of this instrument, and the high pointing accuracy of the sun-tracker, the shapes of the lines measured may be determined. This allows some attempt at profiling the amount of an absorber above the balloon to be made through the difference in collision broadened line widths of the measured lines as a function of altitude. Terrestrial lines may be easily separated from solar features because of the considerable difference in their widths.

The results obtained by ZANDER (1973) indicate a mean mixing ratio of (3.5 ± 1.5) ppmm above the balloon at 25 km. In order to eliminate the effects of water vapour inside the spectrometer itself, a tungsten lamp was flown which

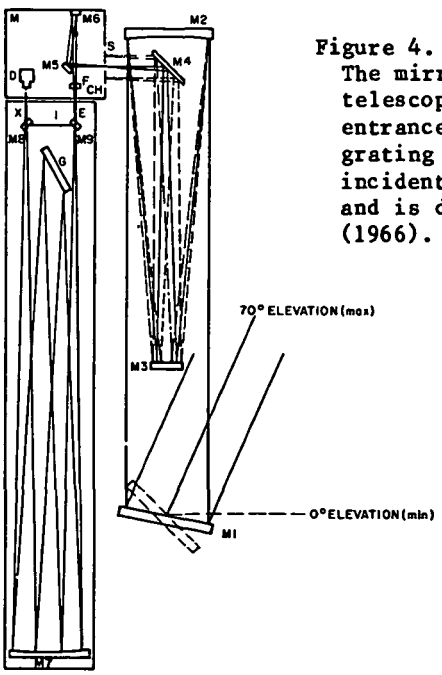

Figure 4. Optical layout of the Ebert spectrometer. The mirrors M_1 through M_4 form a servo-controlled telescope used to image the sun on the spectrometer entrance slit at S. Mirrors M_7 to M_9 and the grating G form an Ebert design spectrometer. The incident radiation is passed through a chopper (CH) and is detected by the detector (D). After ZANDER (1966).

could be turned on in flight and scanned to allow the amount of water vapour in the instrument to be measured and subtracted from the column amount calculated from the solar observations.

The water vapour measurements were based on the intensities of 80 isolated water vapour lines. The author makes the point that the results are totally dependent on a good knowledge of spectral data for water vapour. Since the column amount determined here is for the path from the instrument upward to the sun, there will be a path contribution due to water vapour emitted by the balloon and payload. The effects of this contamination problem are discussed by ZANDER (1966) in an earlier paper.

INFRARED EMISSION RADIOMETRY

The downward flux of radiation in the stratosphere due to the emission of radiation from vibrationally and rotationally excited water vapour has been used by a number of investigators to measure the stratospheric water vapour mixing ratio. The instruments used for this measurement technique range from cooled spectro-radiometers and filter radiometers, to submillimeter interferometers.

BROOKS (1972) describes a small grating spectrometer designed to be cooled to liquid nitrogen temperatures and to observe the spectral region 16-30 μm. The instrument has a spectral resolution of 2 cm^{-1} near 25 μm and utilizes a liquid helium-cooled copper-germanium detector. The observed region of the spectrum exhibits features due to CO_2, HNO_3 and water vapour. In the range 24-30 μm only water has a significant emission.

Observations are made during a balloon descent to approximately 30 km. The resulting radiance versus height data are fitted in a model atmosphere using data from the AFCRL atmospheric transmittance program, in a line-by-line calculation. The amount of water vapour observed during this particular flight was about 0.6 ppmm around 17 km, and 4 ppmm at 25 km.

WILLIAMSON (1965) described the use of a liquid nitrogen cooled wideband radiometer which sensed thermal emission in the spectral range 5.5-8.0 μm (1820-1250 cm^{-1}). A band calculation following the method of GOODY (1964), was used to estimate the amount of water vapour in the lower stratosphere at 3 ppmm. A large residual signal at the highest flight altitude of 25 km was inconsistent (by 3 orders of magnitude) with estimates of the overburden of water vapour at that height.

Because of the difficulty in understanding the WILLIAMSON (1965) data, PICK (1969) developed a new radiometer. Figure 5 illustrates the principal elements. There are several notable features in the radiometer design. All the optical elements in the field of view of the detector, and the detector itself, are cooled to nearly the temperature of liquid air by radiation to the walls, which form the liquid air reservoir. In addition the gas evolved as the radiometer ascends or is warmed by heat entering the reservoir, is exhausted through the opening through which radiation is allowed to enter. This eliminates the need for a cooled window to prevent the accumulation of ice inside the instrument.

The detector surface is imaged by reflecting optics to accept radiation entering the instrument through a field of view of 15° half angle. A motor driven filter wheel with six interference filters, and a brass blank is situated in front of the gold doped germanium detector. The radiation impinging on the detector is chopped at a point between the detector and the filter wheel. The filters have a spectral resolution of approximately 0.3 μm. The instrument is flown so the center line of its field of view is mounted at 45° to the zenith.

Inflight radiometric calibration is accomplished by periodically moving a

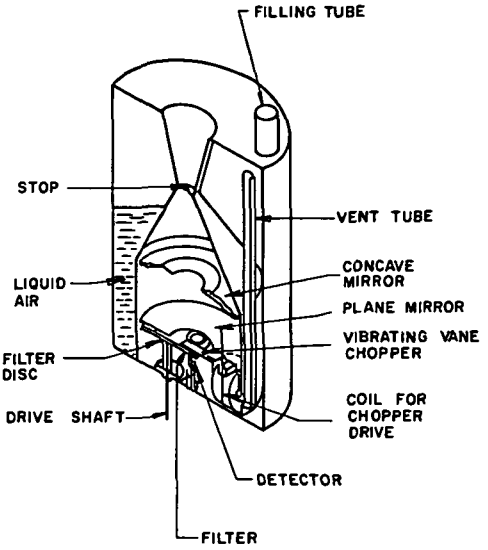

Figure 5. The radiometer assembly shown is a cross section along a diameter of the cylindrical copper can which holds the cryogenic coolant. From PICK (1969).

blackbody at ambient temperature (measured) into the instrument's field of view. Because the radiation passes through the interference filters at a range of angles up to 15°, the wavelength passband is broadened toward longer wavelengths than the nominal one for each filter. This necessitated that the instrument be calibrated against a Golay cell detector in monochromatic radiation on the ground, to determine its true spectral response. The main systematic error is reported as being due to the error in the determination of the inflight blackbody temperature. A 1% uncertainty in blackbody temperature translates to a 4% uncertainty in radiance measured.

The measurements confirmed Williamson's measurement of anomalous fluxes in two spectral intervals measured. The amount of water vapour was calculated by a procedure identical to that of the previous paper, and was reported as 3 ppmm, constant up to 25 km in the stratosphere. The anomalous radiation has since been identified as due to nitric acid.

LONG PATH SOLAR ABSORPTION MEASUREMENTS WITH INFRARED INTERFEROMETERS

The measurement procedures of FARMER (1980) and NIPLE (1980) provide good examples of the use of interferometry in the infrared region of the spectrum. The instruments are both Michelson Interferometers, but are rather different in design philosophy and execution. Both Murcray and Farmer are currently very active in the measurement of stratospheric species and they are therefore particularly good examples to cite as users of the interferometric technique.

The use of a high resolution Michelson at relatively short wavelengths in a balloon-based situation is a challenging task. Each group has solved the difficulties of alignment, data collection and analysis in its own way.

The basic interferometer used by FARMER (1980) is described by SCHINDLER (1970). The instrument is a modified Michelson interferometer in which the usual plane mirrors have been replaced by a pair of cat's-eye retroreflectors.

The retroreflectors are used in a double pass mode where a beam incident on one side of the cat's-eye exits on the other, reflects from a stationary plane mirror and retraces its path back through the cat's-eye. The arrangement is illustrated in Figure 6 which was taken from Schindler's paper.

The use of the cat's-eye reflector in this mode has some advantages. Because of the double pass which occurs in the path to the moving cat's-eye, the path difference will be double that of a conventional Michelson arrangement. Because the cat's-eye is a retroreflector, the arrangement is relatively

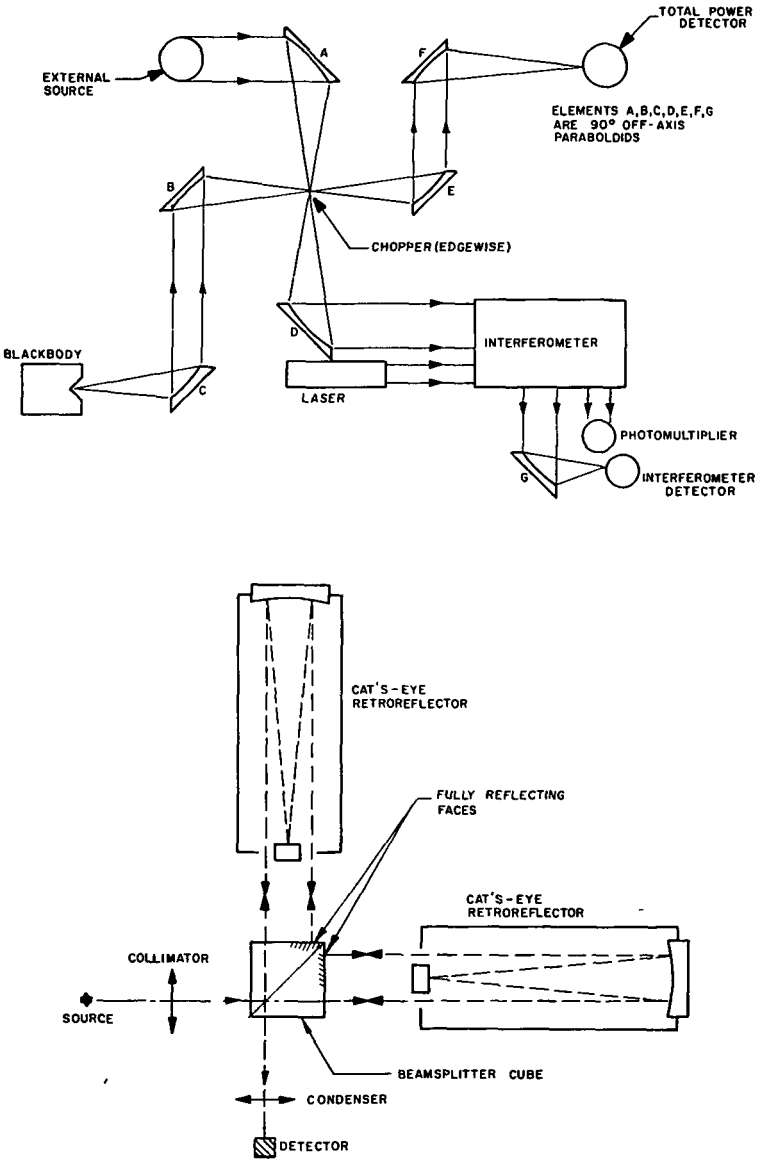

Figure 6. The optical layout of the interferometer (top) and the foreoptics arrangements. Taken from SCHINDLER (1970).

tolerant of small angular misalignments. In addition, since the beam from the beam splitter and the beam from the stationary plane mirror are parallel, the system is also tolerant of lateral misalignments of the cat's-eye mirrors as well. These features tend to make the complete instrument generally resistant to small misalignments.

In order to accurately measure the path difference through which the moving mirror has travelled, a monochromatic light source, a helium-neon laser, is imaged through the interferometer onto a photodetector. This signal is modulated by the motion of the moving mirror.

In fact the control system is much more complicated than this. A moving coil actuator is used to make the large physical movement needed for the motion of the moving cat's-eye. Fine control on the order of a wavelength is provided by a pîezo-electric stack which makes small adjustments to the secondary mirror of the cat's-eye. An elaborate digital control system steps the mirror assembly from one laser wavelength position to another in either direction. The necessary sensing signals for this process are derived from the phase sensitive rectification of a small amplitude modulation of the laser interference signal by a high frequency oscillation of the secondary mirror of the stationary cat's-eye. This process generates a signal which is 180° out of phase with the detected total intensity of the laser signal, since the modulation depends on the differential of the laser amplitude, which is a sinusoidal function of the moving mirror position. The use of the total intensity and demodulated differential signal together allows the electronics to determine the position and direction of motion of the moving mirror at any time. It is, therefore, possible to command the control system to move to a particular fringe position.

Finally, to allow the point-by-point normalization of the interferogram of an external source to its integrated intensity, the interferometer is rapidly (1000 Hz) chopped between the observed source and a local blackbody reference source. While this chopping occurs, complementary chopping is done between the same two sources for a total power detector included to provide the normalization signal. The chopper is a tuning fork type and because of its small size, it is situated at the focus of collimating optics so the beam that needs to be interrupted is also very small.

The quoted performance for this instrument (FARMER, 1980) is as follows: spectral range, 1800-7900 cm^{-1}; unapodized resolution 0.3 cm^{-1}; time for one scan, 200 seconds; detector, InS_b; liquid nitrogen cooled.

The water vapour profiles are recovered from measurements of lines in the $2\nu_2$ band at 3152 cm^{-1}.

The amount of water vapour in the path to the instrument was determined by a line-by-line calculation of synthetic spectra, which were matched to the observed data. Twelve lines in the water vapour spectrum were used to do the analysis. The spectral line parameters were taken from McCLATCHEY et al. (Air Force Cambridge Research Laboratory, 1973).

The results of aircraft measurement flights were analyzed and published, with figures available for the amount of water vapour in both the Northern and Southern Hemispheres. The Southern Hemisphere mixing ratios was determined as 1.2 ppmm, at 22 km, rising to 3.7 ppmm at 36 km. In the Northern Hemisphere the 22 km mixing ratio was 3.1 ppmm, rising to 3.7 ppmm at 36 km.

The Murcray group (NIPLE; 1980) has reported the acquisition of high resolution spectral data obtained by the use of a Michelson interferometer as well. They have begun the systematic application of a novel design interferometer to the measurement of atmospheric constituents in the solar occultation mode.

The instrument was designed and constructed by Bomem Company (BUIJS, 1980) and is a conventional plane mirror Michelson interferometer in its optical design. In order to construct an instrument with dependable alignment characteristics, which is essential for remote operation, the interferometer is equipped with a laser servo control system which maintains the alignment of the interferometer. The layout of the instrument is shown in Figure 7. A small portion of the aperture of the interferometer is used for the detection beam. This beam is derived from the helium-neon laser which is fitted with a beam expander. A lens is placed in the output beam of the interferometer which images straight line fringes localized at the stationary mirror position (BORN, 1975). These fringes have their maximum density along the line of maximum relative tilt between the two Michelson mirrors. Since one mirror is moving, the fringes travel across the field in the direction of maximum density.

Three detectors are placed in the field of view and the output of two are phase detected relative to the third. A signal which is proportional to the amount and direction of the relative mirror tilt is developed. This signal is then used to drive a two axis servo system, aligned with the detector axes, to maintain the "stationary" mirror accurately in plane alignment with the image of the moving mirror.

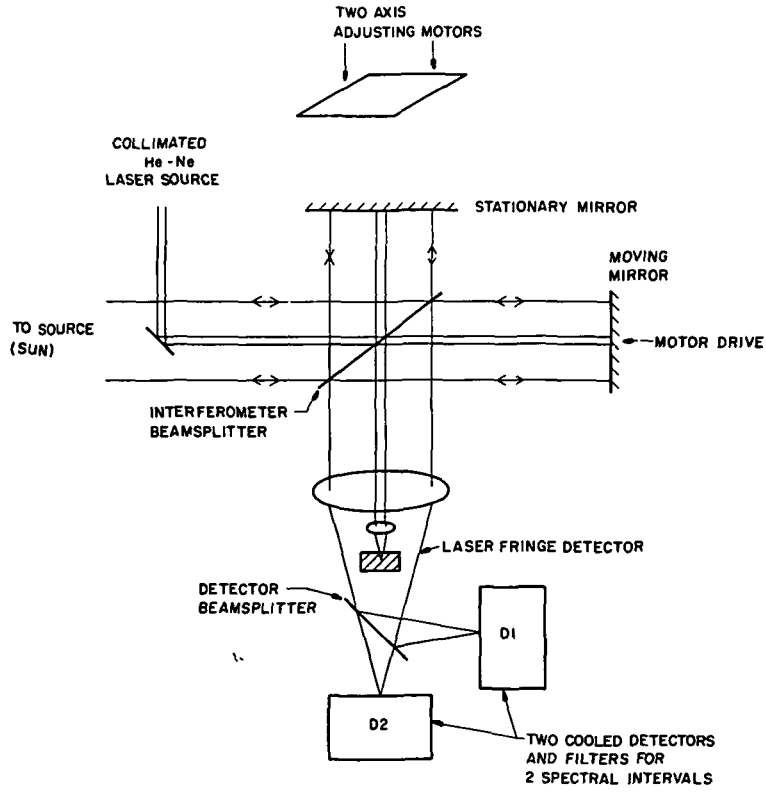

Figure 7. The Bomem interferometer. The tilt of the "stationary" mirror is adjusted using information from the laser fringe detection system so that the image of its surface in the beam splitter remains dynamically parallel to the surface of the moving mirror.

Clearly, if the phase difference (tilt) between the two detectors is a multiple of one full wavelength of the laser light, the servo-system will be nulled. In order to ensure that this occurs for the plane parallel condition, and not some multiple of the one wavelength tilt, the amplitude of the laser signal is sensed. The system searches in a preprogrammed manner, to make the amplitude of the modulation from the interference large enough to satisfy a preset criterion for correct alignment.

Since the wavelength of the laser light is much shorter (0.6 μm compared to 6 μm) than the wavelengths measured, this alignment procedure will ensure correct alignment of the mirrors over their full field for the infrared, even though the laser detectors take up only a fraction of the full instrumental beam width. In aligning the instrument, procedures are used to align the infrared detection optical axis with that of the laser alignment subsystem. This ensures that when fringe detection is used to "measure" the position of the moving mirror relative to zero path difference, the wavelength scale of the resultant interferogram transform will be directly in accurate wavelength units. These units will be correct, independent of the refractive index of the environment of the instrument.

The use of an automated alignment system results in an instrument of unusually small size and light weight (about 50 kg). It is relatively immune to isolated shocks since it realigns itself after they have occurred. It is not particularly insensitive to vibration while operating, but since balloon payloads are relatively free of vibration, the instrument provides good performance in the balloon environment. The automated alignment system greatly reduces the thermal stabilization time, and also provides the important information as to whether the instrument is properly aligned at any given time, so that data analysis can be properly done.

The instrument described by NIPLE (1980) is capable of simultaneously measuring nitrogen dioxide and water vapour. It has an unapodized resolution of 0.02 cm^{-1}, and can produce a complete interferogram in approximately 50 seconds.

The 1603.0-1607.4 cm^{-1} region of the spectrum was observed for the detection of both water vapour and NO_2. This region includes 232 NO_2 lines and 19 H_2O lines.

Because of the optical characteristics of the instrument (channel spectra and instrument apodization) it was decided to improve the analysis procedure by including the known instrumental properties explicitly in the analysis procedure, rather than attempting to remove or explain them in their resultant effects on the transformed spectra.

This is accomplished by determining the infinite resolution spectrum appropriate for some first guess model atmosphere, using published spectral data for the constituents considered. The high resolution spectrum is Fourier transformed, and the transform is modified according to the known properties of the observing instrument. Both the observed interferogram and the simulated one are then transformed to spectral space and compared. An interaction scheme is operated to correct for differences between the two, using a least squares metric to quantify the fit. The model atmosphere producing the spectrum with minimal error is taken to describe the real atmosphere at the time of the observations.

The flight described by NIPLE (1980) determined the stratospheric water vapour mixing ratio to be 2.4 ppmm at 17 km, rising to 3.9 ppmm at about 30 km. This paper references various others which describe in detail the algorithms used for the analysis of the interferograms obtained.

FILTER RADIOMETERS FOR ROTATION BAND MEASUREMENTS

BREWER (1972) reported the development of a long wavelength filter radiometer designed to observe the emission from water vapour in the 20-60 μm region of the spectrum. The instrument design is illustrated in Figure 8. It consists of a Barnes thermistor bolometer on which radiation is imaged after passing through a waveband selecting filter. The filter was compounded from beryllium oxide and carbon black, which were embedded in polyethylene. The filter is transparent to wavelengths longer than 20 μm.

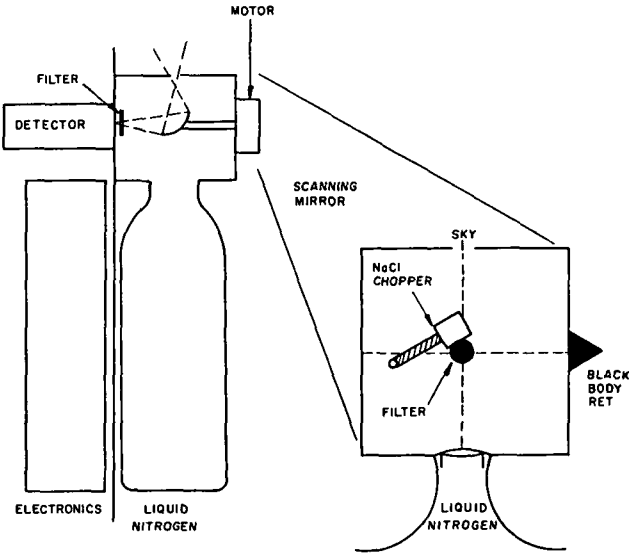

Figure 8. The Brewer-Thomson radiometer. The detector is successively exposed to radiation from the sky, an ambient temperature black body, and the liquid nitrogen reservoir. The detector is chopped by a salt crystal chopper driven by a stepping motor. From BREWER (1972).

The signal detected by the bolometer is chopped by a 32 Hz stepping motor chopper. The chopper blade is made of sodium chloride, since the polyethylene filter has a small transmission around 5 μm. Sodium chloride transmits in that region of the spectrum, but cuts off rapidly to wavelengths longer than 20 μm. Therefore the resultant output of the phase detector is due to radiation of wavelengths longer than 20 μm. The signal is then phase detected and telemetered to the ground. The chopper temperature in flight is not known, so the collimating mirror which images the sky on the detector is turned periodically to sample either a black body at ambient temperature, or a flask of liquid nitrogen which is carried along with the radiometer.

A standard radiosonde is flown along with the radiometer to measure temperature and pressure. The instrument is light weight and can be flown on a 2.5 kg balloon or two radiosonde balloons.

Three ascents were made with the radiometer and yielded a lower stratosphere water vapour mixing ratio of 2 ppmm.

HYSON (1974a,b; 1978) describes a small radiometer for the detection of water vapour in the stratosphere. The instrument is similar in principle to that of the Brewer, but has a few interesting differences. The instrument is illustrated in Figure 9 taken from HYSON (1976).

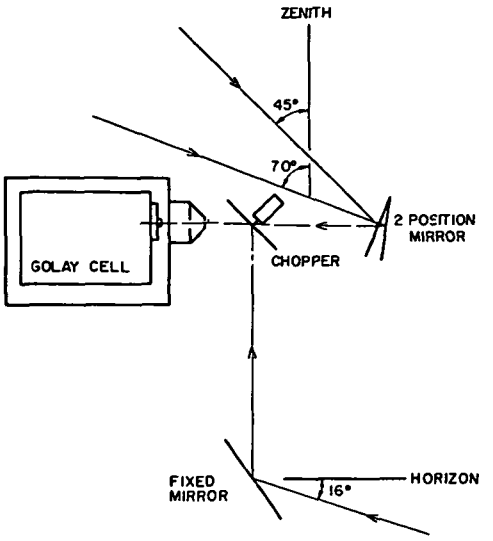

Figure 9. The Golay cell receives radiation from one of two sources; the intensity of radiation from the sky above the radiometer is compared to the (assumed) saturated signal from emission by water vapour at ambient temperature below the horizontal direction. The sources are compared through the use of a reflective chopper. After HYSON (1974b).

The instrument uses a Golay cell detector, which is alternately illuminated by radiation from the sky above the radiometer, or the atmosphere below at a depression angle of 16° relative to the local horizontal. The radiation from the sky may be examined at zenith angle of 45° or 70°.

The instrument uses a polyethylene filter to pass radiation in the 40-200 μm region of the spectrum to the detector. The detector beam is chopped with a reflecting chopper between the upward looking and downward looking mirrors. The chopping rate is 14 Hz and the Golay cell signal is phase detected.

Since the amount of water vapour below the instrument is very large, the signal arriving from that direction is taken to be representative of a blackbody at ambient temperature.

Water vapour amounts in the Australian stratosphere have been reported by Hyson. It was found that the water vapour mixing ratio is between 2.3 and 3.1 ppmm in the altitude range 15 to 21 km and approximately 5 ppmm at 25 km.

DIFFERENTIAL ABSORPTION RADIOMETER

BURKERT (1974) describes a filter radiometer for the measurement of water vapour in long path solar absorption. The instrument is shown in Figure 10. When a gas is measured in absorption, the measurement depends on the detection of the amount of radiation removed from the beam on passing through the absorbing gas. Since gases, in general, do their absorbing in very narrow lines, the detection of the net depletion of a beam by a broadband sensor will show only small changes for substantial changes in the amount of absorber in the

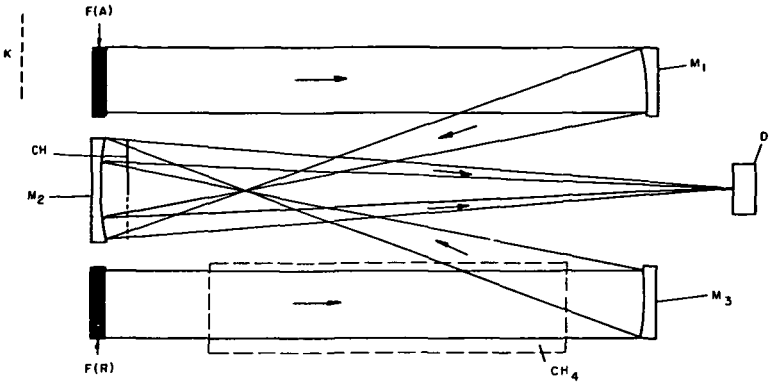

Figure 10. Signals are alternately detected by the detector D, which originate from two telescopes formed by mirrors M_1 and M_2. The telescopes are fitted with two narrow-band interference filters; one chosen to lie on an appreciable water vapour absorption feature, and one nearby where the absorption from water vapour is negligible. After BURKERT (1974).

beam. This signal may be lost in noise sources such as fluctuations in the source intensity, or changes in the detector sensitivity. The signal to noise ratio may be improved by using spectrometers or interferometers of higher resolution, but with the attendant costs of increased size, complexity and the loss of speed.

A filter radiometer is a very small and simple instrument, but suffers from the signal to noise problem discussed above. It is possible to gain some of the signal to noise advantage of a high resolution device, while maintaining the simplicity of the filter radiometer. With reference to Figure 10 taken from BURKERT (1974), it is possible to select narrow band interference filters (50 cm^{-1}) chosen to lie on, and just beside a water vapour absorption feature. If incident radiation is allowed to reach a detector after being absorbed by these two different filters, the difference in the amount of radiation taking these two paths will be more sensitive to the absorber than either of the two beams.

This technique will automatically reduce the dependence of the final instrument signal on the source intensity or the detector sensitivity (BURKERT, 1974). In order to calculate the amount of absorber on the solar beam arriving at the instrument, it is necessary to know what the instrument output would be if there were no absorbing gas in the atmosphere. By allowing the instrument to observe the sun at high sun angles, at float altitude for some time, a Langley plot may be prepared (a plot of instrument output versus atmospheric path length) and the intercept of this plot will be the value the instrument would read with zero absorber amount in the atmosphere.

This extraterrestrial value, together with the known instrumental response to changes in absorber amount, will allow the determination of the total amount of absorber in the path to the sun.

On the balloon flight reported in BURKERT (1974) two filters were used to select narrow bands at 2.606 μm and 2.280 μm with a bandwidth of 50 cm^{-1}. The extraterrestrial constant for the instrument was determined during a float interval at 29.5 km. This, together with data taken during balloon descent, allowed the calculation of the total amount of water vapour in the incident path as a function of altitude. The conversion from instrument reading to water vapour amount was done by using the laboratory measured spectral response of the

instrument in a line by line calculation, assuming a Voigt line profile for the absorption by water vapour. By calculating from float height downward a vertical profile can be determined.

The published profile exhibits a minimum mixing ratio of (0.8 ± 0.2) ppmm at 20 km, which is about 2 km above the tropopause for that flight. The mixing ratio rises to about 8 ppmm by 30 km but the uncertainty due to possible instrument outgassing is approximately ±3 ppmm.

RESULTS OF WATER VAPOUR INVESTIGATIONS

It is appropriate to introduce a discussion of the results of water vapour investigations by following ELLSAESSER (1983) in quoting GUTNICK (1961): "Lack of a tenable explanation of the various reports on stratospheric humidity casts doubt on the accuracy of part or all of the data". Figure 11 is replotted from ELLSAESSER (1983) and is representative of recent data. The large variability of the measurements is difficult to reconcile with the Brewer hypothesis for the circulation of air through the stratosphere. Not the least of the difficulties is the variation in the vertical gradient of water vapour amount, which ranges from near zero to a change of 5 ppmm between the tropopause level and 30 to 40 km altitude.

In 1961 Gutnick called upon the scientific community to carry out a co-operative research program to assess the size and sources of the differences between measurements made using different techniques and different instruments. Just twenty years after this call, the Federal Aviation Administration (FAA) of the United States and the National Aeronautics and Space Administration (NASA)

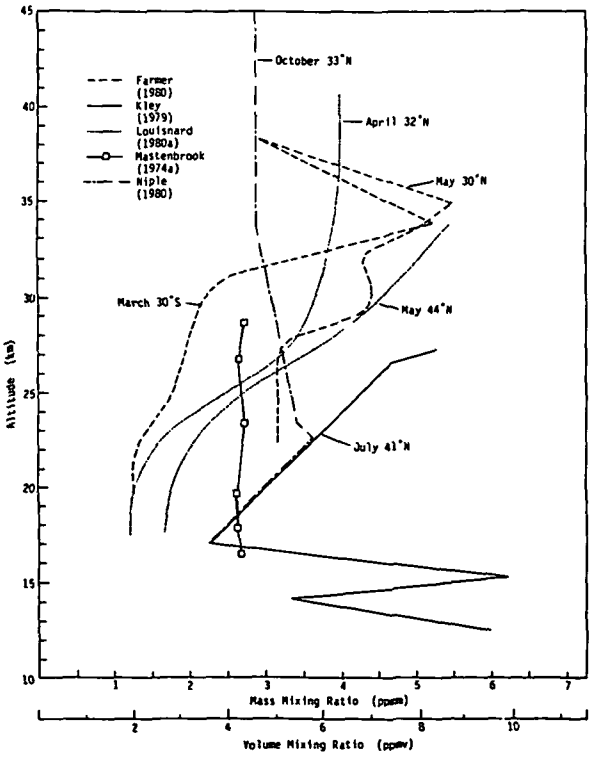

Figure 11. A comparison of some water vapour measurements made from stratospheric research balloons. After ELLSAESSER (1983).

agreed to jointly administer a water vapour intercomparison program. The goal and details of the program were reported in the UPPER ATMOSPHERIC PROGRAMS BULLETIN (1981). Table 1 lists the cooperating investigators. The set of instruments chosen to participate in the program provides a cross section of the techniques used in the past for water vapour measurement.

When the preliminary results are examined (UPPER ATMOSPHERIC PROGRAMS BULLETIN, 1981, 1982) the agreement between the different techniques is seen to be reasonably good (Figure 12). This result helps to clarify some of the uncertainties raised by ELLSAESSER (1983) in his review.

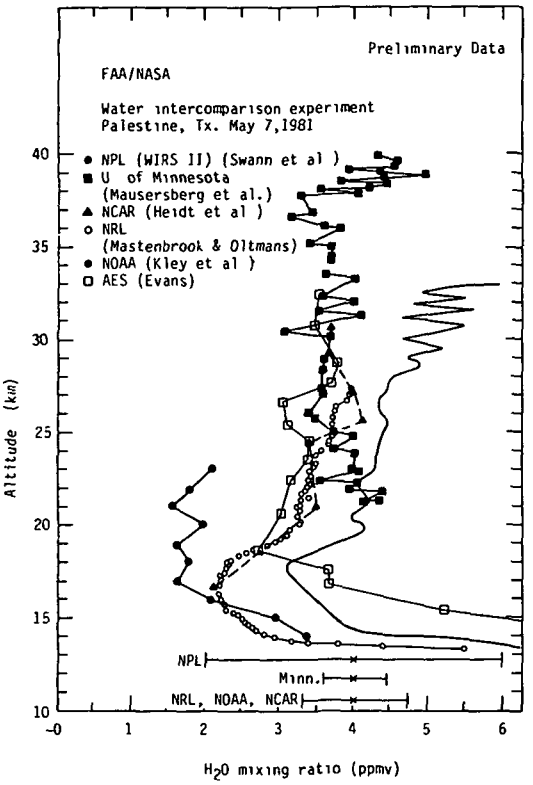

Figure 12. Preliminary results from the 1981 comparison of stratospheric water vapour instrumentation. Published in the UPPER ATMOSPHERIC PROGRAMS BULLETIN (1981, 1982).

It will be noted that in situ and remote sensing instruments agree on a difference in the vertical of 1.2 to 1.5 ppmm between the minimum mixing ratio level near 17 km and an altitude of 30 km. This is in contrast to the long-standing difference between past MASTENBROOK (1974b) results taken with the frost point hygrometer and those observations made by remote sensing measurements made by the solar occultation technique (MURCRAY, 1966; FARMER, 1980). This would suggest that there is a much larger variability in the water vapour mixing ratio profiles with respect to time and place than had previously been expected.

The preliminary results (1.7 ± 0.4 ppmm) are compatable with the previously accepted levels of water vapour measured by Mastenbrook, which were in the region of 2.0 ppmm in the lower stratosphere. This level of humidity is comparable to that which NEWELL's (1981) stratospheric fountain would introduce

Table 1. A partial list of investigators of the water vapour mixing ratio in the stratosphere.

INVESTIGATOR	MEASUREMENT TECHNIQUE	LOCATION	ALTITUDE (km)	MIXING RATIO (ppmm)
BARRETT (1972)	Emission 18-23 μm Downward Emission		low strat.	2.4-2.6
BREWER (1972)	Emission 20-60 μm Downward Emission	Ontario Canada (1969-70)	low strat.	1.4-3.0
Bonnetti (BANGHAM; 1980)	Emission 5-80 cm^{-1} Long Path		18 36	2.5 5
GOLDMAN (1972)	Emission 25 μm Ascent	New Mexico USA (1971)	16 25	<1.0 3-4
HARRIES (1973)	Submillimeter Emission Long Path	England (1971)	mid strat	1-3
HYSON (1974)	Emission 30 μm		15-18	4
KLEY (1979)	Lyman Alpha Photodissociation		17 30	2.4 4.8
LOUISNARD (1983)	Absorption 5-6 μm Solar Occultation	CNES France	20 40	1.8 5.5
MASTENBROOK (1974)	Frost Point Hygrometer	Washington D.C., USA (1960 -)	18 22	2 3
MURCRAY (1966)	Absorption 2.6 μm Ascent	New Mexico USA (1964)	16 30	<2.0 >10.0
MURCRAY (1969)	Absorption 2.6 μm Solar Occultation	New Mexico USA (1964)	25 30	2.5 3.0
MURCRAY (1973)	Emission 2.5 μm Ascent	Hyderabad India (1972)	16 25	4-5 <1.0
PICK (1969)	Emission 5.8-6.8 μm Ascent	England (1967)	low strat 25	3.0 3.0
WILLIAMSON (1965)	Emission 5.5-8.0 μm Ascent	England (1963)	low strat 25	3.0 3.0
ZANDER (1973)	Absorption 1.8, 2.5 μm Solar Occultation		15-25	3.5

into the stratosphere. The observed amount of water vapour leaves little margin for any other sources of water, such as tropical hot tower convection (ELLSAESSER, 1983) which might inject additional water into the stratosphere. The results of the intercomparison also seem to be consistent with the observation by KLEY (1979) of a hygropause, which is a mixing ratio minimum in the water vapour profile located a couple of kilometers above the tropopause height.

There remains the possibility that some other mechanism for drying air, both in the troposphere and in the stratosphere, remains to be elucidated (ELLSAESSER, 1983).

OZONE

The limited extent to which vertical profile information may be obtained from ground-based measurements of ozone (GOTZ, 1934) lead investigators to devise methods for the direct sampling of the ozone distribution. REGENER (1938) flew an ultra violet spectrograph on board a balloon payload to make a determination of the ozone vertical profile. Similar measurements were reported by PAETZOLD (1955). Since these techniques produce only moderate vertical resolution of the ozone profile and are little used, they will not be discussed here.

REGENER OZONE SONDE

REGENER (1960, 1964) developed a chemiluminescent sonde to make a direct determination of ozone concentration through a chemical detection process. This sonde depends on the reaction of ozone in the atmospheric sample with Rhodamine-B. This substance reacts with ozone with a characteristic fluoresence, the intensity of which is related to the ozone concentration. The fluorescence signal is detected with a photomultiplier to produce an output which is used as an indicator of the ozone concentration in the measurement chamber.

In use as a stratospheric sounder the measurement device is aspirated with a diaphragm pump which draws outside air into the reaction vessel. The resulting signal is telemetered to the ground via a standard radiosonde, which is flown along with the instrument to measure the background atmosphere. While the instrument was used for a number of years by the United States Weather Service, it was eventually phased out. While the dry chemistry involved in the sonde was an advantageous simplification, the lack of an absolute calibration, difficult preparation and poor instrument stability were among its problems. The instrument was also difficult to use operationally since a preflight calibration with an accurately determined ozone source was required.

BREWER OZONE SONDE

BREWER (1960) reported the development and use of a wet chemical method for the detection of ozone. The method depends on the ability of ozone to release iodine in a solution of potassium iodide according to the reaction:

$$2KI + O_3 + H_2O \rightarrow 2KOH + I_2 + O_2 \qquad (10)$$

Two electrodes are placed in the electrolyte solution. If a current is allowed to flow, the following reactions will take place at the anode and cathode respectively:

$$I_2 + 2e \rightarrow 2I^- \qquad (11)$$

$$2I^- \rightarrow I_2 + 2e \qquad (12)$$

Actually the I^- exists in the form I_3^-, but the net result of the chemistry is as indicated here. If the I_2 produced is free to recirculate, a current may be maintained without the continual addition of iodine. In the Brewer system this re-circulation is prevented by using one electrode of platinum and one of silver. The silver electrode is the anode, and the iodine formed at the anode by reaction R3 is immediately converted to AgI which is insoluble in the electrolyte solution. The net result is the formation of an electrochemical system which allows the circulation of a current of two electrons in the external circuit, for each molecule of ozone dissolved and reacted in the electrolyte according to reaction R1.

In the light of recent knowledge of the behaviour of ozonesondes in the presence of sulphur dioxide and other atmospheric pollutants, it is interesting to note that Brewer observed the presence of an absorber which caused an effect in the sense of "negative" ozone amounts in some of his early work, and he concluded that the observed effect was "clearly due to negative shifts of the telemetry system". In addition he noted that the response time of the sonde seemed to be a function of altitude, an effect which was studied in more detail by DE MUER (1980). This determination of the sonde response time is not compatible with the response times determined in the laboratory.

The advantage of the Brewer sonde is that it needs no absolute calibration. Operationally, however, the flights are usually normalized to a nearby total ozone reading made by a Dobson or Brewer spectrophotometer. The magnitude of the correction coefficient is taken as indicative of the absolute accuracy of the ozonesonde in performing a measurement of ozone.

THE ELECTROCHEMICAL CONCENTRATION CELL

KOMHYR (1967, 1969) reported the development of an electrochemical concentration cell for the measurement of ozone. The cell system is made up of several components and is depicted in the sketch in Figure 13. The cell consists of anode and cathode containers and a larger reservoir for the cathode electrolyte.

DETAIL OF CONSTRUCTION OF
ELECTROCHEMICAL CONCENTRATION CELL
FOR GAS ANALYSIS

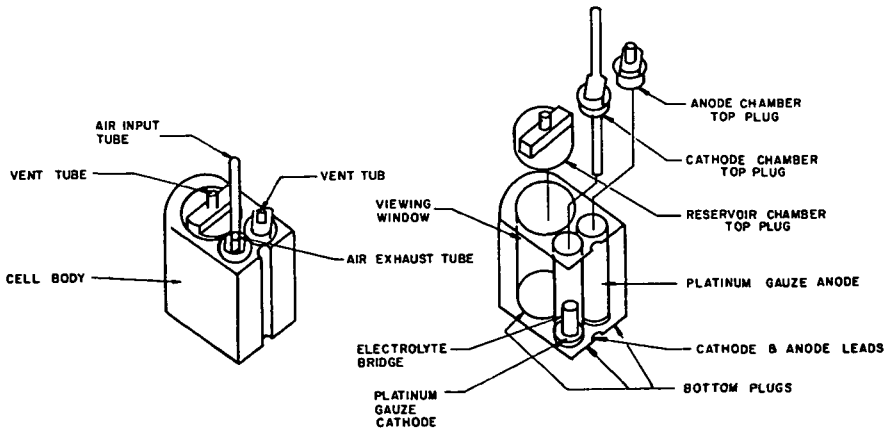

Figure 13. Details of the construction of the electrochemical concentration cell for gas analysis. From KOMHYR (1969).

The cathode cell consists of a platinum electrode immersed in a dilute, buffered solution of potassium iodide. The anode container is connected to the cathode by an electrolyte bridge composed of tightly packed asbestos fibers. The bridge prevents bulk flow, but allows the exchange of ions between the cathode and anode regions. The anode electrolyte is a concentrated potassium iodide solution, and the anode is platinum.

In the cathode region iodine is reduced according to the following reaction:

$$I_2 + 2e \rightarrow 2I^- \tag{13}$$

In the anode region oxidation takes place according to the reaction:

$$3I^- \rightarrow I_3^- + 2e \tag{14}$$

The electrons produced or consumed are exchanged through an external circuit and constitute the measurement of the iodine consumed by the reduction reaction in the cathode area. The measurement of ozone is accomplished through the production of iodine in the cathode compartment by the reaction of ozone with potassium iodide. This reaction proceeds according to the following reaction:

$$2KI + O_3 + H_2O \rightarrow 2KOH + I_2 + O_2 \tag{15}$$

The ozone is introduced into the cathode solution by a small teflon pump which drives the air sample into the cathode region. The gas is allowed to bubble up through the electrolyte, where the ozone goes into solution and reacts with the potassium iodide.

The chemistry of the electrochemical cell is quite complex (see THORNTON, 1982; TORRES, 1978) and the cell concentrations were adjusted empirically to achieve a calibrated response to ozone. In use it is found that the cell has a "zero-signal" with air bubbled through it in the absence of ozone. Thornton has identified this as due to the removal of I_3^- which is normally present in the cathode chamber immediately after the cell is filled. This constant background signal is subtracted from the ozone induced response of the cell to yield the measured signal.

In operational use the ECC sonde is connected to a standard radiosonde and uses the radiosonde's transmitter to telemeter the ozone profile information to the receiving station. In practice it is found that it is useful to normalize the ozone profile obtained to a nearby Dobson or Brewer spectrophotometer total ozone value.

In the context of research ballooning the measurement of the ambient ozone concentration is usually done in conjunction with a measurement flight intended to measure other stratospheric constituents. The usual end goal of a measurement flight is that of providing suitable profile information for the development and verification of photochemical models designed to explain the observed properties of the stratosphere. In order to accomplish this goal, it is essential to measure the state of the stratosphere at the time that any particular trace constituent measurement is made. One reason for this is the well known large temporal and spatial variability of the ozone profile. In addition some measurements such as long path infrared absorption measurements require a detailed knowledge of the concentration profile of background species to allow the calculation of their effects on the observed spectra.

Generally, the performance characteristics of the Brewer and Komhyr ozonesonde systems are quite similar. It is found operationally that the correction

factors needed to bring ground-based total ozone measurements and ozonesonde measurements into agreement are slightly different for the two instruments. Table 2, taken from MATEER (1977), illustrates the typical mean response of Brewer-Mast sondes in relation to Dobson total ozone amount. It is found that the ozonesonde amounts must be scaled by approximately 1.2 to 1.3 to yield a value for the total ozone which is comparable to that measured by a nearby spectrophotometer. A similar table for the ECC ozonesonde is presented as Table 3 which is taken from KIRCHOFF (1983). It can be seen that the correction factor for the ECC sonde is closer to unity for the largest set of observations reported than that of the Mast sonde, and the range of the correction factors observed is smaller. The ECC sonde is a somewhat better choice for the investigator who is supporting a balloon flight without the support of a ground-based measurement of ozone.

Table 2. Typical normalization factors for Brewer-Mast ozonesondes compared to Dobson total ozone reading. After MATEER (1977).

LOCATION	SAMPLE SIZE	CORRECTION FACTOR	TOTAL OZONE (DOBSON UNITS)
Churchill	92	1.309 ± 0.187	377 ± 58
Edmonton	161	1.236 ± 0.165	351 ± 50
Goose	244	1.301 ± 0.199	377 ± 54
Resolute	159	1.186 ± 0.113	412 ± 86

Table 3. Statistical parameters of ozone total column amount measured by ECC and Dobson instruments. From KIRCHHOFF (1983).

	ECC	DOBSON	DIFFERENCE	PERCENT DIFFERENCE
Geraci and Luers (1970-1975 data, 95 days)				
Mean	0.319	0.320	-0.001	-0.30
Standard Deviation	0.050	0.034	0.038	12.19
Geraci and Luers (1973 data, 16 days)				
Mean	0.338	0.320	0.017	5.25
Standard Deviation	0.043	0.024	0.026	7.74
Natal Data (1978-1981, 43 days)				
Mean	0.286	0.276	0.010	3.84
Standard Deviation	0.025	0.013	0.027	9.65

DASIBI

The Dasibi ozone measuring instrument is a widely used device for the ground-based monitoring of atmospheric ozone (Dasibi operating and instruction manual, Model 1003 AH). The Dasibi instrument measures ozone by measuring the extinction of 253.7 nm radiation from an internal mercury lamp. The light is made to transverse a known length of absorption tube and the measured light intensity is indirectly compared to the intensity the same lamp-detector contribution would exhibit if there were no ozone in the absorption tube. This normalized measurement is accomplished by comparing the reading the detector system recorded when the air sample was passed through an ozone destroying filter of manganese dioxide before being admitted to the absorption cell, with that obtained when the air sample containing ozone is measured.

In addition to this comparison procedure which eliminates the effect of absorption cell changes, the instantaneous fluctuations of the light source are also eliminated by the use of a second detector which views the light source without an intervening absorption cell. This detector controls the sensing electronics in such a way as to remove the dependence of the final measurement on the absolute intensity of the mercury line source.

The principle of the Dasibi laboratory instrument has been adapted to a successful instrument for the measurement of stratospheric ozone. Robbins (Johnson Space Centre; private communication) reports the details of the balloon version of the instrument.

REFERENCES

Antikainen, V. and V. Hyvonen (1983), The accuracy of the Vaisala RS80 radiosonde, *Fifth Symp. on Meteo. Observations and Instrum.*, Amer. Meteo. Soc., Toronto, Canada, 134-140.

Bain, S., C. L. Mateer and W. F. J. Evans (1976), Meteorological and ozone data for the project STRATOPROBE balloon flights of 8 and 22 July 1974, Atmosphere, 14, 147-154.

Bangham, M. J., A. Bonetti, R. G. Bradsell, B. Carli and J. E. Harries (1980), F. Mencaraglia, D. G. Moss, S. Pollitt, E. Rossi and N. R. Swann (1980), Measurements of stratospheric trace gases using infrared and submillimeter spectroscopy, Proc. Quad. International Ozone Symp., Ed. J. London, Boulder, CO, 2, 759-767.

Barclay, F. R., M. J. W. Elliott, P. Goldsmith and J. V. Kelley (1960), A direct measurement of the humidity in the stratosphere using a cooled-vapour trap, Quart. J. Roy. Met. Soc., 86, 259-264.

Barrett, E. W., L. R. Herndon, Jr. and H. J. Carter (1950), Some measurements of the distribution of water vapour in the stratosphere, Tellus, 2, 302-311.

Bertaux, J. and A. Delannoy (1978), Vertical distribution of H_2O in the stratosphere as determined by UV fluorescence in-situ measurements, Geophys. Res. Lett., 5, 1017-1020.

Born, M. and E. Wolf (1975), Principles of Optics, Fifth Ed., Pergamon Press, Toronto, 300-302.

Brewer, A. W. (1949), Evidence for a world circulation provided by measurements of helium and water vapour distribution in the stratosphere, Quart. J. Roy. Met. Soc., 75, 351-363.

Brewer, A. W. and J. R. Milford (1960), The Oxford-Kew ozonesonde, Proc. Roy. Met. Soc. London A, 256, 470-495.

Brewer, A. W. and K. P. B. Thomson (1972), A radiometer for observing stratospheric emission due to water vapour in its rotational band, Quart. J. Roy. Met. Soc., 98, 187-192.

Brooks, J. N., A. Goldman, J. J. Kosters, D. G. Murcray, F. H. Murcray and W. J. Williams (1972), Balloon-borne infrared measurements, Physics and Chemistry of Upper Atmospheres, Ed. B. McCormac, D. Reidel Publishing Co., Boston, MA, 278-285.

Brown, J. A., Jr. and E. J. Pybus (1964), Stratospheric water vapour soundings at McMurdo Sound Antarctica: Dec. 1960 - Feb. 1969, J. Atmos. Sci., 21, 597-602.

Buijs, H. L., G. L. Vail, G. Tremblay and D. J. W. Kendall (1980), Simultaneous measurement of the volume mixing ratios of HCl and HF in the stratosphere, Geophys. Res. Lett., 7, 205-208.

Burkert, P., D. Rabus and H.-J. Bolle (1974), Stratospheric water vapour and methane profiles, Proc. International Conf. on Structure, Composition and General Circulation of the Upper and Lower Atmosphere and Possible Anthropogenic Perturbations, Melbourne, Australia, 267-274.

Chleck, D. (1966), Aluminum oxide hygrometer: laboratory performance and flight results, J. Appl. Meteor., 5, 878-886.

Chleck, D. (1979), Measurements of upper atmospheric water vapour made in-situ with a new moisture sensor, Geophys. Res. Lett., 6, 379-381.

Cluley, A. P. and M. J. Oliver (1978), Aircraft measurements of humidity in the low stratosphere over southern England 1972-1976.

Danielson, E. G. (1982), A dehydration mechanism for the stratosphere, Geophys. Res. Lett., 9, 605-608.

De Muer, D. (1980), A correction procedure for electrochemical ozone soundings and its implication for the tropospheric ozone budget, Proc. Quad. International Ozone Symp., Boulder, CO, 88-95.

Dobson, G. M. B. (1930), Proc. Roy. Soc. London A, 129, 411.

Dobson, G. M. B., A. W. Brewer and B. Cwilong (1946), Proc. Roy. Soc. London A, 190, 137.

Ellsaesser, H. W. (1983), Stratospheric water vapour, J. Geophys. Res., 88, 3897-3906.

Fabry, C. and M. Buisson (1921), J. Phys. Radium. Ser. 6, 2, 197.

Farmer, C. B. (1974), Infrared measurements of stratospheric composition, Can. J. Chem., 52, 1544-1559.

Farmer, C. B., O. F. Raper, B. D. Robins, R. A. Toth and C. Muller (1980), Simultaneous spectroscopic measurements of stratospheric species O_3, CH_4, CO, CO_2, N_2O, H_2O, HCl and HF at northern and southern mid-latitudes, J. Geophys. Res., 85, 1621-1632.

Girard, A. (1963), Spectrometre a grille, Appl. Optics, 2, 79-87.

Goldman, A., D. G. Murcray, F. H. Murcray, W. J. Williams and J. N. Brooks (1973), Distribution of water vapour in the stratosphere as determined from balloon measurements of atmospheric emission spectra in the 24-29 μm region, Appl. Optics, 12, 1045-1053.

Goody, R. M. (1964), Atmospheric Radiation, Oxford University Press.

Gotz, F. W. P., A. R. Meethan and G. M. B. Dobson (1934), The vertical distribution of ozone in the atmosphere, Proc. Roy. Soc. London A, 145, 416-446.

Gutnick, M. (1961), How dry is the sky?, J. Geophys. Res., 66, 2867-2871.

Hofmann, D. J., J. M. Rosen, T. J. Pepin and J. L. Kroening (1972), Global measurements of stratospheric aerosol, ozone, and water vapour by balloon-borne sensors, Second Conf. on CIAP, DOT-TSC-OST-73-4, 23-33.

Houghton, J. T. (1966), Effect of contamination on spectroscopic detection of stratospheric water vapour, Quart. J. Roy. Met. Soc., 92, 281.

Hyson, P. (1974a), Radiometric measurements of H_2O in the southern Hemisphere, J. Geophys. Res., 79, 5001.

Hyson, P. (1974b), Recent measurements of stratospheric water vapour over Australia, Proc. International Conf. on Structure Comp. and General Circulation of the Upper and Lower Atmosphere, and possible Anthropogenic Perturbations, Melbourne, Australia, 257-266.

Hyson, P. (1978), Stratospheric water vapour measurements over Australia, Quart. J. Roy. Met. Soc., 104, 225-228.

Kirchhoff, V. W. J. H., E. Hilsenrath, A. G. Motta, Y. Sahai and R. A. Medrano-B (1983), Equatorial ozone characteristics, J. Geophys. Res., 88, 6813.

Kley, D. and E. J. Stone (1978), Measurement of water vapour in the stratosphere by photodissociation with Lyman alpha (1216A) light, Rev. Sci. Instru., 49, 691-697.

Kley, D., E. L. Stone, W. R. Henderson, J. W. Drummond, W. J. Harrop, A. L. Schmeltekopf, T. L. Thompson and R. H. Winkler (1979), In-situ measurements of the mixing ratio of water vapour in the stratosphere, J. Atmos. Sci., 36, 2513-2524.

Komhyr, W. D. (1967), Nonreactive gas sampling pump, Rev. Sci. Instru., 38, 981-983.

Komhyr, W. D. (1969), Electrochemical concentration cells for gas analysis, Ann Geophys., 25, 203-210.

Lenhard, R. W. (1970), Accuracy of radiosonde temperature and pressure-height determination, Bull. Amer. Meteor. Soc., 52, 842-846.

Lenhard, R. W. (1973), A revised assessment of radiosonde accuracy, Bull. Amer. Meteor. Soc., 54, 691-693.

Louisnard, N., G. Fergent and A. Girard (1980), Simultaneous measurements of methane and water vapour vertical profiles in the stratosphere, Proc. Quad. International Ozone Symp., Boulder, CO, 797-802.

Louisnard, N., G. Fergent, A. Girard, L. Gramont, O. Lado-Bordowsky, J. Laurent, S. Le Boiteux and M. P. Lemaitre (1983), Infrared absorption spectroscopy applied to stratospheric profiles of minor constituents, J. Geophys. Res., 88, 5365-5376.

Lueb, R. A., D. H. Ehalt and L. E. Heidt (1975), Balloon-borne low temperature air sampler, Rev. Sci. Instru., 46, 702-705.

Mastenbrook, H. J. and J. F. Dinger (1961), Distribution of water vapour in the stratosphere, J. Geophys. Res., 66, 1437.

Mastenbrook, H. J. (1965), Frost-point hygrometer measurements in the stratosphere and the problem of moisture comtamination, Humidity and Moisture Measurement Control in Science and Industry, 2, 480-485.

Mastenbrook, H. J. (1968), Water vapour distribution in the stratosphere and high troposphere, J. Atmos. Sci., 25, 299-311.

Mastenbrook, H. J. (1971), The variability of water vapour in the stratosphere, J. Atmos. Sci., 28, 1495-1501.

Mastenbrook, H. J. (1974a), Water-vapour measurement in the lower stratosphere, Can. J. Chem., 52, 1527-1531.

Mastenbrook, H. J. (1974b), Stratospheric water vapour distribution and variability, Proc. International Conf. on Structure, Composition and General Circulation of the Upper and Lower Atmosphere and Possible Anthropogenic Perturbations, Melbourne, Australia, 233-248.

Mastenbrook, H. J. and R. E. Daniels (1979), Measurements of stratospheric water vapour using a frost-point hygrometer, Atmospheric Water Vapour, Ed. A. Deepak, T. D. Wilkerson and L. H. Ruhnke, Academic Press, NY, 329-342

Mateer, C. L. (1977), Method of Evaluation of Canadian Ozonesonde Data, Atmospheric Environ. Service Internal Rep. No. APRB 89 D 7, Environment Canada.

McClatchey, R. A. and J. H. Shaw (1969), A spectrometric measurement of the atmospheric temperature above 30 km near sunrise, J. Atmos. Sci., 26, 153.

McClatchey, R. A., W. S. Benedict, S. A. Clough, E. D. Burch, R. F. Calfee, K. Fox and L. S. Garing (1973), AFCRL atmospheric absorption line parameters compilation, AFCRL-TR-0096, Environment Res. Paper, 434, Air Force Cambridge Research Laboratory, Bedford, MA

Murcray, D. G., F. H. Murcray and W. J. Williams (1962), Distribution of water vapour in the stratosphere, J. Geophys. Res., 759-766.

Murcray, D. G., F. H. Murcray and W. J. Williams (1966), Further data concerning the distribution of water vapour in the stratosphere, Quart. J. Roy. Met. Soc., 92, 159-161.

Murcray, D. G. (1967), A balloon-borne grating spectrometer, Appl. Optics, 6, 191.

Murcray, D. G., T. G. Kyle and W. J. Williams (1969a), Distribution of water vapour in the stratosphere as derived from setting sun observation data, J. Geophys. Res., 74, 5369-5373.

Murcray, D. G., F. H. Murcray, W. J. Williams, T. G. Kyle and A. Goldman (1969b), Variation of the infrared solar spectrum between 700 cm^{-1} and 2240 cm^{-1} with altitude, Appl. Optics, 8, 2519-2536.

Murcray, D. G., A. Goldman, F. H. Murcray, W. J. Williams, J. N. Brooks and D. B. Barker (1973), Vertical distribution of minor atmospheric constituents as derived from airborne measurements of atmospheric emission and absorption infrared spectra, Second Conf. on CIAP, DOT-TSC-OST-73-4, 86-98.

Murcray, D. G., A. Goldman, W. J. Williams, F. H. Murcray, J. N. Brooks, R. N. Stocker and D. E. Snider (1974), Stratospheric mixing ratio profiles of several trace gases as determined from balloon-borne infrared spectrometers, Proc. International Conf. on Structure, Composition and General Circulation of the Upper and Lower Atmosphere and Possible Anthropogenic Perturbations, 292-303.

Newell, R. E. and S. Gould-Stewart (1981), A stratospheric fountain?, J. Atmos. Sci., 38, 2789-2796.

Niple, E., W. G. Mankin, A. Goldman, D. G. Murcray and F. J. Murcray (1980), Stratospheric NO_2 and H_2O mixing ratio profile from high resolution infrared solar spectra using non-linear least squares, Geophys. Res. Lett., 7, 489-492.

Oliver, M. J. and A. P. Cluley (1978), A systematic error in the measurement of frost point using the Meteorological Office Mk 3 hygrometer, Quart. J. Roy. Met. Soc., 104, 503-509.

Paetzold, H. K. (1955), New experimental and theoretical investigations on the atmospheric ozone layer, J. Atmos. Terr. Phys., 7, 128-140.

Phillips, P. D. and H. Richner (1983), SONDEX - the ALPEX radiosonde intercomparison, Fifth Symp. on Meteor. Observations and Instru., Amer. Meteor. Soc., Toronto, Canada, 141-147.

Pick, D. R. and J. T. Houghton (1969), Measurements of atmospheric infrared emission with a balloon-borne multifilter radiometer, Quart. J. Roy. Met. Soc., 95, 535-543.

Pollock, W., L. E. Heidt, R. Lueb and D. H. Ehalt (1980), Measurement of stratospheric water vapour by cryogenic collection, J. Geophys. Res., 85, 5555-5568.

Regener, V. (1938), Phys. Z., 35, 788.

Regener, V. (1960), On a sensitive method for the recording of atmospheric ozone, J. Geophys. Res., 65, 3975-3977.

Regener, V. (1964), Measurement of atmospheric ozone with the chemiluminescent method, J. Geophys. Res., 69, 3795-3800.

Richner, H. and P. D. Phillips (1981), Reproducibility of VIZ radiosonde data and some sources of error, J. Appl. Meteor., 20, 954-962.

Schindler, R. A. (1970), A small high speed interferometer for aircraft, balloon, and spacecraft applications, Appl. Optics, 9, 301-306.

Schmidlin, F. W. (1982), Can the standard radiosonde meet special atmospheric research needs?, Geophys. Res. Lett., 9, 1109-1112.

Shaw, J. H., M. T. Cahine, C. B. Farmer, L. D. Kaplan, R. A. McClatchey and P. W. Schaper (1970), Atmospheric and surface properties from spectral radiance observations in the 4.3 micron region, J. Atmos. Sci., 27, 773-780.

Snider, D. E. (1975a), Refractive effects in remote sensing of the atmosphere with infrared transmission spectroscopy, J. Atmos. Sci., 32, 2178-2184.

Snider, D. E. and A. Goldman (1975b), Refractive effects in remote sensing of the atmosphere with infrared transmission spectroscopy, BRL Report No. 1790, Ballistics Research Laboratory, Aberdeen Proving Ground, MD.

Thornton, D. C. and N. Niazy (1982), Sources of background current in the ECC ozonesonde: Implications for total ozone measurement, J. Geophys. Res., 87, 8943-8950.

Torres, A. L. and A. R. Bandy (1978), Performance characteristics of the electrochemical concentration cell ozonesonde, J. Geophys. Res., 83, 5501-5504.

Upper Atmospheric Programs Bulletin (1981), 81-4, Office of Environment and Energy, Federal Aviation Administration, Washington, DC, 1-8.

Upper Atmospheric Programs Bulletin (1982), 82-5, Office of Environment and Energy, Federal Aviation Administration, Washington, DC, 3-4

Williamson, E. J. and J. T. Houghton (1965), Radiometric measurement of emission from stratospheric water vapour, Quart. J. Roy. Met. Soc., 91, 330-338.

Zander, R. J. (1966), Moisture contamination at altitude by balloon and associated equipment, J. Geophys. Res., 71, 3775-3778.

Zander, R. (1973), Water vapour above 25 km altitude, Pure Appl. Geophys., 106, 1346-1351.

2. MEASUREMENTS OF NEUTRAL CONSTITUENTS USING INFRARED AND VISIBLE REMOTE SENSING

N. Louisnard* and S. Pollitt**

*Office National d'Etudes et de Recherches Aerospatiales
BP 72, 92322 Chatillon Cedex
France

**National Physical Laboratory
Teddington, Middlesex
United Kingdom

ABSTRACT

Remote sensing from balloon platforms by visible and infrared spectrometry has been extensively used for the past 10 years to measure the concentration profiles of stratospheric species. A brief review of the instrumentation and method of analysis is made. Recent results concerning HCl, ClO, HF, NOx, HNO_3, CO, CH_4, N_2O, H_2O and O_3 are presented.

INTRODUCTION

Infrared spectroscopy and radiometry are very powerful techniques for remote sensing of trace concentrations of atmospheric gases. The unique spectra associated with molecular transitions enables gases to be identified and the data obtained from the spectra can be used to determine quantitative information. Two spectroscopic techniques are currently available for remote atmospheric monitoring from balloons; these are:

(1) Absorption spectroscopy which measures the transmission of radiation through the atmosphere from a distant source, in most cases the sun;

(2) Emission spectroscopy which measures the atmospheric thermal emission.

These two techniques are now well established in the field of atmospheric monitoring and it is these which we shall review in this chapter.

(a) The Mid-Infrared Spectrum of the Atmosphere

Before reviewing the measurement techniques and instrumentation, let us first briefly examine the mid-infrared atmospheric spectrum. Langley in 1884 was the first to record the transmission of sunlight through the atmosphere in the infrared. There have been many atmospheric infrared atlases produced during the last century; the reader is referred to the recent atlases produced by the Denver group (GOLDMAN et al., 1982) which are compiled from high resolution solar absorption spectra measured from the ground and from balloons.

The mid-infrared region is bounded by intense absorption features due to carbon dioxide at 2.7, 4.3 and 15 microns. Water vapour has strong rotation-vibration bands at 1.9, 2.7 and 6.3 microns. Other bands due to ozone, methane and nitrous oxide occur at 9.6, 7.6 and 7.8 microns, respectively. Between these absorption bands, there are regions known as "atmospheric windows" where the atmosphere is less opaque. Some absorption in these window regions is still present in the lower atmosphere due to the wings of lines in the water vapour bands and, at sea level, large portions of the infrared spectrum are very heavily, if not totally absorbing. However, detailed spectroscopic investigations in the window regions from mountain observations, high flying aircraft and balloons have led to the identification of a large number of minor stratospheric constituents. The position of the major vibration-rotation bands which are

known to exist in the mid-infrared are shown in Figure 1 which also shows the spectral emittance of a blackbody at typical stratospheric temperatures.

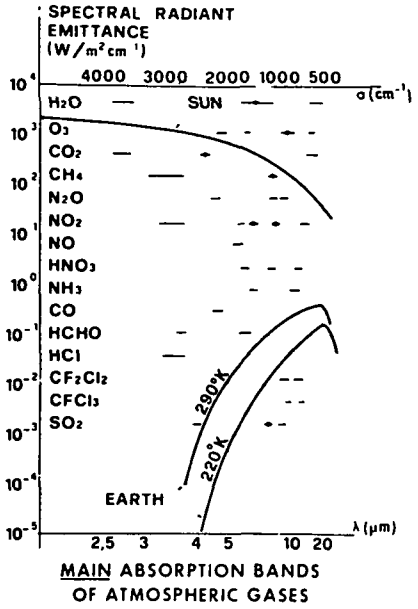

Figure 1. Main absorption bands of atmospheric gases in the infrared and spectral radiant emittance (W/m^2 cm^{-1}) for the sun and two typical stratospheric temperatures.

(b) Measurements from Balloons

Balloons made from modern plastics are able to carry payloads of several tons to altitudes of 35-40 km. From these altitudes balloon-borne spectrometers can make observations over a large range of zenith angles from more than 40° to 96°, limited on one side by the balloon entering the field of view and on the other by the earth. The mass path along the line of sight increases with zenith angle; for zenith angles greater than 90° the mass path can be orders of magnitude greater than that for a vertical column and so it is ideal for the detection of molecules with weak emission or absorption features; it may also be shown that most of the absorption or emission is located in a rather narrow layer, roughly one scale height thick, above the point along the line of sight where the latter is tangential to the earth's surface. The vertical concentration profile of trace species below the spectrometer can be determined from spectral measurements made at zenith angles between 90° and 96°. This technique, known as limb scanning, has been discussed in detail by Gille and House (GILLE and HOUSE, 1971) and is the most important technique for the remote monitoring of atmospheric species from balloons and satellites. Some information can also be deduced from spectra measured at zenith angles less than 90°, for example the mean mixing ratio and the total amount of the species above the altitude of the balloon. The main disadvantage of the limb-scanning technique is that, because the line of sight is near horizontal, a large horizontal scale applies to the measurement.

THE EQUATION OF RADIATIVE TRANSFER

In order to interpret atmospheric emission or absorption spectra, it is necessary to understand how an electromagnetive wave interacts with the atmosphere. The radiative transfer process through the real atmosphere is complex; two assumptions are made to simplify the calculation; (1) scattering is not appreciable, so that only processes of absorption and emission are important; (2) the atmosphere is in local thermodynamic equilibrium.

For a plane parallel non-scattering atmosphere, the transfer equation is (GODY, 1964):

$$dI_\nu = -k_\nu c(I_\nu - B_\nu)\, ds \tag{1}$$

where I_ν is the intensity of the incident radiation per unit frequency interval per unit solid angle, B_ν is the locally defined Planck function, k_ν is the spectral absorption coefficient, c is the density and s is the linear dimension along the ray path.

The solution to equation (1) can be written as:

$$I_\nu(s) = I_\nu(o)\, \tau_\nu(s,o) + \int_o^s B_\nu(s')\, \tau_\nu(s,s')\, k_\nu(s')\, c(s')\, ds' \tag{2}$$

where $\tau_\nu(s,s')$, the fractional transmittance from s' to s, is given by:

$$\tau_\nu(s,s') = \exp - \int_{s'}^{s} k_\nu(s)\, c(s)\, ds \tag{3}$$

The first term on the right hand side of equation (2) represents the radiation from an external atmospheric source I(o) modified by its transmission through the atmosphere by the fractional transmittance $\tau(s,o)$. The second term represents the emission, dI, from elements ds':

$$dI = B(s')\, k_\nu(s')\, c(s')\, ds' \tag{4}$$

but again modified by the fractional transmittance from s' to s.

Taking the derivative of τ along the line of sight, we find:

$$d\tau_\nu(s,s') = -k_\nu(s')\, c(s')\, \tau_\nu(s,s')\, ds \tag{5}$$

hence substituting (5) in equation (2):

$$I_\nu(s) = I_\nu(o)\, \tau_\nu(s,o) + \int_s^o B_\nu(s')\, \frac{d\tau_\nu}{ds}(s,s')\, ds' \tag{6}$$

This is a convenient form of the equation for numerical computation of radiative transfer; the radiation flux at s is simply expressed in terms of τ, the fractional transmittance, and B_ν the Planck function.

The spectral absorption coefficient, k_ν, is the key parameter for calculation of the transmittance function $\tau(s)$. For a single line the absorption coefficient is:

$$k_\nu = Sf(\nu)$$

where s, the line strength, is equal to the integrated absorption coefficient, $S = \int k_\nu d\nu$, and $f(\nu)$ is the line shape function.

The pressure broadened line shape, due to Lorentz, is given by:

$$f(\nu) = \frac{\gamma_L}{\pi} [(\nu - \nu_o)^2 + \gamma_L^2]^{-1}$$

where the halfwidth γ_L is related to the value γ_o at a standard pressure P_o and temperature T_o by:

$$\gamma_L/\gamma_o = (P/P_o) \cdot (T/T_o)^n$$

where n, usually assumed to be -0.5, is not well known; depending on the molecule it could vary between -0.5 and -1.0.

At low pressures (high altitudes) Doppler broadening becomes dominant and the Doppler line shape is given by:

$$f(\nu) = \frac{1}{\gamma_D\sqrt{\pi}} \exp(-(\nu - \nu_i)^2/\gamma_D^2)$$

where γ_D, the Doppler halfwidth, is:

$$\gamma_D = 3.58 \times 10^{-7} \nu_i (T/M)^{1/2}$$

ν_i is the central frequency of the line and M is the molecular weight of the gas at temperature T.

In the middle stratosphere the line shape can be represented by a convolution of Lorentz and Doppler line shapes known as the Voigt line shape. In practice the absorption coefficient at a given frequency is made up from the contributions of the individual lines close by.

We can now go into the details of the two main spectroscopic techniques.

(a) Absorption Spectroscopy

A distant source like the sun or a star has an intensity I(o) much higher than the emission of the atmosphere. Referring to equation (6), the second term on the right hand side can be neglected, hence

$$I(s) = I(o)\, \tau(s,o) \quad . \qquad (7)$$

Therefore the signal-to-noise ratio which can be achieved using absorption spectroscopy is much greater than that which can be achieved using emission spectroscopy. This signal-to-noise advantage can, in classical instruments, be traded for increased spectral resolution in order to isolate absorption features with little or no contamination from other species.

Since this technique requires a hot source at the limb the measurements are restricted to sunrise or sunset when the sun is used as a source, periods which are particularly undesirable for the observation of short-lived photochemically produced species. Measurements using stars as a source are more flexible, permitting observations to be made over an extended period of time. However the intensity of these sources is considerably weaker than the sun, so measurements have been made only in the visible and UV spectral regions where their emission is greatest. These measurements are only made at night to avoid spurious signals from scattered sunlight.

(b) Emission Spectroscopy

Measurements are made against the cold background of space. The first term on the right hand side of equation (6) can now be neglected:

$$I_\nu(s) = \int_{s'}^{s} B_\nu(s,T) \frac{d\tau_\nu}{ds}(s,s')\, ds' \qquad (8)$$

The radiative flux, determined by the Planck function, is reduced by $d\tau/ds$, which is referred to as the weighting function since it "weights" the Planck function along the path of the ray and indicates from where the emitted radiation originates. Figure 2 indicates the weighting functions versus altitude for CO_2.

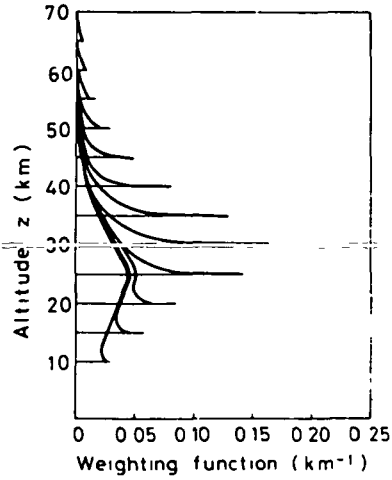

Figure 2. Weighting function of limb sounding; a single spectral CO_2 band has been used (585-705 cm^{-1}) and the different curves correspond to different observational zenith angles (from GILLE and HOUSE, 1971).

This function depends on the concentration and molecular transition strengths of the gas. For the more abundant stratospheric gases, such as ozone and carbon dioxide, this term can approach unity and the observed thermal emission is close to the maximum determined by the Planck function. However, for less abundant species this term is often much less than unity.

Because the radiative flux is determined by the Planck function reduced by a weighting function, the following constraints are imposed on the emission technique:

(1) Limitation of the spectral range to the 10-2000 cm^{-1} where the atmospheric thermal emission is greatest;

(2) The need to know accurately the Planck function and hence atmospheric temperature. This can be a particularly acute problem beyond 1500 cm^{-1} where the Planck function varies rapidly with temperature;

(3) Extremely sensitive instrumentation to detect the low levels of radiation. The instruments are often cooled to keep other sources of radiation to a minimum. Also elaborate baffle systems are required to prevent radiation from the earth entering the instrument when operating in the limb scanning mode.

All these constraints are balanced by the fundamental advantage of this technique not requiring a hot source such as the sun. Therefore, unlike absorption spectroscopy, measurements made using the limb-scanning technique are not restricted to particular times of the day but can be made at any time of day and night and along any compass bearing.

Hence the emission technique is invaluable for making studies of the diurnal variation of stratospheric species concentrations and for studying short lived photo-chemically produced species.

INSTRUMENTATION

(a) General Considerations

We will characterise the performance of instruments designed to measure profiles of minor stratospheric constitutents by two basic criteria which broadly determine the accuracy of the measurement: (1) signal-to-noise ratio, and (2) spectral resolution. These criteria also determine more specific constraints such as instrument weight and ability to work on stratospheric balloon platforms.

Signal-to-noise ratio. The incident flux on the detector, S, is always a linear function of the following parameters:

- L, luminance of the source,
- G, instrumental throughput, equal to the product of the entrance aperture and the field of view,
- T_r, instrumental transmission,
- Δt, integration time for one sample,
- $\Delta\sigma$, spectral interval.

$$S = LGT_r \, \Delta t \, \Delta\sigma$$

The dominant noise can be detector noise (independent of the photon flux) or photon noise.

Until recently the performance of infrared instruments has been limited by detector noise while that of UV and visible instruments is limited by photon noise.

There are two fluxes of radiation incident on the detector:

- F_B is the background flux,
- F_S is the source flux. According to the type of instrument as will be shown in a later section, the source flux can be composed of two components,
- F_{Su} is the signal to be analysed,
- F_{Sp} can be considered as parasitic because it will not be discriminated by the electronics but contributes to the noise (interferometer, grille spectrometer, ...).

In the detector noise limited case:

$$S/N = (F_S + F_B)/I_n$$

while in the photon noise limited case:

$$S/N = (F_{Su} + F_B)/(F_{Su} + F_{Sp} + F_B)^{1/2}$$

Spectral resolution. The natural width of lines in the stratosphere varies with pressure. In the lower stratosphere where the Lorentz profile is predominant, a typical halfwidth lies between 0.005 and 0.01 cm^{-1}. In the upper stratosphere the Doppler profile is predominant. Since the molecular weight of most stratospheric species falls between 20 and 80 then the Doppler halfwidths typically lie between 10^{-3} and 6×10^{-4} cm^{-1} at 1000 cm^{-1}.

The visible and infrared spectral regions are rich in spectral lines. These lines can only be observed with minimum contamination from adjacent lines using an instrument with resolution less than the natural halfwidth of the lines (i.e., $\leq 10^{-3}$ in the upper stratosphere). The only measurements with such a resolution are reported by Menzies (MENZIES, 1979; MENZIES et al., 1981) using a laser heterodyne spectrometer. The resolution of other instruments is generally limited by the technical problems associated with operating them on balloon borne platforms.

Since the spectral resolution can vary from 0.02 cm^{-1} to more than 0.1 cm^{-1} in instruments using absorption techniques and up to several wavenumbers in instruments using emission techniques, the observed spectral features can be very broad with the peak height reduced in proportion due to the convolution of the natural line shape with the instrumental function. In general, as the spectral resolution of the instrument decreases, the contamination of a spectral line by adjacent lines of the same gas or of other gases becomes more of a problem; the inversion process tends to become more prone to errors, needs more spectroscopic data and limits the accuracy of the result (see section on 'method of analysis').

(b) Instruments and Techniques

The instruments described below are divided into two types classified by the relationship between resolution and throughput.

Strong dependence between throughput and resolution. Radiometers and classical grating spectrometers with slits are in this class. Improving the resolution leads to a decrease in throughput and therefore in luminosity.

Filter radiometers, using individual interference filters or circular variable filters with resolution typically equal to 2% of the center wavelength, make measurements integrated over part or whole of a spectral band. In most cases, the radiation is modulated by a chopper. Radiometers measuring atmospheric emission are often cooled to liquid nitrogen temperature in order to achieve the best performance. This technique is only suitable for monitoring species such as ozone, water vapour or nitric acid whose spectral bands are relatively free from contamination by other species.

The main advantages of radiometers are that they are small, have few moving parts and have a good light gathering efficiency.

Although Classical spectrometers used on balloon platforms have given good results for almost 20 years, we will only illustrate the state of the art by two examples.

Solar absorption spectroscopy is carried out by the group from Liege University using the largest grating spectrometer which ever has been flown (ZANDER, 1970).

It consists of a 38 cm aperture telescope and a 2.5 m focal length spectrometer operating in a double pass configuration. The spectral resolution is usually about 0.03 to 0.05 cm^{-1} with signal-to-noise ratios in excess of 100 in the 4000 cm^{-1} region. The weight of the instrument is 300 kg. High quality spectra are obtained with this instrument but the time available for an observation limits the number of species that can be detected during the same occultation.

Emission spectroscopy with an Ebert-Fastie type of grating instrument is performed by the Upper Atmosphere Group from the National Physical Laboratory, England. The resolution at 1000 cm^{-1} is 0.25 cm^{-1}. It covers a spectral region from 600 to 2000 cm^{-1}.

Figure 3 indicates the configuration of the instrument. A telescope focuses radiation on to the input slit of the spectrometer; a large concave mirror then collimates the radiation onto the diffraction grating. The radiation is dispersed into its spectral components by the grating, only a narrow spectral interval of radiation is then focused by the concave mirror onto the output slit and detector optics.

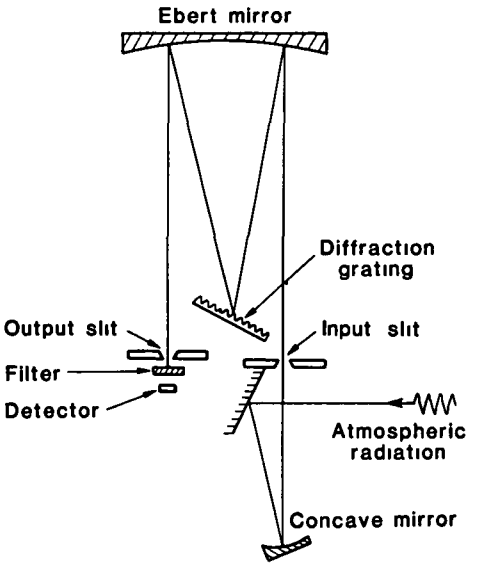

Figure 3. The cooled NPL grating spectrometer for emission measurements in the stratosphere.

Three liquid helium cooled copper doped germanium detectors are used and permit simultaneous spectra of different species to be measured. As the detectors are photon noise limited, all the optical components are cooled to liquid nitrogen temperature. The weight of the instrument is 150 kgs.

Weak dependence between throughput and resolution. The following instruments employ techniques of spectral filtering which eliminate, to first order, the reciprocal relationship between throughput and resolution. These instruments usually have a greater resolution-luminosity product than classical instruments. This can be used to increase the resolution, reduce the sample time (and hence allow more species to be observed) or reduce the size of the instrument. However, since the incident flux on the detector is considerably

greater than in classical spectrometers, these advantages tend to disappear when photon limited detectors are used.

Four examples will be described. The grille spectrometer is a variant of the grating instrument, invented and developed by Girard (GIRARD, 1963). The entrance slit is replaced by a grille which is an array with hyperbolic structure having alternate opaque and transparent bands. The radiation is reflected from the grille (Figure 4) then through a conventional Littrow mounting grating system and finally passes through the grille. It is then filtered to select the order of the grating. The resolution is determined by the narrowest step of the grille while the throughput is determined by the total area of the grille.

A 60 cm focal length grille spectrometer using a 30 cm diameter telescope has been used to make stratospheric absorption measurements from balloon platforms. The resolving power is 20000 and the weight of the instrument is 80 kg.

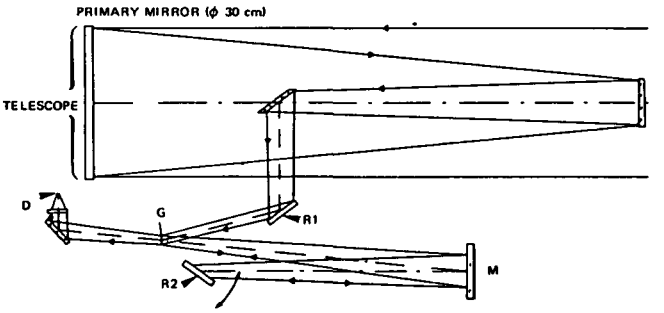

Figure 4. Optical scheme of the ONERA grille spectrometer for solar absorption measurements. M, off axis (F = 600 mm); R_1, predispersing grating; R_2, main grating; G, grille; D, detector.

The Fourier transform interferometer (Figure 5) consists of a beam splitter (for example, germanium coated KCl or KBr), a fixed mirror, a moving mirror and a detector. Incoming radiation is split into two beams, each beam is reflected back to the beam splitter where they recombine and are focused onto the detector. The interferogram, produced at the detector, is obtained by moving one of the mirrors and hence changing the path of one beam relative to the other. Monitoring the path difference is usually performed by counting the fringes when monochromatic radiation from a laser traverses the paths. The fringes can be used to trigger the signal electronics to sample the interferogram. In most modern interferometers "corner-cube" reflectors are used instead of plane mirrors.

The interferometer combines Felgett's Multiplex Advantage (FELGETT, 1958) with the Throughput Advantage of Jacquinot (JACQUINOT, 1958). All spectral elements are analysed simultaneously and the resolution is determined by the maximum optical path difference and is independent of throughput to first order.

The main disadvantage of an interferometer is that a spectrum is not available in real time, the interferogram must be transformed by a computer. A badly sampled point in the interferogram can severely degrade the whole of the transformed spectrum. An interferometer is sensitive to vibration and changes in its operating environment which can displace the mirrors from their true position and therefore distort the interferogram.

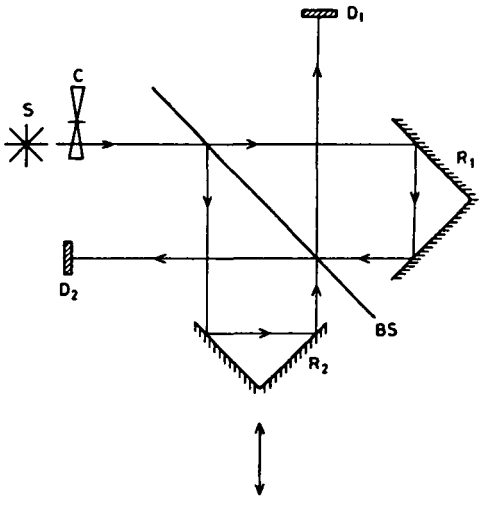

Figure 5. The Michelson interferometer: an example shown without collimation. S, source; C, chopper; BS, beam splitter; D_1 D_2, detectors; R_1 R_2, "roof top" reflectors. The R_2 reflector is moved along the optical axis in order to produce a difference of optical path between the two beams.

When used for limb-scanning absorption spectroscopy the interferogram must be sampled in a short time so as to keep the change in the position of the source to a minimum and therefore obtain the maximum possible height resolution in the measured concentration profile. In the instrument described by FARMER et al. (1980), the interferogram is sampled in 100 s which results in a height resolution varying from 1 km in the upper stratosphere to 4 km in the lower stratosphere.

Several instruments are now currently used from balloon platforms (see SCHINDLER, 1970 and MURCRAY et al., 1981).

Gas correlation instruments use a sample of the constituent itself within a cell to produce a filter sensitive only to those wavelengths corresponding to molecular transitions of the gas. The spectral bandwidth is comparable with the line width of the gas, typically 10^{-3} cm^{-1}, giving a resolving power of 10^6 in the infrared, quite independent of throughput. In practice radiation is collected from many lines and therefore the energy falling on the detector is considerably greater than in most high resolution instruments.

One practical example of this technique, the pressure modulator radiometer, has been developed for atmospheric remote sensing by Houghton and colleagues at Oxford University (TAYLOR et al., 1972). The principle of operation can be understood by referring to Figure 6. A cell is placed between the collecting and detector optics; the pressure of gas within the cell is modulated by a piston at frequency f. If the maximum and minimum pressures within the cell are P_2 and P_1 respectively, then the transmission through the cell in the region of the spectral line at these two pressures varies between τ_2 and τ_1 which leads to a modulated signal at frequency f proportional to the difference between τ_2 and τ_1 (Figure 7). Operating the cell at a high mean pressure makes the instrument suitable for studying gases with strong pressure broadened lines where information concerning the profile is contained within the wings.

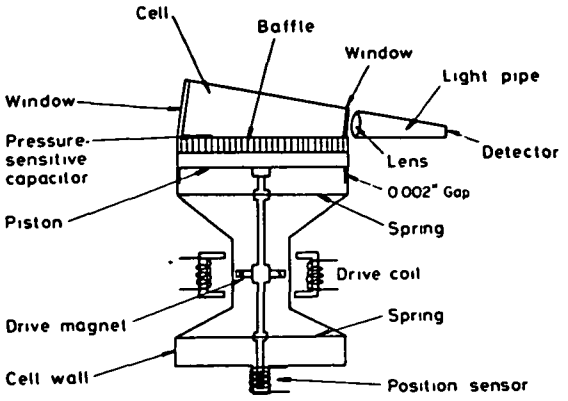

Figure 6. The pressure modulator radiometer used by the Clarendon Laboratory (from HOUGHTON et al., 1971). Radiation traverses the cell before being focused onto the detector. Pressure modulation is effected by a resonant piston driven electromagnetically.

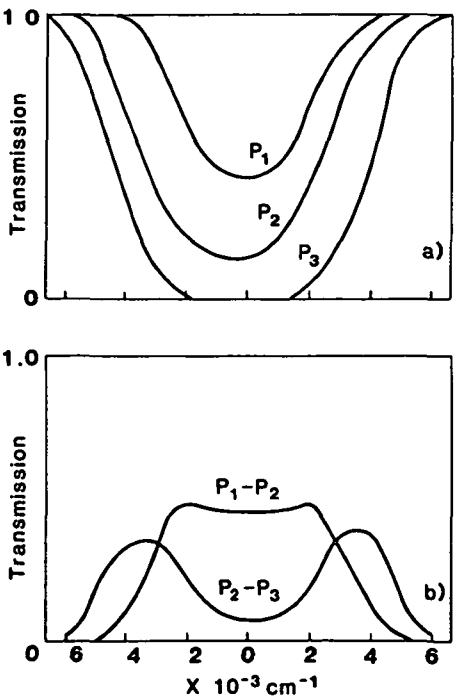

Figure 7. Illustration of the principle of the PMR instrument. a) Spectral line transmission at pressures P_1, P_2, P_3. b) Cell transmittance. Modulation between pressures P_1 and P_2 leads to the P_1-P_2 transmittance curve. Modulation between pressures P_2 and P_3 leads to the P_2-P_3 curve.

Despite the large resolving power and light collecting efficiency, a pressure modulator radiometer can be mechanically simple and robust. The problem with such an instrument is in the containment of gases in the cell for long periods without deterioration; many gases of atmospheric interest are extremely unstable, corrosive or both.

Laser heterodyne radiometer. Infrared heterodyne detection is achieved by allowing radiation from a coherent local oscillator (frequency ν_1) and from a source (frequency ν_2) to illuminate a square law detector (photomixer). The heterodyne signal has a frequency $\nu_1 - \nu_2$. It is passed through a radio frequency filter of bandwidth B then through a second square law detector and time averaged (MUMMA et al., 1978).

Recent developments in high speed infrared detectors and in tunable lasers make infrared spectroscopy very attractive to achieve high spectral resolution ($0.001\ cm^{-1}$) and so completely resolve the profile of a spectral line.

The heterodyne technique eliminates the effect of detector and background radiation noise but at the expense of having to operate with large bandwidths and narrow fields of view.

This technique is limited by the availability of suitable local oscillators, so that only selected spectral intervals can be studied.

Technical difficulties are still limiting balloon borne applications. Nevertheless ClO results have been obtained by solar spectroscopy (MENZIES et al., 1981) and have recently been reevaluated using improved spectroscopic data (MENZIES, 1983).

METHOD OF ANALYSIS

When a set of atmospheric spectra is obtained, either by an emission or by an absorption technique, the task remains of "inverting" the results to get an altitude concentration profile for the species of interest. This means that, from equation (6) which expresses radiation as a function of atmospheric state, one has to express the atmospheric state in terms of that radiation.

The solution to such a problem is not unique since in practice there are only a finite number of observations and also, because there is noise in all physical measurements. Therefore the problem is one of estimation, finding the appropriate criteria which determines the best solution from all possible ones which are consistent with the observations. The problem can be expresed mathematically in the following way; let us assume that the spectroradiometer has measured several atmospheric radiances R(i); these may be measurements at several zenith angles or at a constant zenith angle and at several altitudes. We want to find the concentration profile, C_j, so that the calculated radiance $R_i(C_j)$ is in agreement with the measured radiance to within some constant factor; mathematically we need to minimize

$$F(\overline{R} - R(C(z)))$$

subject to certain constraints on C_j. The function F in a simple form is the sum of the squares.

(a) Calculation of the Radiances

Practically the calculation of the radiances, R(i), is made by dividing the atmosphere into homogeneous layers.

For absorption spectra the transmission function $\tau(\nu)$ is usually computed line by line using the expression;

$$\tau(\nu) = \exp - \int_{P_1}^{P_2} ds \sum_j C_j \sum_i k_{ijn}$$

n, j, and i respectively refer to the number of layers, absorbing species and lines of each species, s is the optical length in each layer and k_{ijn} is the absorption coefficient.

The starting point is the calculation of the monochromatic absorption coefficient which requires data on the individual vibration-rotation lines of atmospheric molecules. Several groups have collected data for the atmospheric species (ROTHMAN et al., 1983; HUSSON et al., 1982). They are very useful tools, but work has still to be done in several cases to improve the precision.

The way the atmosphere is divided into layers influences the precision of the results. Thin layers (say 1 km thick) will lead to the best approximation but introduce more steps into the calculation. A compromise has to be found between precision and calculation time.

(1) Layers may be simply defined by choosing boundaries corresponding to the tangent heights of the observations.

(2) In the FSCDATM program of AFGL (CLOUGH et al., 1982), the selection of the boundaries is determined by an acceptable line width differential through the layer, the variation of the mean line width staying lower than a factor of two from one layer to the next.

(3) Mankin's method (MANKIN, 1979) uses an isothermal layer in which both the pressure and absorber concentrations vary along the line of sight.

In all cases, the average pressure and temperature are defined by the Curtis-Godson approximation in each layer,

$$\overline{P} = \int P dm / \int dm \qquad \overline{T} = \int T \, dm / \int dm$$

where dm is the differential air mass.

The calculation of the optical path in each layer must include refraction by the atmosphere at large zenith angles (tangent altitude lower than 25 km (SNIDER, 1975)).

Instrumental effects, such as apodization and phase distortion, have to be included. Usually the calculated radiances are finally convolved with the instrumental function.

An original algorithm has been developed by MANKIN (1979) for calculating transmittances by Fourier transforms of the absorption coefficients which greatly reduces the time required to generate synthetic spectra.

For solar absorption spectroscopy the intensity of the source $I_o(\nu)$ is, in some spectral intervals, severely contaminated by absorption lines in the solar spectrum; one has to simulate correctly this absorption (see GOLDMAN et al., 1973). Spectra obtained from high altitudes and low zenith angles can be used as a reference. To simulate these spectra one single layer of CO at 4500 K and a Doppler line shape can be used with good approximation. A sophisticated solar model (MULLER and SAUVAL, 1975) can obviously be used.

For emission spectra, which are usually measured with low resolution, line by line calculations over large spectral intervals can be very costly on computer time. So it has proved desirable to develop techniques for averaging over the finest structure. A few line spacings is a sufficient range of averaging to smooth out lines without destroying the band contour. This leads to the idea of a band model.

In a band model the lines within a band are replaced by an infinite array of lines of uniform statistical properties. An interval of this array is taken to have similar properties to those of an interval of the band under consideration. The best known model for dealing with bands of asymmetric top models is due to GOODY (1964); the mean transmittance, $\bar{\tau}$, in any spectral interval $\Delta\nu$ is given by,

$$\bar{\tau} = \exp - \frac{\bar{s}}{d} u \left(1 + \frac{s}{\gamma} \frac{\mu}{\pi p}\right)^{-1/2}$$

where (s/d) is the mean value of the integrated absorption strengths in $\Delta\nu$, S, divided by the mean line spacing d, γ is the mean width, u the absorber amount and p the pressure. The Goody model assumes that the lines are pressure broadened, although corrections to the band model for Doppler effects have been considered by GILLE and ELLINGSEN (1968).

To simplify the evaluation of the radiative transfer equation along a path through an inhomogeneous atmosphere, the Curtis-Godson approximation is used to represent the mean atmosphere.

From equation (8),

$$R(s) = \int_{\nu_1}^{\nu_2} \int_{s'}^{s} B \frac{d\tau}{ds}(s,s')\, ds' d\nu$$

If the frequency interval, $\Delta\nu = \nu_1 - \nu_2$, is small, then the Planck function can be replaced by an average value $B(\bar{T},s')$. Therefore,

$$R(s) = \int_{s'}^{s} B(s') \int_{\nu_1}^{\nu_2} \frac{d\bar{\tau}}{ds}(s,s')\, ds' d\nu$$

where B(s') is the mean Planck function evaluated at the n^{th} step and $\bar{\tau}$ is the mean transmittance from the observer up to and including the n^{th} step. The atmospheric radiance can now be calculated rapidly using a band model to evaluate τ_n.

More sophisticated methods of evaluating the atmospheric radiance have been developed, some such as Lowtran (SELBY et al., 1976) use an empirical model while others use multiparameter analytical methods to perform the calculation.

(b) *Inversion Process*

The radiative transfer function, deduced from equation (6) by integrating over the frequency range ν_1 to ν_2 is a nonlinear function of the concentration profile c(z). To simplify the calculation, the function R(c) can be expanded as a Taylor series about a guessed value, c_g, of the solution:

$$R(c) = R(c_g) + \frac{\partial R}{\partial c}(c - c_g) + \frac{\partial^2 R}{\partial c^2} \frac{(c - c_g)^2}{2} \ldots$$

If the second and higher order terms are ignored, then a set of linear equations in c remain. Linear matrix techniques can then be used to determine c(z). The procedure can be iterated to obtain the optimum values for c(z).

It is not always necessary to perform a matrix inversion since it is possible to solve the equations sequentially as in the "onion peeling" technique, which will serve to illustrate a simple inversion algorithm. With reference to Figure 8, the values R correspond to the atmospheric radiances measured at zenith angles $\theta(\theta > 90°)$; the atmosphere is divided into shells whose boundaries are defined by the tangent heights at each zenith angle. An initial guess is made at the concentration, c, in the outermost shell, S, from which $R(c_j)$ is calculated. The calculation is iterated until,

$$R - R(c_j) \leq \varepsilon$$

where ε is a constant comparable with the experimental error in R. Knowing the amount in the first shell, the amount in the second shell is determined and so on down to the lowest layer. It may not be apparent that any constraint has been put on C_j; in fact, we have constrained c_j by assuming that the values are constant within each shell. Care has to be taken when inverting noisy data since it often increases the effect of noise by propagating it downwards. For example, if there is a positive error in R_i, then the value c_i will be overestimated resulting in an underestimation in shell $i + 1$, irrespective of the noise there.

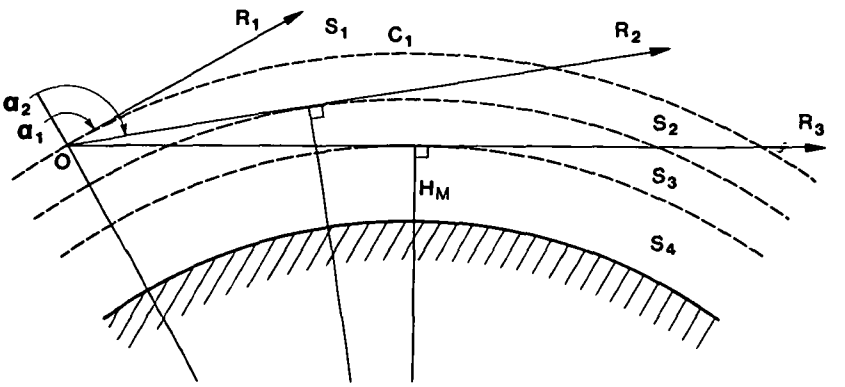

Figure 8. Geometry of a limb remote sensing experiment. H_M, altitude of the tangent ray; R_1 R_2 R_3, direction of observation; a_1, a_2, zenith angle; S_1 S_2 S_3 S_4, different layers in the atmosphere with respectively C_1 C_2 C_3 C_4 concentration for gases.

In order to avoid this drawback, Mill has suggested a method for limb inversions which is the reverse of the onion peeling method (MILL, 1977), the procedures being performed from the lowest to the highest levels. In general, since the emission or absorption profiles decrease with altitude the data with the highest signal-to-noise ratio is given in preference, making this method suitable for the inversion of noisy spectra.

Some other examples and numerical solutions are given in references GOLDMAN and SAUNDERS, 1979; NIPLE et al., 1980; WANG and GOULAG, 1975.

RESULTS

Remote sensing of diatomic species, like HCl, HF, CO and NO is usually

performed with the absorption technique since the fundamental 1-0 transitions are located in the near infrared ($\lambda < 5.5$ microns) where the blackbody emission is too small to be detected using current emission techniques (Figure 1). Other species have often been measured by both techniques. Only recent results obtained by remote sensing from balloons are discussed.

(a) HCl and ClO

The 1-0 band of HCl consists of regularly spaced pairs of lines due to ^{35}Cl and ^{37}Cl between 2700 and 3000 cm^{-1} with the center at 2905 cm^{-1}. A complete analysis of this region has been made by FARMER et al. (1976). Using the AFGL line listing supported by extensive laboratory measurements on CH_4, Farmer pointed out that under stratospheric conditions several lines appear to be uncontaminated:

R_1, R_2, R_3, P_5, P_6 for $H^{35}Cl$

R_1, R_2, R_3 for $H^{37}Cl$

The R_1 and R_2 lines of HCl have been used exclusively where the published profiles have been derived from observations of individual lines. The PMR technique has been used by EYRE and ROSCOE (1977), to measure the solar absorption by all the lines in the band. In all cases the spectroscopic data of TOTH et al. (1970) have been used.

A compilation by RAPER (1977) has discussed the various results, pointing out some discrepancies even when measurements were made at the same latitude. (See ACKERMAN et al., 1976; WILLIAMS et al., 1976a; EYRE and ROSCOE, 1977.)

More recent observations are now available. Measurements of the latitude distribution of HCl have been made by MANKIN and COFFEY (1983) and GIRARD et al. (1982) from aircraft flying at 10-12 km. The total column exhibits a minimum close to the equator with an increase of approximately 1.5 between 0° and 30° and 1.8 between 30° and 60° latitude. Therefore only profiles measured at the same latitude can be compared.

Recent HCl balloon observations are shown in Figure 9. They all indicate a continuous increase from 20 to 40 km with a volume mixing ratio greater than 10^{-9} above 30 km. Although these profiles have been obtained at different latitudes (from 30° to 65°) they do not clearly show the latitude variation mentioned above for the total column. More precision is still needed to make a valuable conclusion.

The ClO fundamental vibration-rotation band is located near 850 cm^{-1}. The low ClO concentration in the middle stratosphere and the low strength of the band make it difficult to measure by current spectroscopic techniques. ClO features in the atmospheric spectrum can only be isolated using high resolution spectroscopy and consequently the line positions must be known accurately.

Recent laboratory measurements by Maki (MAKI et al., 1982) have been made with an accuracy of 2×10^{-3} cm^{-1} which have allowed the solar balloon heterodyne spectra obtained in 1979 by MENZIES (1983) to be interpreted. The band intensity comes from MARGOLIS et al. (1978). Identification of ClO is made difficult because the spectral region also contains weak lines of NO_2 and O_3.

The observations and altitude profiles (Figure 10) were made during sunset and are compared with the results of a photochemical model.

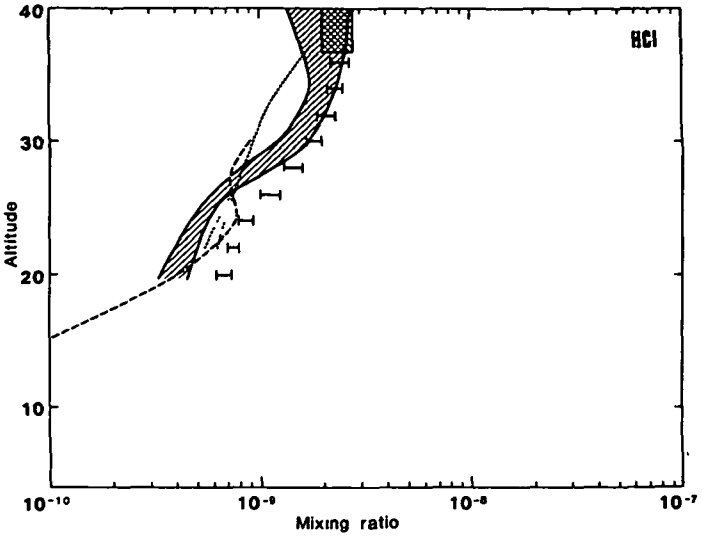

		Latitude	Resolution cm^{-1}	Flight	Altitude km
⊢⊣	LOUISNARD et al. (1983) Gr. Gr. Spectrometer	44°N	0.2	May 1982	39.2
▨	ZANDER et al. (1981b) Gr. Spectrometer	31°N	0.09	Oct. 1978 Sept. 1979	30.3 36.8
.....	FARMER et al. (1980) Interferometer	31°N 30°S	0.13	May 1976 Mar. 1977	37 39
——	BUIJS et al. (1980) Interferometer	65°N	0.05	May 1976	30.1

Figure 9. HCl profiles (3.4 μ).

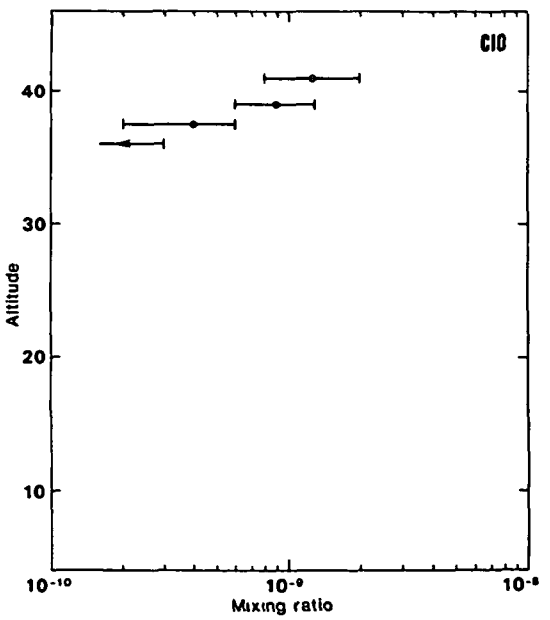

Figure 10. ClO profile obtained at sunset near 11.0 μ with a laser heterodyne spectrometer with 0.001 cm^{-1} resolution (MENZIES, 1983).

This result illustrates the possibility of making very high resolution spectroscopic measurements of the atmosphere from balloon borne platforms.

(b) HF

The fundamental band of HF is centered at 4005 cm^{-1}. The main absorption features in this spectral region come from H_2O, however solar CO lines are also present. ZANDER et al. (1977) concludes that the R_1 line at 4038.975 cm^{-1} is the most suitable for measuring the HF concentration since it is the strongest line at stratospheric temperature not obscured by any other absorption feature. Nevertheless, the P_1 line at 4000.99 cm^{-1} can also be used if the instrumental resolution is sufficient to isolate the HF line from the water vapour and solar CO lines. All the published HF concentration profiles due to remote sensing in the IR come from an analysis of either one of these two lines. However the lines at 3877.71, 3920.32 and 3833.68 cm^{-1} have beeen considered.

Because of the importance of HF and HCl in the CFM problem and because the HF/HCl ratio provides information on the ratio of natural and anthropogenic sources of atmospheric Cl and F, these two gases are often measured simultaneously. The latitudinal variation of these two gases exhibits the same trend (MANKIN and COFFEY, 1983; GIRARD et al., 1982).

Zander first detected HF above 27.5 km in 1975; further results have now been obtained with the same instrument. The spectral data used by Zander in the analysis of the R_1 line is due to CONNES et al. (1967). The results are presented as a mean mixing ratio above the measurement altitude; they clearly show an increase in HF concentration from 1976 to 1979.

BULJS et al. (1980), during a flight over Alaska, measured the HF column density with a precision of ±25%. The volume mixing ratio profile which they obtain has an error of ±50% near 30 km and ±10% below 25 km.

From a large set of spectra obtained during sunset, FARMER et al. (1980) deduce an HF mixing ratio profile showing an increase with altitude with an uncertainty of about ±20%. Spectral parameters are due to Goldman (GOLDMAN et al., 1974).

These profiles are shown in Figure 11. Although the 65°N profile appears distinctly higher than the profile measured at 30°N, in good agreement with the predicted latitudinal variation, the total column measured by Zander et al. is contradictory to this latitude variation. More measurements are still needed to draw a conclusion on the variability of the results.

(c) Freons 11 and 12

Chlorofluoromethanes have been extensively measured by in-situ sampling techniques. These species can be detected in the lower stratosphere by remote sensing techniques. However, the concentration profiles which are deduced are less accurate than those measured by in-situ techniques due to the lack of spectroscopic data.

Absorption features due to CFM 11 and CFM 12 at 10.8 and 11.8 microns, respectively, were first observed in solar occultation measurements from a balloon by WILLIAMS et al. (1976b). These features are very weak at stratospheric altitudes due to the rapid decrease of CFM density above the tropopause resulting from photolysis. The profiles of CFM 11 and CFM 12 measured by Williams and coworkers are shown in Figures 12 and 13. Also shown are profiles determined by POLLITT et al. (1979) using emission spectroscopy.

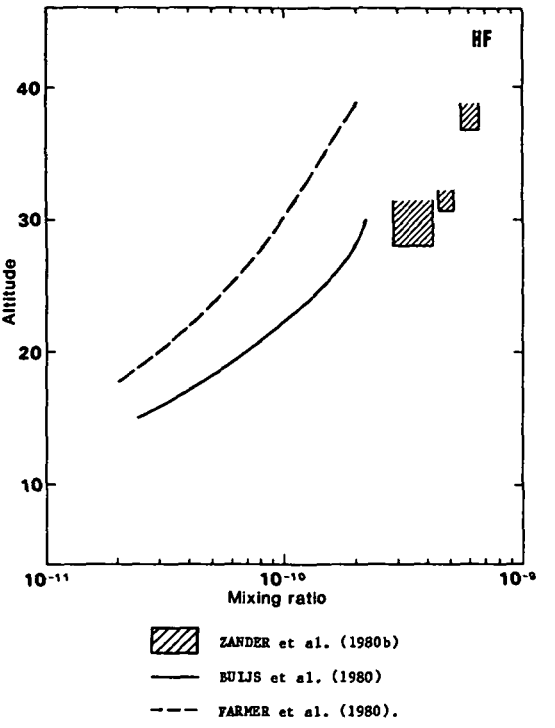

Figure 11. HF profiles. Characteristics of the flights (2.5 μ) are the same as for HCl, Figure 9.

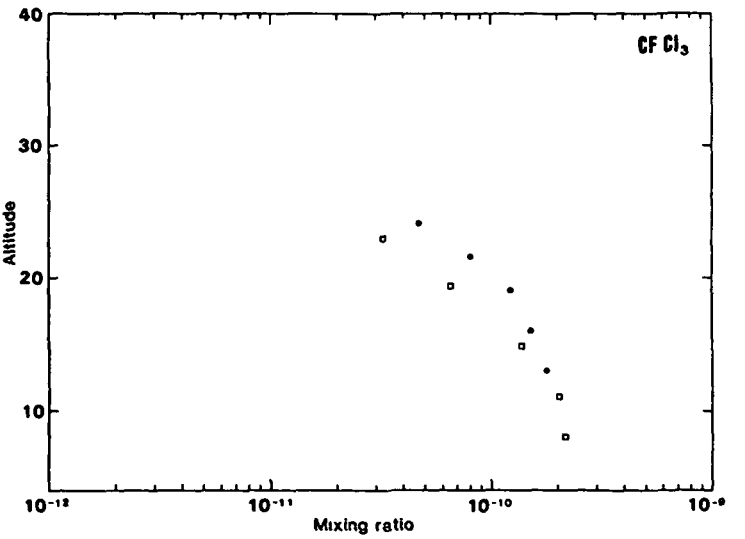

Figure 12. $CFCl_3$ profiles at 32°N.

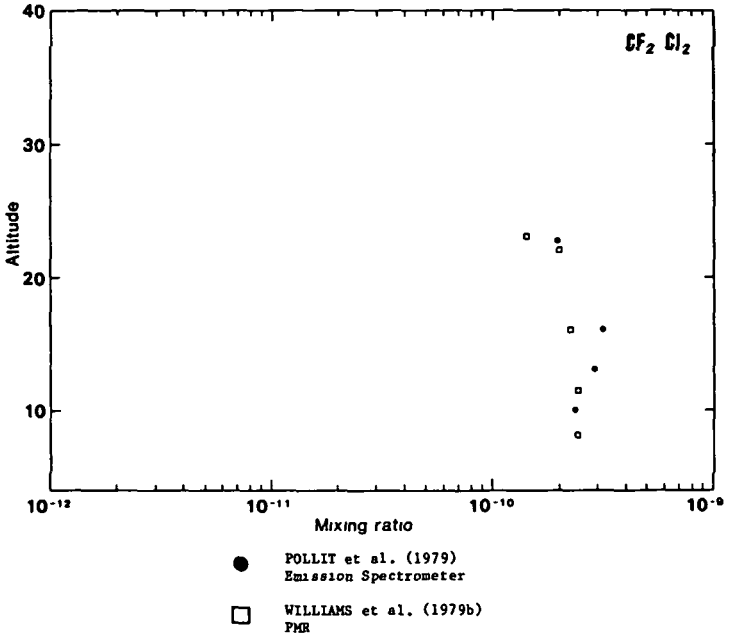

Figure 13. $CFCl_2$ profiles at 32°N.

(d) NO and NO_2

Using solar occultation techniques to determine the concentration of such short-lived photochemically produced species is open to question. The variation of sunlight during the occultation period introduces ambiguities in interpreting the measured absorption in terms of meaningful atmospheric abundances.

Calculation of the photolysis rates for a spherical atmosphere (equinox, 45° latitude) with a simple scattering approximation has been made by BOUGHNER et al. (1980). They conclude that sunset NO measurements below 30 km have to be corrected for variations in twilight. However, the correction is highly dependent on the photochemical model used. Therefore, remote absorption measurements of NO and NO_2 are often suspect, especially in the lower stratosphere. For these reasons, remote sensing measurements of NO are coupled with NO_2 measurements in order to get a good estimate of the NO + NO_2 profile.

The 1-0 fundamental band of NO, located at 1876 cm^{-1}, is difficult to measure using emission techniques because the energy radiated from this part of the spectrum is very weak. However, a PMR instrument using this technique has measured NO successfully (DRUMMOND and JARNOT, 1978; ROSCOE et al., 1981). Although the accuracy of these measurements is relatively low they clearly show the diurnal variation of NO and NO_2.

Two other sets of NO and NO_2 results have been obtained using the solar occultation technique in the same spectral region and using the same spectroscopic data (AFGL, ROTHMAN et al., 1978).

In preliminary work, MURCRAY et al. (1980) show only NO column densities while NIPLE et al. (1980) obtained a profile. A more complete analysis has been made by BLATHERWICK et al. (1980) which included a simplified photochemical model. The NO and NO_2 profiles are shown in Figures 14 and 15, respectively. The photochemical correction, quite negligible for NO_2, becomes important for NO below 25 km and reaches a factor of 2 around 21 km.

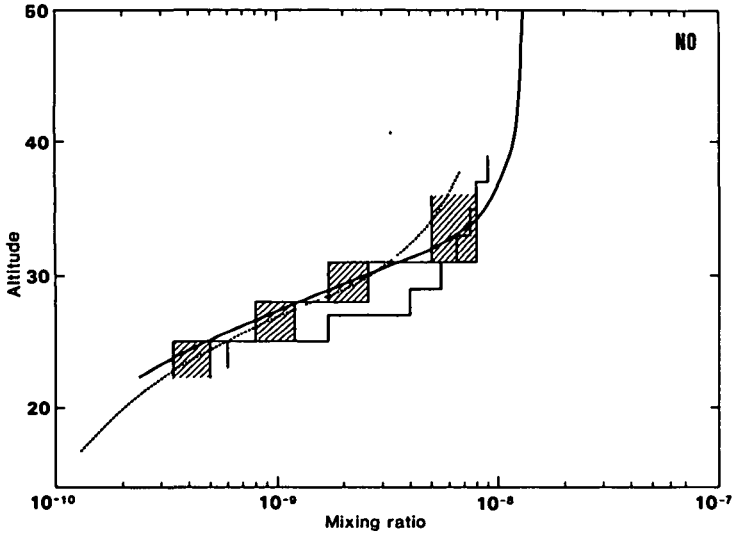

		Flight	Altitude km
..... BLATHERWICK et al. (1980) Interferometer	sunset	Oct. 1979	33
LOUISNARD et al. (1983) Gr. Gr. Spectrometer	sunset	Sept. 1980	40
LOUISNARD et al. (8-5-1982)	sunrise	May 1982	39.2
—— DRUMMOND and JARNOT (1978) PMR	day	June 1975	38

Figure 14. NO profiles (5.3 μ)

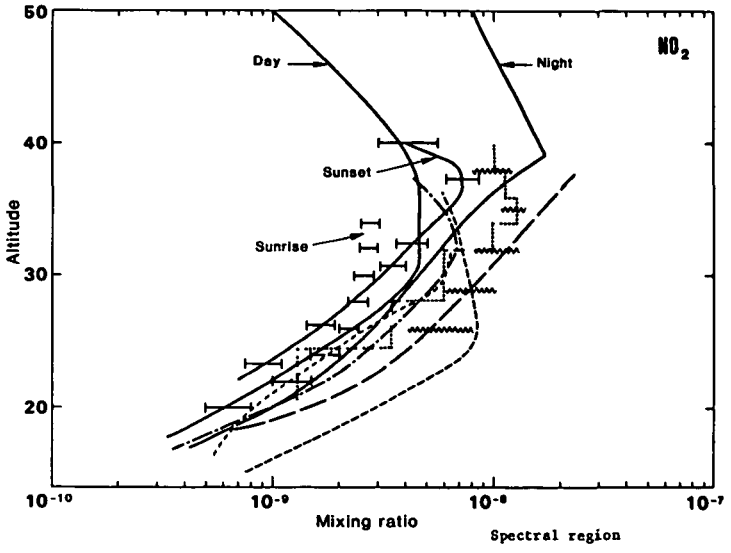

			Spectral region
——	DRUMMOND and JARNOT (1978) PMR	day night	6.2 μ
·	GOLDMAN et al. (1978)	sunset	450 nm
—|—	LOUISNARD et al. (8-5 1982)	sunrise	6.2 μ
—/—	LOUISNARD et al. (1983)	sunset	6.2 μ
—·—	BLATHERWICK et al. (1980)	sunset	6.2 μ
----	OGAWA et al. (1981)	sunset	450 nm
~~	NAUDET et al. (1984)	night	450 nm
— —	KENDALL and BUIJS (1983)	sunset	3.5 μ
▬▬	EVANS et al. (1981)	sunset	450 nm

Figure 15. NO_2 profiles.

From a more recent balloon flight, LOUISNARD et al. (1983) have obtained profiles which do not include any photochemical correction. The profiles which are shown in Figures 14 and 15 assume that the mixing ratios remain constant as the solar zenith angle varies. They observe a discrepancy below 30 km in the NO mixing ratio profiles measured at sunrise and sunset while the discrepancy appears above 30 km in the NO_2 profiles. In both cases the total column is lower at sunrise than at sunset in agreement with the total column measurements by LAURENT et al. (1981) from a plane.

Also in the infrared, the weak $\nu_1 + \nu_2$ band of NO_2 has been observed by KENDALL and BUIJS (1983) using a high resolution (0.02 cm^{-1}) interferometer.

NO_2 has also been measured by the solar occultation technique in the visible near 450 nm. In this spectral region numerous Fraunhofer lines appear and also corrections for Rayleigh scattering and absorption due to O_3 and H_2O have to be included in the analysis. Profiles have been obtained by GOLDMAN et al. (1978), OGAWA et al. (1981) and EVANS et al. (1982). Observations of the diurnal variation in the NO_2 total column have been made by POMMEREAU (1982) but have not been confirmed by other experiments.

The original technique of NAUDET et al. (1984) uses a star at the limb to make atmospheric absorption measurements of NO_2 at night. By using a star as the source instead of the sun not only is the spectral contamination due to solar lines removed but also errors in the measurement due to the rapid variation of NO_2 at sunrise and sunset. The concentration of NO_2 measured by Naudet (Figure 15) is clearly greater than the results obtained by other workers even though there is a large variation in the measurements.

(e) N_2O_5

This species has a complex vibration-rotation band centered at 1247 cm^{-1}, the density of lines within the band is so great that they cannot be resolved and therefore appear as a continuum. Under stratospheric conditions the band is severely contaminated by N_2O and CH_4 making spectroscopic detection very difficult.

MURCRAY et al. (1978) has looked for N_2O_5 in the 8.1 micron region of emission spectra without a positive identification and hence gives an upper limit of 1.2×10^{15} cm^{-2} above 18 km. EVANS et al. (1978) have a tentative identification of N_2O_5 a few hours after sunset; they obtain 2 ppb at 30 km. ROSCOE (1982), using a gas cell of CH_4 as a filter, has observed an "N_2O_5-like" substance having the same day-night variation which the models predict for N_2O_5.

(f) $ClONO_2$

Although $ClONO_2$ has absorption bands in the infrared at 780.2, 1292 and 1730 cm^{-1} it is very difficult to detect because these bands are contaminated by strong absorption features of other stratospheric gases such as CH_4, N_2O, CO_2 and O_3. The density of lines within the Q-branches is so great that even at a resolution of 0.01 cm^{-1} no structure can be resolved.

The only observation of $ClONO_2$ has been made by MURCRAY et al. (1979) using an interferometer with a resolution of 0.02 cm^{-1}. They obtain a mixing ratio of 0.9 ± 0.2 ppbv at 30 km although interference by other species makes interpretation of their spectral data extremely difficult.

(g) NO_3

The only balloon measurement of NO_3 has been made by RIGAUD et al. (1983) using visible spectroscopy of the 661 nm absorption feature. The measurement was made at night using the occultation technique with a bright star (Venus, Arcturus) as a source. From a balloon borne platform at 38.8 km they were able to measure, with good accuracy, the profile of NO_3 from 30 to 40 km, the region where the concentration is a maximum. The profile is shown in Figure 16. Ozone was also measured simultaneously to assist in the interpretation of the data.

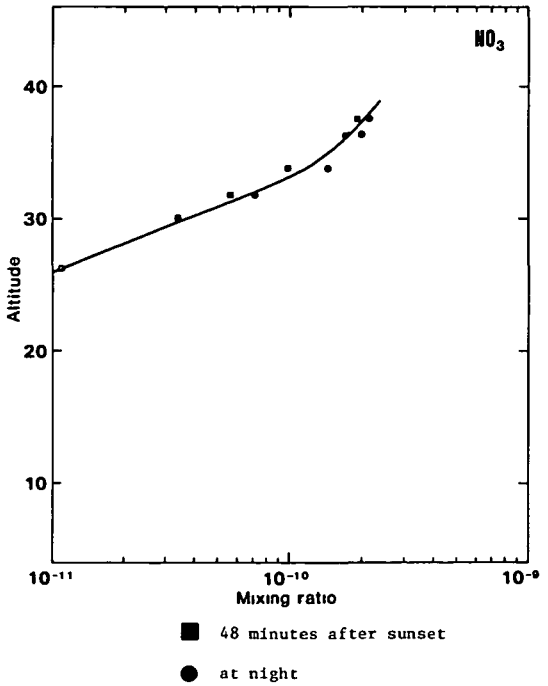

Figure 16. NO_3 profile obtained near 660 nm by RIGAUD et al. (1983)

(h) Nitric Acid

Nitric acid has strong vibration-rotation bands at 5.9, 7.5 and 11.3 microns; individual lines within the bands can be resolved only with high resolution spectroscopic techniques. GOLDMAN et al. (1971, 1981) have determined the statistical band model parameters for the three IR bands and BROCKMAN et al. (1978) have measured the positions and strengths of over 1000 lines in a part of the 11.3 micron band. However, the lack of spectroscopic data, especially the temperature dependence of the absorption coefficients, makes analysis very difficult.

The 11.3 micron band is relatively free from contamination by other species and therefore low resolution spectroscopic and radiometric observations in this band allows stratospheric nitric acid concentrations to be determined (POLLITT et al., 1979; EVANS et al., 1982; FISCHER et al., 1980). Contamination from the wings of the Freon 11 and Freon 12 bands centered at 10.8 and 11.8 microns becomes significant in the lower stratosphere.

The other bands of nitric acid are contaminated by features due to H_2O, CH_4 and N_2O. The Q-branch at 1326 cm^{-1} can be resolved with medium resolution spectrometers and has been used to determine nitric acid concentrations (LOUISNARD, 1983).

Since nitric acid is a relatively long-lived species, dynamics play a significant role in its distribution in the lower stratosphere, both with latitude and altitude. Latitude surveys of the total column of nitric acid have been made from aircraft by MURCRAY et al. (1975), GIRARD et al. (1982) and COFFEY et al. (1981). All these results show a minimum in total nitric acide at the equator rising by an order of magnitude towards the poles.

Recent measurements of nitric acid, made both in emission and absorption, are shown in Figure 17. Although all but one of these profiles were measured at the same latitude it is not possible to determine how much of the scatter is due to natural variability rather than measurement error.

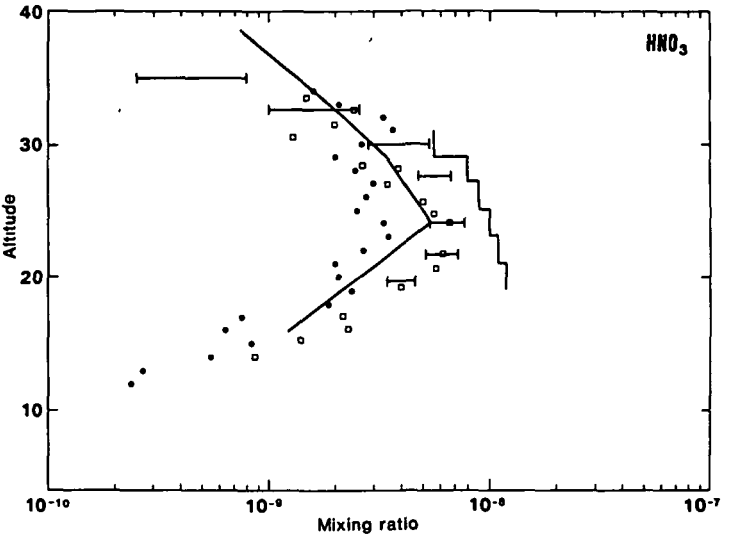

		Latitude	Resolution cm^{-1}	Spectral region
⊢⊣	POLLITT et al. (1979) Emission Spectrometer	32°N	0.25	11.5 μ
⌐¬	LOUISNARD et al. (1983) Absorption Spectrometer	44°N	0.09	7.5 μ
——	GOLDMAN et al. (1980) Absorption Interferometer	32°N	0.02	5.8 μ
●	EVANS et al. (1982) Emission Radiometer	32°N		11.3 μ
□	FISCHER et al. (1980) Emission Radiometer	32°N		11.3 μ

Figure 17. HNO_3 profiles.

(i) CO

The 1-0 fundamental transition of CO is centered at 2143 cm^{-1}. Ozone ($\nu_1 + \nu_3$) and nitrous oxide also have strong absorption bands in this spectral region; weak absorption features due to water vapour and CO_2 are present. However, the greatest difficulty in using absorption spectroscopy to measure CO concentration arises from the solar photsphere; a significant fraction of the equivalent width of each line is due to solar CO (see earlier section). The telluric absorption by CO can be obtained from spectra measured at high altitudes and small zenith angles where the atmosphere mass path is very small.

Several lines (R_0, R_2, R_5, P_1 and P_2) have been analysed by a number of experimenters using spectroscopic data from the AFGL compilation. The most recent results are summarized in Figure 18.

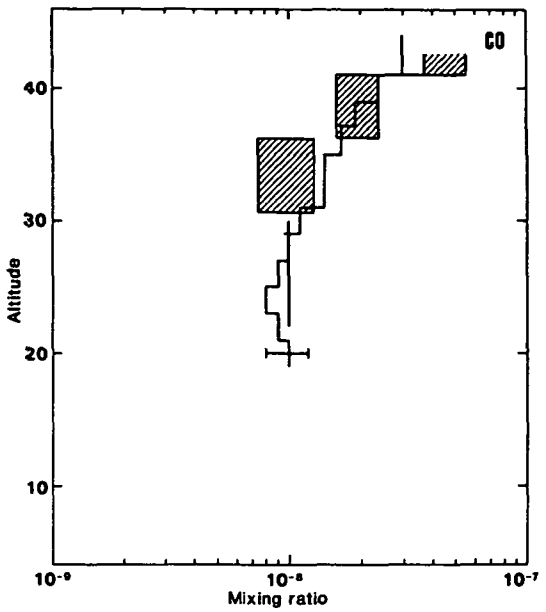

	Latitude	Resolution cm^{-1}	Flight	Altitude km
FARMER et al. (1980)	31°N	0.13	May 1976	37
LOUISNARD and LADO-BORDOWSKY (1983)	44°N	0.12	Sept. 1980	40
ZANDER et al. (1981a)	31°N	0.04	Oct. 1978 Sept. 1979	30.3 36.3

Figure 18. CO profiles (4.6 μ).

FARMER's (1980) result shows a constant volume mixing ratio of 1×10^{-8} between 21 and 30 km with uncertainties of $\pm 0.2 \times 10^{-8}$ at the lower altitude and $\pm 0.5 \times 10^{-8}$ at the upper bound.

ZANDER (1981a) using only zenith angles less than 90°, has deduced values of the mean mixing ratio above the balloon altitude: $2.1 \pm 0.3 \times 10^{-8}$ above 30.6 km and $3.7 \pm 0.4 \times 10^{-8}$ above 36.8 km.

From a balloon at 40 km and using the limbscanning technique, LOUISNARD and LADO (1983) have measured CO profiles between 20 and 40 km. A minimum in the CO mixing ratio is observed around 22-25 km followed by an increase with altitude.

There is general agreement between these three results within the quoted errors.

(j) Methane and Nitrous Oxide

CH_4 and N_2O, with volume mixing ratios close to 10^{-6} and 10^{-7}, respectively, have been measured extensively by cryogenic sampling techniques with good accuracy. Although strong absorption features appear in numerous spectral regions the accuracy which can be obtained by remote sensing is limited by the uncertainties in the spectroscopic data; the precision of remote sensing techniques is still lower than the precision of in-situ techniques. Nevertheless, profiles of CH_4 and N_2O have been measured using solar occultation spectroscopy and are presented in Figures 19 and 20, respectively.

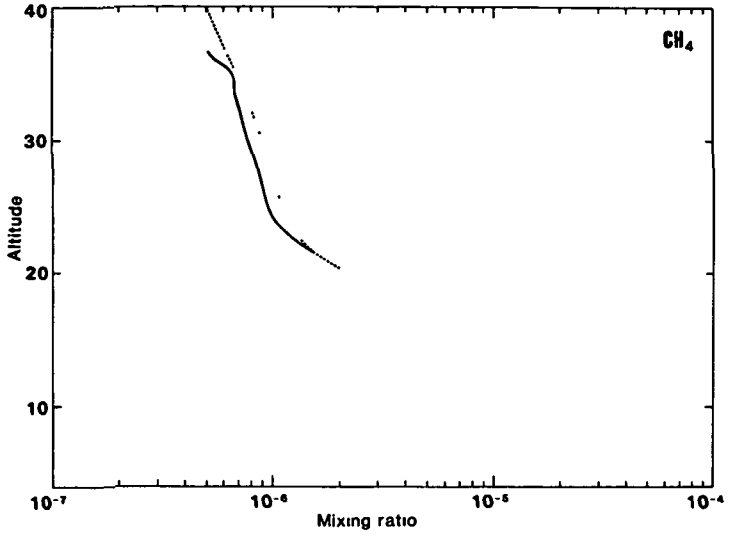

		Latitude	Spectral region
·····	LOUISNARD et al. (1983)	44°N	7.5 μ
——	FARMER et al. (1980)	31°N	3.8 μ

Figure 19. CH_4 profiles.

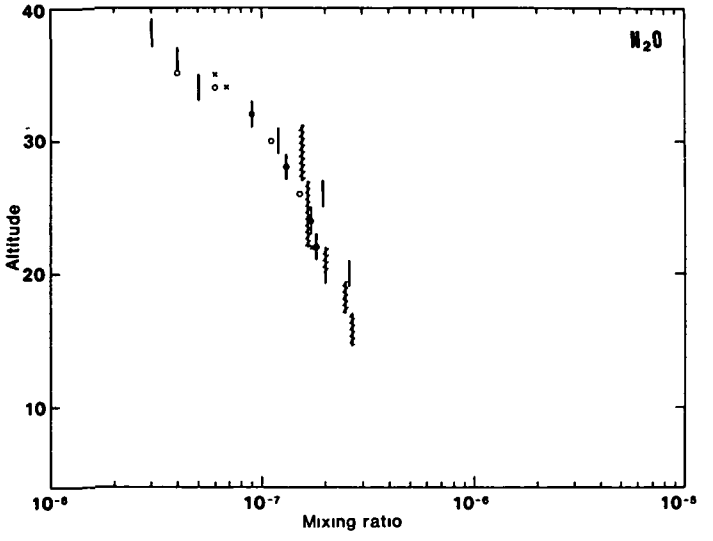

		Latitude	Resolution cm^{-1}	Spectral region
O ×	FARMER et al. (1980)	31°N 30°S	0.13	2.9 μ
——	LOUISNARD et al. (1983)	44°N	0.09	7.8 μ
//////	RINSLAND et al. (1982)	33°N	0.02	5.3 μ

Figure 20. N_2O profiles.

(k) Water Vapour

Although water vapour is one of the most abundant of minor species in the stratosphere it still remains one of the least understood both in terms of dynamics and photochemistry. The vibration-rotation spectrum of water vapour is rich and complex; its characteristically random appearance being caused by the great difference between its three moments of inertia.

Like other molecules with a complex spectra, the spectral line data for water vapour is far from perfect and serious discrepancies can sometimes be found between measured and calculated spectra in the regions away from the band centers where high rotational energy states occur. Not all water vapour lines are suitable for determining concentration profiles since many of the lines are saturated even at low concentrations.

Remote sensing techniques for the measurement of water vapour over long atmospheric paths offer a distinct advantage over in-situ techniques since they are less likely to suffer from errors caused by local contamination due to water vapour outgassing from the instrument and balloon. Local water vapour contamination at float altitude can be determined by studying the variation of the water vapour signal with zenith angle for small zenith angles.

Some recent measurements of stratospheric water vapour profiles are shown in Figure 21. Most of them have been obtained from measurements in the ν_2 band centered at 6.29 microns by absorption or emission. Primary interfering gases in this region are CH_4 and molecular oxygen. Although there is a large spread in the profiles they all show an extremely dry lower stratosphere with the mixing ratio increasing with altitude in the upper stratosphere.

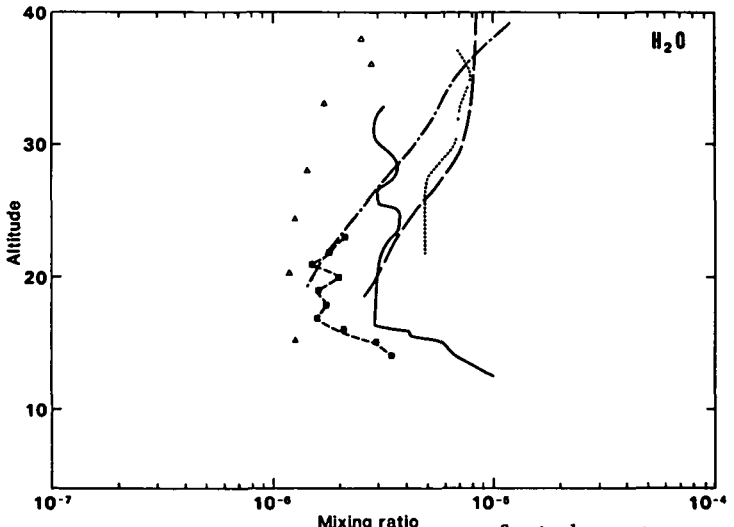

		Spectral region
△	FISCHER et al. (1980) Absorption Radiometer	6.3 μ
—·—	CHALONER et al. (1978) Emission PMR	6.3 μ
———	EVANS et al. (1981) Emission Radiometer	6.3 μ
-■--	SWANN et al. (1981) Emission Radiometer	100 μ
— — —	LOUISNARD et al. (1983) Absorption Spectrometer	6.3 μ
·····	FARMER et al. (1980) Absorption Spectrometer	6.3 μ

Figure 21. H_2O profiles.

(1) Ozone

Stratospheric spectra of ozone have been measured in several spectral regions.

Pollitt (POLLITT et al., 1979) has made emission measurements of the ν_1 and ν_3 bands at 9.6 microns, close to the maximum of the Planck function at stratospheric temperatures. These two bands have been extensively studied by spectroscopists.

Absorption spectra at sunset have been obtained by Farmer (FARMER et al., 1980) in the $\nu_1 + \nu_2 + \nu_3$ bands at 2785 cm^{-1} and the $3\nu_3$ band at 3041 cm^{-1}. The absolute accuracy of the O_3 mixing ratio derived from the spectra is limited by the uncertainty in the O_3 line strengths for these bands (±25%). Obviously this uncertainty affects the total ozone burden but not the shape of the profile.

Solar absorption spectra in the ν_1 and ν_3 bands have been obtained by Louisnard (LOUISNARD et al., 1983). They obtain two different profiles from analysis of these bands; this discrepancy is due to uncertainties in the line strengths used. However, they point out that the uncertainty in the Lorentz halfwidth, and especially its variation with temperature, is also a contributing factor.

Ozone profiles at night (using stellar occultation) have been obtained by Rigaud (RIGAUD et al., 1983) from measurements in the 640-670 nm spectral region where the O_3 absorption cross section is well known and is independent of pressure and temperature; water vapour is only weakly absorbing in this spectral region.

The profiles obtained by remote sensing techniques are shown in Figure 22 and are in good agreement with those obtained using in-situ techniques.

CONCLUSION

This review of recent stratospheric measurements obtained by remote sensing techniques in the visible and infrared illustrates how the measuring techniques have developed and brings out certain points which are summarized below.

Comparison of results obtained by different experimenters shows that it is very important to be able to distinguish between the natural variability in concentration and the error in the measurement. Profiles measured with greater accuracy are required to validate photochemical models of the stratosphere. In a recent paper, HARRIES (1982) suggests that key stratospheric species need to be measured to an absolute accuracy of 2%; even though such an accuracy has not been achieved the trend is in this direction.

International intercomparison campaigns (CNES, NASA, MAP/GLOBUS) have brought together identical and complementary measurement techniques with the aim of making simultaneous measurements of the same species within the same air mass. The results from these campaigns, still being analyzed in most cases, do not appear in this review. These campaigns have encouraged experimenters to pay rigorous attention to instrumental calibration and data analysis in order to minimize all sources of error.

In parallel, the work of laboratory spectroscopists has brought about improvements in the spectral parameters of key stratospheric species. However, many of the heavy molecules (HNO_3, N_2O_5, Freons) have received less attention and the lack of spectral data limits the accuracy with which these can be measured.

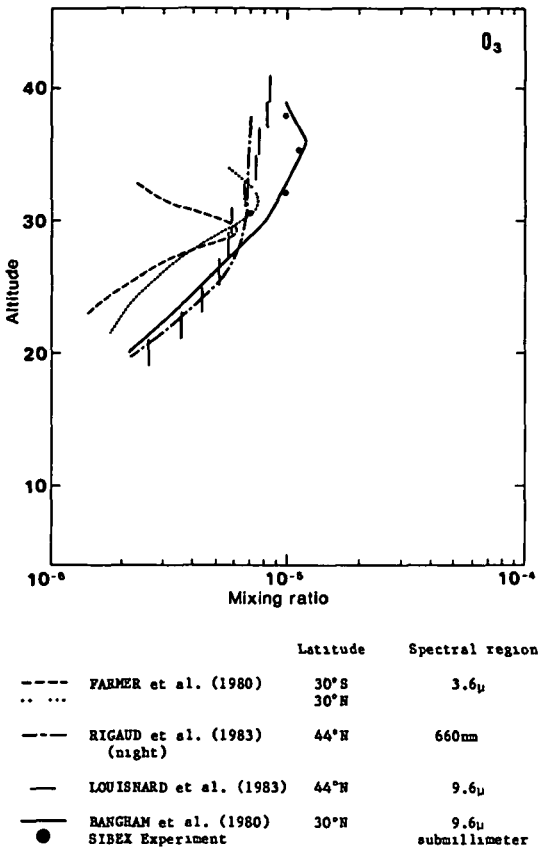

Figure 22. O_3 profiles.

The simultaneous measurement of several species with identical or complementary instruments has proved to be indispensible for obtaining cross-correlated sets of data on key species and for studying their natural variations. A Fourier Transform interferometer, being able to multiplex spectral information would appear more suitable for making simultaneous measurements of groups of species than instruments which carry out spectral measurements line by line. However, grating spectrometers can reduce this advantage considerably by scanning the grating rapidly and by using different orders to analyze several spectral regions in parallel.

The development of remote sensing instruments must continue in two directions to allow new species to be detected and to enable measurements to be made with greater accuracy.

(a) Resolution

The report of the detection of ClO by IR heterodyne absorption spectroscopy illustrates the possibility of making atmospheric spectral measurements at very high resolution comparable with the Doppler line widths. At present measure-

ments are limited to the 8-12 micron region where the technology of CO_2 and N_2O laser local oscillators is well developed. However, by using tunable diode lasers as a source of local oscillator power it will become possible to make very high resolution measurements anywhere in the infrared spectral region.

Although laboratory interferometers have been developed for obtaining high resolution spectra (0.0025 cm^{-1}) it appears unlikely that balloon borne infrared interferometers will be able to match the resolution which heterodyne systems are potentially capable of achieving.

All the high resolution instruments that have been reported use absorption spectroscopy; there exists a requirement for the development of a high resolution mid infrared emission instrument for studying the diurnal variation of photochemically active species.

(b) Signal-to-Noise

The progress in the field of infrared detector technology promises a real improvement in the signal-to-noise ratio and therefore an improvement in the accuracy of measurements. Photon limited detectors are most suited for use in high resolution cooled grating spectrometers where the photon flux on the detector is small; their full potential is not realised in interferometers unless the spectral bandwidth (and hence multiplex advantage) is severely reduced by using cooled narrowband filters.

Although there will be an increasing shift towards remote sensing of stratospheric species from satellites, remote sensing from balloons will still have an important role to play in:

(1) detecting new species,
(2) addressing specific points of stratospheric composition,
(3) testing new instrumentation, and
(4) validating satellite measurements.

REFERENCES

Ackerman, M., D. Frimout, A. Girard, M. Gottignies and C. Muller (1976), Stratospheric HCl from infrared spectra, Geophys. Res. Lett., 3, 81.

Bangham, M., A. Bonetti, R. Bradsell, B. Carli, J. Harries, F. Mencaraglia, D. Moss, S. Pollitt, E. Rossi and N. Swann (1980), Proc. Quadrennial International Ozone Symp., Colorado, 759-764.

Boughner, R., J. C. Larsen and M. Natarajan (1980), The influence of NO and ClO variations at twilight on the interpretation of solar occultation measurements, Geophys. Res. Lett., 7, 231.

Blatherwick, R. D., A. Goldman, D. G. Murcray, F. J. Murcray, G. R. Cook and J. W. Van Allen (1980), Simultaneous mixing ratio profiles of stratospheric NO and NO_2 as derived from balloon-borne infrared solar spectra. Geophys. Res. Lett., 7, 471.

Brockman, P., C. H. Baw and F. Allano (1978), High resolution spectral measurement of the HNO_3 11.3 μ band using tunable diode lasers, Appl. Opt., 17, 91.

Buijs, H. L., G. L. Vail, G. Tremblay and D. J. W. Kendall (1980), Simultaneous measurement of the volume mixing ratios of HCl and HF in the stratosphere, Geophys. Lett. Res., 7, 205.

Chaloner, C. P., J. R. Drummond, J. T. Houghton, R. F. Jarnot and H. K. Roscoe (1978), Measurement of stratospheric composition, Proc. Roy. Soc., 364, 145.

Clough, S. A., F. X. Kneizys, L. S. Rothman and W. O. Gallery (1982), Atmospheric spectral transmittance and radiance FASCOD IB, AFGL Hanscom Air Force Base, MA 01731.

Coffey, M., W. Mankin and A. Goldman (1981), Simultaneous spectroscopic determination of the latitudinal, seasonal and diurnal variability of stratospheric N_2O, NO, NO_2 and HNO_3, J. Geophys. Res., 86, 7331.

Connes, P., J. Connes, W. S. Benedict and L. D. Kaplan (1967), Traces of HCl and HF in the atmosphere of Venus, Astrophys. J., 1230.

Drummond, J. R. and R. F. Jarnot (1978), Measurement of stratospheric composition, Proc. Roy. Soc., 364, 237.

Evans, W. F. J., H. Fast, J. B. Kerr, C. T. McElroy, R. S. O'Brine, D. I. Wardle, J. C. McConnell and B. A. Ridley (1978), Proc. of WMO Symp., n°511, Toronto. June.

Evans, W. F. J. and coworkers (1981), Upper Atmospheric Program Bulletin 81-4.

Evans, W. F. J., C. T. McElroy, J. B. Kerr and J. C. McConnell (1982), Simulation of the October 23, 1980 stratosprobe flight, Geophys. Res. Lett., 9, 223.

Eyre, J. R. and H. K. Roscoe (1977), Radiometric measurements of HCl, Nature, 226, 243.

Farmer, C. B., O. F. Raper and R. H. Norton (1976), Spectroscopic detection and vertical distribution of HCl in the troposphere and stratosphere, Geophys. Res. Lett., 3, 13n Jan.

Farmer, C. B., O. F. Raper, B. D. Robbins, R. A. Toth and C. Muller (1980), Simultaneous spectroscopic measurements of stratospheric species O_3, CH_4, CO, CO_2, N_2O, H_2O, HCl and HF at Northern and Southern mid-latitudes, J. Geophys. Res., 85, 1621.

Felgett, P. B. (1958), J. Phys. Radium, 19, 187.

Fischer, H.,F. Fergg and D. Rabus (1980), Int. Rad. Symp., Fort Collins, August.

Gille, J. and Elingsen (1968), Corrections of random exponential band transmittance for Doppler effects, Appl. Opt., 7, 471.

Gille, J. and F. House (1971), J. Atmos. Sci., 28, 1427.

Girard, A. (1963), Spectrometre a grille, App. Optic, 2, 79.

Girard, A., L. Gramont, N. Louisnard, S. Le Boiteux and G. Fergant (1982), Latitudinal variations of HNO_3, HCl and HF vertical column density above 11.5 km, Geophys. Res. Lett., 9, 135.

Girard, A., G. Fergant, L. Gramont, O. Lado-Bordowsky, J. Laurent, S. Le Boiteux, M. P. Lemaitre and N. Louisnard (1983), Latitudinal distribution of ten stratospheric species deduced from simultaneous spectroscopic measurements, J. Geophys. Res., 88, 5377.

Goldman, A., T. G. Kyle and F. S. Bonano (1971), Statistical band model parameters and integrated intensities for the 5.9 μ, 7.5 μ and 11.3 μ bands of HNO_3 vapour, Appl. Opt., 10, 65.

Goldman, A., D. G. Murcray, F. H. Murcray and W. J. Williams (1973), Solar absorption in the CO fundamental region, The Astrophysics J., 182, 581-584.

Goldman, A., S. C. Schmidt, J. R. Riter and R. M. Blunt (1974), Infrared spectral radiance of hot HF and DF in the $\nu = 1$ bands region as seen from an atmospheric path, J.Q.S.R.T., 14, 299.

Goldman, A., F. G. Fernald, W. J. Williams and D. G. Murcray (1978), Vertical distribution of NO_2 in the stratosphere as determined from balloon measurements of solar spectra in the 45000 Å region, Geophys. Res. Lett., 5, 257-260.

Goldman, A. and R. S. Saunders (1979), Analysis of atmospheric infrared spectra for altitude distribution of atmospheric trace constituents, J.Q.R.S.T., 21, 155.

Goldman. A., D. G. Murcray, F. J. Murcray and E. Niple (1980), High resolution IR balloon-borne solar spectra and laboratory spectra in the HNO_3 1720 cm^{-1} region: an analysis, Appl. Opt., 19, 22, 3721.

Goldman, A., F. S. Bonano, F. P. J. Valero, D. Goorwitch and R. W. Boese (1981), Temperature dependence of HNO_3 absorption in the 11.3 μ region, Appl. Opt., 20, 167.

Goldman, A., R. D. Blatherwick, F. J. Murcray, J. W. Van Allen, F. J. Murcray and D. G. Murcray (1982), New atlas of stratospheric IR absorption spectra, Dept. of Phys. Univ. of Denver, January.

Goody, R. M. (1964), Atmospheric Radiation, Oxford University Press.

Harries, J. E. (1982), Stratospheric composition measurements as tests of photochemical theory, J. Atmos. Terr. Phys., 44, 7, 591-597.

Houghton, J. T., G. D. Peskett and C. D. Rodgers (1971), A scientific proposal to employ the PMR to sound the temperature and composition of the stratosphere and mesosphere, Oxford Univ.

Husson, N., A. Chedin, N. A. Scott, J. Cohen-Hallaleh and A. Berroir (1982), La banque de donnees "GEISA", LMD n°116, Palaiseau.

Jacquinot, P. (1958), J. Phys., 19, 223.

Kendall, D. J. W. and H. Buijs (1983), Stratospheric NO_2 and upper limits of CH_3, Cl and C_2H_6 from measurements at 3.4 μ, Nature, 303.

Laurent, J., M. P. Lemaitre and L. Gramont (1981), Contribution a l'etude experimentale des variations diurnes et saisonnieres du dioxyde d'azote, C.R. Acad. des Sc., 293, 903.

Louisnard, N. and O. Lado-Bordowsky (1983), Spectroscopic measurements of carbon monoxide in the stratosphere, J. Geophys. Res., 88, 3789.

Louisnard, N., G. Fergant, A. Girard, L. Gramont, O. Lado-Bordowsky, J. Laurent, S. Le Boiteux and M. P. Lemaitre (1983), Infrared absorption spectroscopy applied to stratospheric profiles of minor constituents, J. Geophys. Res., 88, 5377.

Maki, A. G., F. J. Lovas and W. B. Olson (1982), J. Mol. Spect., 92, 410.

Mankin, W. G. (1979), Fourier transform method for calculating the transmittance of inhomogeneous atmospheres, Appl. Optics, 18, 3426.

Mankin, W. G. and M. T. Coffey (1983), Latitudinal distribution and temporal changes of stratospheric HCl and HF, J. Geophys. Res., 88, 10776.

Margolis, J. S., R. T. Menzies and E. D. Hinkley (1978), Appl. Optics, 17, 1680.

Menzies, R. T. (1979), Geophys. Res. Lett., 6, 151-154.

Menzies, R. T. (1983), A re-evaluation of laser heterodyne radiometer ClO measurements, Geophys. Res. Lett., 10, 729.

Menzies, R. T., C. W. Rutledge, R. A. Zanteson and D. L. Spears (1981), Balloon borne laser heterodyne radiometer for measurement of stratospheric trace species, Appl. Optics, 20, 536.

Mill, J. D. (1977), An efficient method for investigating limb radiance profiles with application to the fluorocarbons, Report No. 013624, Hael Univ. of Michigan, Ann Arbor.

Muller, C. and A. J. Sauval (1975), The CO fundamental bands in the solar spectrum, Astron. Astrophys., 39, 445.

Mumma, M. J.., T. Kostiuk and D. Buhl (1978), A 10 μ laser heterodyne spectrometer for remote detection of trace gases, Opt. Eng., 17, January.

Murcray, D., D. Barker, J. Brooks, A. Goldman and W. Williams (1975), Seasonal and latitudinal variation of the stratospheric concentration of HNO_3, Geophys. Res. Lett., 2, 223.

Murcray, D. G., W. J. Williams, D. B. Barker, A. Goldman, C. Bradford and C. Cook (1978), Proc. of the WMO Symp., No. 511, Toronto, June.

Murcray, D. G., A. Goldman, F. H. Murcray, F. J. Murcray and W. J. Williams (1979), Stratospheric distribution of ClO NO_2, Geophys. Res. Lett., 6, 857.

Murcray, F. H., F. J. Murcray, D. G. Murcray and W. J. Williams (1981), Cryogenic infrared balloon experiment - A 0.1 cm^{-1} cooled balloon-borne Fourier transform spectrometer system, AFGL-TR-81-0186, May.

Murcray, F. J., A. Goldman, D. G. Murcray, G. R. Cook, J. W. Van Allen and R. D. Blatherwick (1980), Identification of isolated NO lines in balloon borne infrared solar spectra, Geophys. Res. Lett., 7, 673.

The Stratosphere Present and Future (1979), NASA, Ref. Pub. 1049, Ed. Hudson and E. I. Reed, December.

Naudet, J. P., P. Rigaud and D. Huguenin (1984), Stratospheric NO_2 at night from balloons, accepted J. Geophys. Res.

Niple, E., W. G. Mankin, A. Goldman, D. Murcray and F. J. Murcray (1980), Stratospheric NO_2 and H_2O mixing ratio profiles from high resolution infrared solar spectra using nonlinear least squares, Geophys. Res. Lett., 7, 489.

Ogawa, T., K. Shibasaki and K. Suzuki (1981), Balloon observations of the stratospheric NO_2 profile by visible absorption spectroscopy, J. of Met. Soc. of Japan, 59, 410.

Pollitt, S., M. J. Bangham, R. H. Bradsell, J. E. Harries, D. G. Moss and N. R. Swann (1979), SIBEX (Submillimeter Infrared Balloon Experiment), Final Rep. to the CMA, October.

Pommereau, J. P. (1982), Observation of NO_2 diurnal in the stratosphere, Geophys. Res. Lett., 9, 850.

Raper, O. F., C. B. Farmer, R. A. Toth and B. D. Robbins (1977), The vertical distribution of HCl in the stratosphere, Geophys. Res. Lett., 4, 531.

Rigaud, P., J. P. Naudet and D. Huguenin (1983), Simultaneous measurements of vertical distributions of stratospheric NO_3 and O_3 at different periods of the night, J. Geophys. Res., 88, 1463.

Rinsland, C., A. Goldman, F. M. Murcray, M. Smith, R. Seals, J. Larsen and P. Rinsland (1982), Stratospheric N_2O mixing ratio profile from high resolution balloon borne absorption spectra and laboratory spectra near 1880 cm^{-1}, Appl. Optics, 21, 4351.

Roscoe, H. K. (1982), Tentative observations of stratospheric N_2O_5, Geophys. Res. Lett., 9, 901.

Roscoe, H. K., J. R. Drummond and R. F. Jarnot (1981), Infrared measurements of stratospheric composition - The daytime changes of NO and NO_2, Proc. R. Soc. Lond., 375, 507.

Rothman, L. S. (1978), Appl. Optics, 17, 3517-3518.

Rothman, L. S. (1981), AFGL atmospheric absorption line parameters compilation, 1980 version, Appl. Optics, 20, 791.

Rothman, L. S., R. R. Gamache, A. Barbe, A. Goldman, J. R. Gillis, L. R. Brown, R. A. Toth. J. M. Flaud nd C. Camy-Peyret (1983), AFGL atmospheric absorption line parameters compilation: 1982 edition, Appl. Optics, 22, 2247.

Schindler, R. A. (1970), A small, high-speed interferometer for aircraft, balloon and spacecraft applications, Appl. Optics, 9, 301.

Selby, J., E. Shettle and R. Mac Clatchey (1976), Atmospheric transmittance from 0.25 to 28.5 μ supplement LOWTRAN, AFGL-TR-76-0258.

Snider, D. E. (1975), Refractive effects in remote sensing of the atmosphere with infrared transmission spectroscopy, J. Atmos. Sci., 32, 2178.

Swann, N. and Coworkers (1981), Upper Atmospheric Program. Bulletin 81-4.

Taylor, S. W., J. T. Houghton, J. D. Peskett, C. D. Rodgers and E. J. Williamson (1972), Radiometer for remote sounding of the upper atmosphere, Appl. Optics, 11, 135-141.

Toth, R. A., R. H. Hunt and E. K. Plyler (1970), Line strengths, line widths and dipole moment function for HCl, J. Mol. Spec., 35, 110.

Wang, J. Y. and R. Goulag (1975), Numerical solutions in remote sensing, Appl. Optics, 14, 862.

Williams, W. J., J. J. Kosters, A. Goldman and D. G. Murcray (1976a), Measurements of the stratospheric mixing ratio of HCl using infrared absorption technique, Geophys. Res. Lett., 3, 383.

Zander, R. (1981b), Recent observations of HF and HCl in the upper stratosphere, Geophys. Res. Lett., 8, 413.

Zander, R., H. Leclercq and L. D. Kaplan (1981a), Concentration of carbon monoxide in the upper stratosphere, Geophys. Res. Lett., 8, 365.

Zander, R., G. Roland and L. Delbouille (1977), Confirming the presence of hydrofluoric acid in the upper stratosphere, Geophys. Res. Lett., 4, 117.

Williams, W. J., J. J. Kosters, A. Goldman and D. G. Murcray (1976b), Measurements of stratospheric halocarbon distributions using infrared techniques, Geophys. Res. Lett., 3, 379-382.

Zander, R. (1970), Observations, par ballon stratospherique, du spectre solaire a 1.85 microns avec un pouvoir de resolution de 135 000, Acad. Roy. Belgique, Cl. Sci., 5 eme serie, Tome LVI, 729-739.

3. MEASUREMENTS OF NEUTRAL CONSTITUENTS USING FAR INFRARED REMOTE SENSING TECHNIQUES

B. Carli* and J. E. Harries**

*Instituto Di Ricerca Sulle Onde Elettromagnetiche
Via Panciatichi 64
50127 Firenze
Italy

**Rutherford Appleton Laboratory
Chilton, Didcot
Oxfordshire OX11 0QX
England

INTRODUCTION

The history of submillimetre atmospheric research began in 1957 with the publication by GEBBIE (1957) of the first measurements of atmospheric transmission at wave numbers between 10 and 35 cm^{-1} at a spectral resolution of 0.2 cm^{-1}. These data were recorded using a large aperture (300-mm) lamellar grating interferometer and a Golay cell detector at the Jungfraujoch mountain observatory in Switzerland. The spectrum observed is reproduced in Figure 1 and shows, for the first time, the existence of several transmission windows between 12 and 28 cm^{-1}. Many of the observed spectral features were identified as due to water vapour H_2O and others were provisionally assigned to ozone O_3. Subsequent laboratory spectroscopy (STONE, 1964; GEBBIE et al., 1966) confirmed that numerous O_3 lines were present in the observations, along with magnetic dipole transitions in molecular oxygen (GEBBIE et al., 1969).

The development of submillimetre atmospheric research from 1957 until about the end of 1976 has been reviewed by HARRIES (1977). Following the early activities just described, a number of groups carried out studies of the submillimetre emission spectrum of the lower atmosphere from aircraft (HARRIES et al., 1972; BUSSOLETTI and BALUTEAU, 1974; MARTEN and CHAUVEL, 1975; MANKIN, 1975). During these studies, new methods such as phase modulation (CHAMBERLAIN, 1971, 1979) and new helium cooled detectors were introduced, and spectral resolutions of 0.06 cm^{-1} were achieved. Figure 2 illustrates two stratospheric emission spectra in the 12-27 cm^{-1} range recorded from an aircraft at an altitude of 12 km, a zenith angle of 75° and with a spectral resolution of 0.06 cm^{-1}. These observations showed the existence of highly reproducible spectral structure due to O_3 and other molecules.

Experiments following that were mounted on balloon platforms (HARRIES et al., 1973, 1976; CLARK and KENDALL, 1976). At the higher altitudes accessible by such methods, lines were narrow (particularly H_2O, which causes considerable opacity still at aircraft altitudes), and it became possible to detect weak lines of other species and to use limb-sounding methods to derive concentration-height profiles throughout the stratosphere for a number of species. Figure 3 shows an example of an emission spectrum measured from a balloon floating at 35 km with a zenith angle of 92° (HARRIES et al., 1976). The molecular assignments made at the time for many of the emission lines are indicated in the figure.

Considerable progress was made, also, in the early 1970's in the availability of laboratory spectra of stratospheric trace gases, mainly through the work of Fleming and co-workers (e.g., FLEMING and WAYNE, 1975; FLEMING, 1976a,b). Figure 4 shows a beautiful result from FLEMING and WAYNE (1975): a laboratory measurement of the transmission spectrum of 18 torr of ozone in a 1-m cell (Figure 4b) in comparison with a calculated spectrum (Figure 4a), showing excellent agreement between the two.

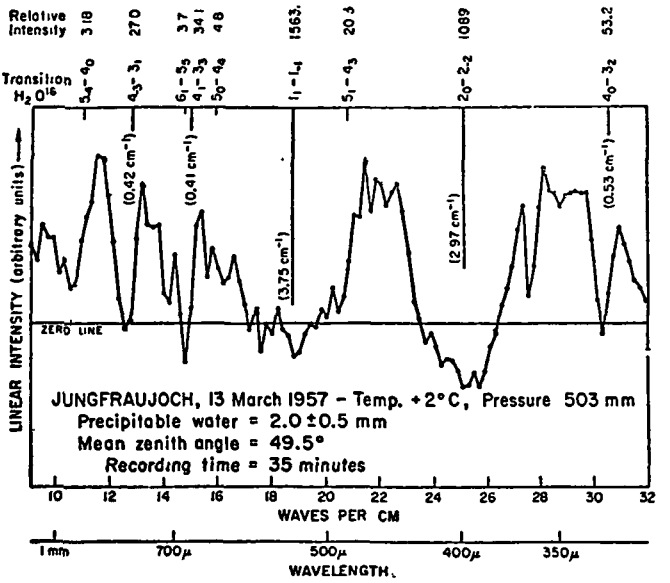

Figure 1. The solar absorption spectrum in the submillimetre region measured using a lamellar grating interferometer at an altitude of 3.58 km, a temperature of 2°C, a pressure of 503 torr, precipitable water of 2 $\pm$ 0.5 mm, and a mean zenith angle of 49.5°. Recording time 35 min. This represents the first observation of the transmission windows at 12, 14, 16, 11 and 28 cm^{-1}. From GEBBIE (1975).

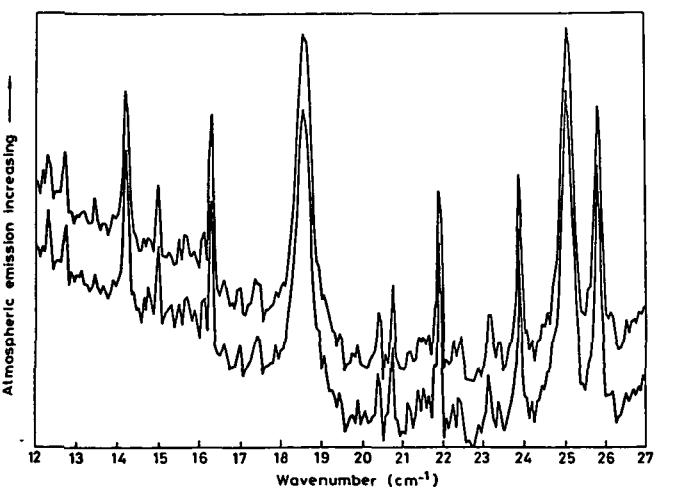

Figure 2. Stratospheric emission spectra in the 12 - 27 cm^{-1} region measured from an aircraft at an altitude of 12 km, a zenith angle of 75°, and a spectral resolution of 0.06 cm^{-1}. From HARRIES et al. (1972).

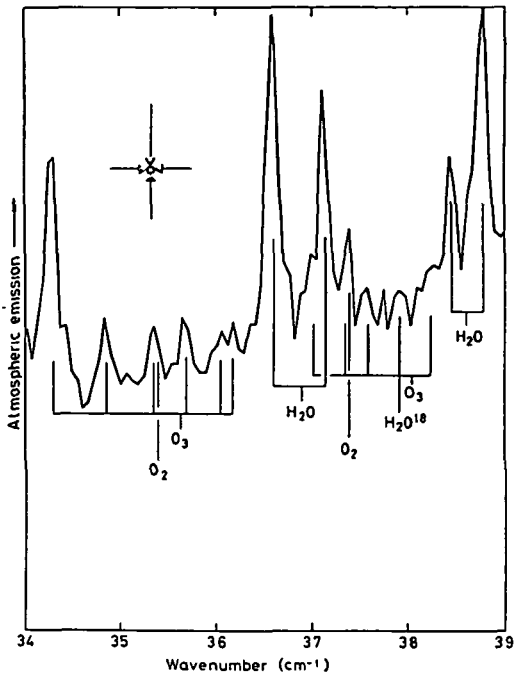

Figure 3. Stratospheric emission spectra in the 34 - 39 cm^{-1} region measured from a balloon at an altitude of 35 km, a zenith angle of 92°, and a spectral resolution of 0.07 cm^{-1}. From HARRIES et al. (1976).

Since the time of the HARRIES (1977) review, progress has occurred both in the direction of considerably improved experimental measurements from balloons and in the area of theoretical studies of the far infrared spectrum. The first aspect will be discussed in the section "Recent Experimental Results" and the second in "Theoretical Calculations and Spectroscopic Data". In the light of the recent results, our present understanding of the far infrared and submillimetre spectrum is reviewed in the last section.

RECENT EXPERIMENTAL RESULTS

Kendall and Clark of the University of Calgary have reported further measurements of the stratospheric emission spectrum from balloon altitudes, using a rapid-scan Michelson interferometer and a cooled detector (KENDALL and CLARK, 1978, 1979a,b, 1981; KENDALL, 1979). These data were measured at a resolution up to 0.07 cm^{-1} over the 30-110 cm^{-1} range. A number of flights were made, details of which may be found in KENDALL (1979).

In this work the most notable result has been the possible detection of OH. The question of OH emission has been investigated in some detail by these authors (KENDALL, 1979; KENDALL and CLARK, 1979b), including a calculation of the line positions and strengths, and it appears that the spectral resolution of their measurements was just on the limit for the detection of OH. Figure 5 shows an example of an emission spectrum from KENDALL and CLARK (1979b): The top curve is the experimental result (see caption for details), and the lower curve is a line-by-line calculation including H_2O and O_3 only. The arrows mark the predicted OH line positions, and it can be seen that features have been detected that might be due to OH.

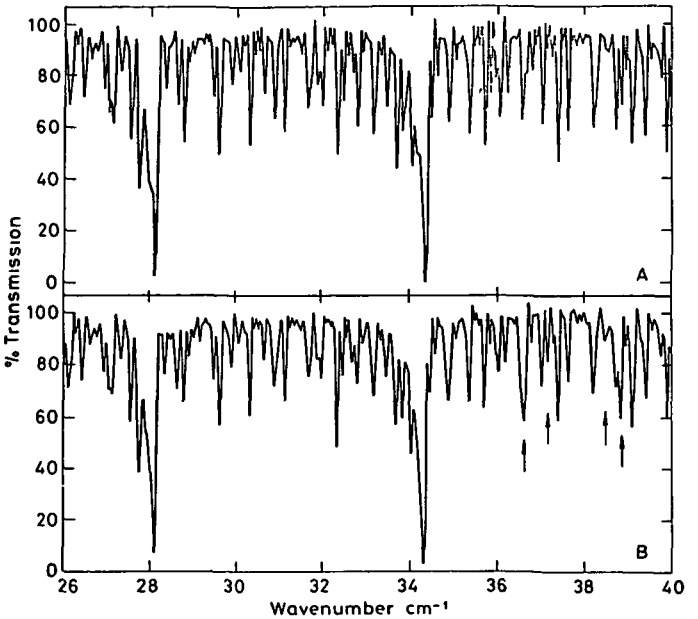

Figure 4. Comparison of synthetic (a) and experimental (b) transmittance spectra of ozone for laboratory conditions (room temperature approximately 296 K; path length 1.0 m; pressure 18 torr O_3 + 12 torr O_2; spectral resolution 0.05 cm^{-1}). The arrows indicate the positions of strong H_2O lines, which influence the experimental spectrum. From FLEMING and WAYNE (1975).

GROSSMAN and OFFERMAN (1978) reported rocket-borne measurements of the 63 μm emission from thermospheric atomic oxygen OI ($^3P_1 - ^3P_2$ fine structure transition in the ground state). An interesting interpretation of the data is given by these authors in terms of the breakdown of local thermodynamic equilibrium at the height of the measurements (about 80 km), which results in much lower emission intensity than previously assumed. The significance of this result, of course, is that this emission line represents a much less effective radiative cooling mechanism than previous calculations (assuming LTE) had indicated.

CARLI et al. (1980, 1982, 1983) have recently measured the emission spectrum of the stratosphere in the 7-85 cm^{-1} interval with an unapodized resolution of 0.0033 cm^{-1}. This significant improvement in resolution, made possible by the use of both a high efficiency polarizing Michelson interferometer (MARTIN and PUPLETT, 1969) and new sensitive bolometers, has provided very detailed information on the complex structure of the stratospheric submillimetre spectrum. Some of the difficulties encountered in the early assignments have been explained and several new constituents have been identified.

New measurements at higher frequencies have recently been obtained by Chance and Traub. These measurements cover the 70-260 cm^{-1} interval with an unapodized resolution of 0.032 cm^{-1} and have made possible the study of a new spectral interval and the identification of several lines due to important stratospheric species such as HF, HCl and OH (CHANCE et al., 1980; TRAUB and CHANCE, 1981; CHANCE and TRAUB, 1984b).

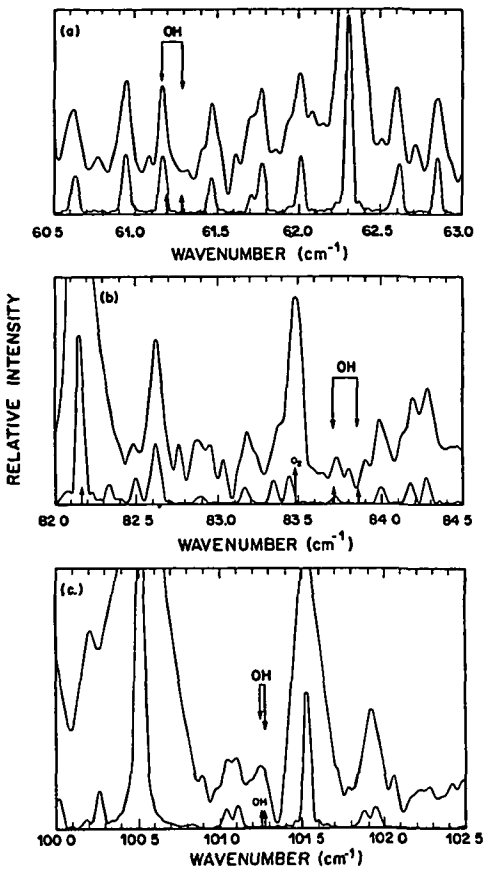

Figure 5. Measured submillimetre stratospheric emission spectrum obtained using a Michelson interferometer at a spectral resolution of 0.08 cm^{-1} from a balloon at approximately 35 km altitude (top curve) compared with a calculated spectrum for a standard atmosphere of H_2O and O_3 on which the positions of OH lines have been marked by arrows; an O_2 line is similarly indicated. From KENDALL and CLARK (1979b).

The results of the recent measurements by Carli et al. and by Chance and Traub together provide a full coverage at high resolution of the emission spectrum of the stratosphere in the far infrared and submillimetre region, and will be reviewed in the last section.

THEORETICAL CALCULATIONS AND SPECTROSCOPIC DATA

In France, Rabache and Rebours continued their studies of the submillimetre spectrum of the lower stratosphere. RABACHE (1977) studied the details of the pure rotation spectrum of nitric oxide, NO, and provided a listing of line positions and strengths. He concluded, however, that the NO lines made such a weak contribution to the spectrum by contrast with lines of O_3, H_2O and O_2 that they were essentially undetectable, given the current instrumental per-

formances at the time. REBOURS and RABACHE (1979) discussed the method proposed by BURROUGHS and HARRIES (1970) for making quantitative estimates of stratospheric H_2O concentration using an "internal calibration" procedure against O_2 lines. Rebours and Rabache were able to show that the method gave reasonably accurate results (±20%) in the case of H_2O which generally decreases in density with height in the stratosphere in a monotonic way. However, much larger errors (± 100% and more) were found in the case of O_3, which is distributed in the atmosphere in the form of a layer: In this case, clearly the method breaks down and cannot be used.

At the National Physical Laboratory, UK, BANGHAM (1978a,b) carried out a number of line-by-line spectral emission computations, generally for the case of limb sounding geometry with an observer on a balloon or spacecraft. These calculations were carried out in order to deduce the amount of retrievable information contained in the submillimetre spectrum at a resolution of about 0.01 cm^{-1} (the best resolution achievable at this time) as well as to analyse existing data. An example of this work is given in Figure 6, where the spectrum near 41 cm^{-1} is calculated in the case of a high resolution limb-scanning submillimetre spectrometer mounted on a spacecraft at 250 km looking at the atmospheric limb at a tangent height of 20 km. The solid line is for H_2O, O_2 and O_3 only: The broken line shows the effect of adding HCl and HF with a relative concentration of 1 part in 10^9 by volume (constant with height). This result should be compared with the more recent observational results shown in Figure 12.

Several laboratory measurements and calculations have been made in order to improve the spectroscopic data available in the far infrared. Useful new information has been included in the revision of 1982 of the AFGL Atmospheric Absorption Line Parameter Compilation (ROTHMAN et al., 1983b) and in the new AFGL Trace Gas Compilation that also appeared in 1982 (ROTHMAN et al., 1983a). Furthermore, a new catalogue has been started at JPL (POINTER and PICKETT, 1980) for frequencies up to 100 cm^{-1}, on the basis of new microwave measurements and theoretical calculations. This catalogue, of which two revisions have already been produced in 1981 and 1984, now provides a rather exhaustive data base as far as constituents, line position and line strength are concerned.

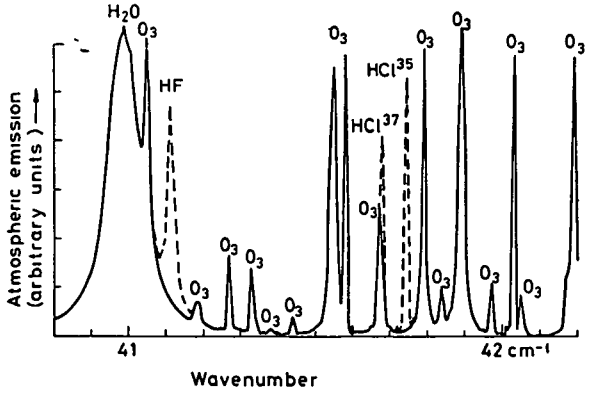

Figure 6. A calculated spectrum of the submillimetre atmospheric emission spectrum in the 42 - 42 cm^{-1} region for a standard atmosphere containing H_2O, O_2, and O_3, plus HCl and HF completely mixed at a mole fraction of 10^{-9}. The calculation was undertaken for the same observational geometry and spectral resolution as that in Figure 5. From BANGHAM (1978a).

High resolution measurements in the submillimetre region have recently been carried out at the Instituto Di Ricerca Sulle Onde Elettromagnetiche. The pure rotational spectra of several minor atmospheric constituents, including O_3, SO_2, H_2, NO_2, and H_2O_2, have been measured in the 10-80 cm^{-1} spectral region with a frequency accuracy of the order of 2.10-4 cm^{-1} (BALDECCHI et al., 1984). A full analysis has been completed in the case of SO_2 (CARLOTTI et al., 1984a) and ozone (CARLOTTI et al., 1984b) and is in progress for the others. An example of the results obtained is shown in Figure 7 in the case of nitrogen dioxide (CARLI et al., 1984a). The high resolution makes it possible to resolve most of the transitions and provides important information on the extension of the microwave data to higher frequencies.

In the 100-250 cm^{-1} spectral interval laboratory measurements of $ClONO_2$ (CHANCE and TRAUB, 1982) and HOCl (CHANCE and TRAUB, 1983) have been made at the Smithsonian Astrophysical Observatory. These molecules play a major role in the ozone chemistry, but are difficult to measure in the stratosphere.

While these measurements and calculations are rapidly filling the gaps as far as the knowledge of line position is concerned, large uncertainties still exist in the value of the half width of most transitions of the stratospheric spectrum and new measurements of this quantity will be required in the future for a more precise data analysis.

THE FAR INFRARED STRATOSPHERIC SPECTRUM

(a) The Main Features

A pictorial representation of the far infrared spectrum of a selection of stratospheric constituents is shown in Figure 8 (PARK et al., 1981). This figure is not updated and in fact some constituents like SO_2 and HBr have not yet been detected in the far infrared stratospheric spectrum while some more recent measurements like HCN and OH are not included. Nevertheless, the figure

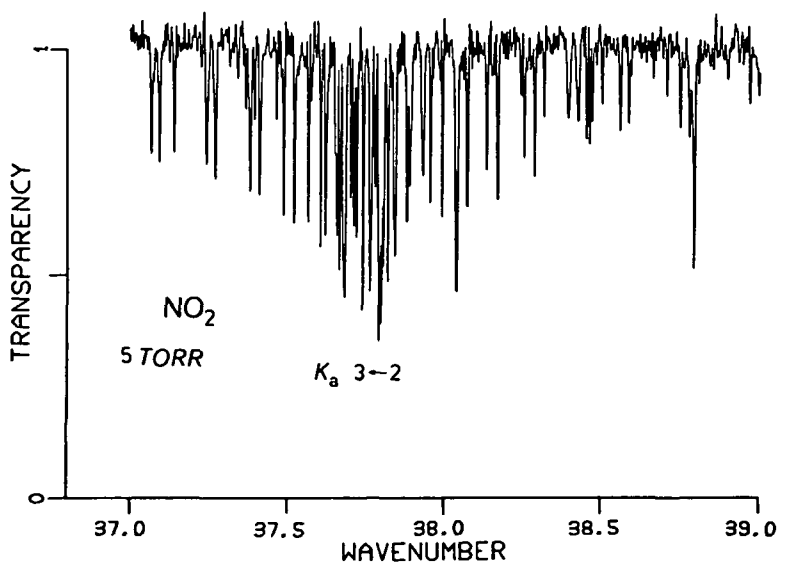

Figure 7. Laboratory measurements of the NO_2 absorption spectrum between 37 and 39 cm^{-1}. The unapodized resolution of 0.003 cm^{-1} makes it possible to resolve most of the individual rotational transitions within this Q-branch.

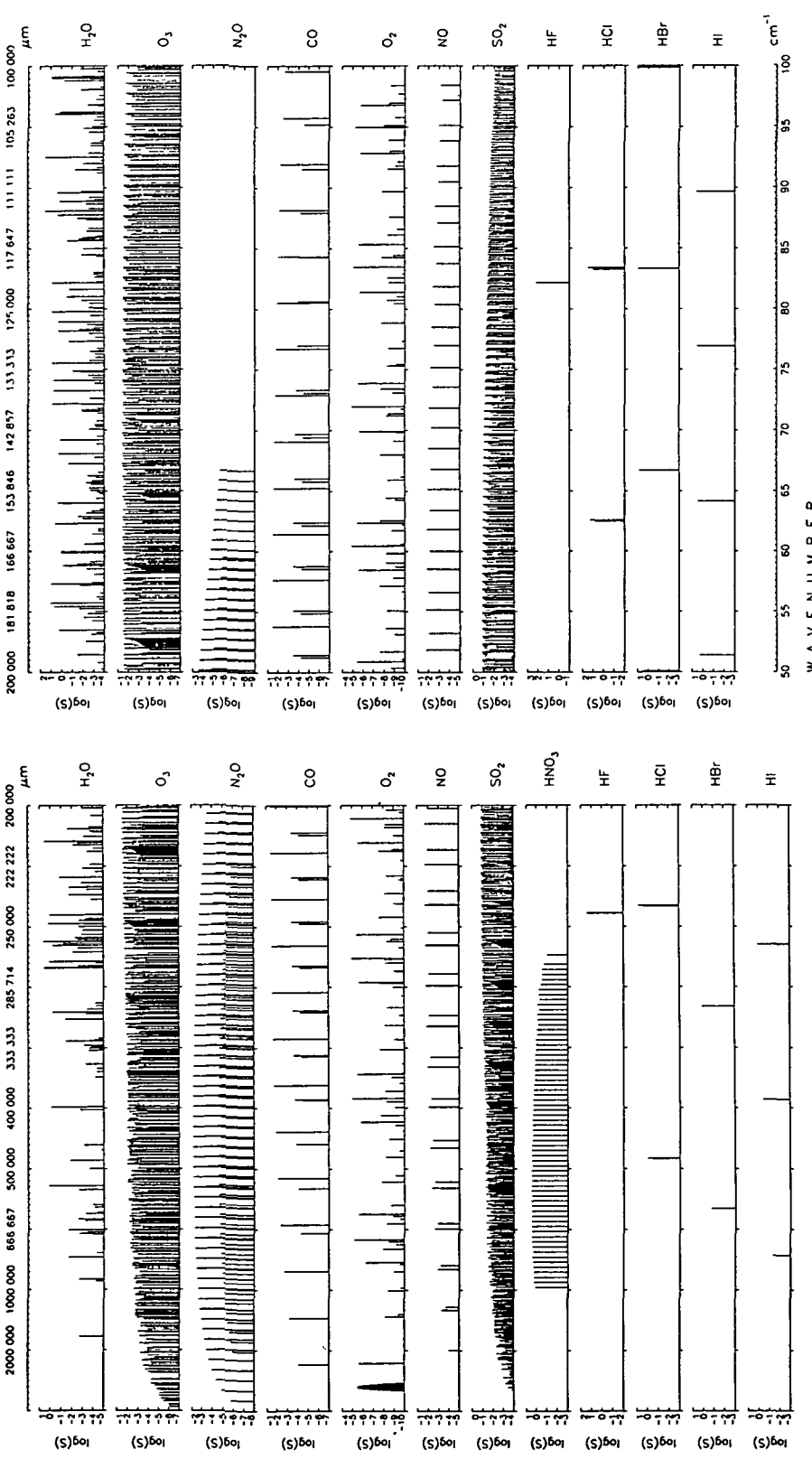

Figure 8. The logarithm of the line strength at 296 K as a function of the frequency for a few atmospheric gases, from PARK et al. (1981). This diagram provides a useful pictorial representation of the position and strength of the transitions that contribute to the stratospheric emission spectrum in the 0 - 250 cm-1.

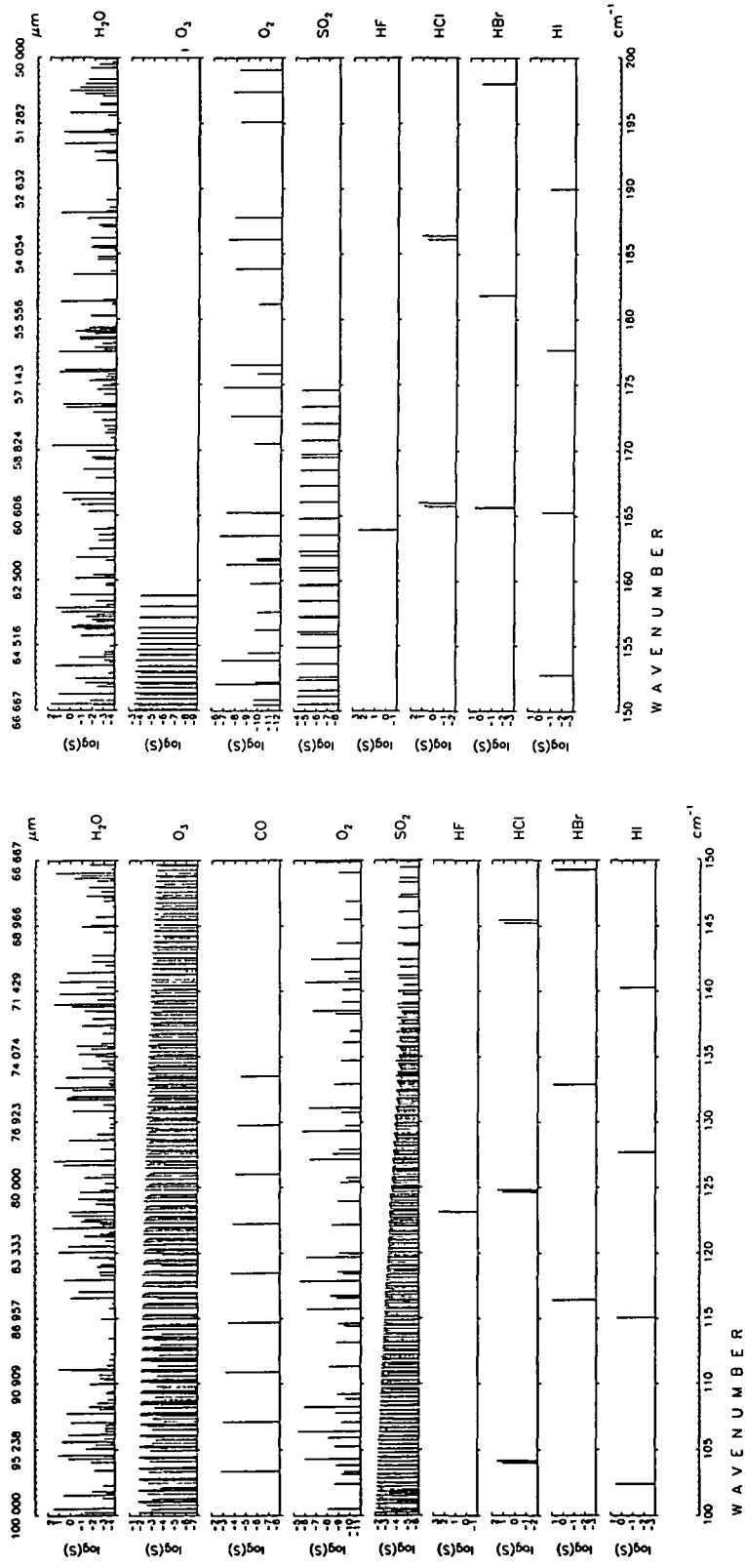

Figure 8 continued.

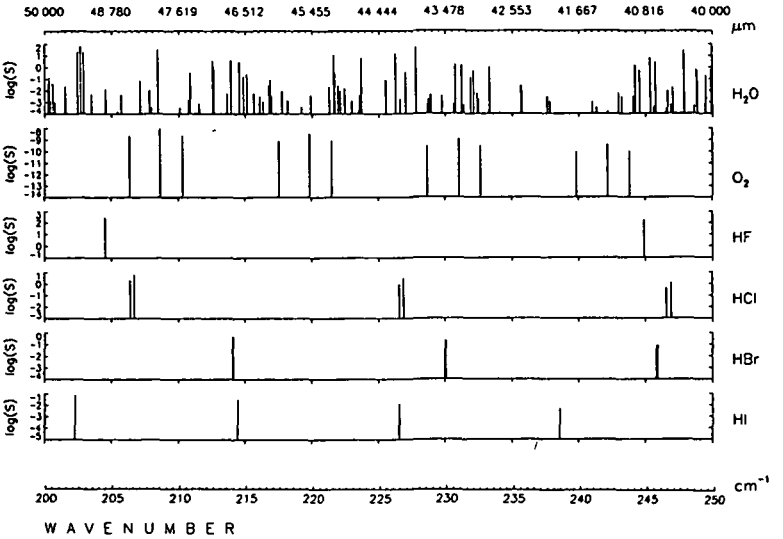

Figure 8 continued.

provides some very useful information on the position and the density of the lines that compose the stratospheric spectrum.

Magnetic dipole transitions of molecular oxygen and pure rotational transitions of both water vapour and ozone are the dominant features because of the relatively high concentration of these constituents. Oxygen is present in the entire spectral interval with a few strong and easily resolved lines that are grouped in a typical sequence of triplets. At high resolution also, weaker transitions due to the isotropic form $^{16}O^{18}O$ become visible (CARLI et al., 1980).

Water vapour also is present in the entire spectral interval with several features irregularly spaced. The strong water vapour lines can grow into broad features and eventually make the full spectral interval opaque when a sufficiently high column density is present along the observation path. At high resolution several sharp transitions due to HDO, $H_2{}^{18}O$, $H_2{}^{17}O$ and water vapour excited to the first level of the ν_2 vibrational state become visible (CARLI et al., 1980).

Ozone is present with a sequence of numerous closely spaced transitions that extend from the submillimetre region up to about 150 cm^{-1}. A decreasing density of ozone lines can be noticed in the 100-150 cm^{-1} region. The Q-branches of ozone can also be easily detected in very low resolution spectra, but a relatively high resolution is needed to detect individual transitions. With a resolution of 0.003 cm^{-1}, most features of the ozone spectrum are resolved and several transparent "windows", where transitions of other minor constituents can be studied, become visible. Transitions of rotational spectra of ozone isotopes $^{16}O^{18}O^{16}O$ and $^{18}O^{16}O^{16}O$ and of vibrationally excited ozone to the first ν_1, ν_2 and ν_3 levels have also been identified in the 10-100 cm^{-1} region, stressing the dominant role that ozone plays in the submillimetre stratospheric spectrum (CARLI et al., 1980, 1982).

(b) Nitric Acid, HNO_3

Nitric acid was first identified in submillimetre spectra measured with a resolution of 0.06 cm^{-1} (HARRIES, 1973) and its detection has been confirmed

by measurements at higher resolution. Two features occur in the spectral interval shown in Figure 9, but are not sufficiently strong for a positive detection, because of the geometry of observation (tangent height of about 28 km). At lower altitudes the concentration of HNO_3 increases and several lines can be detected in spectra with a tangent height of 16 km (see Figure 10) in the spectral interval from 9 cm^{-1} to about 24 cm^{-1}. The detection becomes difficult at higher frequencies because of both the decreasing intensity of HNO_3 features and the increasing opacity of the spectrum.

(c) Nitrous Oxide, N_2O

Nitrous oxide is a linear molecule and its equispaced lines have a period of about 0.84 cm^{-1}. The detection of this molecule was already possible in spectra at 0.06 cm^{-1} resolution (HARRIES, 1973). With a resolution of 0.003 cm^{-1} more than 16 lines of nitrous oxide can be resolved going from the J" = 11 transition at 10.055 cm^{-1} to the J" = 41 transitions at 35.145 cm^{-1}. One example is shown in Figure 10.

(d) Nitric Oxide, NO

The concentration of nitric oxide undergoes a diurnal cycle so that its monitoring throughout a 24 hour period with an emission measurement is important for the study of the photochemistry of this constituent. As pointed out by RABACHE (1977) nitric oxide shows only some rather weak features in the sub-millimetre stratospheric spectrum, but with the sensitivity of more recent measurements some small signal has been detected (CARLI et al., 1982). The strongest and better resolved feature is the $\pi_{3/2}$, J" = 9.5 transition at 36.077 cm^{-1} as shown in the stratospheric spectrum of Figure 11.

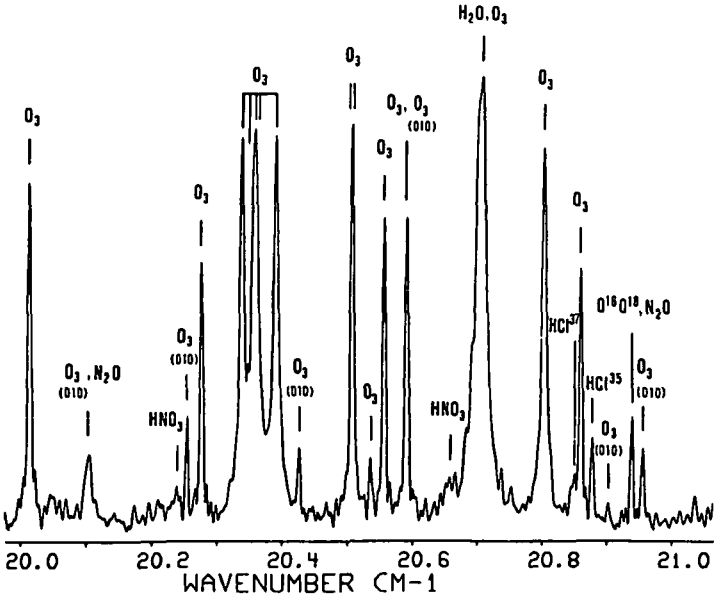

Figure 9. Stratospheric emission spectrum with an unapodized resolution of 0.003 cm^{-1} measured from a floating altitude of 38 km with a tangent height of 28 km. In this interval the two features of hydrochloric acid are easily resolved, while the emission features of nitrous oxide are blended and the emission of nitric acid is insufficient for a positive detection.

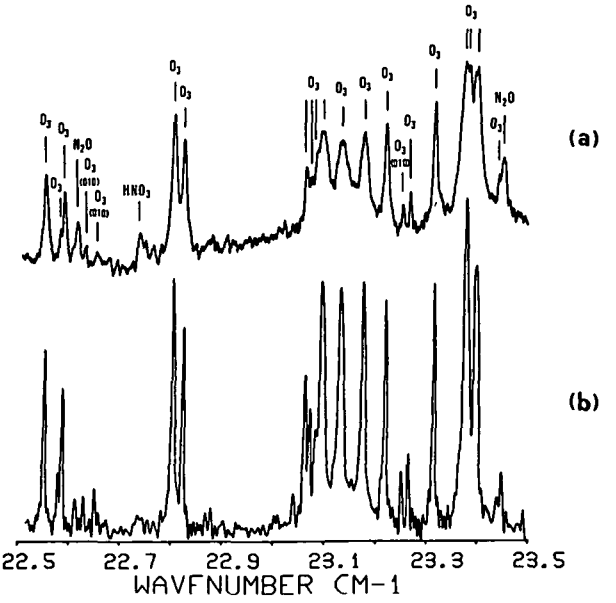

Figure 10. Stratospheric emission spectra measured with an unapodized resolution of 0.003 cm^{-1} from a floating altitude of 38 km in the case of a tangent height of 16 km (curve (a)), and the the case of a tangent height of 28 km (curve (b)). In this interval two features of nitrous oxide are resolved and a strong signal due to nitric acid becomes visible at low tangent heights.

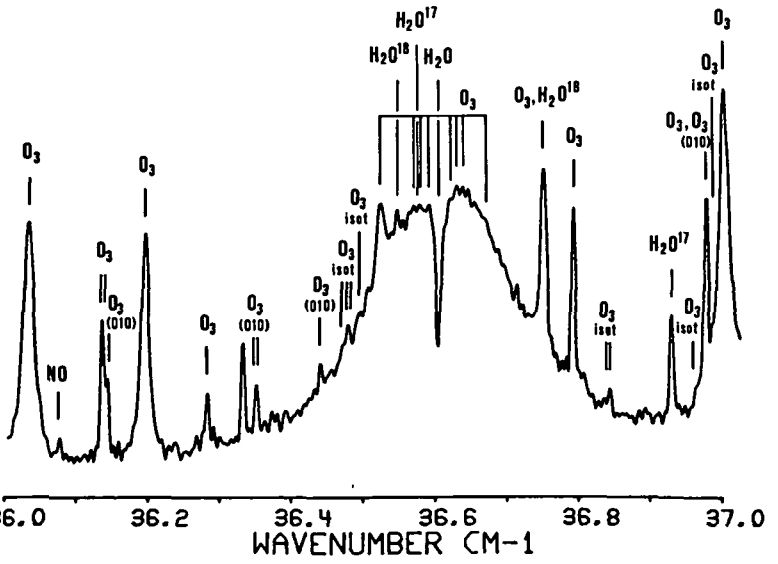

Figure 11. Stratospheric emission spectrum measured with an unapodized resolution of 0.003 cm^{-1} from a floating altitude of 38 km with a tangent height of 28 km. In this interval a small feature of nitric oxide has been detected. The negative signal at the centre of the strong water vapour line at 36.6 cm^{-1} is an instrumental artifact due both to the use of the zenithal signal as a reference zero level and to water absorption within the instrument.

(e) Nitrogen Dioxide, NO_2

As in the case of NO, the concentration of stratospheric nitrogen dioxide shows some diurnal variation and the detection of this constituent with an emission technique is of great interest. From recent high resolution laboratory measurements (CARLI et al., 1984), an emissivity of about 3% is expected from stratospheric NO_2 both in the interval between 52.657 cm^{-1} and 52.665 from the $^2Q_3$ branch and in the 0.003 cm^{-1} spectral element around 67.345 cm^{-1} from the $^2Q_4$ branch. Much lower emissivity is expected from the other Q-branches with the present resolution. The first feature is unfortunately covered by an ozone Q-branch, but the second occurs in a relatively open spectral interval. A positive assignment is made difficult by the weakness of the signal and by the blending with other small features at 67.3518 and at 67.3525 cm^{-1} due to ozone and isotopic ozone respectively, but some evidence exists that a signal from stratospheric NO_2 has been detected, see Figure 14 (CARLI et al., 1983). It is clear that the measurement of stratospheric nitrogen dioxide in the far infrared region requires a sensitivity and a resolution higher than those used up to now and it may be possible only in the 67.345 cm^{-1} region.

(f) Hydrofluoric Acid, HF

The first transition of the rotational spectrum of HF is clearly detected in the stratospheric spectrum at 41.111 cm^{-1}, see Figure 12. A small feature at 41.114 cm^{-1} due to ozone excited to the first v_2 vibrational level and the tail of the strong water vapour line at 40.988 cm^{-1} are superimposed on the HF line, but are not sufficient to mask the contribution that clearly emerges above the other signals (CARLI et al., 1983). The same does not occur in the case of the next two transitions at 82.171 and 123.130 cm^{-1} that are covered by strong lines of water vapour at 82.155 and 123.129 cm^{-1}, respectively, and cannot be resolved. At higher frequencies, three other HF features, that are free from blending effects with strong water vapour lines, have been measured by TRAUB and CHANCE (1981).

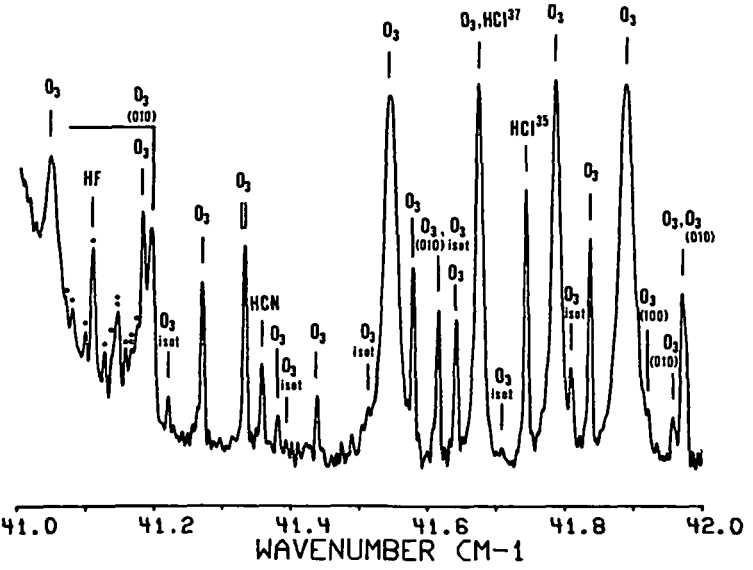

Figure 12. Stratospheric emission spectrum measured with an unapodized resolution of 0.003 cm^{-1} from a floating altitude of 38 km with a tangent height of 28 km. In this interval HF, HCl and HCN display strong features that can be resolved and used for their measurement.

(g) Hydrochloric Acid, HCl

The two isotopes of chlorine, ^{35}Cl and ^{37}Cl, occur naturally with an abundance ratio of about 3 to 1 so the pure rotational spectrum of HCl displays two adjacent sequences of equispaced lines with a period of about 20.8 cm^{-1}. Some of the features that can be measured below 100 cm^{-1} are shown in Figures 9, 12 and 15 (CARLI et al., 1980, 1983). Pressure broadening in measurements with a low tangent height introduces some slight blending between the J" = 0 $H^{37}Cl$ transition at 20.874 cm^{-1} and the ozone line at 20.860 cm^{-1} (see Figure 9), and a serious blending between the J" = 1 $H^{37}Cl$ transition at 41.681 and the ozone line at 41.675 cm^{-1} (see Figure 12). No blending has been observed for the J" = 0 and the J" = 1 transitions of the other isotope and for the J" = 2 and J" = 3 transitions of both isotopes.

Several other transitions are present about 100 cm^{-1}. In particular, the J" = 4, 5, 6 of $H^{35}Cl$ at 104.139, 124.827, 145.440 cm^{-1} and the J" = 6 of $H^{37}Cl$ at 145.223 cm^{-1} have been successfully used by TRAUB and CHANCE (1981) to measure a profile of HCl in the stratosphere (see Figure 16).

(h) Hydrogen Cyanide, HCN

Hydrogen cyanide is a linear molecule with a large dipole moment which displays in the submillimetre a strong rotational spectrum. About 12 transitions of this molecule can be resolved in the stratospheric spectrum going from the J" = 3 transitions at 11.825 cm^{-1} up to at least the J" = 21 transitions at 64.918 cm^{-1} (CARLI et al., 1982). An example of an HCN line that has been resolved in the stratospheric spectrum is shown in Figure 12.

(i) Carbon Monoxide, CO

The rotational spectrum of carbon monoxide displays a sequence of equispaced lines with a period of about 3.8 cm^{-1} and a maximum line strength around 50 cm^{-1}. Among about half-a-dozen lines that have been identified in the stratospheric spectrum (CARLI et al., 1980), the J" = 12 transition at 49.932 cm^{-1} (see Figure 13) provides the strongest and best resolved signal of CO in the far infrared stratospheric spectrum.

(j) Hydroxyl Radical, OH

The measurement of hydroxyl radical is of great importance for the study of the ozone chemistry because of the role of this molecule in many stratospheric reactions. The possibility of measuring this constituent in the far infrared, first suggested by KENDALL and CLARK (1979b) (see Figure 6), was confirmed by the recent high resolution measurements.

The far infrared spectrum of OH starts at 60 cm^{-1} and has its strongest features in the 150 cm^{-1} region. The first four weak features, respectively at 61.200, 61.303, 83.724 and 83.868 cm^{-1}, have been clearly identified in spectra at high resolution (CARLI et al., 1983). An example of these results is shown in Figure 15. The second and fourth transitions are seen as isolated lines down to tangent heights lower than about 33 km, as shown in Figure 15.

Furthermore, a total of twelve transitions of OH have been identified in the 80-200 cm^{-1} in stratospheric spectra recorded by CHANCE and TRAUB (1984b). An example of these measurements is shown in Figure 17.

(k) Other Constituents

The far infrared spectral region continues to be analyzed in order to identify other constituents that can usefully be measured in these regions.

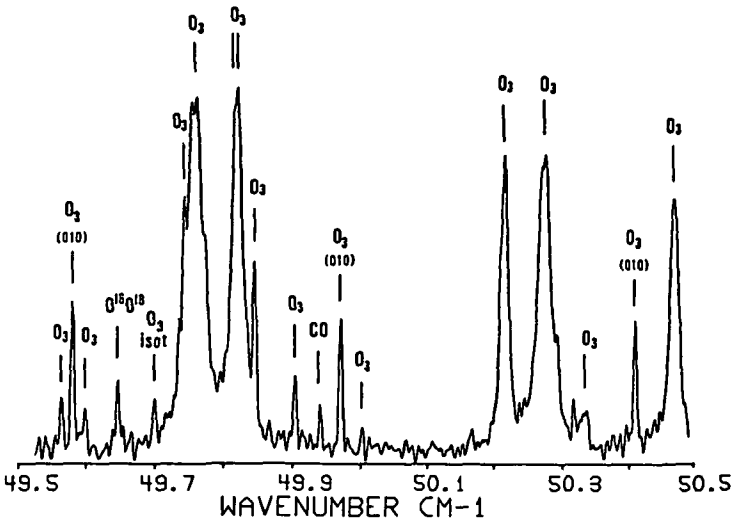

Figure 13. Stratospheric emission spectrum measured with an unapodized resolution of 0.003 cm^{-1} from a floating altitude of 38 km with a tangent height of 28 km. In this interval a small feature due to carbon monoxide is clearly visible close to one of the few transparent spectral intervals that are present in the submillimetre stratospheric spectrum.

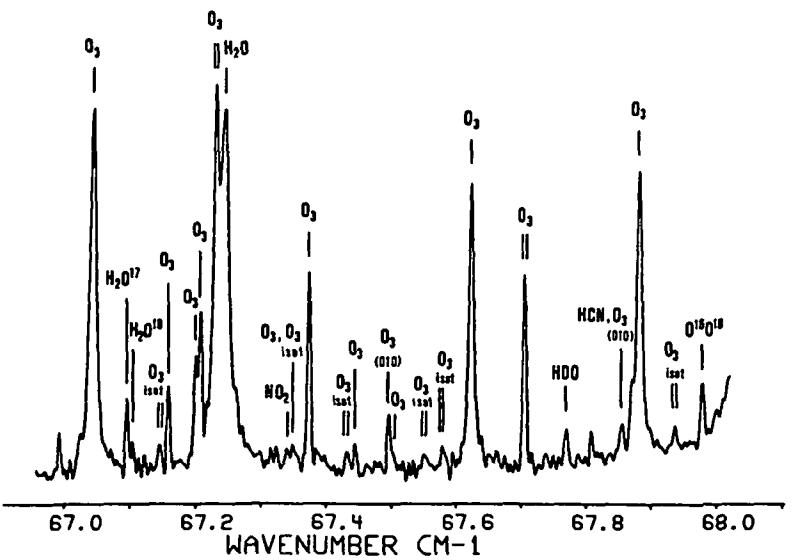

Figure 14. Stratospheric emission spectrum measured with an unapodized resolution of 0.003 cm^{-1} from a floating altitude of 38 km with a tangent height of 35 km. A small feature, that is tentatively assigned to nitrogen dioxide, suggests the possibility of the measurement of this constituent, given a larger signal-to-noise ratio.

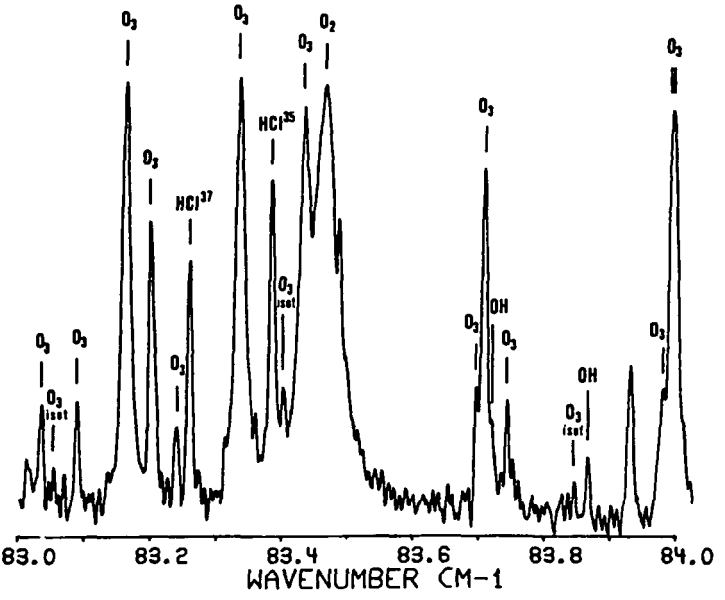

Figure 15. Stratospheric emission spectrum measured with an unapodized resolution of 0.003 cm^{-1} from a floating altitude of 38 km with a tangent height of 28 km. In this spectral interval, features due to hydrochloric acid and hydroxyl radical are clearly resolved.

Some new results have been obtained very recently.

First, on the basis of an expected feature of hydrogen peroxide at 112 cm^{-1} a firm 2σ upper limit of 0.05 ppb was determined for H_2O_2 stratospheric mixing ratio near 26.5 km by CHANCE and TRAUB (1984a).

Second, a feature of ClO has been identified at 22.89 cm^{-1} (CARLI et al., 1984b) in recent high signal-to-noise ratio stratospheric spectra recorded with ^{3}He cooled detectors.

CONCLUSIONS

The understanding of the far infrared stratospheric spectrum has improved continuously since the early measurements by H. A. Gebbie. A rather exhaustive picture of the constituents that can be detected and of the spectral intervals that provide the most useful measurement is now available.

The results obtained show that far infrared remote sounding can provide valuable and unique information on stratospheric composition and its evolution. Further improvements are expected in the case of a few molecules from the measurement of better line parameters (half width in particular), in the case of lines that are not fully resolved even at higher resolution and, probably most important of all, from measurements with better signal-to-noise ratio, as is possible with high sensitivity detectors associated to cooled narrow band filters.

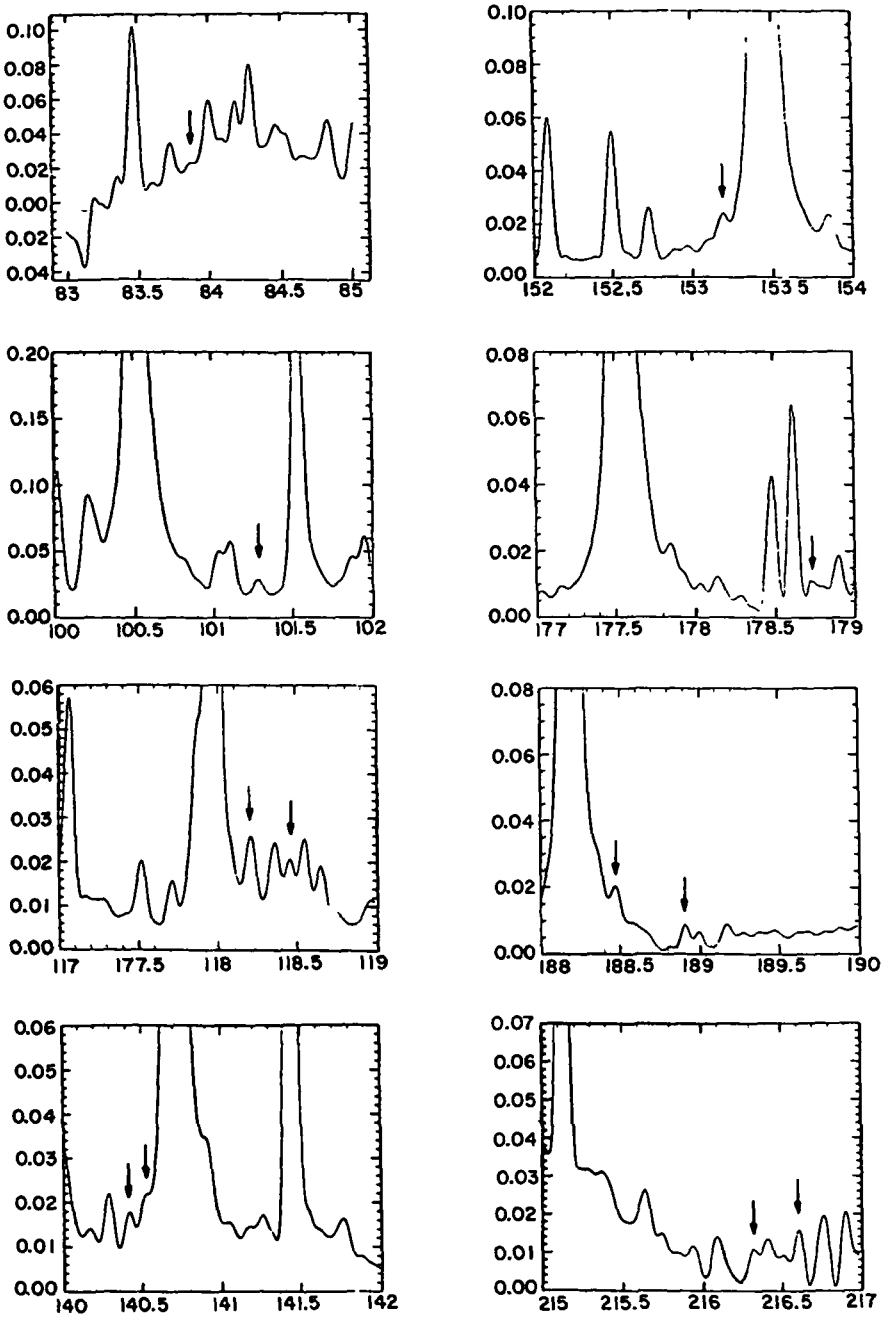

Figure 16. Examples of lines of hydroxyl radical that have been detected in the 80 - 220 cm^{-1} interval in the stratospheric emission spectrum obtained by CHANCE and TRAUB during the balloon flight of 23 January 1983. The abscissa scale is in cm^{-1}.

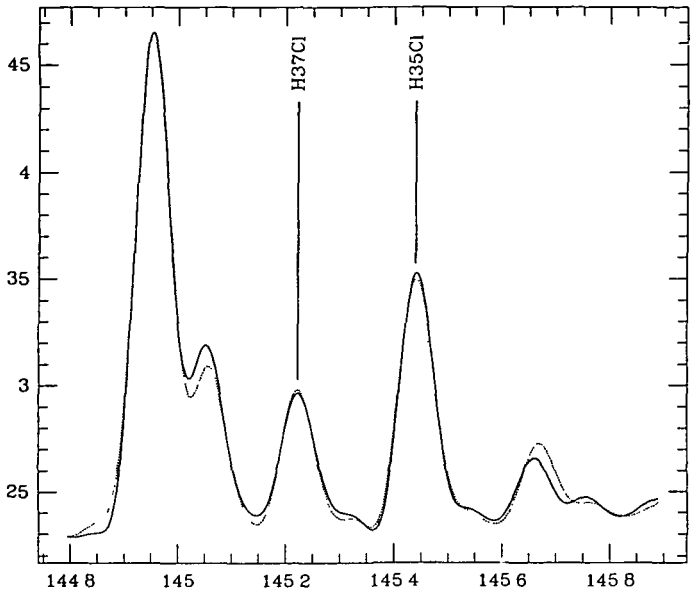

Figure 17. Example of lines of hydrochloric acid that have been detected in the far infrared stratospheric spectrum obtained by CHANCE and TRAUB during a balloon flight on 20 June 1984. The dotted line is a nonlinear least-square fit to the observed spectrum (solid line).

REFERENCES

Baldecchi, M. G., B. Carli, M. Carlotti, G. Di. Lonardo, F. Forni, F. Mencaraglia and A. Trombetti (1984), Int. J. Infrared & Millimeter Waves, 5, 381-402.

Bangham, M. J. (1978a), Infrared Phys., 18, 357-359.

Bangham, M. J. (1978b), Infrared Phys., 18, 799-801.

Burroughs, W. J. and J. E. Harries (1970), Nature, 227, 824-825.

Bussoletti, E. and J. P. Baluteau (1974), Infrared Phys., 14, 293-302.

Carli, B., F. Mencaraglia and A. Bonetti (1980), Int. J. Infrared & Millimeter Waves, 1, 263-276.

Carli, B., F. Mencaraglia and A. Bonetti (1982), Int. J. Infrared & Millimeter Waves, 3, 385-394.

Carli, B., F. Mencaraglia, A. Bonetti, B. M. Dinelli and F. Forni (1983), Int. J. Infrared & Millimeter Waves, 4, 475-488.

Carli, B., M. Carlotti, F. Mencaraglia, A. Mahmoudi, C. Camy-Peyret and J. M. Flaud (1984a), Mol. Phys., 51, 1505-1509.

Carli, B., M. Carlotti, B. M. Dinelli, F. Mencaraglia and I. Nolt (1984b), Private communication.

Carlotti, M., G. Di Lonardo, L. Fusina, B. Carli and F. Mencaraglia (1984a), J. Mol. Spectr., 106, 235-244.

Carlotti, M., G. Di Lonardo, L. Fusina, A. Trombetti, A. Bonetti, B. Carli and F. Mencaraglia (1984b), J. Mol. Spectr., 107, 84-93.

Chamberlain, J. (1971), Infrared Phys., 11, 25-55.

Chamberlain, J. (1979), The Principles of Interferometric Spectroscopy, Wiley, New York.

Chance, K. V., J. C. Brasunas and W. A. Traub (1980), Geophys. Res. Lett., 7, 704-706.

Chance, K. V. and W. A. Traub (1982), J. Mol. Spectr., 95, 306-312.
Chance, K. V. and W. A. Traub (1983), J. Quantum Spectrosc. & Rad. Transf., 29, 81-84.
Chance, K. V. and W. A. Traub (1984a), Submitted to J. Geophys. Res.
Chance, K. V. and W. A. Traub (1984b), Private communication.
Clark, T. A. and D. J. W. Kendall (1976), Nature, 260, 31-32.
Fleming, J. W. (1976a), J. Quant. Spectrosc. Radiat. Transfer., 16, 63-68.
Fleming, J. W. (1976b), Spectrochim. Acta, Part A, 32A, 787-795.
Fleming, J. W. and R. P. Wayne (1975), Chem. Phys. Lett., 32, 135-140.
Gebbie, H. A. (1957), Phys. Rev., 107, 1194.
Gebbie, H. A., N. W. B. Stone, G. Topping, E. K. Gora, S. A. Clough and F. X. Kneizys (1966), J. Mol. Spectr., 19, 7-24.
Gebbie, H. A., W. J. Burroughs and G. R. Bird (1969), Proc. R. Soc. London Ser. A., 310, 579-590.
Grossman, K. U. and D. Offerman (1978), Nature, 276, 594-595.
Harries, J. E. (1973), Nature, 241, 515-519.
Harries, J. E. (1976), Rev. Geophys. Space Phys., 14, 565-575.
Harries, J. E. (1977), J. Opt. Soc. Am., 67, 880-894.
Harries, J. E., N. R. Swann, J. E. Beckman, P. A. R. Ade (1972), Nature, 236, 159-161.
Harries, J. E., N. R. Swann, G. P. Carruthers and G. A. Robinson (1973), Infrared Phys., 13, 149-155.
Harries, J. E., D. G. Moss, N. R. Swann, G. F. Neill and P. Gildwarg (1976), Nature, 259, 300-302.
Kendall, D. J. W. (1979), Ph.D. Thesis, Univ. of Calgary, Canada.
Kendall, D. J. W. and T. A. Clark (1978), Infrared Phys., 18, 803-813.
Kendall, D. J. W. and T. A. Clark (1979a), Appl. Opt., 18, 346-353.
Kendall, D. J. W. and T. A. Clark (1979b), J. Quant. Spectrosc. Radiat. Transfer., 21, 511-526.
Kendall, D. J. W. and T. A. Clark (1981), Int. J. Infrared & Millimeter Waves, 2, 783-809.
Mankin, W. G. (1975), Proc. Soc. Photo-Opt. Instrum. Eng., 67, 69-75.
Marten, A. and Y. Chauvel (1975), Infrared Phys., 15, 205-209.
Martin, D. H. and E. F. Puplett (1969), Infrared Phys., 10, 105-109.
Park, J. H., L. S. Rothman, C. P. Rinsland, M. A. H. Smith, D. J. Richardson and J. C. Lorsen (1981), NASA Reference Publication, 1084.
Pointer, R. L. and H. M. Pickett (1980), Submillimeter & Microwave Spectral Line Catalogue, JPL Publication, 80-23.
Rabache, P. (1977), J. Quant. Spectrosc. Radiat. Transfer., 17, 673-678.
Rebours, B. and P. Rabache (1979), Infrared Phys., 19, 107-113.
Rothman, L. S., A. Goldman, J. R. Gillis, R. R. Gamache, H. M. Pickett, R. L. Pointer, N. Husson and A. Chedin (1983a), Appl. Opt., 22, 1616-1627.
Rothman, L. S., R. R. Gamache, A. Barbe, A. Goldman, J. R. Gillis, L. R. Brown, R. L. Toth, J. M. Flaud and C. Camy-Peyret (1983b), Appl. Opt., 2, 2247-2256.
Stone, N. W. B. (1964), Ph.D. Thesis, Univ. of London.
Traub, W. A. and K. V. Chance (1981), Geophys. Res. Lett., 8, 1075-1077.

4. MICROWAVE LIMB SOUNDER FOR STRATOSPHERIC MEASUREMENTS

J. W. Waters, J. C. Hardy, R. F. Jarnot, H. M. Pickett, and P. Zimmerman

Jet Propulsion Laboratory
California Institute of Technology
Pasadena, CA 91109

ABSTRACT

The Balloon-borne Microwave Limb Sounder (BMLS) measures atmospheric thermal emission from millimeter wavelength spectral lines to determine vertical profiles of stratospheric species. The instrument flown to date operates at 205 GHz to measure ClO, O_3, and H_2O_2. A 63 GHz radiometer will be added to test the technique for determining tangent point pressure from the MLS experiment on the Upper Atmosphere Research Satellite (UARS). Many additional species could also be measured by the BMLS. A radiometer at 270 GHz would provide measurements of HO_2, NO_2, HNO_3, N_2O, $^{16}O^{18}O^{16}O$, and HCN. With this addition the BMLS can test the current theory of O_3 photochemical balance in the upper stratosphere.

INTRODUCTION

As part of NASA's Upper Atmosphere Research Program, a balloon-borne microwave limb sounder (BMLS) has been developed to perform measurements of the earth's stratosphere. The BMLS followed earlier development of an aircraft instrument for the same purpose (WATERS et al., 1979, 1980) and was a step towards development now underway of a similar instrument (WATERS et al., 1978) for the Upper Atmosphere Research Satellite (UARS) planned by NASA for launch in 1989.

The BMLS is the first use of microwave remote sensing techniques for limb sounding. Good reviews of the principles and application of microwave remote sensing are by STAELIN (1969), SCHANDA (1976), and NJOKU (1982). The major advantages of limb sounding over other viewing geometries are that (1) it provides the largest possible signals from species with small abundances, and (2) it has much better vertical resolution than ground-based or aircraft-based measurements which obtain vertical resolution from spectral line shape. Technology is now available for balloon-based instruments operating at frequencies below approximately 300 GHz (wavelengths longer than 1 millimeter). Advances in technology are currently being made which can provide instrumentation to much higher frequencies. Figure 1 illustrates some of the many species and spectral lines which are available for measurement in the 200-300 GHz frequency range alone. The species abundances which were used for the calculations in Figure 1 are given in Table 1. Spectroscopic data used for these calculations are from the JPL catalogue (POYNTER and PICKETT, 1981) with the latest revisions as of March 1984. Figure 2 compares the vertical resolution of limb sounding and ground-based or aircraft-based microwave measurements. Other general advantages of microwave sounding include (1) the composition measurements are very much less sensitive to uncertainties in the atmospheric temperature profile than are infrared emission measurements, and (2) continuous measurements can be made during both day and night. The major disadvantage of limb sounding is that the instrument must be above the atmospheric layer being measured to fully exploit the technique.

Development of the BMLS was motivated by the need for measurements of stratospheric ClO which is one of the best indicators of stratospheric ozone depletion by industrial chlorofluocarbons (CFCs) (e.g., MOLINA and ROWLAND, 1974; STOLARSKI and CICERONE, 1974; CRUTZEN et al., 1978; WUEBBLES, 1983). The ClO rotational line at 204.352 GHz was selected for measurement because of its

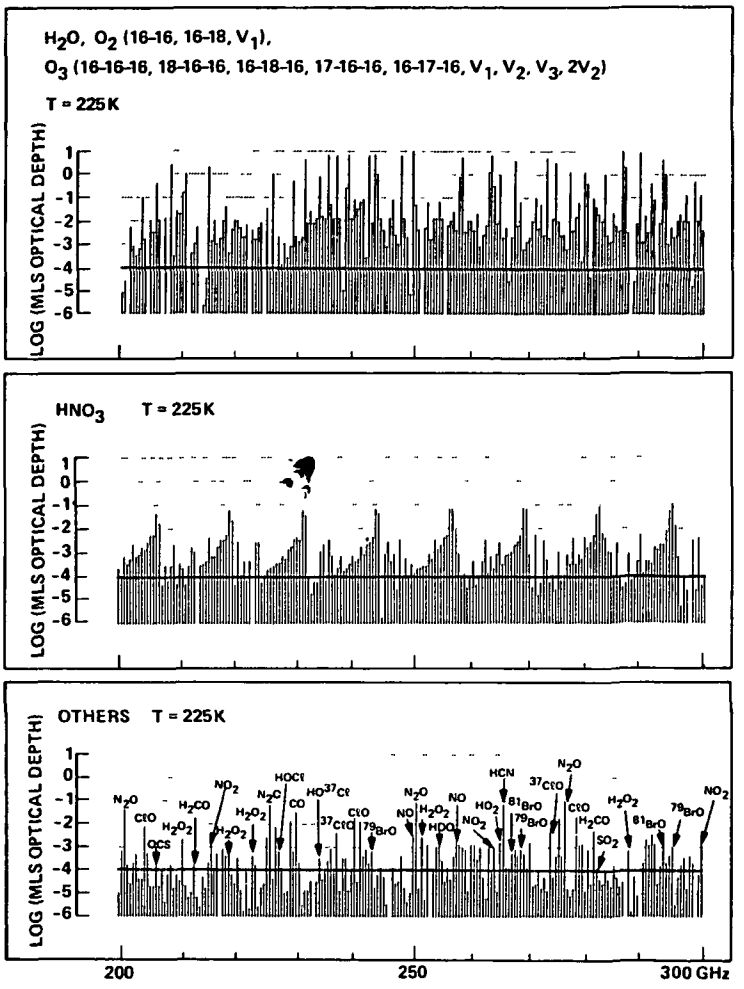

Figure 1. Atmospheric spectral lines in the 200-300 GHz range. The vertical scale is the logarithm of the calculated optical depth for a limb sound path through the middle stratosphere. Species abundances used for the calculation are in Table 1. Within each 0.5 GHz interval all spectral lines from a given species are summed. The heavy horizontal line is the approximate noise level for emission measurements using a state-of-the-art radiometer with a few minutes integration and spectral resolution to resolve the stratospheric lines.

freedom from interference by other atmospheric lines and to optimize measurement signal-to-noise. (Line strengths increase with frequency whereas instrument sensitivity decreases.) An O_3 spectral line at 206.132 GHz and an H_2O_2 line at 204.575 GHz were also selected for simultaneous measurement. The O_3 line was chosen because of the insensitivity of its emission to stratospheric temperature variations. A stratospheric temperature variation of 10°C changes the 206.132 GHz O_3 limb emission by only one per cent (WATERS, 1980). The H_2O_2 line was chosen because it could be measured by the same radiometer which measures ClO and O_3. Initial measurement results are described by WATERS et al. (1981).

Table 1. Stratospheric species abundances. Abundances given here are relative to total number density by volume. Species are listed in order of increasing mass.

Species	Log (Abundance)	Species	Log (Abundance)
H_2O	-5.3	$^{16}O^{17}O^{16}O$	-8.7
HDO	-9.1	$^{16}O^{16}O^{17}O$	-8.3
HCN	-9.8	$^{16}O^{18}O^{16}O$	-7.8
CO	-7.0	$^{16}O^{16}O^{18}O$	-7.5
H_2CO	-10.0	ClO	-9.4
NO	-8.0	HOCl	-9.8
O_2	-0.7	^{37}ClO	-9.9
HO_2	-9.7	$HO^{37}Cl$	-10.3
$^{16}O^{18}O$	-3.1	OCS	-10.7
H_2O_2	-9.5	HNO_3	8.7
N_2O	-7.0	SO_2	-11.0
NO_2	-8.0	^{79}BrO	-11.1
O_3	-5.2	^{81}BrO	-11.1

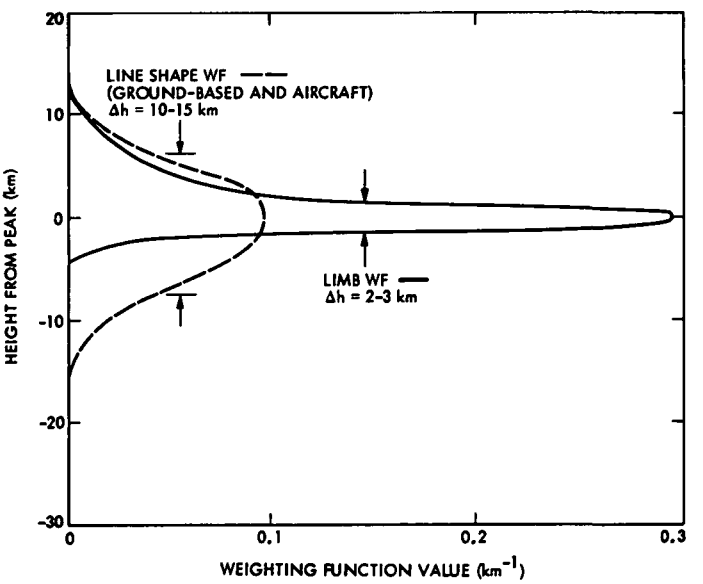

Figure 2. Weighting functions for limb and spectral line shape microwave measurements. These functions describe the vertical resolution of the technique; the measured signal is proportional to the integral, through the observed atmospheric path, of the product of this function and the mixing ratio of the species being measured. The curves shown here have been normalized to unity area. The limb curve includes smearing by the BMLS antenna when pointed at 15 km tangent height from a float height of 40 km; for higher tangent heights this curve is narrower. The line shape curve is calculated for infinitesimally spaced spectral channels with infinitesimal resolution.

INSTRUMENT DESCRIPTION

(a) Summary

The BMLS consists of (1) an antenna and optics system; (2) a heterodyne radiometer with three intermediate-frequency output bands; (3) electronic filter banks for spectral analysis; (4) command and data handling systems; (5) power supply and thermal control systems; and (6) a ground support system. An overall block diagram is shown in Figure 3. The BMLS mass (including batteries for a 24 hour flight) is approximately 350 kg and it consumes approximately 300 W power. Additional mass of the gondola required for a solo BMLS flight is approximately 300 kg.

(b) The Antenna and Optics

The antenna is an offset Cassegrain with a 50 cm diameter main reflector of machined aluminum. Vertical scanning of the field of view is performed by a flat mirror in front of the main reflector. This scanning mirror is pivoted at its lower end and discretely driven by a stepping motor-screw drive mechanism in 0.2° increments. A shaft encoder gives the mirror position. The scan sequence is read from a programmable memory. There are 64 scan positions available.

Figure 4 shows measured 205 GHz antenna patterns at every fourth scan position. The measured full width at half power points on the patterns is 0.30°. For a 40 km balloon float height this width corresponds to a vertical resolution at the limb of 3 km for an observation path having 15 km tangent height and 1.5 km for a path having 35 km tangent height.

(c) The Radiometer

Initial flights with the BMLS were with a radiometer having an ambient temperature second harmonic mixer (ZIMMERMAN and MATTAUCH, 1979) and a phase-

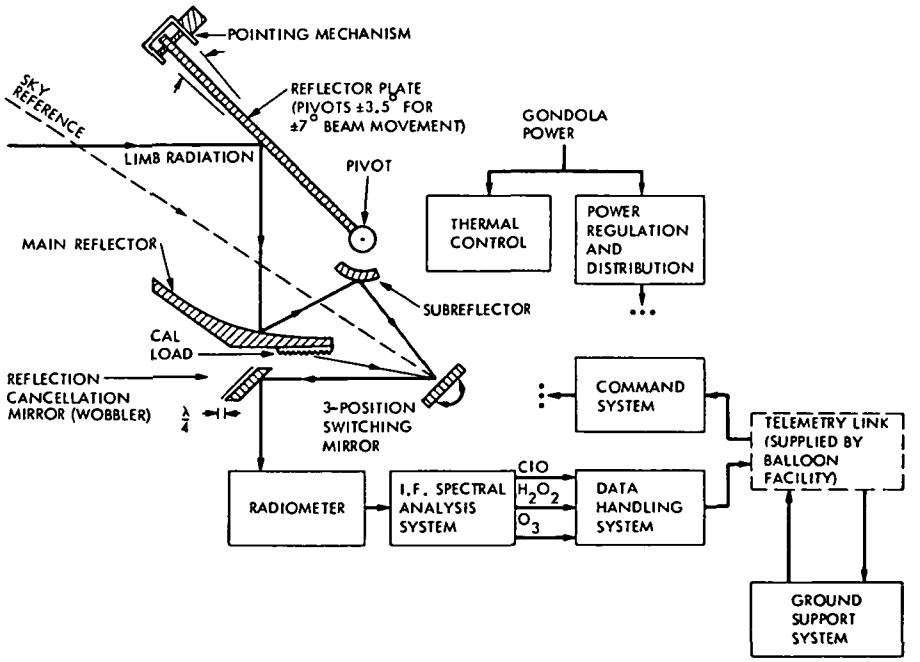

Figure 3. Overall BMLS block diagram.

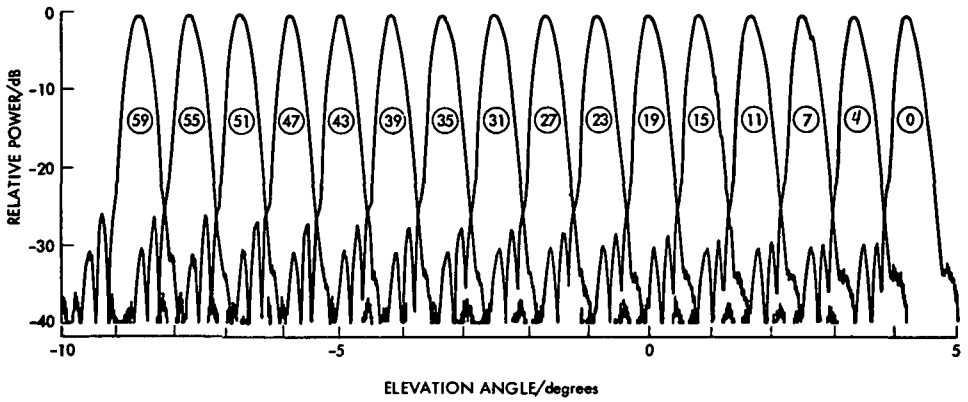

Figure 4. Measured BMLS antenna patterns. The circled numbers indicate the scan position for that pattern.

locked 104 GHz klystron local oscillator. The intermediate-frequency (i.f.) output of the mixer was split into one band at 4 GHz and another band at 2 GHz. GAS-FET amplifiers were used for the first stage amplification. The overall single sideband system noise temperature of this radiometer was approximately 10,000 K. (For microwave radiometry it is customary to measure power in terms of the equivalent temperature of a thermal source.)

To improve sensitivity by a factor of approximately 10, the initial BMLS radiometer has been replaced by a radiometer with a liquid nitrogen cooled mixer and preamplifier. A block diagram of the cooled radiometer is shown in Figure 5. The mixer, fabricated at JPL, is a fundamental waveguide mixer using Schottky diodes from the University of Virginia. A phase-licked commercial Gunn oscillator at 67.7556 GHz is tripled, using a waveguide multiplier developed at JPL, to provide the local oscillator at 203.2669 GHz. The local oscillator and signal from the BMLS antenna are combined with a folded quasi-optical Fabry-Perot whose design principles are discussed by PICKETT and CHIOU (1983).

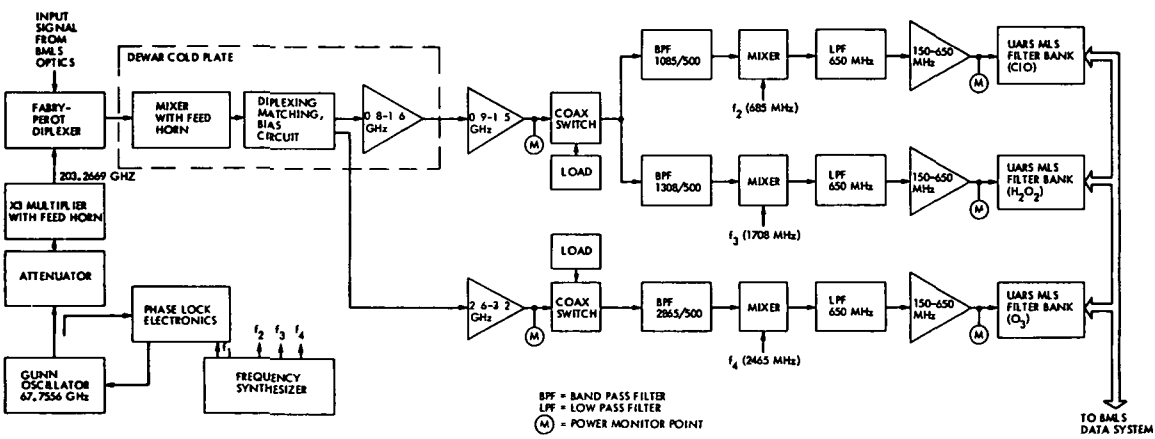

Figure 5. Block diagram of the cooled 205 GHz BMLS radiometer.

The optical layout is shown in Figure 6. This layout also indicates a dichroic plate where a beam will be separated for input to a 63 GHz radiometer which will be added to the BMLS to test the technique of measuring tangent point pressure on the UARS MLS. The layout also indicates the location of a polarization grid which can be used to separate the beam for a 270 GHz addition to the BMLS which is discussed later. The optical components were fabricated at JPL. The dewar was procured commercially; its 5 liter volume gives a measured hold time of approximately 80 hours.

Table 2 gives the noise budget for the radiometer. The rms noise ΔT for a filter bandwidth B and integration time t is obtained from the overall noise temperature T_N (given in this table) by the formula

$$\Delta T = CT_N/(Bt)^{1/2}$$

where C = 1 for total power measurements and C = 2 for square wave switching.

(d) The Spectral Analysis System

The three spectal bands are down-converted in frequency by heterodyning. Three identical filter banks then simultaneously perform spectral analysis of these bands.

The heterodyning arrangement used for BMLS flights performed to date is shown in Figure 7. For these flights each filter bank contained 35 filters.

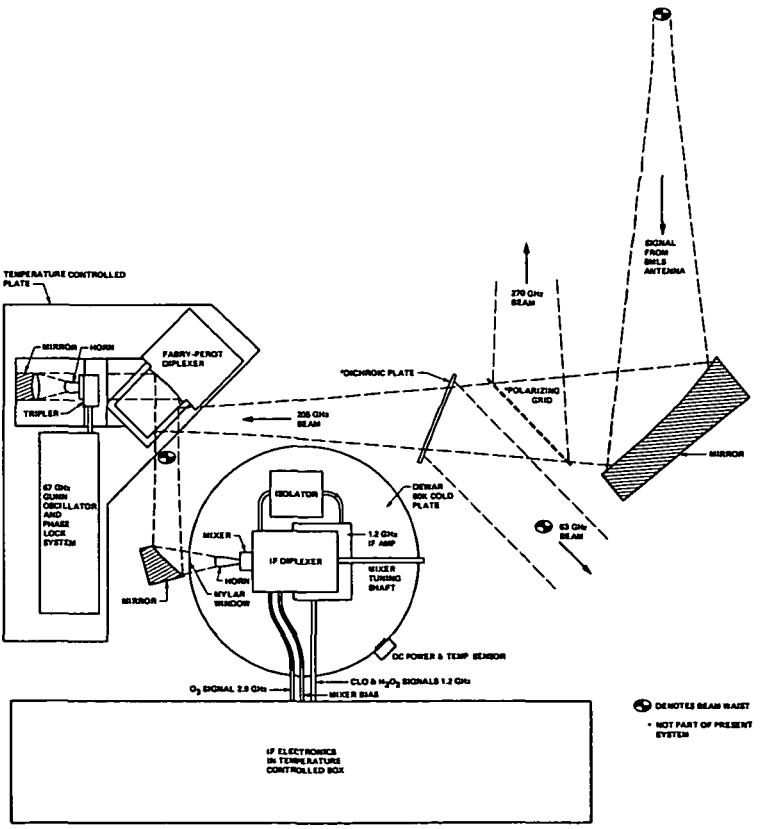

Figure 6. Optics layout of the cooled 205 GHz BMLS radiometer.

Table 2. Cooled 205 GHz BMLS radiometer noise budget. All values are measured and are single sideband.

	ClO and H_2O_2 band	O_3 band
loss before mixer (dB)	0.5	0.5
mixer conversion loss (dB)	8.0	8.0
mixer excess noise temperature (K)	600	600
i.f. diplexer loss (dB)	1.0	1.0
i.f. noise temperature (K)	30	200
overall noise temperature, T_N (K)	1000	2500

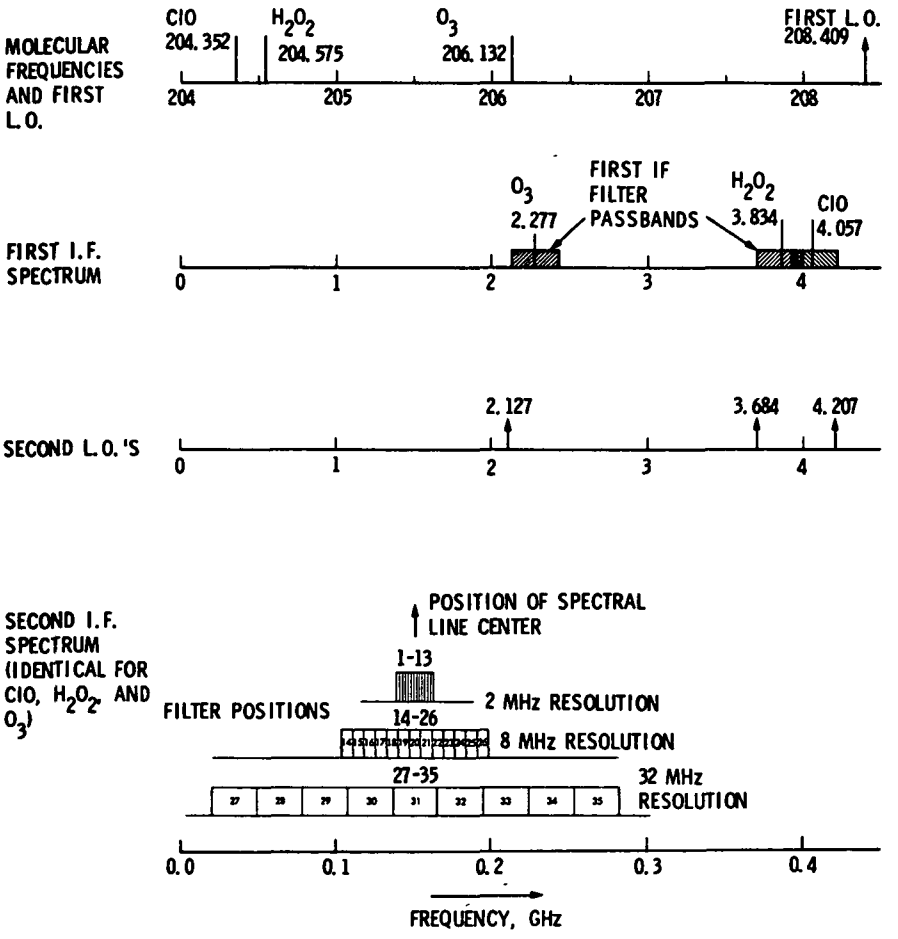

Figure 7. Heterodyning arrangement used on BMLS flights to date.

All filters operate simultaneously so that no spectral scanning is required. The individual filters were six-pole and constructed of discrete elements on printed circuit boards. Their positions and widths were chosen to fully cover and resolve the spectral lines. Three widths (nominally 2, 8 and 32 MHz) are used in the filters. Figure 8 shows examples of measured filter response. The output from each filter is detected with a square-law diode. The detected signal is then passed through synchronous filters which give two outputs proportional to the power received on the two halves of the switching cycle. Differencing of the signals from the two halves of the switching cycle is done during data analysis by the BMLS ground support system computer.

For future flights the BMLS filter banks are being replaced by copies of filter banks developed for the UARS MLS. These filter banks have a center frequency of 400 MHz and contain 15 channels. They are composed of both lumped element (L-C) and surface acoustic wave (SAW) filters and have better spectral characteristics, greater thermal stability, better integrators, and less digitization noise than the current BMLS filter banks. Table 3 gives the filter characteristics. Figure 9 shows their coverage of the 204 GHz CℓO line. The horizontal width of each bar indicates the width for that filter. The vertical bar gives the rms instrument noise with a one minute integration for measurements in total power mode and, equivalently, for a four minute integration for measurements with a 50 percent chopping as was the case in previous BMLS flights. The amount of chopping required will be between these limits and must be determined by tests on the full system after it is completely assembled.

The power at each filter output is measured by a tunnel diode detector, chosen because of its low noise and low thermal drift. An input matching network provides a nominal -31 dBm power level which is well within the tunnel diode square law range, and which gives an output voltage of approximately 1 mV.

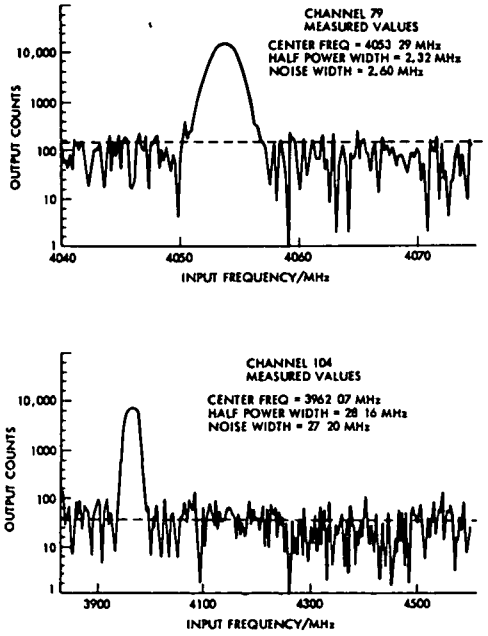

Figure 8. Examples of measured BMLS filter response. Top: a narrow bandwidth filter; Bottom: a broad bandwidth filter. The noise at the dashed line level is due to the measurement scheme.

Table 3. UARS MLS filter bank characteristics.

Channel	Center frequency f_o (MHz)	3 dB Bandwidth B (MHz)	Percentage Bandwidth (B/f_o x 100%)	Filter Type
1	209	128	61.2	L-C
2	305	64	21.0	L-C
3	353	32	9.1	L-C
4	377	16	4.2	L-C
5	389	8	2.1	SAW
6	395	4	1.0	SAW
7	398	2	0.5	SAW
8	400	2	0.5	SAW
9	402	2	0.5	SAW
10	405	4	1.0	SAW
11	411	8	1.9	SAW
12	423	16	3.8	L-C
13	447	32	7.2	L-C
14	495	64	12.9	L-C
15	591	128	21.7	L-C

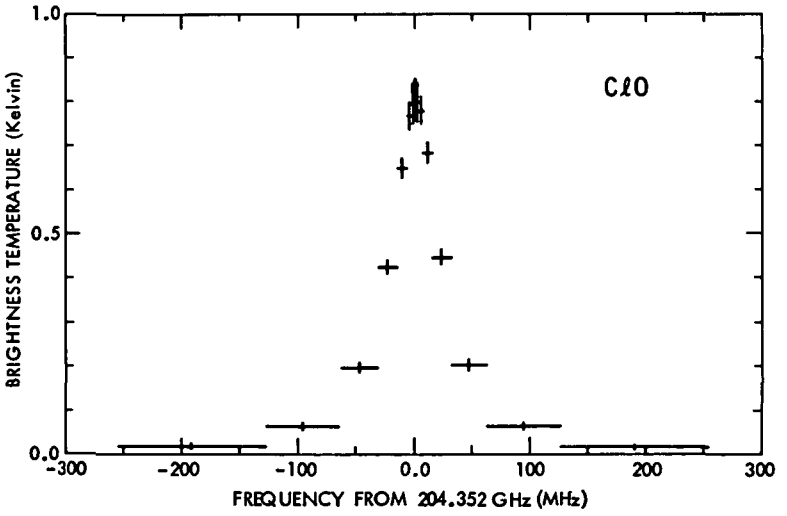

Figure 9. Coverage of the 204.352 GHz ClO spectral line by the UARS MLS filter bank.

A low noise/low drift Precision Monolithics OP-27E operational amplifier provides first stage amplification of the signal from the detector. This signal is further amplified by a National LM108A operational amplifier to a level of approximately 3 volts. The voltage is then applied to a voltage to frequency converter whose output is counted for 1.8 s, and the counter contents read by the data handling system.

(e) The Command and Data Handling System

A block diagram of the BMLS command system is shown in Figure 10 and a block diagram of the data handling system is shown in Figure 11. These systems interface the BMLS with the telemetry system of the balloon launch facility.

(f) Power Supply and Thermal Control Systems

Electrical power for the BMLS is provided by lithium cell batteries. Typically, a flight will include approximately 15 packs of 11 cells per pack. This provides approximately 450 ampere hours at 28 volts. The battery voltage is converted and regulated to various dc voltages required by BMLS subsystems.

During flight the instrument is thermally insulated by completely covering the gondola and certain subassemblies with thermal insulation. The optical path in front of the antenna is covered with 4 cm thick styrofoam which has a loss at 205 GHz measured to be less than 1%. Polyethylene foam, which is more resistant to ultraviolet, is used elsewhere for thermal insulation. Thermal control is by regulating the exchange of heat between the instrument and a radiator plate. Heat exchange is by circulating ethylene glycol between the heat producing elements and the radiator. Regulation is by feedback control of the pumps which circulate the coolant fluid. There are three separate thermal control circuits which independently regulate (1) the local oscillator assembly, (2) the intermediate frequency amplifier assembly, and (3) the filter banks and data system assembly.

Figure 12 shows selected BMLS temperatures throughout the flight of 11 May 1981 from the National Scientific Balloon Launch Facility in Palestine, Texas (32°N). Also shown is the balloon height and outside air temperatures. Below

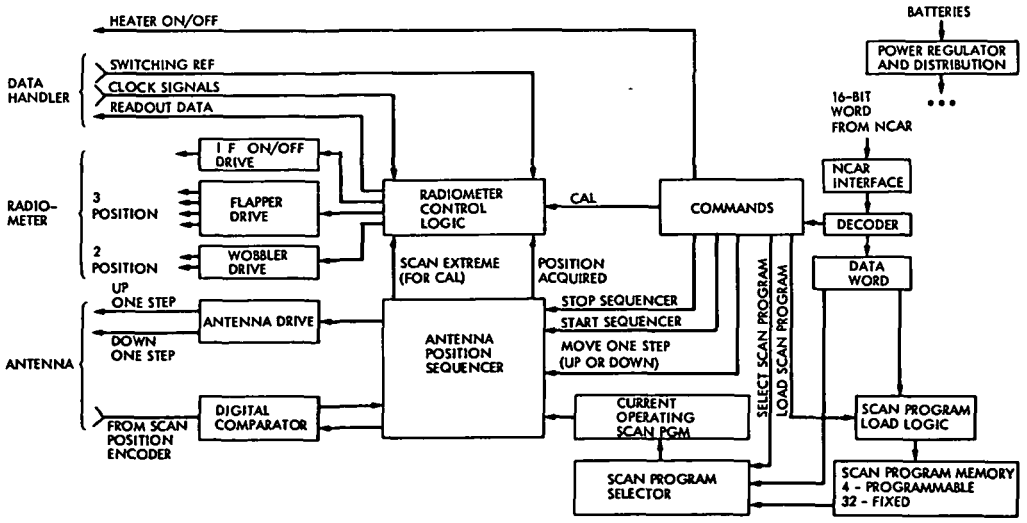

Figure 10. The BMLS command system.

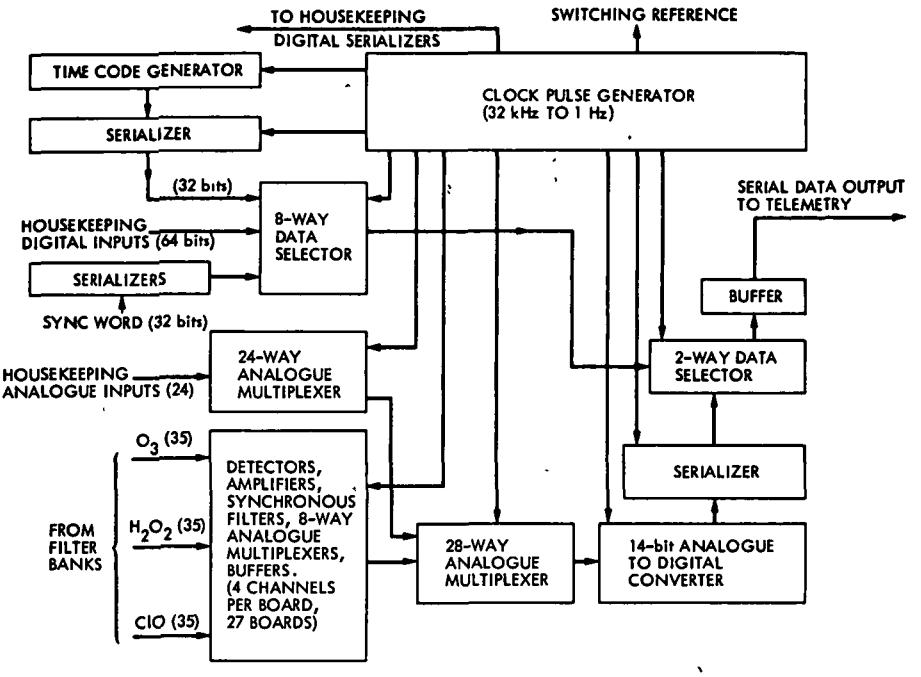

Figure 11. The BMLS data handling system.

40 km the outside air temperatures were measured by a radiosonde launched from Longview, Texas (~100 miles north of Palestine), at approximately 6 a.m. on 12 May 1981. The outside air temperature at 40 km is from climatology for 30°N May (CIRA, 1972).

(g) The Ground Support System

The BMLS ground support system processes the data stream received from the balloon launch facility telemetry. It produces a magnetic tape record of the unprocessed data, performs averaging and initial calibration of radiometric data, and provides outputs needed for in-flight decisions. The system is based on a Hewlett-Packard HP-1000 computer and is housed in an air-conditioned air-ride trailer which is taken to the launch facility for flights.

During flight several programs are simultaneously run on the ground support system computer. The first program receives the data frame from the telemetry, produces a one-line screen output indicating the data were received and the antenna scan position and other information on the data frame, and integrates the data by either a preset integration time or whenever a configuration change (e.g., change in scan position) occurs in the instrument. The second program reads a data buffer produced by the first program, performs calibration of the data and stores it in a disc file, and creates a log output describing the received data. A third program produces a continuous screen display, with optional hard copies, of all engineering data. A fourth program accesses the disc files of calibrated data and performs various operations on these data such as averaging and plotting.

DATA ANALYSIS

The first step in data analysis is to radiometrically calibrate the outputs from the BMLS filter channels. This is accomplished by using the linearity of

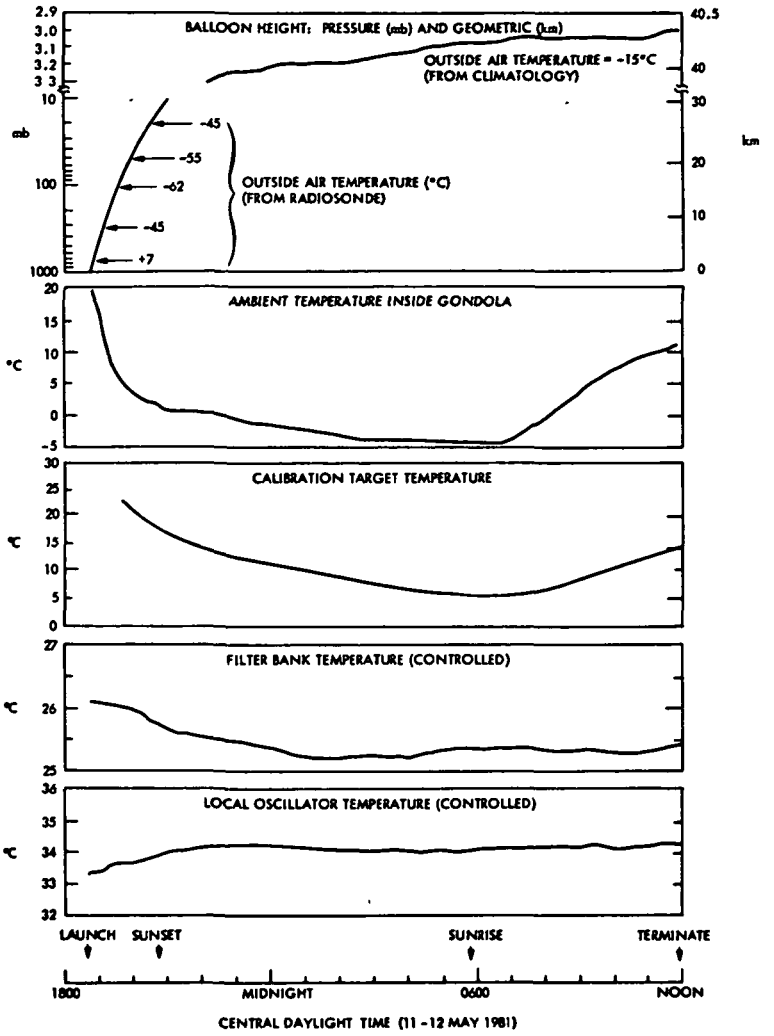

Figure 12. Measured temperatures during the BMLS flight of 11 May 1981. The balloon height and outside air temperatures are also shown.

the detected filter output relative to the input power and two calibration references. One calibration reference is the ambient temperature target at the radiometer input. The second calibration is the "sky view" at approximately 50 degrees elevation. Tests on the current BMLS indicate this calibration is accurate to approximately 5%. Plans are underway to add the UARS MLS calibration target to the BMLS which should provide 1% or better calibration accuracy.

A second step in data analysis is to calibrate the BMLS pointing. The pointing reference is the sharp increase in water vapor emission as the BMLS field-of-view is scanned downwards through the tropopause. The measured increase in emission is compared with that calculated for the water vapour distribution from radiosonde measurements made at nearly the same time and place as the BMLS measurements. Figure 13 shows results from the 22 September 1983 flight in which there was an 0.3° offset between nominal and inferred pointing. The theoretical expressions for calculating the water vapor emission are given

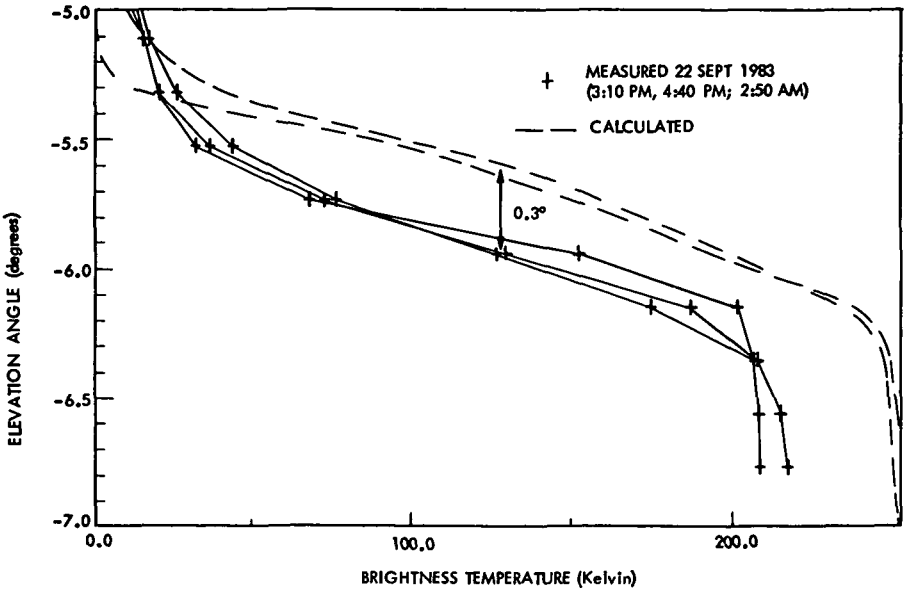

Figure 13. Measured and calculated emission for the BMLS field-of-view scanned through the tropopause. On this flight the pointing was approximately 0.3 degrees (one beamwidth) from the nominal a priori value. Approximately 15% loss in the optics accounts for the difference between measurement and calculation below -6.3 degrees elevation. The two calculated curves are for 0 and 15% relative humidity between 10 and 18 km. The radiosonde measurement of humidity stopped at 10 km where 15% relative humidity was measured.

in WATERS (1976); the Van Vleck - Weisskopf line shape was used and the Gaut - Reifenstein empirical correction was included. Calculated emission was also compared with ground-based measurements of 205 GHz emission versus elevation angle at a time when the total column water vapor was measured by an infrared solar absorption instrument calibrated against radiosonde measurements. The comparison between measurements and calculation is shown in Figure 14. Agreement is within 10% which translates to a BMLS pointing error of approximately 0.1 degree or less.

The calibrated BMLS data are then used in a retrieval process to obtain vertical profiles of the species being measured. The retrieval technique now being used for the BMLS is one of constrained least squares. Say $\{p_j\}$ are a set of parameters to be estimated, e.g., points on a vertical profile. We make an initial estimate of these parameters and from them calculate the brightness temperature $\tilde{T}_{B_i}$ for BMLS channel i

$$\tilde{T}_{B_i} = \iiint W(\{p_j\}, \ldots)\, ds\, d\nu\, d\Omega \qquad (1)$$

where the integrations are over the observation path s, solid angle Ω, and channel frequency interval ν. The antenna gain pattern, filter spectral characteristics, and effects of radiative transfer and other atmospheric parameters are included in $W(\{p_j\}, \ldots)$. From the preceding equation we numerically calculate the partial derivation C_{ij}

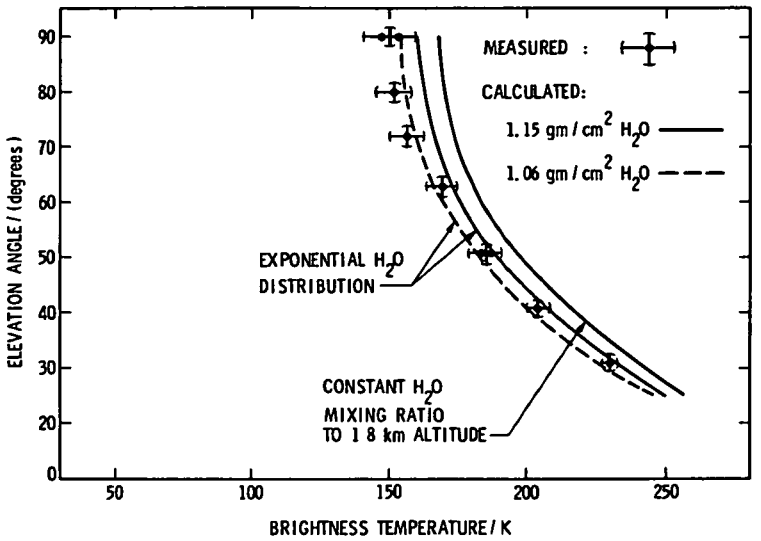

Figure 14. Comparison of ground-based measurements and calculations of atmospheric emission at 205 GHz. At the time and place of the 205 GHz measurements a calibrated infrared solar absorption instrument measured 1.1 ± 0.1 gm/cm^2 vertically integrated water vapor. Calculations are given for 1.06 and 1.15 gm/cm^2 integrated water vapor.

$$C_{ij} = \partial \tilde{T}_{Bi} / \partial p_j \tag{2}$$

Expanding (1) in a Taylor series of Δp_j about p_j and keeping linear terms gives

$$\underline{\tilde{T}}_B' = \underline{\tilde{T}}_B + \underline{\underline{C}} \cdot \Delta \underline{p} \tag{3}$$

where a single underline indicates a vector and a double underline indicates a matrix. We now require that the difference between calculated brightness $\underline{\tilde{T}}_B$ and measured brightness $\underline{T}_B$ be approximately equal to the measurement noise

$$\epsilon^2 \triangleq (1/N) \sum_i (T_{B_i} - \tilde{T}_{B_i})^2 \tag{4}$$

where ϵ is the rms measurement noise and N is the number of measurement channels. If we require better agreement than this, then we will likely retrieve a profile fit to noise which is undesirable. Equation (4) imposes a constraint on the solution for Δp_j. As written above it assumes equal noise in all channels; modification for unequal channel noise is straightforward.

In general there is no unique solution for Δp_j due to the smearing described by the integrals in (1) and due to uncertainties introduced by measurement noise. We must establish a criterion for choosing one of several possible solutions which agrees with the measurements to within the noise. One reasonable criterion is choosing the "smoothest" profile consistent with (4). The smoothest profile as measured by the second differences of the points on the profile is obtained by minimizing the scalar quantity

$$s^2 = \underline{p}^T \cdot \underline{\underline{K}}^T \cdot \underline{\underline{K}} \cdot \underline{p} \tag{5}$$

where superscript T indicates transpose and the square matrix K is given by

$$\underline{\underline{K}} = \begin{matrix} 0 & 0 & 0 & 0 & \cdot & \cdot & \cdot \\ -1 & 2 & -1 & 0 & & & \\ 0 & -1 & 2 & -1 & & & \\ 0 & 0 & -1 & 2 & & & \\ \cdot & & & & 2 & -1 & 0 \\ \cdot & & & & -1 & 2 & -1 \\ \cdot & & & & 0 & 0 & 0 \end{matrix} \qquad (6)$$

whose number of rows and columns equals the number of elements in the parameter vector.

Minimizing (5) subject to the constraint (6) gives the solution

$$\underline{\Delta p} = [\underline{\underline{C}}^T\underline{\underline{C}} + \zeta\underline{\underline{K}}^T\underline{\underline{K}}]^{-1} \cdot \underline{\underline{C}}^T \cdot (\underline{T}_B - \underline{\tilde{T}}_B) \qquad (7)$$

which can be integrated if necessary to account for nonlinearities. The parameter ζ in (7) determines the relative weight given to smoothing versus fitting to measurement. If ζ is chosen to be zero no weight is given to the smoothing requirement and the standard least squares solution is obtained; as ζ is made larger less weight is given to the measurement. In practice ζ is set to the value which makes the difference between calculated and measured brightness equal the noise. Selection criteria other than maximum smoothness as defined by second differences can be implemented simply by changing the form of $\underline{\underline{K}}$ from that given in (6). TWOMEY (1977) gives some examples and further discussion of this point. RODGERS (1976) gives a more sophisticated and comprehensive discussion of retrieval techniques. One feature of microwave limb sounding which is of significance to the retrieval process is that only those elements of the data vector $\underline{T}_B$ which correspond to optically thin signals at all points in the spectral channel being measured are included in the retrievals. This makes the procedure much more linear than would otherwise be the case and, for example, means that the partial derivatives (2) need only be calculated once.

This profile retrieval technique was used to determine the accuracy of obtaining ClO and O_3 profiles from the BMLS measurements. In this process the BMLS measurement is simulated by calculating the emission for a specific profile. This simulated measurement is then used in the retrieval algorithm to obtain a profile which is compared with the original profile. Error bars for the retrieved profile points are obtained from the retrieval matrices using the expected measurement noise. For simulated retrievals shown below, the species mixing ratio profile was represented as a continuous piece-wise linear function. Values at the ends of the individual linear segments were inferred by the retrieval process. The smoothing parameters ζ was set to zero in order to obtain independence of the different points.

Results of the ClO retrieval simulations are shown in Figure 15. The two cases shown are, respectively, for mid-day and midnight ClO profiles as predicted by current theory. The simulated measurement was for the 15 UARS MLS filters, eight elevation angles, and a typical balloon altitude of 40 km. The error bars are for an integration time per elevation angle corresponding to 1 minute for non-switched (or 4 minute for switched) operation of the radiometer. Thus, complete profiles with the accuracies indicated in Figure 15 should be possible with time resolution of between 8 and 32 minutes.

Results of the O_3 retrieval simulations are shown in Figure 16. As for the ClO retrievals, the simulated measurement was for the 15 UARS MLS filter channels and eight elevation angles from 40 km height. The error bars are for the same integration time as for ClO and for the larger system noise temperature of the O_3 band (see Table 2). These results indicate that very accurate O_3 profiles can be retrieved from the BMLS measurement. They also demonstrate the

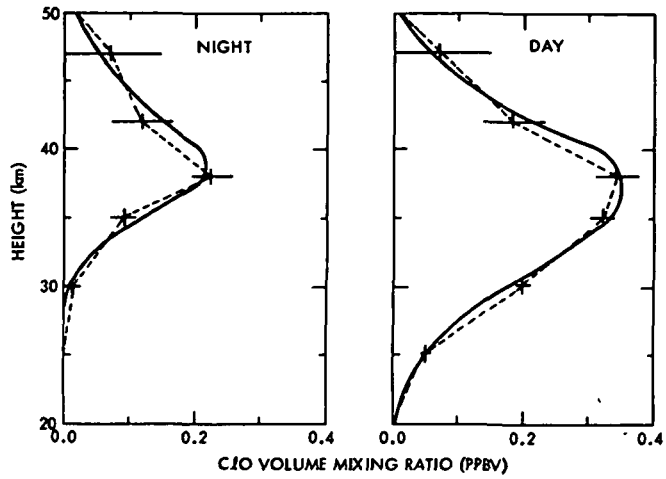

Figure 15. Results of simulated ClO retrievals. The solid curves are the "true" profiles and the dashed curves the retrieved. The horizontal extent of the crosses on the retrieved profiles indicate their rms uncertainty for the measurement sensitivity of the instrumentation discussed in the text with one minute total power integration time at each of eight elevation angles. Profile points above 40 km have degraded accuracy because they are obtained from the information in the spectral line shape instead of information in the limb scan.

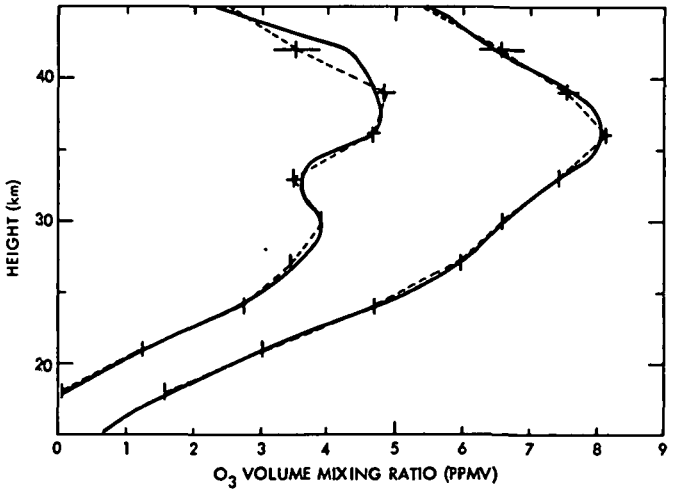

Figure 16. Results of simulated O_3 retrievals. The two profiles are, respectively, for the KRUEGER-MINZNER (1976) standard O_3 profile and this standard profile minus three standard deviations as also given by Krueger-Minzner. The solid curves are the "true" profiles and the dashed curves the retrieved. The horizontal extent of the crosses on the retrieved profiles indicate their rms uncertainty for the measurement sensitivity as discussed in the text.

capability of the technique to measure vertical structure with 3 km or better resolution.

MEASUREMENTS OF HO_2, NO_2, HNO_3, HCN, N_2O AND $^{16}O^{18}O^{16}O$ BY ADDING A 270 GHz RADIOMETER TO THE BMLS

Understanding of the stratosphere is now so sufficiently advanced that simultaneous measurements of several species are extremely important, if not essential, for further progress. In order to make such measurements practical, both logistically and economically, it is desirable to obtain several species from single instruments. In the case of the BMLS, many additional species could be measured as suggested in Figure 1. However, because of resource limitations, compromises must be made. One very attractive compromise is to add to the BMLS a single 270 GHz radiometer which simultaneously measures six additional species of HO_2, NO_2, HNO_3, HCN, N_2O and $^{16}O^{18}O^{16}O$. This radiometer also simultaneously measures O_3.

Some specific justifications for these additional measurements are discussed in the following subsections.

(a) Test of O_3 Photochemical Balance

The largest percentage depletion of O_3 by CFC's is predicted to occur between heights of 30 and 45 km. Current theory (WUEBBLES, 1983) predicts a 40% O_3 depletion at 40 km if CFC releases continue at their present rate. This region should thus provide the best early warning of these effects. The chemistry there is expected to be less complex than at lower altitudes, and reactions are sufficiently fast that transport processes should not upset photochemical balances. One expects, therefore, the theory for this region to be more reliable than for lower altitudes. However, there is a serious discrepancy between measured and calculated O_3 abundances above about 35 km. Measurements are approximately 50% higher than calculated, as shown in Figure 17. The discrepancy is not likely due to measurement errors, as several measurement techniques have yielded similar results. It is also not likely due to O_3 variability, which is measured to be less than approximately 20% at these heights. This discrepancy must be resolved in order to have confidence in the theory.

The O_3 photochemical balance expected to occur above about 35 km can, when second order effects are neglected, be written (e.g., FROIDEVAUX, 1983; see also ANDERSON et al., 1980):

$$J_{02}[O_2] = (J_{03}[O_3]/k_1[O_2][M])(k_2[O_3] + k_3[HO_2] + k_4[NO_2] + k_5[ClO])$$

where [A] is abundance of species A. The left side is the O_3 production rate, limited by the rate J_{02} of breaking the O_2 bond. The right side is the O_3 destruction rate. The first factor on the right is the predicted abundance of atomic O, in equilibrium between O_3 photolysis at rate J_{03} and recombination with O_2 (in the presence of another molecule M) at rate k_1. The rate constants k_2, k_3, k_4, k_5 refer, respectively, to the O_3 destruction rate-limiting reactions: $O + O_3$, $O + HO_2$, $O + NO_2$, and $O + ClO$.

All abundances in the above equation are measured by the BMLS with the 270 GHz addition ($[O_2]$ and [M] are obtained from the 63 GHz pressure measurements which will be made when the UARS 63 GHz radiometer is added to the BMLS). This provides the possibility of the BMLS performing a needed test of the O_3 photochemical balance. Such a test, which has not been done to date, should give valuable insight concerning the cause for the discrepancy between measured and calculated O_3 in the upper stratosphere.

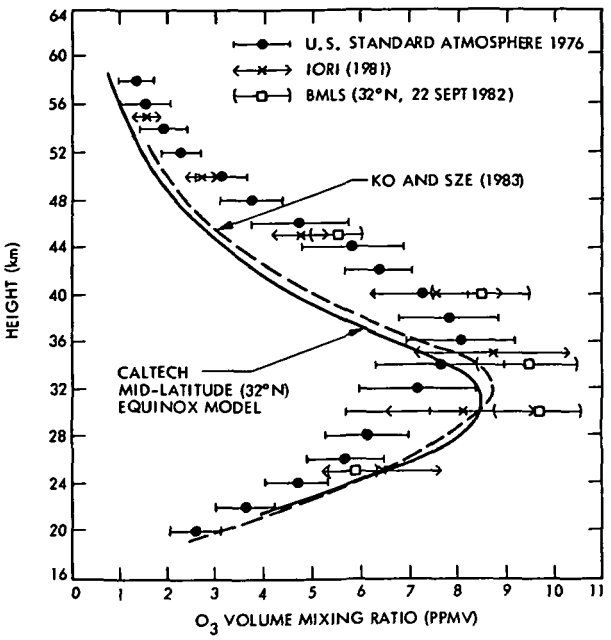

Figure 17. Measured and theoretical O_3 profiles. The mid-latitude Caltech equinox model is shown (see FROIDEVAUX (1983)). the KO and SZE profile is also theoretical, for equinox and 30°N. The U.S. Standard Atmosphere Profile is that of KRUEGER and MINZNER (1976) based on measurements. The IORI profile was measured during an international ozone rocket intercomparison campaign. The BMLS measurements made on 22 September 1982 from Palestine, Texas (32°N) are also shown. The full widths of the horizontal bars on all measurements are two standard deviations.

The accuracy of the BMLS O_3 photochemical balance test can be estimated by considering the relative importance of the various terms in the balance equation, and the accuracy with which the BMLS can measure the respective abundances. At 35-40 km altitudes the relative importance of the terms in the second factor on the right side of the balance equation are (FROIDEVAUX, 1983) $k_2[O_3] \sim 10\%$; $k_3[HO_2] \sim 10\%$; $k_4[NO_2] \sim 60\%$; $k_5[ClO] \sim 20\%$. The appropriate abundances which go into the equation are daytime averages, so a reasonable time to allow for the BMLS measurements is one hour. With one hour integration the BMLS accuracies for daytime measurements will be: $\sim 1\%$ for O_3, $\sim 5\%$ for HO_2, $\sim 25\%$ for NO_2, and $\sim 5\%$ for C O. Thus the uncertainty in the test due to BMLS daytime measurement uncertainty will be $\sim 20\%$. Additional uncertainty will be introduced by uncertainties in J_{02}, J_{03} and k_n. The uncertainty in J_0 and J_{03} should be less than 10% (Froidevaux, private communication; the BMLS measurement gives total O_3 overburden which reduces uncertainty in J_{03}). The effects of uncertainties in k_n should also be less than 10% (these have been measured and the atmospheric temperature profile at the time of BMLS flights is also measured which allows the k_n temperature-dependence to be accounted for). Thus, an overall accuracy of $\sim 30\%$ is expected for the O_3 photochemical balance test from daytime BMLS measurements. This accuracy is useful since the discrepancy between measured and calculated O_3 in the upper stratosphere is $\sim 50\%$. (It should be possible to further improve the accuracy of the test by using the more accurate BMLS nighttime NO_2 measure-

ments to help infer average daytime NO_2 values; M. Allen, private communication.)

Since the uncertainty in the BMLS O_3 photochemical balance test is largely dominated by the uncertainty in the NO_2 measurement, simultaneous NO_2 measurements by other techniques would be very desirable. A technique which can provide these measurements both day and night, as well as measurements of the important related species NO, is balloon-borne infrared pressure-modulated radiometry (PMR), (DRUMMOND and JARNOT, 1978; ROSCOE et al., 1981). A balloon PMR can be flown together with the BMLS.

It would also be very desirable to have simultaneous measurements of [O] to independently test the validity of the first factor on the right side of the preceding photochemical balance equation. One measurement has been performed which indicates this expression is valid (see WMO, 1908; Figure 1-54) more evidence for its validity is needed, since as noted by FROIDEVAUX (1983), the measured O_3 abundances in that test were substantially lower than most O_3 measurements (and in atypical good agreement with theory).

(b) HO_2

Microwave spectroscopy is the only demonstrated method for remotely measuring HO_2 (DE ZAFRA et al., 1984) which, with OH, is intimately involved in all of what are now thought to be the major catalytic cycles of stratospheric O_3 destruction.

HO_x strongly influences the NO_x catalytic destruction of O_3 by reactions such as:

$$HO_2 + NO \rightarrow NO_2 + OH$$

and

$$NO_2 + OH + M \rightarrow HNO_3 + M$$

where the HNO_3 diffuses downward and is removed by rain.

HO_x increases the $C\ell O_x$ catalytic destruction of O_3 by converting inactive chlorine in $HC\ell$ to active atomic chlorine by the reaction

$$OH + HC\ell \rightarrow H_2O + C\ell$$

HO_x itself catalytically destroys O_3 by reactions such as:

$$OH + O_3 \rightarrow HO_2 + O_2$$

and

$$HO_2 + O \rightarrow OH + O_2$$

and by a similar chain where HO_2 reacts with O_3.

Thus, knowledge of the distribution and variation in stratospheric HO_x is key to general understanding of stratospheric O_3 destruction. Below about 40 km HO_2 is expected to be the most abundant stratospheric species of HO_x but only a few stratospheric HO_2 measurements have been made to date.

Chemical models of the stratosphere are especially sensitive to the OH/HO_2 ratio and, for a specific test of stratospheric chemistry theory,

simultaneous OH measurements are needed with HO_2. Such measurements could be made from a single balloon carrying the BMLS and submillimeter or far-infrared instruments. It would also be desirable to simultaneously measure H_2O and other chemically coupled species; this could also be done from the same balloon.

(c) NO_2, HNO_3, N_2

These species have key roles in the NO_x catalytic destruction of O_3 which is predicted to account for approximately 70% of total O_3 destruction. Understanding of this catalytic cycle is crucial.

NO_2 is a key radical in the cycle, for which the rate limiting reaction is

$$NO_2 + O \rightarrow NO + O_2$$

which, coupled with

$$NO + O_3 \rightarrow NO_2 + O_2$$

destroys O_3. However, there are only a limited number of NO_2 measurements and most of these were taken during sunset or sunrise which does not observe the diurnal variation in NO_2. The BMLS NO_2 measurements throughout a complete diurnal cycle could provide this essential information. These will be especially valuable when made simultaneously with NO measurements.

HNO_3 removes active NO_x from the lower stratosphere by downward diffusion and rainout. Above 25 km, theoretical models of the stratosphere have predicted significantly more HNO_3 than measured, by as much as a factor of 3 at 30-35 km (e.g., WMO, 1981). Very recent models, e.g., FROIDEVAUX (1983) may have reduced this discrepancy, but more reliable measurements of connected species are needed. A specific test of model predictions would be obtained by simultaneous measurements of HNO_3, NO_2 and OH, all of which could be performed throughout a complete diurnal cycle from a single balloon carrying the BMLS and far infrared or submillimeter instruments for OH.

N_2O, upwardly transported from the troposphere and oxidized by $O(^1D)$, provides the major source of stratospheric NO_x. The measurement of the decrease in stratospheric N_2O mixing ratio gives information on this source and transport processes.

(d) HCN

Stratospheric HCN has been measured from aircraft-based infrared solar absorption by COFFEY et al. (1981), and from balloon-based submillimeter thermal emission by CARLI et al. (1982). Only very recently (CICERONE and ZELLNER, 1983) has a stratospheric model been developed which includes HCN chemistry. Predictions of HCN from this model agree with the Coffey et al., measurements in the lower stratosphere, but are a factor of 2 below the Carli et al., measurements at 40 km. The BMLS measurements of HCN will extend to 40 km or higher, and will provide additional data needed to test the model.

(e) $^{16}O^{18}O^{16}O$

Balloon-borne mass spectroscopic measurements of MAUERSBERGER (1981) show a pronounced altitude-dependent enchancement of heavy ozone (O_3, containing one ^{18}O atom). The measured enhancement is largest at 32 km altitude where it is a factor of 1.4 above the expected $^{18}O/^{16}O$ ratio. Although enhanced photodissociation of heavy O_2 in the upper stratosphere is predicted (CICERONE and MCCRUMB, 1980; BLAKE et al., 1983), reactions between ^{18}O and $^{32}O_2$ are

sufficiently fast that no such enhancement in the abundance of ^{18}O or heavy ozone is expected (FROIDEVAUX, 1983; KAYE and STROBEL, 1983). Thus, the Mauersberger heavy ozone measurements are inconsistent with current theory and it is important that they be checked.

(f) O_3

The BMLS 270 GHz radiometer also measures a strong ozone line at 276.923 GHz. This line provides an independent check on the current BMLS ozone measurement using the 206.132 GHz line. Such a check is important to help verify that ozone measurements can be performed by the BMLS and UARS MLS to the expected accuracy of approximately 1 per cent.

EXPECTED 270 GHz SIGNALS AND MEASUREMENT ACCURACY

The signals expected for the 270 GHz measurements can be determined by using the expected stratospheric abundances of the respective species in an atmospheric radiative transfer calculation (see, e.g., WATERS, 1976). The calculations done here break the atmosphere into layer approximately 0.5 km thick and integrate the radiative transfer equation through the limb path, accounting for spherical atmospheric geometry. The full Voigt spectral line shape and the 1976 U.S. Standard Atmosphere model of temperature and pressure are used. Strengths of the respective lines, and their temperature dependence, were taken from the JPL catalogue (POYNTER and PICKETT, 1981), with latest revisions as of March 1984, and are believed accurate to 1% or better (all appropriate dipole moments are known to 0.1% and uncertainties in the transition matrix elements do not exceed 1%). Line width uncertainties introduce less than 5% uncertainty in retrieved profiles, based on simulated retrievals; this is due to height information being obtained principally from limb scan and not line shape. Frequencies of all the lines have been measured to the required accuracy.

Figures of calculated signal levels given in the following subsections also include a cross showing the noise level of the 270 GHz instrumentation (described later) for an indicated integration time. The vertical extent of this cross is 2 standard deviations for the instrument operated in non-switched mode and 1 standard deviation for square-wave switching.

(a) HO_2

Expected abundances of HO_2 are shown in Figure 18. The recent ground-based measurements of DE ZAFRA et al. (1984) have now demonstrated that HO_2 can be measured from microwave emission lines near 270 GHz. In fact, this is the only demonstrated method by which HO_2 can be remotely measured.

Figure 19 shows calculated emission from the 265.770 GHz HO_2 line which is one of the triplet of HO_2 lines near 265.7 GHz measured by DE ZAFRA et al. (1984). All three of the HO_2 triplets would be simultaneously measured by the BMLS 270 GHz radiometer. A pressure-broadening coefficient of 3.1 MHz/mb at T=300 K with $T^{-0.75}$ temperature dependence was used for the calculation, following DE ZAFRA et al. (1984). The curves in Figure 19 indicate the expected range of daytime HO_2 signals. The lower profile 2 is consistent with the de Zafra et al., ground-based measurement.

Since there is a significant mesospheric contribution to the HO_2 signal, it is difficult to estimate, from only measurement signal-to-noise, the accuracy with which stratospheric HO_2 profiles can be retrieved from BMLS measurements. To determine this accuracy we used the profile retrieval procedure described earlier. Results are shown in Figure 20. The simulated measurement for these

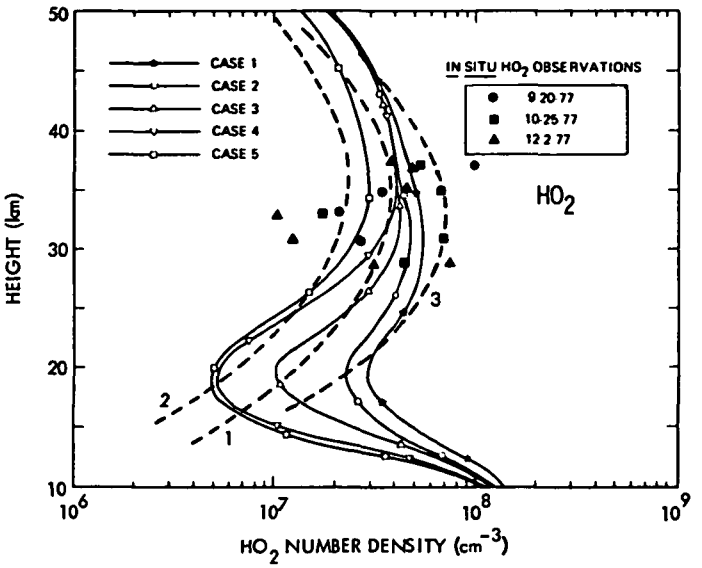

Figure 18. Stratospheric HO_2 abundances. From WMO (1981).

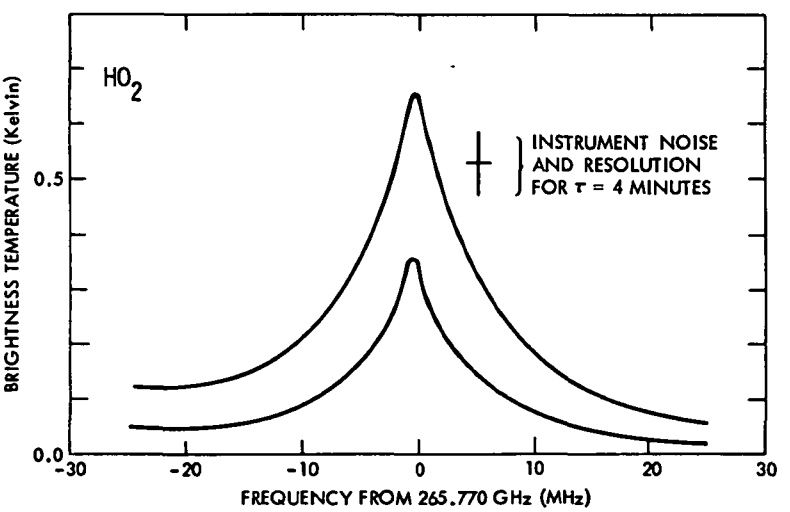

Figure 19. Calculated limb emission from the 265.767 GHz HO_2 line. These calculations are for an elevation angle of -1^2 degree from 40 km. The two curves are for dashed profiles 2 and 3 of Figure 18, respectively. Also shown is the rms noise and the spectral resolution for the instrumentation described in the text with 4 minute integration.

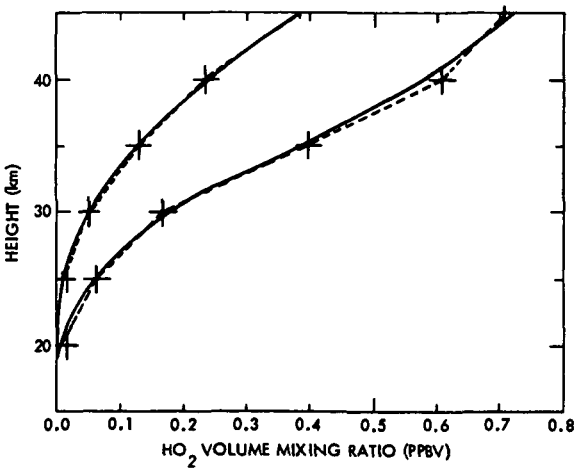

Figure 20. Results of simulated HO_2 retrievals. The dashed lines give the retrieved profile and the solid lines are the "true" profile. The horizontal width of the retrieved profile points gives the rms uncertainty due to the instrument noise as discussed in the text.

retrievals used the same 8 elevation angles as for the CIO retrievals described earlier. Channels 2 MHz wide within 20 MHz of line center were used. The initial estimate for the retrievals was dashed curve 1 of Figure 18 and retrievals were performed on the simulated data vector calculated separately for dashed profiles 2 and 3. The rms measurement noise was that for the 270 GHz instrumentation described with 4 minute integration per elevation angle for non-switched radiometer operation (equivalent to 16 minutes per elevation angle for switched operation).

The results shown in Figure 20 indicate that useful HO_2 accuracy can be obtained to altitudes as low as approximately 25 km. In fact integration times a factor of four shorter than those assumed for the retrieval simulations done here should provide useful measurements. This means that useful HO_2 profiles between 25 and 40 km could be obtained with time resolution of approximately 1/2 hours or better.

(b) NO_2

Expected stratospheric abundances of NO_2 are shown in Figure 21. The symbols are measurements made near sunset (WMO, 1981) and the solid curves are predictions by the Caltech model (L. Froidevaux, private communication) for noon and midnight. Figure 22 shows calculated emission by the 265.560 GHz NO_2 line for the noon and midnight theoretical profiles of Figure 2.3-5 and for elevation angles of $-1°$ and $-3°$ from 40 km. A pressure-broadened linewidth parameter of 3.0 MHz/mb with $T^{-0.75}$ temperature dependence was used for the calculations. This line is one of three NO_2 lines which could be simultaneously measured by the 270 GHz instrumentation described below. The BMLS NO_2 signals are stronger at night because of the nighttime increase in NO_2. A 15 minute integration at midnight will give an expected signal to noise of approximately 10 in the 30-40 km altitude region. During midday a one hour integration is required for a signal-to-noise of approximately 10 at 30 km; one hour integration gives a signal to noise of approximately 2 at 40 km. Data from all three NO_2 lines, which have approximately equal strengths, can be combined to improve signal-to-noise by a factor of approximately 1.7 over these values.

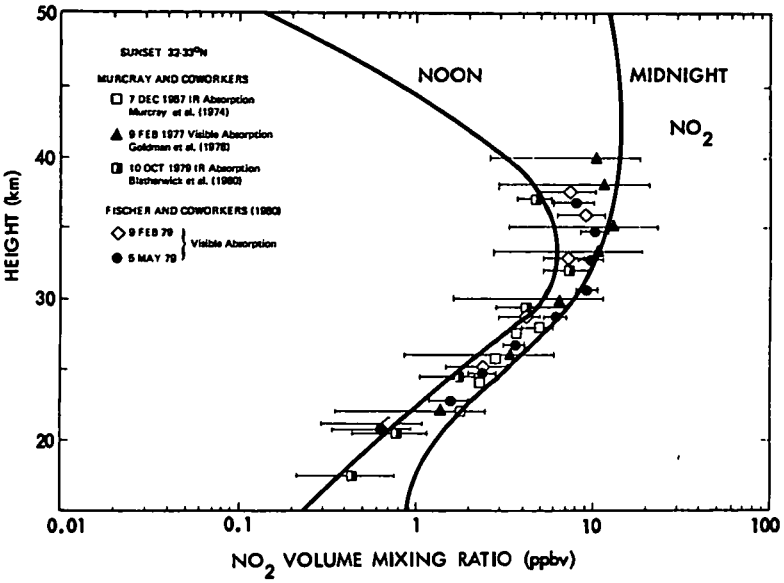

Figure 21. Stratospheric NO_2 abundances. From WMO (1981)

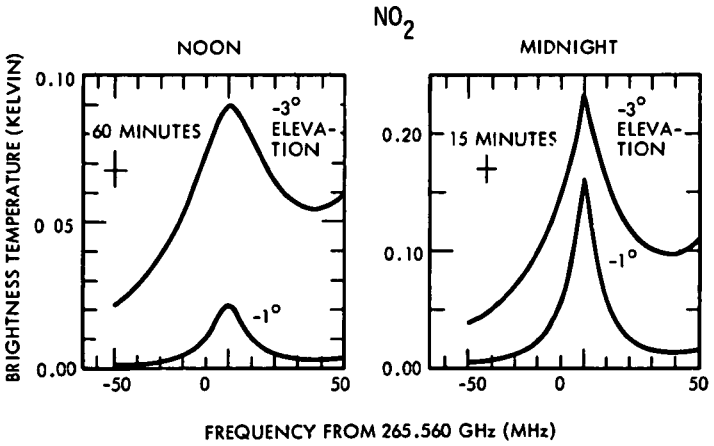

Figure 22. Calculated limb emission by the 265.560 GHz line at elevation angles of -1 degree and -3 degrees from 40 km altitude. These angles correspond to observation paths having tangent heights of 39 and 31 km, respectively. Note the difference in vertical scale for the noon and midnight signals. The instrument noise for 20 MHz spectral resolution and integration times of 60 minutes at noon and 15 minutes at midnight are shown.

(c) HCN

COFFEY et al. (1981) detected stratospheric HCN from aircraft infrared absorption and obtained an average HCN mixing ratio above 12 km of 0.17 ppbv. CARLI et al. (1982) detected several submillimeter HCN lines from balloon measurements of thermal limb emission and obtained a mixing ratio of 0.13 to 0.26 ppbv in the 20-40 km altitude range. CICERONE and ZELLNER (1983) calculate an HCN profile which has 0.15 ppbv at 15 km decreasing to 0.06 ppbv at 50 km. To determine the expected strength of the 265.886 GHz HCN line in stratospheric emission we used a constant HCN mixing ratio of 0.1 ppbv between 15 and 50 km. This profile is intermediate between the theoretical and measured values in the middle stratosphere. A collision linewidth parameter of 3.0 MHz/mb quoted by DE ZAFRA et al. (1984) for HCN was used with a temperature dependence of $T^{-0.75}$. Results of the calculation are shown in Figure 23. It can be seen that this line is very strong, having a brightness temperature of nearly 50 K for -1 degree elevation angle. Measurement of this line with a signal-to-noise of 100 can be achieved with a few seconds integration. Expected HCN profile accuracies are a few percent.

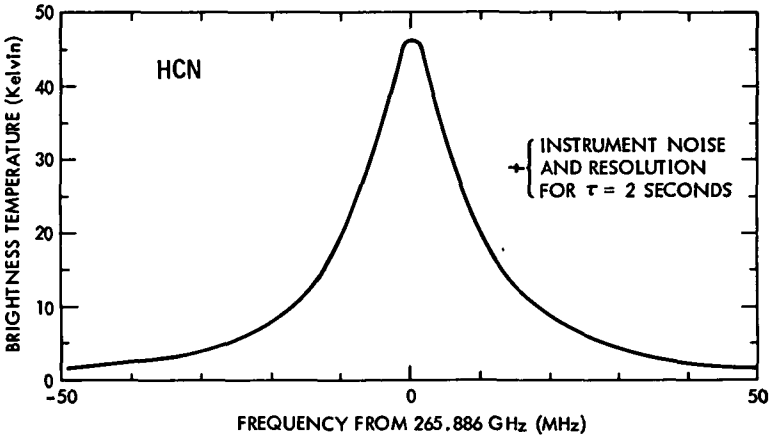

Figure 23. Calculated limb emission by the 265.886 GHz HCN line for -1 degree elevation angle from 40 km altitude. The instrument noise for a 2 second integration is indicated.

(d) HNO_3

Measured stratospheric abundances of HNO_3 are shown in Figure 24. We used the dashed profile in the mid-range of these abundances to calculate HNO_3 emission at 269.2 GHz. Results of the calculations are shown in Figure 25. HNO_3 emission near this frequency is from ∿10 separate lines which are merged together by pressure broadening. A pressure broadening parameter of 3.0 MHz/mb at T=300 K based on the 2.2 Debye dipole moment of HNO_3 and the plot of linewidth versus dipole moment by DE ZAFRA et al. (1984) was used. The HNO_3 signal is very strong and signal-to-noise of 100 for a mid-range profile point is achieved with an integration time of a few seconds. An integration time of 4 minutes will provide an expected signal-to-noise of approximately 10 at 40 km altitude.

(e) N_2O

Stratospheric N_2O profiles are shown in Figure 26. The lower dashed line in this figure was used to calculate the N_2O limb emission shown in Figure 27.

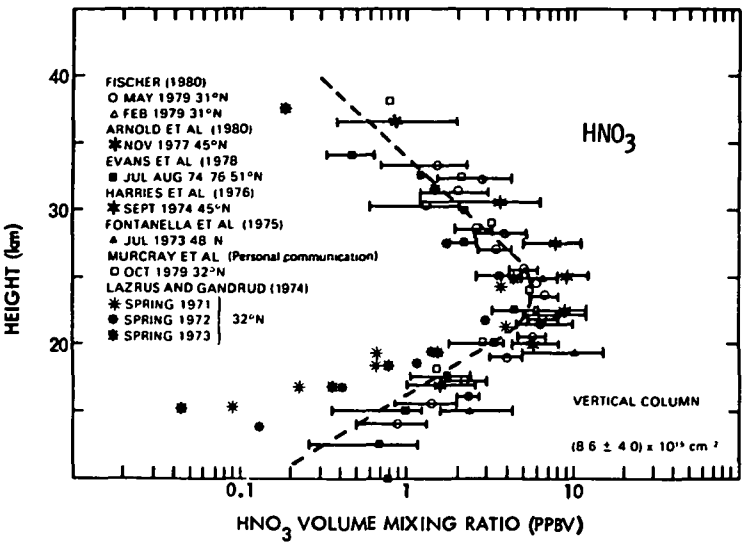

Figure 24. Stratospheric HNO_3 abundances. From WMO (1981).

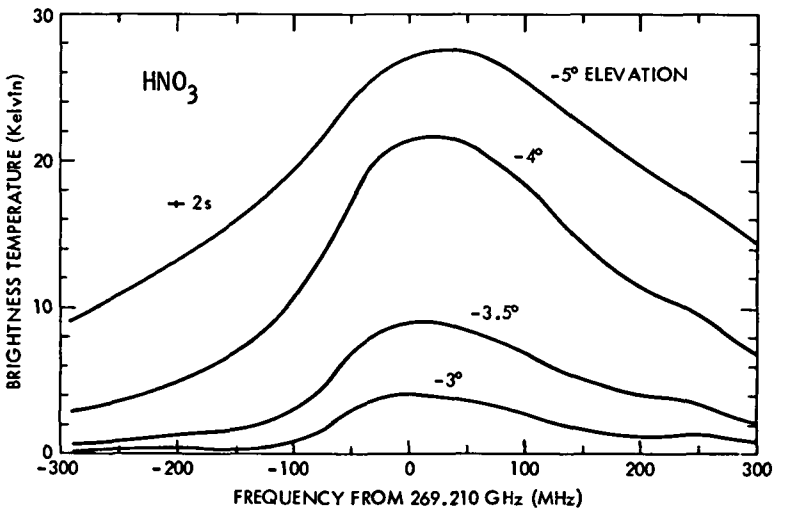

Figure 25. Calculated HNO_3 limb emission near 269.2 GHz for several elevation angles from 40 km altitude. This spectral region could be covered by the UARS MLS filter bank with filter positions and resolution as indicated in Figure 9. The instrument noise for an intermediate resolution filter with 2 seconds integration time is indicated.

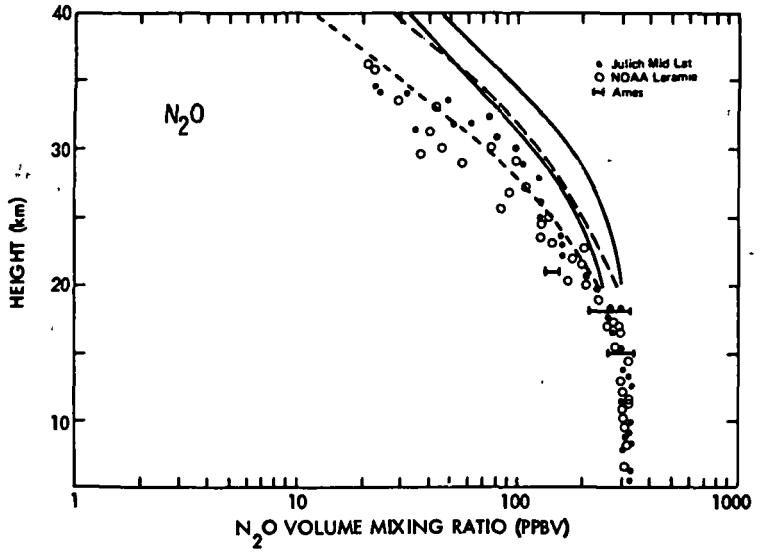

Figure 26. Stratospheric midlatitude N_2O profiles. From WMO (1981). The points are measured and the dashed and solid lines are model predictions.

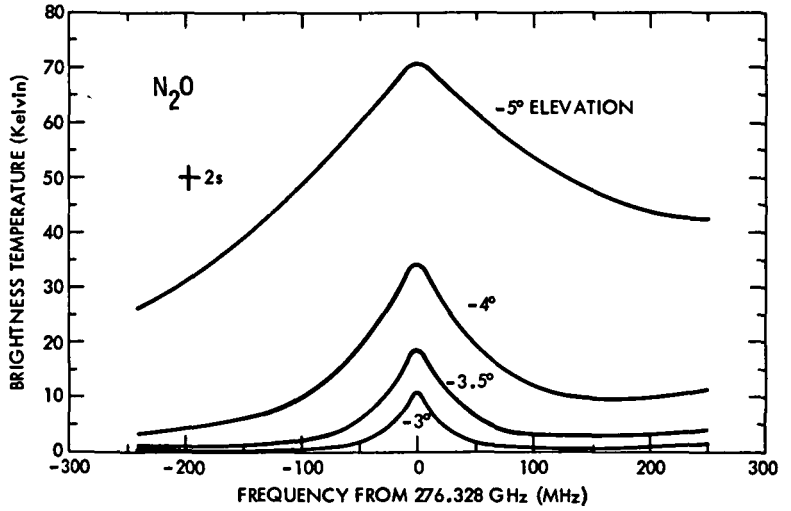

Figure 27. Calculated limb emission by the 276.328 GHz N_2O line for several elevation angles from 40 km altitude. This spectral region could be covered by the UARS MLS filter bank with filter positions and resolution as indicated in Figure 9. The instrument noise for an intermediate resolution filter with 2 seconds integration time is indicated.

A pressure-broadening parameter of 2 MHz/mb was used. The N_2O line is very strong and a signal-to-noise of 100 is achieved with a few minutes integration.

(f) $^{16}O^{18}O^{16}O$

Figure 28 shows calculated emission from the 265.623 GHz line of $^{16}O^{18}O^{16}O$. The vertical profile of $^{16}O^{18}O^{16}O$ used for the calculations was the standard KRUEGER-MINZNER (1976) O_3 profile scaled at all altitudes by the factor 2.04×10^{-3} for the cosmic abundance of ^{18}O relative to ^{16}O (e.g., LEIGHTON, 1959). This abundance of $^{16}O^{18}O^{16}O$ is consistent with the ground-level mass spectroscopic measurements of MAUERSBERGER (1981) which gave 6.3×10^{-3} relative abundance for total heavy ozone, since the expected amount of heavy ozone in the $^{16}O^{18}O^{16}O$ isomer is one-third (e.g., FROIDEVAUX, 1983). A signal-to-noise of approximately 10 throughout the 20-40 km altitude range is achieved with a few minutes integration. Any enhancement in stratospheric heavy ozone, such as that measured by Mauersberger, will increase the signals from those shown here.

Also shown in Figure 28 is the NO_2 emission line at 265.643 GHz.

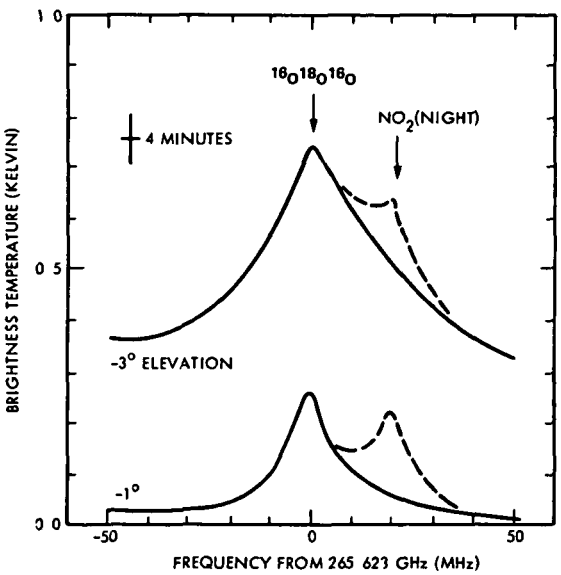

Figure 28. Calculated limb emission by the 265.623 GHz line of $^{16}O^{18}O^{16}O$ with no enhancement of heavy ozone. The instrument noise for 4 minutes integration time with 5 MHz spectral resolution is shown.

(g) O_3

Figure 29 shows calculated limb emission by the 276.923 GHz O_3 line using the KRUEGER-MINZNER (1976) standard O_3 profile. Measurement signal-to-noise of 100 is achieved with a few seconds integration.

270 GHz INSTRUMENTATION

A block diagram of the 270 GHz radiometer which could be added to the BMLS is shown in Figure 30. This radiometer is very similar in design to the

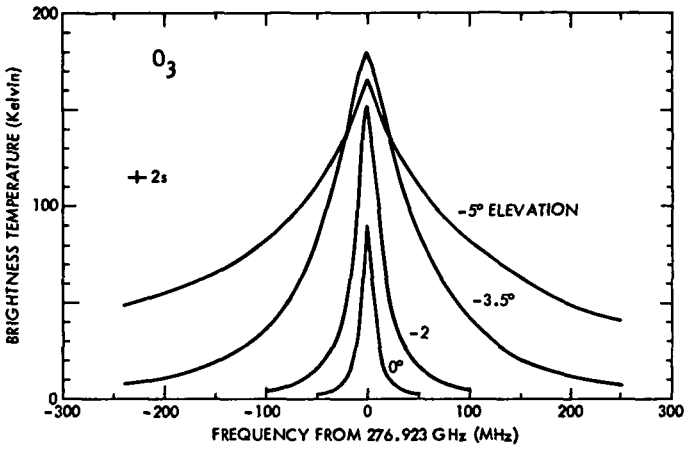

Figure 29. Calculated limb emission by the 276.923 GHz O_3 line for several elevation angles. This spectral region could be covered by the UARS MLS filter bank with filter positions and resolution as indicated in Figure 9. The instrument noise for an intermediate resolution filter with 2 seconds integration time is indicated.

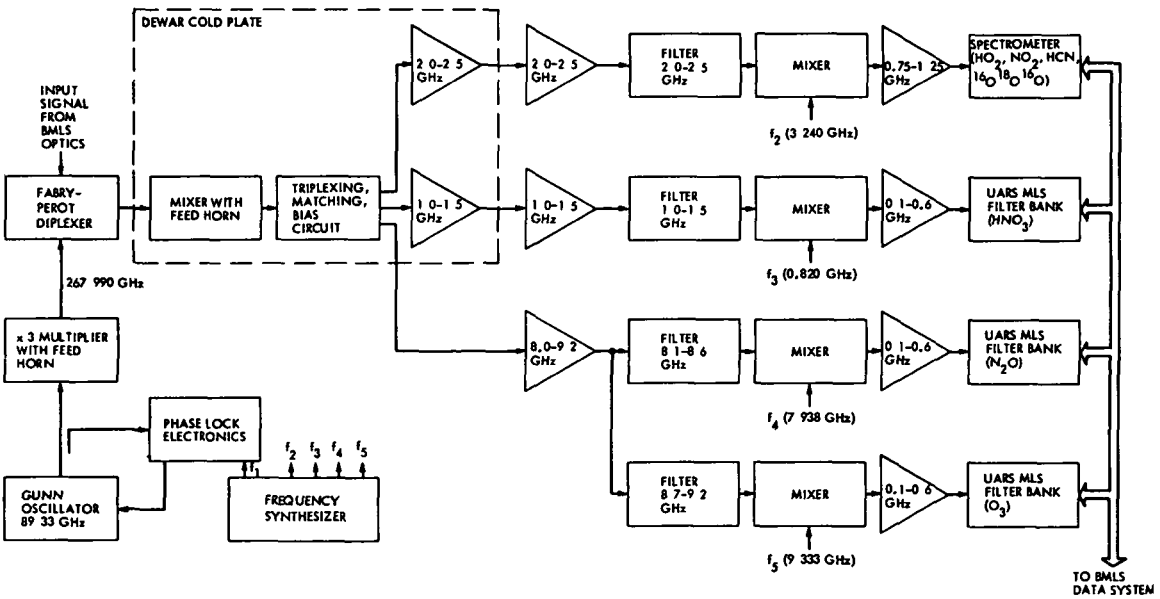

Figure 30. 270 GHz radiometer block diagram.

existing cooled 205 GHz BMLS radiometer described earlier. It uses a Schottky diode waveguide mixer, and local oscillator obtained by tripling a phase-locked Gunn oscillator at 89.33 GHz. Gunn oscillators at 90 GHz are commercially available with at least 30 mW output power. The tripler has an efficiency of at least 2 percent which will provide at least 0.6 mW at the local oscillator frequency of 267.99 GHz. This local oscillator frequency was chosen so that there are no known significant spectral interferences in either sideband with the HO_2, NO_2, HCN, HNO_3, N_2O, and O_3 signals being measured. It also placed a 259.532 GHz HOCℓ line at 8.46 GHz intermediate frequency (i.f.), which is within the passband of the 9 GHz i.f. amplifier for N_2O and O_3; this line is also a candidate for measurement by the BMLS. The Fabry-Perot diplexer which combines local oscillator and signal has less than 0.3 dB loss in the signal path and less than 1.5 dB loss in the local oscillator path.

A layout of the 270 GHz radiometer optical components and dewar is shown in Figure 31. The 270 GHz signal is split from the BMLS antenna optical path by a polarization grid. The location of this grid in the optical path of the current BMLS is shown in Figure 6. All BMLS measurements at 63, 205 and 270 GHz can be performed simultaneously with this arrangement. The Fabry-Perot which combines signal and local oscillator has 3.5 GHz free spectral range and is transmissive to all spectral lines being measured. Figure 32 shows its characteristics.

The signal from the mixer is split into three i.f. bands. The first band from 1.0 to 1.5 GHz contains HNO_3. The second, from 2.0 to 2.5 GHz contains HO_2, NO_2, $^{16}O^{18}O^{16}O$ and HCN. The third, from 8.7 to 9.2 GHz, contains N_2O and O_3. Signals in these bands are amplified and then converted to lower frequency bands for spectral analysis. Refer to Figure 33.

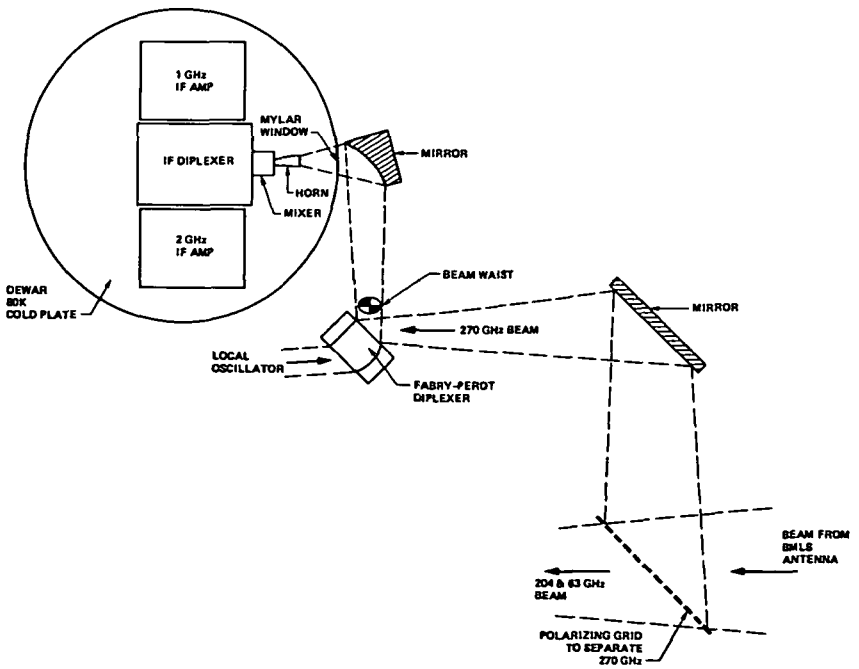

Figure 31. Optical layout for 270 GHz radiometer. The optics producing the local oscillator beam are identical to those shown in Figure 6 for the 205 GHz radiometer.

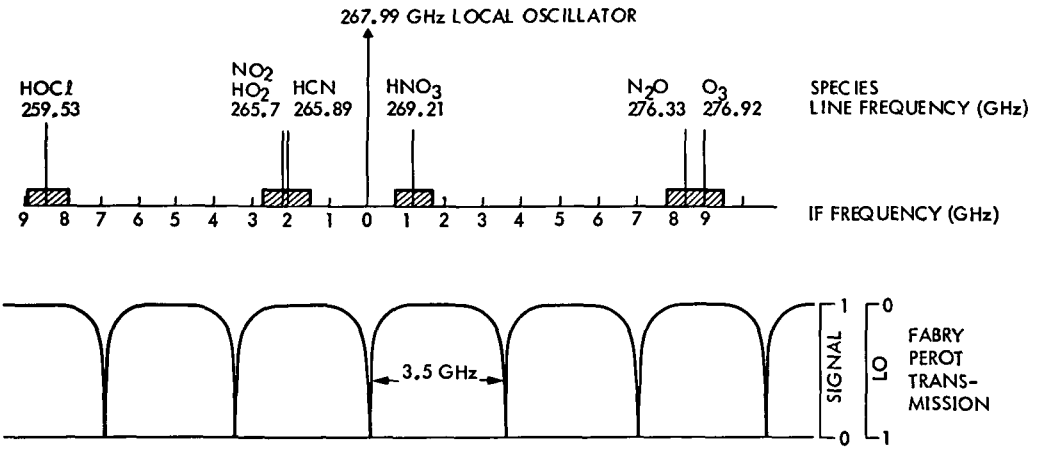

Figure 32. Characteristics of Fabry-Perot for coupling 270 GHz local oscillator and signal.

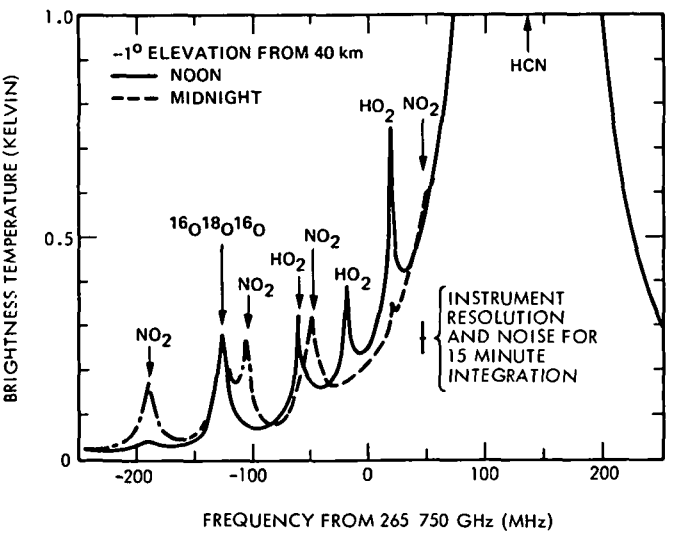

Figure 33. Spectral band containing HO_2, NO_2, HCN, and $^{16}O^{18}O^{16}O$ signals. This spectrum is calculated for emission from 40 km at -1 degree elevation angle. The estimated instrument noise for 15 minutes integration time with 2 MHz resolution is indicated.

Spectral analysis of HNO_3, N_2O and O_3 signals can be performed by copies of the UARS filter banks, described earlier. The HO_2 and NO_2 signals, consisting of several lines of narrower width than those of the other species, require a different spectral analysis system. A spectrometer with 500 MHz bandwidth and 1-2 MHz resolution would simultaneously measure the HO_2, NO_2, HCN and $^{16}O^{18}O^{16}O$ signals. Such a spectrometer could be readily implemented.

An estimated noise budget for the 270 GHz radiometer is given in Table 4.

Table 4. Estimated noise budget of the 270 GHz radiometer. All values are single sideband.

	0.8-1.5 GHz band (HO_2, NO_2, HCN, $^{16}O^{18}O^{16}O$)	1.8-2.5 GHz band (HNO_3)	8.0-9.2 GHz band (N_2O, O_3)
loss before mixer (dB)	0.5	0.5	0.5
mixer conversion loss (dB)	9.0	9.0	11.0
mixer noise temperature (K)	800	800	800
i.f. triplexer loss (dB)	1.0	2.0	3.0
i.f. noise temperature (K)	30	30	200
overall noise temperature, T_N (K)	1300	1400	6500

ACKNOWLEDGEMENTS

Dr. J. J. Gustincic (deceased) designed and fabricated the BMLS antenna system. Dr. W. J. Wilson designed the UARS MLS filter banks. S. Bednarczyk, F. S. Soltis, Dr. H. K. Roscoe, R. D. Stuber, M. M. Schaefer, S. A. Rowe, and R. Zimmermann assisted in various stages of BMLS development. Dr. M.F. Frerking helped with the design of the 270 GHz Fabry-Perot diplexer. Drs. L. Froidevaux and M. A. Allen provided helpful discussions on stratospheric chemistry. The work described here was supported by the National Aeronautics and Space Administration Upper Atmosphere Research Program.

REFERENCES

Anderson, J. G., H. J. Grassl, R. E. Shetter and J. J. Margitan (1980), Stratospheric free chlorine measured by balloon-borne in situ resonance fluorescence, J. Geophys. Res., 85, 2869.

Blake, A. J., S. T. Gibson and D. G. McCoy (1983), Photodissociation of $^{16}O^{18}O$ in the atmosphere, preprint.

Carli, B., F. Mencaraglia and A. Bonetti (1982), New assignments in the submillimeter emission spectrum of the stratosphere, Int. J. Infrared Millimeter Waves, 3, 385.

Cicerone, R. J. and J. L. McCrumb (1980), Photodissociation of isotopically heavy O_2 as a source of atmospheric O_3, Geophys. Res. Lett., 7, 251.

Cicerone, R. J. and R. Zellner (1983), The atmospheric chemistry of hydrogen cyanide (HCN), J. Geophys. Res., 88, 10689.

CIRA (1972), COSPAR International Reference Atmosphere 1972, Akademie-Verlag, Berlin.

Coffey, M. T., W. G. Mankin and R. J. Cicerone (1981), Spectroscopic detection of stratospheric hydrogen cyanide, Science, 214, 333.

Crutzen, P. J., I. S. Isaksen and J. R. McAfee (1978), The impact of the chlorocarbon industry on the ozone layer, J. Geophys. Res., 83, 345.

de Zafra, R. L., A. Parrish, P. M. Solomon and J. W. Barrett (1984), A measurement of stratospheric HO_2 by ground-based mm-wave spectroscopy, J. Geophys. Res., 89, 1321.

Drummond, J. R. and R. F. Jarnot (1978), Infrared measurements of stratospheric composition II. Simultaneous NO and NO_2 measurements, Proc. R. Soc. Lond., A375, 507-528.

Froidevaux, L. (1983), Photochemical modeling of the Earth's stratosphere, California Institute of Technology, Ph.D. Thesis.

Kaye, J. A. and D. F. Strobel (1983), Enhancement of heavy ozone in the Earth's atmosphere?, J. Geophys. Res., 88, 8447.

Krueger, A. J. and R. A. Minzner (1976), A mid-latitude ozone model for the 1976 U.S. standard atmosphere, J. Geophys. Res., 81, 4477.

Leighton, R. B. (1959), Principles of Modern Physics, McGraw-Hill.

Mauersberger, K. (1981), Measurements of heavy ozone in the stratosphere, Geophys. Res. Lett., 8, 935.

Molina, M. J. and F. S. Rowland (1974), Stratospheric sink for chlorofluoromethanes: chlorine atom-catalyzed destruction of ozone, Nature, 249, 810.

Njoku, E. (1982), Passive microwave remote sensing of the earth from space - a review, Proc. IEEE, 70, 728.

Pickett, H. M. and A. F. Chiou (1983), Folded Fabry-Perot quasi-optical ring resonator diplexer: theory and experiment, IEEE Trans. MTT, 31, 373-380.

Poynter, R. L. and H. M. Pickett (1981), Submillimeter, millimeter and microwave spectral line catalog, JPL Publication 80-23, Revision 1.

Rodgers, C. D. (1976), Retrieval of atmospheric temperature and composition from remote measurements of thermal radiation, Rev. Geophys. Space Phys., 14, 609.

Roscoe, H. K., J. R. Drummond and R. F. Jarnot (1981), Infrared measurements of stratospheric composition III. The daytime changes of NO and NO_2, Proc. R. Soc. Lond., A375, 507-528.

Schanda, E. (1976), Passive microwave sensing, in Ecological Studies, 18,: Remote Sensing for Environmental Studies, Springer-Verlag, Berlin.

Staelin, D. H. (1969), Passive remote sensing at microwave wavelengths, Proc. IEEE, 57, 427.

Stolarski, R. S. and R. J. Cicerone (1974), Stratospheric chlorine: a possible sink for ozone, Can. J. Chem., 52, 1610.

Twomey, S. (1977), Introduction to the Mathematics of Inversion in Remote Sensing and Indirect Measurements, Elsevier Publishing Co., Amsterdam.

Waters, J. W. (1976), Absorption and emission of microwave radiation by atmospheric gases, Chap. 2.3 in Methods of Experimental Physics, Vol. 12, Part B, Radio Astronomy, Academic Press.

Waters, J. W. (1980), Microwave measurement of stratospheric and mesospheric ozone, Proc. Quadrennial International Ozone Symp., Boulder, CO, J. London, editor.

Waters, J. W., R. F. Jarnot, H. M. Pickett, P. Zimmermann and R. W. Zurek (1978), Microwave limb sounder, Proposal to the Upper Atmosphere Research Satellites Program, Jet Propulsion Laboratory, Pasadena, CA.

Waters, J. W., J. J. Gustincic, R. K. Kakar, H. K. Roscoe, P. N. Swanson, T. G. Phillips, T. de Graauw, A. R. Kerr and R. J. Mattauch (1979), Aircraft search for millimeter-wavelength emission by stratospheric ClO, J. Geophys. Res., 84, 7034.

Waters, J. W., J. J. Gustincic, P. N. Swanson and A. R. Kerr (1980), Measurements of upper atmospheric H_2O emission at 184 GHz, pp. 229-240 in Atmospheric Water Vapour, edited by A. Deepak, T. D. Wilkerson and L. G. Ruhnke, Academic Press.

Waters, J. W., J. C. Hardy, R. F. Jarnot and H. M. Pickett (1981), Chlorine monoxide radical, ozone, and hydrogen peroxoide: stratospheric measurements by microwave limb sounding, Science, 214, 61.

WMO (World Meteorological Organization) (1981), The Stratosphere 1981: Theory and Measurement.

Wuebbles, D. J. (1983), Chlorocarbon emission scenarios: Potential impact on stratospheric ozone, J. Geophys. Res., 88, 1433.

Zimmermann, P. and R. J. Mattauch (1979), Low noise second harmonic mixer for 200 GHz, IEEE-MIT Symposium, Orlando, FL

5. MEASUREMENT AND IDENTIFICATION OF STRATOSPHERIC IONS

D. Nevejans, J. Ingels and E. Arijs

Belgian Institute for Space Aeronomy
Ringlaan 3, B-1180 Brussels
Belgium

ABSTRACT

Recent progress in the technology of stratospheric ion mass spectrometry is described.

The state of the art as well as some typical measuring problems and needs for future developments are briefly reviewed.

INTRODUCTION

Penetration into the atmosphere of high energy particles and short wave radiation such as solar UV light, X rays and cosmic rays, results in formation of charged particles through direct ionization processes. At sufficiently high gas densities, ions and electrons thus formed make multiple collisions with neutral particles, and electron attachments as well as ion-molecule reactions occur, modifying the identity of the charged particles. In the stratosphere the main ionization source is cosmic radiation and the lifetime of ions is of the order of 100 to 3000 s between 15 and 40 km. The subsequent rapid ion-molecule reactions involve different trace gases so that the terminal ions have a totally different nature than the primary ones.

Until 1977, the experimental data on stratospheric ions were limited to total ion density and mobility measurements (PALTRIDGE, 1965; BRAGIN et al., 1966; ROSE et al., 1972; WIDDEL et al., 1977; BRAGIN, 1967; MORITA et al., 1971; MITCHELL et al., 1977).

Information on positive and negative ion composition below 50 km was based on modelling (FEHSENFELD and FERGUSON, 1969; MOHNEN, 1971; FERGUSON, 1974; REID, 1979), and extending the framework formerly developed for D-region ion chemistry. Therefore it remained merely speculative and incomplete. Nevertheless, such information is important for several reasons:

- Knowledge of the nature of stratospheric ions is essential for our understanding of physical processes in the field of atmospheric electricity. The conductivity of the atmosphere, for instance, depends upon ion mobility and thus on ion composition.
- Also, stratospheric ion mass spectrometry may become an important tool for detection of trace gases with very low concentrations (ARNOLD et al., 1980; ARIJS et al., 1983a,b; VIGGIANO and ARNOLD, 1983).
- Furthermore, stratospheric ions may play an important role in gas to particle conversion and nucleation of stratospheric aersols (MOHNEN and KIANG, 1976; ARNOLD, 1980, 1982), which in turn could influence the Earth's radiation budget and climate.
- Finally, in situ mass spectrometric investigations of stratospheric ion composition can provide experimental thermochemical and kinetic data on ion-molecule reactions taking place under conditions difficult to simulate in the laboratory.

Determination of the nature and abundances of stratospheric ions is therefore a desirable objective and balloon-borne ion mass spectrometers have been and are developed at several places (ARIJS et al., 1978; ARNOLD et al., 1978; OLSON et al., 1978; CUNNINGHAM and HOFMAN, 1982; BALLENTHIN et al., 1983).

The purpose of this paper is to describe the experimental and technological aspects of such ion mass spectrometers as far as they were available in literature. The scientific results obtained with these instruments have been reviewed elsewhere (ARNOLD, 1980; ARIJS, 1983).

EXPERIMENTAL PROBLEMS AND PAYLOAD DESCRIPTION

In situ stratospheric ion identification requires the development of an instrument, wherein ions are sampled through a small orifice, focussed into an appropriate mass spectrometer and detected after filtering according to their mass to charge ratio. This instrument has an associated electronic package taking care of driving the mass filter and focussing device, delivering high voltage to the detector, recording signals and interfacing between the instrument and the ground-borne experimenter.

For ion composition measurements in the D-region, rocket-borne mass spectrometers have been developed by several groups (NARCISI and BAILEY, 1965; GOLDBERG and BLUMLE, 1970; KRANKOWSKY et al., 1972; ZBINDEN et al., 1975).

Use of similar instruments for stratospheric purposes (ARNOLD et al., 1977) however, poses some severe problems among which short measuring times and ion breakup due to induced shock waves are the most important. For stratospheric measurements it is better to make use of more convenient platforms, such as high altitude balloons which are able to lift heavy and large instruments up to 45 km altitude. Present techniques even allow continuous measurements in an altitude range from 45 down to about 15 km by using valve controlled balloons.

Although the philosophy in designing a balloon-borne mass spectrometer for *in situ* sampling of stratospheric ions is similar to the one followed in constructing a rocket-borne payload, some important differences evolve from the nature of the problem itself and from the use of a different platform.

A major difference, for example, is the pumping system required to maintain the mass filter in vacuum. Due to the high ambient pressure and the long duration of a balloon flight, a pumping system with a long standing time (several hours), a large pumping capacity and a high pumping speed will be required for a balloon-borne instrument.

A general view of a typical experimental configuration is shown in Figure 1. The gondola consists of three different parts: a cryopump with the mass spectrometer, an electronics compartment and a mechanical support structure. In the configuration of Figure 1, the electronics compartment consists of a lightweight aluminium cylinder, sealed by a large aluminium flange, on which the cryopump is fixed.

This vessel is pressurized with dry air to avoid high voltage breakdown, and contains several electronic modules mounted on platforms parallel to the sealing flange. Hermetically sealed connectors are also provided on the latter for interfacing to telemetry, to telecommand and to devices located outside and for testing the payload. All sealings are realized with special silicone O-rings qualified for a -55 to +200°C temperature range. The mechanical support structure and crash pad are made completely of metal (aluminium) to avoid charging up problems. Its geometry is adaptable to specific needs, such as flying multiple experiment payloads.

In constructing the payload, the use of heavily degassing materials is avoided as much as possible, in view of contamination problems discussed further on.

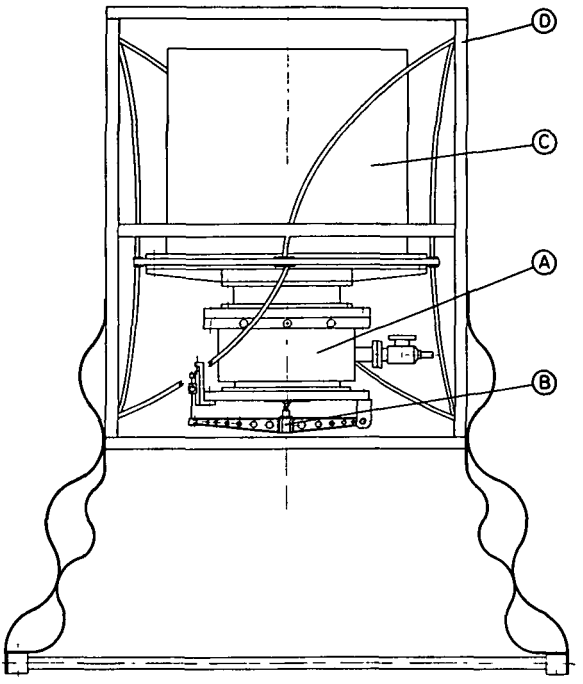

Figure 1. General view of ion mass spectrometer gondola.
A. cryopump; B. opening device; C. electronics container;
D. mechanical support structure.

DETAILED INSTRUMENT DESCRIPTION

(a) High Vacuum Part

The high vacuum part of a typical payload as developed at our institute is pictured in Figure 2. It consists of a high speed cryopump, a sampling hole, a remote opening device and a quadrupole mass filter with an ion focussing device and an ion detector.

In order to prevent scattering of sampled ions by background molecules, to insure proper functioning of the quadrupole mass filter and to avoid H.V. breakdown in the ion detector, a pressure of 10^{-4} Torr or less is required inside the mass spectrometer housing. Since the outside pressure ranges from 1 to 100 mbar, a basic problem of the experiment was designing a balloon-borne pump with high pumping speed. To overcome this difficulty, a liquid helium cryopump was developed, described in detail elsewhere (INGELS et al., 1978) and, therefore, explained here only briefly.

The pump body of the liquid helium cooled cryopump is made of stainless steel and all flanges are sealed with copper or polyimide O-rings. Apart from a glass fibre superinsulation, thermal insulation is achieved through two copper radiation shields, cooled by cold evaporating helium gas passing through an attached spiral. An inner blackened chevron baffle reduces radiation from the ion focussing lens, quadrupole mass filter and ion detector.

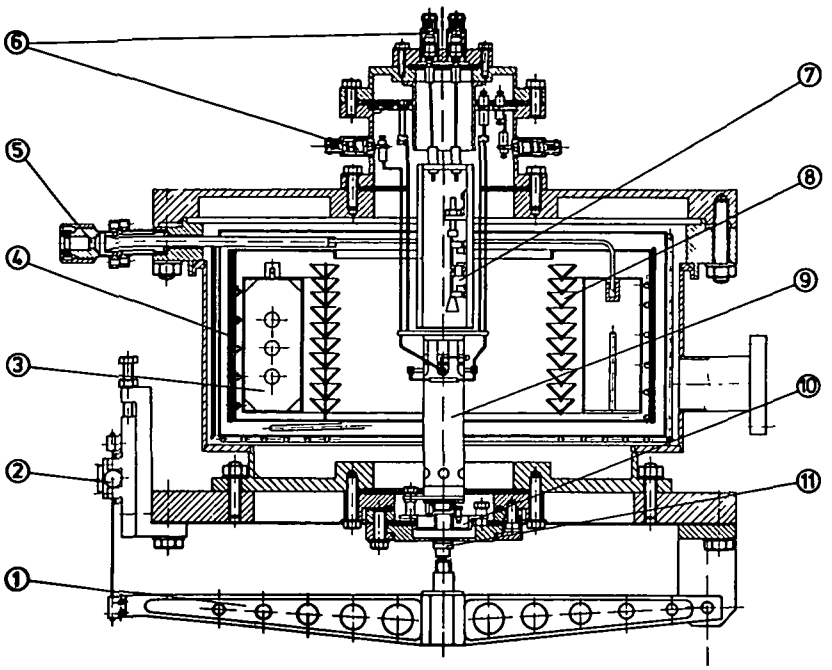

Figure 2. Detailed view of high vacuum part of the mass spectrometer. 1. spring loaded opening device; 2. protechnical cable cutter; 3. liquid helium container; 4. superinsulation; 5. liquid helium filling port; 6. electrical feedthrough; 7. spiraltron ion detector; 8. chevron baffles; 9. quadrupole mass filter; 10. ion lens; 11. polyimide plunger.

The liquid helium content of the reservoir is about 2.3 liter, for a standing time of about 12 hours. Measured pumping speed is about 1,200 liter/sec. OLSON et al. (1978) have designed a somewhat different cryopump for a balloon-borne ion mass spectrometer; whereas, recently Arnold and colleagues (VIGGIANO et al., 1983) have introduced the use of liquid neon pumps for this kind of experiment. Due to the larger heat of evaporation of liquid neon, such pumps have a much longer standing time and, therefore, a simpler, more light-weight design can be used. However, in order to pump light gases such as H_2, He and Ne efficiently, a charcoal absorption layer must be added to the inside of the cryosurfaces.

On the downward looking input flange of the cryopump, a smaller flange is mounted, electrically, of insulated from the pump body. This allows the application of a draw-in potential to attract ambient ions towards the instrument. A sampling aperture is drilled in the central part of the inlet flange, where thickness is reduced to 0.1 mm. The diameter of the sampling hole is a compromise between two conflicting requirements: maximum ion signal and minimum inside pressure. Most of our data were obtained with a sampling hole of 0.2 mm diameter.

Prior to balloon launching the sampling hole is covered with a polyimide plunger, which can be removed by remote control as soon as the gondola has reached the desired working altitude. This opening system has been described in detail previously (INGELS et al., 1978).

In the configuration of Figure 2, the quadrupole mass filter and ion focussing device are mounted rigidly on the sampling flange to avoid centering problems. In previous flights, quadrupoles having a rod radius of 6.3 mm and a length of about 120 mm have been used (type: Finnigan and Vacuum Generators). OLSON et al. (1978) describe the use of a similar mass filter, although application of smaller quadrupoles (rod diameter = 4.5 mmm) has been reported (ARNOLD and QIU, 1984).

In our setup, the ion focussing device consists of a single cylindrical lens element placed in front of an ionizer delivered by the quadrupole manufacturer. The elements of this ionizer can be put at different potentials, according to whether it is used as an electron impact ionizer or as an element of the ion focussing lens. Switching from lens to ion source configuration can be done by remote control. The ionizer has proven to be very useful for in situ calibration of the instrument, which allowed an unambiguous ion mass determination (ARIJS et al., 1980). At present it is merely used for preflight testing.

Although the use of the ion lens contributes to an increase in the ion signal, it also hampers the expansion of the gas beam, which carries ions through the sampling hole. As a result, a rather high pressure exists just behind the inlet aperture. Since in this region ions are accelerated by electric fields the ion abundance data can be falsified to a high degree by field-induced ion dissociation.

To overcome this ARNOLD and QIU (1984) recently used a configuration where no focussing device was used. Ions were simply guided into the quadrupole by a 50 V potential on the mass filter field axis (pole bias).

After passing through the mass filter, the ions are collected by an ion detector. In view of the lower signal, pulse counting techniques have to be applied and, therefore, an appropriate detector needs to be chosen. In our case a continuous dynode electron multiplier (Spiraltron SEM 4219 - Galileo Optics) was used, although the application of other types (Johnston Laboratories MM-1) was also reported (OLSON et al., 1978).

(b) Electronics Package

The various modules located in the pressurized part of the payload are shown in the block diagram of Figure 3. First there is the lens supply unit, furnishing the electrostatic ion lens and the sampling aperture with appropriate voltages of selectable polarity, referenced respectively to the sampling plat and to the metallic structure. It can operate either in an ion sampling or in an ion source mode, the latter mode only being used during in-flight mass scale calibration or for payload testing.

The quadrupole supply unit produces the RF and DC voltages required to drive the quadrupole mass filter. It is designed so that RF and DC voltages can be controlled independently, allowing a great variety of operating modes. The mass range covered by the quadrupole depends upon the selected RF frequency, the maximum attainable RF voltage, the quadrupole dimensions and the desired mass resolution. In the current payload configuration a mass range from 0 to 330 amu at high resolution is realized with 1500 V peak-to-peak RF excitation at 2 MHz and a quadrupole rod diameter of 6.3 mm.

The spiraltron ion detector, located behind the quadrupole mass filter, requires high voltages, delivered by a separate module. About 3 kV between input cone and anode is needed by the spiraltron for proper operation in the saturated pulse counting mode. Furthermore, the module allows for input cone voltage switching between -3 kV or +1.5 kV, in order to accommodate for positive or negative ion acceleration.

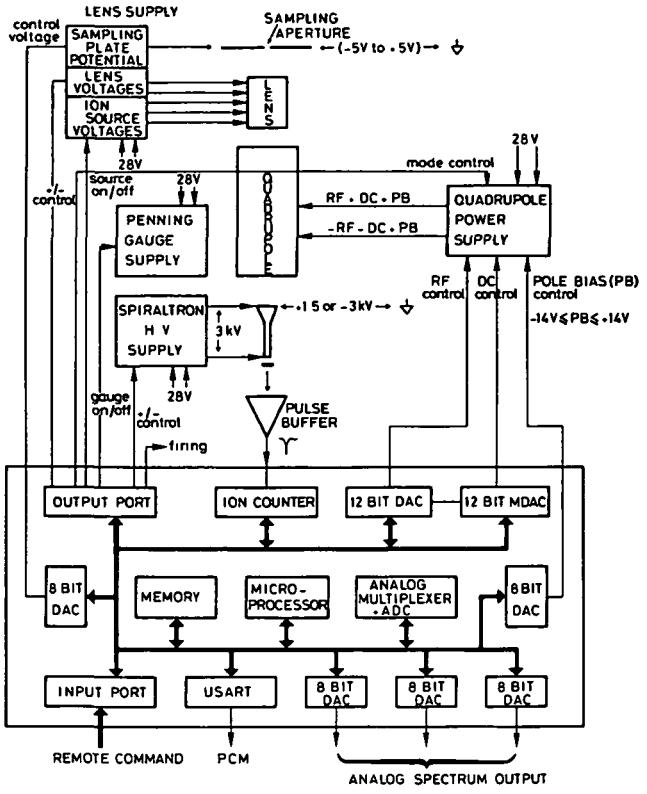

Figure 3. Block diagram of onboard electronics.

In the pulse buffer, which is AC coupled to the anode of the detector, collected charge pulses are converted into voltage pulses with mean amplitudes of a few hundred mV. Instead of using the classical charge amplifier approach, a very simple circuit, based on a high speed, low input capacitance buffer amplifier (NS LH0033), is applied here. The charge cloud leaving the spiraltron is merely integrated on the RC network, formed by the total wiring capacitance (about 20 pf) seen by the anode and by a 1 kΩ leak resistor.

Since collisions with neutrals must be avoided in the mass filter assembly, it must be operated at pressures below about 10^{-4} Torr. Therefore, inside pressure is continuously monitored by a Penning gauge in order to verify the cryopump's operation. Another high voltage unit supplies this gauge with about 2.3 kV. The current consumed by it, which is related to pressure, is measured by a logarithmic electrometer. This value is included in the telemetry format of the payload.

In order to enhance the performance of the balloon-borne mass spectrometer, a microprocessor (INTEL 8080) based control and data management unit has been included in the instrument. The design objectives and its hard- and software implementation have already been described before (NEVEJANS et al., 1982). The unit executes the following main tasks: it controls the polarity of the lens voltage and the spiraltron high voltage; it determines automatically the optimum potential of the sampling aperture; it produces the ramping voltages for the quadrupole supply; it counts the pulses leaving the pulse buffer and stores the

measured values in a spectrum memory; it acquires important parameters of the ambient; it does remote control interpretation and organizes transmission of spectrum and housekeeping data in analog and digital (PCM) formats. All of these duties are governed by software stored in onboard nonvolatile memory. One of the key features of this microprocessor based unit is the selection of an appropriate mass scanning mode. In our instrument, all scan-defining parameters can be optimized: resolution mode, extent of the scan range and number of spectrum channels. Two major resolution modes are implemented (NEVEJANS et al., 1982). The constant resolution mode, wherein ions are filtered with a mass independent, constant, finite resolution ($m/\Delta m$), can be used either to enhance throughput of the mass filter at reduced resolution or to access ion masses, beyond the normal mass range of the instrument. This mode is most often applied during valve controlled balloon flights, when relative abundance profiles of known stratospheric ion species are measured.

An offspring of the constant resolution mode is the integral mode. Here, only RF is supplied to the quadrupole. This results in a shift of the rising edge of all mass peaks towards the low end of the mass scale. Consequently, all mass peaks overlap and, therefore, total ion abundance can be measured at a fixed low level, RF excitation. When the RF voltage is scanned however, the mass filter behaves as a high pass filter.

A second mode is the constant peak-width mode. The resolution ($m/\Delta m$), controlled by the ratio of the DC and RF supply voltage of the quadrupole mass filter, becomes a linear function of mass so that peak-width (Δm) remains constant all over the mass range. The constant peak-width mode is used primarily for the unambiguous determination of mass numbers with a 0.1 to 0.8 amu uncertainty.

(c) Telemetry, Telecommand and Data Reduction

The described assembly of electronic modules is connected to an independent telemetry-telecommand (TM-TC) system. During flights over Southern France a CNES supplied package is used (SITTEL TM-TC), which has nine analog channels (IRIG 5, 6, 7, 9, 11, 12, A, C and E) and a maximum of 27 latching relays (three different addresses with 9 relays each) available to the user. Up to three fully separately powered and integrated mass spectrometers can be interfaced with one such package without any difficulty. Each instrument has then three analog telemetry channels at its disposal: one for the digital serial data stream generated by the on-board microprocessor (PCM rate between 700 and 1300 bits/sec) and two for transmitting analog copies of technological data and mass spectra.

Each mass spectrometer utilizes eight latching relay contacts to form a digital telecommand input and one additional for power on-off switching. The digital information is used by the microprocessor software to select one of the stored measuring programs or to perform service tasks.

The digital data, transmitted over an analog telemetry channel, is handled by a ground borne real-time computer (HP 1000 series), equipped with PCM bit and frame synchronizers (EMR models 720 and 727) and running multitasking software (HP RTE-M III operating system). Housekeeping data about the ambient and internal conditions (pressure, temperatures, voltages, vacuum, etc.) of the payload are displayed and continuously refreshed on a console, while spectrum data are stored on digital tape. The latter data can also be plotted on the console or on a printing plotter.

CALIBRATION OF THE INSTRUMENT

To calibrate the mass scale of our instrument, to check its sensitivity and

to determine the appropriate parameters, which are stored in the memory of the microprocessor control unit, extensive laboratory studies have been performed.

The stratospheric plasma is simulated in a vessel, fitting on the mass spectrometer, by ionizing a nitrogen - nitric oxide gas mixture (typically 1% NO in N_2) with UV irradiation (the 129.6 nm line of a xenon discharge). The pressure of this gas mixture can be stabilized over a wide range (0.1 to 100 Torr) and the ratio NO/N_2 as well as the xenon lamp intensity are kept constant simultaneously.

In this way a reproducible ion population is created having a number density similar to the stratospheric situation, but with a different composition.

The same setup has been used previously (ARIJS et al., 1982a) to investigate the effect of the ion lens field on proton hydrate cluster breakup.

It should be emphasized that so far only relative abundance ratios of different ion species were determined and no absolute ion densities have been deduced from stratospheric ion composition measurements. The derivation of absolute number densities would require a special calibration system, which has not been realized yet, due to the difficulty of independently measuring ion densities.

Another remaining problem is mass discrimination. Since, in most of the present applications of ion composition measurement, moderate resolution spectra have been used, these discrimination effects are believed to be of minor importance. If in the future, however, high resolution spectra will be used, this phenomenon has to be analyzed in the laboratory.

MEASUREMENTS

(a) State of the Art Review

Since 1977 many measurements have been performed with balloon-borne ion mass spectrometer, mainly by two groups (Max Planck Institut fur Kernphysik, Heidelberg and Belgian Institute of Space Aeronomy, Brussels). The results of most of these measurements as well as typical ion spectra have been reported in the literature (see reviews of ARNOLD (1980) and ARIJS (1983) and references cited therein). Therefore, we will only give a concise description of the state of the art and focus more on future advances in the measurement technique, and on problems related to possible misinterpretation of data.

The major positive ions detected in the altitude region 20 to 45 km turned out to be proton hydrates - $H_3O^+(H_2O)_n$ - and nonproton hydrates of the $H^+X_\ell(H_2O)_m$, where X most probably is acetonitrile (CH_3CN) (ARNOLD, 1980; ARIJS, 1983). From the relative ion abundance measurements, the mixing ratio of CH_3CN was derived in the altitude region 45 to 20 km (HENSCHEN and ARNOLD, 1981a; ARIJS et al., 1983a). Although recently an <u>in situ</u> formation mechanism for CH_3CN has been proposed (MURAD et al., 1984), the CH_3CN mixing ratio profiles as deduced from ion mass spectra seem to suggest a release of acetonitrile at the Earth's surface, followed by upward diffusion and destruction by OH in the stratosphere (BRASSEUR et al., 1983).

Apart from the major positive ions, many other positive ions have been detected in the stratosphere (HENSCHEN and ARNOLD, 1981b; ARIJS et al., 1982a). It was shown that the measurements of minor mass peaks offer the possibility of trace gas detection of species such as CH_3OH, NH_3, a.s.o. It should be noted, however, that signal instabilities, which are very pronounced at low ion count rates and possible contamination effects, to be discussed hereafter,

hamper the usefulness of the method as a full grown analytical tool.

The major negative ions observed in the stratosphere are $NO_3^-(HNO_3)_n$ and $HSO_4^-(H_2SO_4)_\ell(HNO_3)_m$ cluster ions (ARNOLD, 1980; ARIJS, 1983).

From the relative ion abundances, both HNO_3 and H_2SO_4 concentration were derived. The derivations of nitric acid vapour mixing ratios, however, are strongly influenced by cluster breakup. The derivations of sulfuric acid ion concentrations, on the other hand, are not subject to these problems and are of great importance for our understanding of the sulfur chemistry and aerosol formation (ARIJS et al., 1981, 1982b, 1983b,d; ARNOLD et al., 1981a, 1982; ARNOLD and BUHRKE, 1983; VIGGIANO and ARNOLD, 1981, 1983; QIU and ARNOLD, 1984). More laboratory data concerning the appropriate ion-molecule chemistry, however, are needed to exploit the data to a full extent.

The detection of minor mass peaks in negative stratospheric ion mass spectra (ARIJS et al., 1982b; MCCRUMB and ARNOLD, 1981) has also opened a way for detecting trace gases so far not measured (such as HCl, HOCl, a.s.o.), but again the same remarks as for positive ions concerning signal instabilities and contamination are valid.

A problem encountered in all in situ analytical techniques and strongly influencing stratospheric ion mass spectrometry data is contamination. It is evident that a technique capable of detecting trace species in the ppt range and lower is extremely sensitive to this problem. It has been established that contamination is mostly influencing the data during measurements obtained in the ascent phase of the balloon flight or at float altitude (VIGGIANO and ARNOLD, 1983; ARIJS et al., 1983a,c). Since contaminants originate from outgassing of the balloon and gondola, the problem is also more acute in daytime measurements. An illustration of the effect of degassing is given in Figure 4, which shows two positive ion spectra obtained by our group at 45.7 km altitude during daytime. Both spectra were recorded at float altitude when the balloon was oscillating between 45.6 and 45.8 km. Spectrum A, containing mass peaks belonging mainly to the natural ions, was obtained during a descending phase of the altitude oscillation, whereas spectrum B was taken during an ascending motion of the payload. It is clear that in spectrum B, contaminants falsify the results considerably. This is explained by the fact that in spectrum B the gondola moves through the wake of the balloon, containing gases released by the balloon and some payload construction materials. These gases are mainly organic vapours, with a high proton affinity and thus are participating in the positive ion chemistry (ARIJS et al., 1983a).

It is also evident that these effects even if not as dramatic as those in Figure 4, may cause misinterpretations, especially in the detection of minor mass peaks.

To overcome these contamination problems, most of the data of our group used so far were obtained at nighttime or during descent in flights with valve controlled balloons. Another remedy which might be envisaged in the future is the use of reel down mechanisms, such as the one recently developed by ANDERSON and HAZEN (1983).

One of the most appealing applications of stratospheric ion mass spectrometry is the detection of trace gases. At present this has been realized by two methods, described to full extent by ARNOLD et al. (1980), namely the steady-state method and the equilibrium method. In the latter one, the partial pressure p(B) of a trace gas B is derived from

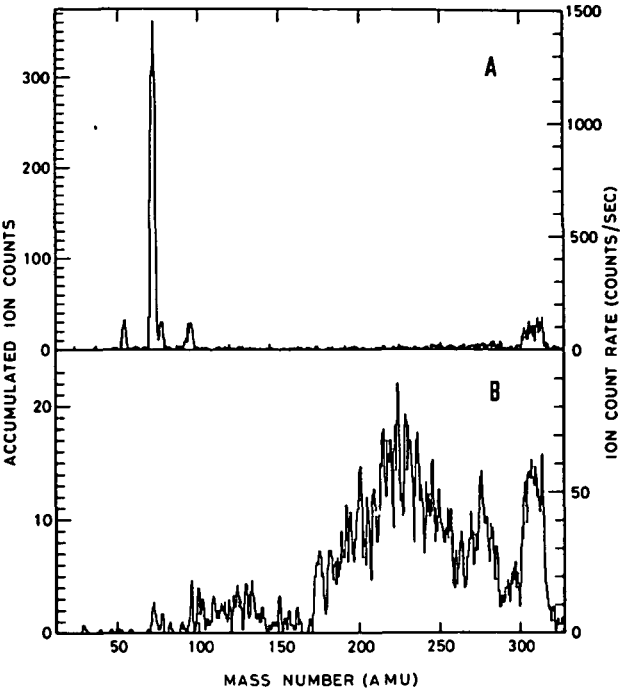

Figure 4. Two typical positive ion spectra obtained around 45 km altitude. Spectrum A is recorded during a descending motion of the balloon, spectrum B during an ascending motion.

$$p(B) = \frac{[A^{\pm} B_{n+1}]}{[A^{\pm} B_n]} \; K^{-1}$$

where square brackets denote number densities and K is the equilibrium constant in atm^{-1}. The core ion $A^{\pm}$ can be positive or negative; major core ions observed in the stratosphere are H_3O^+, $H^+(CN_3CN)$, NO_3^- and HSO_4^-. The main ligands B detected are H_2O, CH_3CN for positive ions and HNO_3 and H_2SO_4 for negative clusters. For some cluster families, such as $H_3O^+(H_2O)_n$ and $NO_3^-(HNO_3)_\ell$, equilibrium constants are known from laboratory measurements and thus p(B) can be derived from the ratio of the fractional ion abundances.

In general, however, the ligands B are weakly bound to the core ions. Immediately behind the sampling aperture of the mass spectrometer, where ions are accelerated by the focussing lens or by the field axis potential of the quadrupole and where pressure is still rather high, the charged particles make many collisions with neutral gas molecules. As a result, field-induced collisional dissociation of a fraction of the ions occurs and some of the ligands B are "boiled orf." Therefore, the measured fractional ion abundance ratio can differ substantially from reality.

A typical example of such measurements is shown in Figure 5, where we have plotted the ratio $H_3O^+(H_2O)_3/H_3O^+$ as measured in a balloon flight performed with a 1,000,000 m^3 Winzen balloon on 23 September 1982 over Southern France.

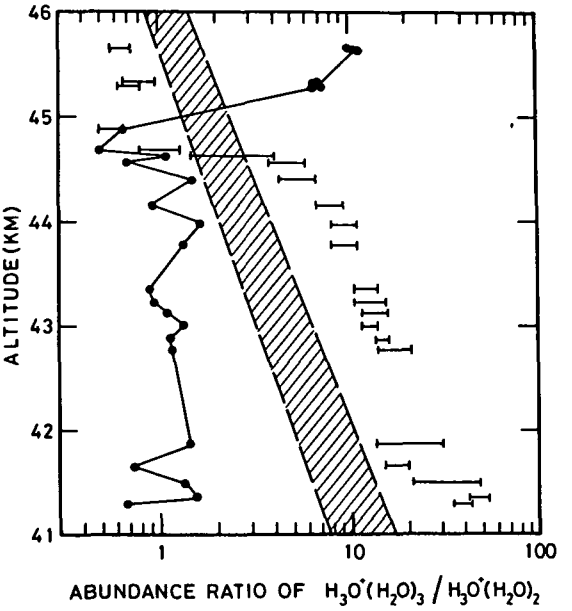

Figure 5. Relative abundance ratio of signal at mass 73 to signal at mass 55 as measured in a high altitude balloon flight.

For comparison, we have also shown the ion abundance derived by

$$[H_3O^+(H_2O)_3]/[H_3O^+(H_2O)_2] = K[H_2O]$$

and

$$-RT \ln K = \Delta H - T\Delta S$$

where the values of LAU et al. (1982) were used for ΔH and ΔS and a constant water vapour mixing ratio of 3 ppm was assumed throughout the whole altitude region considered here.

The shaded area on Figure 5 represents the results of a calculation for standard atmosphere temperature conditions (lower limit for summer and upper limit for spring-fall). Use of the *in situ* measured temperature profile leads to the horizontal bars, the width of which is proportional to the temperature measurement error. As can be seen, the measured ion abundance ratio below 45 km is much lower than expected, which is due to the dissociation of $H_3O^+(H_2O)_3$ into $H_3O^+(H_2O)_2$ in the instrument.

Above 45 km the measured ion abundance ratio is larger than expected. These measurements were taken at float altitude during daytime; whereas the data below 45 km were recorded during descent, due to the cooling of the balloon after sunset.

The too-high ion abundance ratio above 45 km is ascribed to contamination, resulting from balloon and payload outgassing caused by solar heating. One of the major products of this desorption is water, which causes a shift of the proton hydrate distribution towards higher masses. The high signal at mass 73 ($H_3O^+(H_2O)_3$), responsible for the too high ion abundance ratio, partly results from cluster breakup of mass 91 ($H_3O^+(H_2O)_4$).

Figure 5 is at the same time a good illustration of contamination and cluster breakup. It should be pointed out that the effect of cluster breakup is strongly dependent on ambient pressure (altitude) and instrument configuration (diameter of sampling hole, focussing potentials a.s.o.) and may, therefore, vary from flight to flight. For the measurements of Figure 5, a sampling hole of 0.4 mm diameter was used.

It is clear that in order to use ion mass spectrometric data for analytical applications, the cluster breakup effects should be avoided or very well understood so that they can be corrected (ARNOLD et al., 1981b; ARIJS et al., 1982a).

In any case, care should be taken in the interpretation of fractional abundance data, especially if they are used for deriving unknown thermochemical values (ΔH and ΔS) of some clustering reactions.

It should be pointed out that the derivation of CH_3CN number densities from positive ion data and of H_2SO_4 vapour concentrations from negative ion measurements are believed not to be influenced by cluster breakup. In these cases, the fractional ion abundances of two distinct ion families (proton hydrates and nonproton hydrates; NO_3^- and HSO_4^- ions) are compared. Cluster breakup only results in a modification of the distribution within the same ion family and is unlikely to cause the conversion from one family to another.

CONCLUSIVE REMARKS

During the past decade considerable progress has been made in the technology of detection and identification of ambient ions in the stratosphere. The measurements performed hitherto have provided an insight in the major processes governing the ion composition in the altitude region 20 to 45 km. To get a more detailed understanding and to exploit the data to a further extent, however, some developments will be necessary. More extensive calibrations of existing instruments are necessary to be able to convert ion count rates to ion number densities, to correct for cluster breakup and to understand possible mass discrimination effects. New instruments or improvements to existing ones need to be developed to avoid cluster breakup and to increase the sensitivity of mass spectrometers. Since the latter is at lower altitudes mainly limited by ion scattering by residual gas molecules in the instrument, more powerful pumping systems will be part of the new developments. On the other hand, the use of other types of mass filters, such as magnetic mass sector instruments and simultaneous detection techniques may open new perspectives. The altitude range of existing measurements need to be extended and the latitudinal variation of ion compositions should be investigated. To extent the altitude range the use of other measurement platforms such as parachute borne rocket payloads, airplane borne instruments (HEITMANN and ARNOLD, 1983) and the use of reel down mechanisms may become necessary. Finally, in order to interpret the data, more laboratory work on the appropriate ion-molecule reactions is urgently needed.

REFERENCES

Anderson, J. and N. Hazen (1983), New highlights in upper atmospheric bulletin, 83-1, 1-4

Arijs, E. (1983), Positive and negative ions in the stratosphere, Annales Geophysicae, 1, 149-160.

Arijs, E., J. Ingels and D. Nevejans (1978), Mass spectrometric measurement of the positive ion composition in the stratosphere, Nature, 271, 642-644.

Arijs, E., D. Nevejans, P. Frederick and J. Ingels (1981), Negative ion composition measurements in the stratosphere, Geophys. Res. Lett., 8, 121-124.

Arijs, E., D. Nevejans, P. Frederick and J. Ingels (1982b), Stratospheric negative ion composition measurements, ion abundances and related trace gas detection, J. Atmos. Terr. Phys., 44, 681-694.
Arijs, E., D. Nevejans and J. Ingels (1980), Unambiguous mass determination of major stratospheric positive ions, Nature, 288, 684-686.
Arijs, E., D. Nevejans and J. Ingels (1982a), Stratospheric positive ion composition measurements, ion abundances and related trace gas detection, J. Atmos. Terr. Phys., 44, 43-53.
Arijs, E., D. Nevejans and J. Ingels (1983a), Positive ion composition measurements and acetonitrile in the upper stratosphere, Nature, 303, 314-316.
Arijs, E., D. Nevejans, J. Ingels and P. Frederick (1983b), Sulfuric acid vapour derivations from negative ion composition data between 25 and 34 km, Geophys. Res. Lett., 10, 329-332.
Arijs, E., D. Nevejans, J. Ingels and P. Frederick (1983c), Positive ion composition measurements between 33 and 20 km altitude, Annales Geophysicae, 1, 161-166.
Arijs, E., D. Nevejans, J. Ingels and P. Frederick (1983d), Negative ion composition and sulfuric acid vapour in the upper stratosphere, Planet. Space Sci., 31, 1459-1464.
Arnold, F. (1980), Multi-ion complexes in the stratosphere, implications for trace gases and aerosols, Nature, 284, 640-641.
Arnold, F. (1982), Ion nucleation, a potential source for stratospheric aersols, Nature, 299, 134-137.
Arnold, F. (1980), The middle atmosphere ionized component, ESA-PAC Symp. on European Rocket and Balloon Programmes, Bournemouth, 479-496.
Arnold, F., H. Bohringer and G. Henschen (1978), Composition measurements of stratospheric positive ions, Geophys. Res. Lett., 5, 653-656.
Arnold, F. and Th. Buhrke (1983), New H_2SO_4 and HSO_3 vapour measurements in the stratosphere - evidence for a volcanic influence, Nature, 301, 293-295.
Arnold, F., R. Fabian, G. Henschen and W. Joos (1980), Stratospheric trace gas analysis from ions: H_2O and HNO_3, Planet. Space Sci., 28, 681-685.
Arnold, F., R. Fabian and W. Joos (1981a), Measurements of the height variation of sulfuric acid vapor concentrations in the stratosphere, Geophys. Res. Lett., 8, 293-296.
Arnold, F., G. Henschen and E. E. Ferguson (1981b), Mass spectrometric measurements of fractional ion abundances in the stratosphere, Positive ions, Planet. Space Sci., 29, 185-193.
Arnold, F., D. Krankowsky and K. H. Marien (1977), First mass spectrometric measurements of positive ions in the stratosphere, Nature, 167, 30-32.
Arnold, F., A. A. Viggiano and H. Schlager (1982), Implications for trace gases and aerosols of large negative ion clusters in the stratosphere, Nature, 297, 371-376.
Arnold, F. and S. Qiu (1984), Upper stratosphere, negative ion composition measurements and inferred trace gas abundances, Planet. Space Sci., 31, 169-177.
Ballenthin, J. O., A. Bailey, R. Rossi and L. Schmitt (1983), Positive ion measurements at 38 km altitude, EOS, 64, 282.

Bragin, Y. A. (1967), Direct measurements of day and night profiles of concentration of charged particles, Kosmicheskie Issledovanya, 5, 478-479.
Bragin, Y. A., A. D. Danilov and O. K. Kostko (1966), Interpretation of charged particle concentration at the heights of 10-60 km, Space Res. VIII, North-Holland Publ. Co., Amsterdam, 355-359.
Brasseur, G., E. Arijs, A. de Rudder, D. Nevejans and J. Ingels (1983), Acetonitrile in the atmosphere, Geophys. Res. Lett., 10, 725-728.
Cunningham, A. J. and J. H. Hofman (1982), Magnetic mass spectrometer development, Abstracts of the EGS Symp. on Ions in the Middle Atmosphere, Leeds, Aug. 23-27, 116.

Fehsenfeld, F. C. and E. E. Ferguson (1969), The origin of water cluster ions in the D-region, J. Geophys. Res., 74, 2217-2222.

Ferguson, E. E. (1974), Ion chemistry of the normal earth's stratosphere, in: The Natural Stratosphere of 1974, CIAP Monograph I, 5.42-5.54.

Goldberg, R. A. and L. J. Blumle (1970), Positive composition from a rocket-borne mass spectrometer, J. Geophys. Res., 75, 133-142.

Heitmann, H. and F. Arnold (1983), Composition measurements of tropospheric ions, Nature, 306, 747-751.

Henschen, G. and F. Arnold (1981a), Extended positive ion composition measurements in the stratosphere. Implications for neutral trace gases, Geophys. Res. Lett., 8, 999-1001.

Henschen, G. and F. Arnold (1981b), New positive ion species in the stratosphere, Nature, 291, 211-213.

Ingels, J., E. Arijs, D. Nevejans, H. J. Forth and G. Schaefer (1978), Liquid helium cryopump and reliable opening device for a balloon borne mass spectrometer, Rev. Sci. Instr., 49, 782-784.

Krankowsky, D., F. Arnold, H. Wieder and J. Kissel (1972), The elemental and isotopic abundance of metallic ions in the low E-region as measured by a cryogenically pumped quadrupole mass spectrometer, Int. J. Mass Spectr. Ion Phys., 8, 379-390.

Lau, Y. K., S. Ikuta and P. Kebarle (1982), Thermodynamics and kinetics of the gas-phase reactions: $H_3O^+(H_2O)_{n-1} + H_2O \rightarrow H_3O^+(H_2O)_n$, J. Am. Chem. Soc., 104, 1462-1469.

McCrumb, J. L. and F. Arnold (1981), High-sensitivity detection of negative ions in the stratosphere, Nature, 294, 136-139.

Mitchell, J. D., R. S. Sagar and R. Olsen (1977), Positive ions in the middle atmosphere during sunrise conditions, Space Res., 17, 199-204.

Mohnen, V. A. (1971), Discussion of the formation of major positive and negative ions up to the 50 km level, Pure Appl. Geophys., 84, 141-153.

Mohnen, V. A. and C. S. Kiang (1976), Assessment of ion induced stratospheric aerosol formation, Report of Atmospheric Sciences Research Center, State Univ. of New York, Albany.

Morita, Y., H. Ishikawa and M. Kanada (1971), The vertical profile of the small ion density and the electric conductivity in the atmosphere up to 19 km, J. Geophys. Res., 76, 3431-3436.

Murad, E., W. Swider, R. A. Moss and S. Toby (1984), Stratospheric sources of CH_3CN and CH_3OH, Geophys. Res. Lett., 11, 147-149.

Narcisi, R. S. and A. D. Bailey (1965), Mass spectrometric measurements of positive ions from 64 to 112 km, J. Geophys. Res., 70, 3687-3700.

Nevejans, D., P. Frederick and E. Arijs (1982), Microprocessor based data acquisition and control system for a balloon borne quadrupole mass spectrometer, Bull. Acad. Roy. Belg. Cl. Sci., 67, 314-332.

Olson, J. R., R. C. Amme, J. N. Brooks, D. G. Murcray, D.A. Steffen, R. E. Sturm and G. E. Keller (1978), Balloon borne ion sampling package, Rev. Sci. Instr., 49, 643-649.

Paltridge, G. W. (1965), Experimental measurements of the small ion density and electrical conductivity of the stratosphere, J. Geophys. Res., 70, 2751-2761.

Qui, S. and F. Arnold (1984), Stratospheric in situ measurements of H_2SO_4 and HSO_3 during a volcanically active period, Planet. Space Sci., 32, 87-95.

Reid, G. C. (1979), The middle atmosphere, in Middle Atmospheric Electrodynamics, NASA-Rep. CP 2090, 27-42.

Rose, G., H. U. Widdel, A. Azcarraga and L. Sanchez (1972), Experimental evidence for a transient ion layer formation in connection with sudden ionospheric disturbances in the height range 20-50 km, Planet. Space Sci., 20, 871-876.

Viggiano, A. and F. Arnold (1981), Extended sulfuric acid vapour concentration measurements in the stratosphere, Geophys. Res. Lett., 8, 583-586.

Viggiano, A. A. and F. Arnold (1983), Stratospheric sulfuric acid vapor: New and updated measurements, J. Geophys. Res., 88, 1457-1462.
Viggiano, A. A., H. Schlager and F. Arnold (1983), Stratospheric negative ions - detailed height profiles, Planet. Space Sci., 31, 813-820.
Widdel, H. U., G. Rose and R. Borchers (1977), Payload BIII, an instrument package for the measurement of conductivity, concentration and mobility of positive and negative ions in the mesosphere, J. Geophys., 44, 179-188.
Zbinden, P. A., M. H. Hidalgo, P. Eberhardt and J. Geiss (1975), Mass spectrometer measurements of the positive ion composition in the D and E-regions of the ionosphere, Planet. Space Sci., 23, 1621-1642.

6. MEASUREMENTS OF STRATOSPHERIC AEROSOLS

D. J. Hofmann

Department of Physics and Astronomy
University of Wyoming
Laramie, WY 82071

ABSTRACT

The history of measurements of the stratospheric aerosol layer is briefly reviewed. Balloon-borne measurements played a major role both in the discovery of the layer and in the subsequent study of its nature. Following this introduction, stratospheric aerosol sources and balloon-borne measurement techniques are reviewed. Finally, the current status of this research area is outlined with data obtained mainly by balloon-borne techniques. It is concluded that a great deal has been learned in the past five years, due mainly to the increase of the occurrence of major volcanic eruptions, which are the predominant source of stratospheric particles, but also due to the development of instrumentation and techniques which have seen considerable application on the balloon platform.

INTRODUCTION AND BACKGROUND

While knowledge of suspensions of small particles in the upper atmosphere through twilight observations dates back to at least the 18th century, the study of the stratospheric aerosol layer did not become a science until Junge's pioneering measurements in 1959 (JUNGE et al., 1961). Using balloon-borne particle impactors, they determined that a stratospheric relative maximum in the particle concentration existed at about 20 km altitude for particles with radii of about 0.1 μm. They also measured condensation nuclei ($r \sim 0.01$ μm) using expansion cloud chambers and found them to be predominantly a tropospheric phenomenon with only minor concentrations in the stratosphere.

ROSEN (1964) developed a balloon-borne optical individual particle counter which was a forerunner of an instrument now known as a dustsonde used extensively over the past twenty years in balloon applications all over the world. About the same time, laser radar (lidar) was applied to stratospheric aerosol studies (FIOCCO and GRAMS, 1964). In the seventies, balloon-borne particle impactors (BIGG et al., 1970; BIGG, 1975, 1976; BROWNLEE et al., 1976; GRAS and LABY, 1978, 1981) and filter samples (LAZRUS et al., 1971; LAZRUS and GANDRUD, 1974, 1977; CASTLEMAN et al., 1974) were used to study the nature of the aerosol.

Extensive volcanic activity during the 1980-1982 period resulted in a renewed interest and accelerated research on stratospheric particulates by numerous techniques. It is now clear that the concentration of optically active ($r \geq 0.1\,\mu$m) aerosol varies from the order of 1 cm^{-3} during volcanically quiescent periods to at least ten times this value following large volcanic eruptions such as that of Agung in 1963 and El Chichon in 1982. Condensation nuclei ($r \sim 0.01$ μm) typically have tropospheric concentrations of the order of 10^3 cm^{-3} but fall off rapidly in the stratosphere and become part of the normal stratospheric aerosol size distribution.

Under nonvolcanic conditions, the stratospheric aerosol size distribution may be typified by a log normal distribution with a mean radius of about 0.08 μm, a total number concentration of about 10 cm^{-3} and a σ of about 1.8 at an altitude of about 20 km (PINNICK et al., 1976; HOFMANN and ROSEN, 1981; ROSEN and HOFMANN, 1977). The global mass of stratospheric aerosol is estimated to be about 0.5 Tg (1 Tg = 10^6 metric tons) under normal conditions and as

large as 10 Tg following major volcanic eruptions (HOFMANN and ROSEN, 1983a; MCCORMICK and SWISSLER, 1983). The quiescent layer appears to be at a slightly higher altitude in equatorial regions than at the poles but is clearly a continuous global phenomenon (ROSEN et al., 1975).

While stratospheric aerosol contains many trace elements, the overwhelming component is sulfate (LAZRUS et al., 1971). The chemical structure appears to be sulfuric acid with an approximate 75% H_2SO_4, 25% H_2O composition (ROSEN, 1971). Recent measurements suggest that the acid fraction probably varies from 60-80% depending on temperature and water vapor concentration (HOFMANN and ROSEN, 1983a). That the aerosol exists as a liquid droplet has been suggested from its appearance following impaction and also from the generally good agreement obtained in comparing in situ measurements with lidar backscatter measurements (NORTHAM et al., 1974; PINNICK et al., 1976; SWISSLER et al., 1982; HOFMANN et al., 1983), a comparison which relies on the particles being spherical droplets of aqueous sulfuric acid.

STRATOSPHERIC AEROSOL SOURCES

While >98% of the aerosol which persists in the stratosphere is composed of sulfuric acid under both background and volcanically disturbed conditions, the precursor sulfurous gas appears to be quite different in the two cases. Most of the volcanic gas is SO_2 with possibly some H_2S which is rapidly converted to SO_2. Thus, following volcanic eruptions, H_2SO_4 vapor is formed through the chemical oxidation of SO_2. Recent studies suggest that the most plausible chain of reactions involves the hydroxyl radical OH but in a catalytic manner so that OH is conserved in the process (MCKEEN et al., 1983):

$$SO_2 + OH + M \rightarrow HOSO_2 + M$$
$$HOSO_2 + O_2 \rightarrow SO_3 + HO_2$$
$$HO_2 + NO \rightarrow OH + NO_2$$
$$SO_3 + H_2O \rightarrow H_2SO_4$$

net: $SO_2 + O_2 + NO + H_2O \rightarrow H_2SO_4 + NO_2$

The lifetime for this process in the stratosphere (25 km) is estimated to be about 40 days. SO_2 decay and aerosol growth observations at 25 km following the El Chichon eruption are in agreement with this estimate (HEATH et al., 1983; HOFMANN and ROSEN, 1983b).

The lifetime of SO_2 in the troposphere is considerably shorter owing to its water solubility and rapid washout resulting in the quiescent SO_2 level in the lower stratosphere being only about 10-100 parts per trillion by volume (JAESCHKE et al., 1976; GEORGII and MEIXNER, 1980; INN et al., 1981). Thus, nonimpulsive anthropogenic emissions of SO_2 at the surface, which by far exceed eruptive volcanic emissions, are not effective as stratospheric aerosol precursor gas sources. It is believed that the surface sulfur source for the background stratospheric aerosol is naturally produced and anthropogenic carbonyl sulfide (OCS) which has a relatively long lifetime (∿500 days) in the troposphere, diffuses into the stratosphere where it is photo-dissociated, eventually forming SO_2 (TURCO et al., 1979).

Most of the very large particles (greater than 1 μm radius) in the stratosphere appear to be composed of aluminum oxide (BROWNLEE et al., 1976) which are apparently deposited there through the exhaust of solid fuel rockets. Due to their small number (approximately 1 m^{-3} above a radius of 1 μm before 1976), they do not contribute substantially to the total mass distribution but warrant continued observations as the use of solid fuel propellants increases.

BALLOON-BORNE MEASUREMENT TECHNIQUES

Table 1 summarizes and references techniques which have been used to study the stratospheric aerosol and its precursor gas (H_2SO_4) from the balloon platform. While the reference list may not be exhaustive, the table includes all techniques which have contributed to the understanding of this phenonmenon. In the following we will briefly identify the advantages and disadvantages of each.

(a) Impactors

This technique involves the physical impaction of the particles (or droplets) on a surface which is then subjected to analysis by optical or electron microscopes or by spectroscopic techniques. Advantages include size and shape discrimination and some compositional information. Disadvantages include possibility of particle loss or contamination prior to analysis, poorly known efficiency for the smaller particles and manpower intensive analysis requirements.

(b) Filters

This method of sampling involves the trapping of the aerosol in a filter matrix with subsequent removal and analysis using standard chemical techniques.

Table 1. Balloon-borne aerosol measurement techniques.

METHOD	TYPE	REFERENCES
Impactors	Cascade/Optical Microscope Electron Microscope	JUNGE et al., 1961 BIGG et al., 1970 BIGG, 1975 BROWNLEE et al., 1976 GRAS and LABY, 1978
Filters	IPC Cellulose	LAZRUS et al., 1971 LAZRUS and GANDRUD, 1974, 1977 SEDLACEK et al., 1983
Optical Particle Counters	White Light	ROSEN, 1964 GRAS and LABY, 1981 HOFMANN and ROSEN, 1982
	Laser	MIRANDA and FENN, 1974
Condensation Nuclei Counters	Expansion Chambers	JUNGE et al., 1961 KASELAU et al., 1974
	Growth Chamber/Optical Particle Counter	ROSEN and HOFMANN, 1977
Ion Mass Spectrometers		ARNOLD and FABIAN, 1980 ARIJS et al., 1981 ARNOLD and BUHRKE, 1983
Remote Sensing	Solar Occultation	PEPIN, 1969, 1970 THOMPSON, 1981

Advantages include accurate chemical composition determinations and inherent simplicity in obtaining a sample. Disadvantages include lack of size distribution information and possibility of contamination.

(c) Optical Particle Counters

These instruments pass an air sample through a beam of light and measure the amount of light scattered by individual particles or droplets in the sample. Advantages include large amounts of data easily collected, relatively good size specificity given the aerosol composition and shape (e.g., for sulfuric acid droplets) and simple determination of volatile or nonvolatile state of aerosols. Disadvantages include necessity for accurate calibration, lack of compositional information other than degree of volatility, degradation of size information for unknown distributions of nonspherical particles and a lower size limit of about 0.1 μm due to the inability of discriminating light scattered by smaller particles from that due to air molecules.

(d) Condensation Nuclei Counters

While these instruments also generally rely on a particle's ability to scatter light, they are distinguished from an optical particle counter because they incorporate a growth chamber wherein particles normally too small (<0.1μm) to be detected by light scattering, are caused to grow by passing them through a region of supersaturation of a working fluid (water or ethylene glycol). Supersaturation is either caused by expansion or by a thermal gradient or transition. Following growth to optically active sizes, the particles are counted either individually by light scattering (using photography or optical particle counters) or collectively by the amount of light they absorb. Advantages include the small sizes (∿0.01 μm) which may, in principle, be detected, the possibility of varying effective size by varying the degree of supersaturation and the ability to handle high concentrations. Disadvantages include poor overall size discrimination, lack of composition discrimination and poor resolution of low particle concentrations for instruments that use photographic detection or collective light absorption. In addition, any instrument which attempts to measure particles smaller than 0.1 m, must contend with loss of particles due to preferential diffusion of small particles to the walls of the instrument.

(e) Ion Mass Spectrometers

These devices are capable of obtaining the mass spectrum of charged molecular clusters and thus address the measurement of aerosols in their earliest stage of growth. Advantages include the ability to obtain the H_2SO_4 vapor concentration and the relative mass distribution for cluster masses less than several hundred amu. Disadvantages include the inability of obtaining the ion density so that concentrations of clusters cannot be determined and the susceptibility to ion fractionation at the inlet to the instrument.

(f) Remote Sensing

This technique involves the measurement of the extinction (absorption and scattering) of sunlight by the stratospheric aerosol layer through a tangent atmospheric pathlength during sunrise or sunset. Advantages include a relatively large signal and aerosol/molecular resolution through wavelength discrimination. Disadvantages include the reliance on an optical model of the aerosol for data interpretation, poor horizontal resolution due to the long atmospheric pathlength (∿200 km) and a need for high pointing accuracy to obtain desired vertical resolution (<1 km).

CURRENT STATUS

The last five years (1978-1983) have seen a revolution in the study of the distribution of particulate matter in the upper atmosphere. Most of what is now known about the sources and detailed formation processes of the quiescent and disturbed stratospheric aerosol layer was pieced together through observation and theory during this period. The first two years of this period (1978-1979) were characterized by minimal major volcanic activity and consequent low background conditions for the stratospheric aerosol layer. Thus HOFMANN and ROSEN (1981), through numerous balloon soundings using the dustsonde, were able to identify a background aerosol level of about 0.5 cm^{-3} for radii greater than 0.15 μm at about 20 km. Comparisons with Junge's measurements in 1959, also a period of minimal volcanic activity, suggested an increase of about 9% per year. Total sulfate measurements by SEDLACEK et al. (1983) between 1973 and 1979 (two periods thought to be relatively free of major volcanic eruptions) suggested a 6.2% per year increase and when compared with Junge's measurements, an 8% per year increase. Such an increase rate is not surprising in view of the increase in the burning of fossil fuel and the concomitant release of OCS, a known source gas for the quiescent stratospheric aerosol layer.

The period 1980-1982 saw the eruption of four volcanos which caused major stratospheric perturbations. These include Mt. St. Helens (46.2° N) in the state of Washington on May 18, 1980, Alaid (50.8°N) in the Kurile Islands on April 28, 1981, an apparently unobserved and thus unidentified eruption in early January, 1982, and the series of eruptions of El Chichon (17.3°N) in Mexico on March 28, April 3 and April 4, 1982. These eruptions, due either to their accessible location or sheer magnitude, provided the opportunity to study the process of gas to particle conversion in the stratosphere. The nucleation of new sulfuric acid droplets from the vapor phase and their subsequent growth to optically active sizes were observed and studied carefully.

In the following we will summarize the current status of stratospheric aerosol measurements. A great majority of this information has been gathered through the use of balloon-borne sensors. Indeed, the height of the El Chichon volcanic injection (25-30 km) dictated the use of balloons for *in situ* measurements as currently available research aircraft have ceiling altitudes in the vicinity of 21 km.

(a) Precursor Gases

Figure 1, from ARNOLD and BUHRKE (1983), shows H_2SO_4 and HSO_3 measurements made by balloon-borne ion-mass spectrometers in southern France (44°N) in 1982 and include the possible identification of a sulfuric acid layer at about 25 km, on June 10, 1982, believed to be due to the eruption of El Chichon. No *in situ* measurements of the sulfuric acid vapor precursor, SO_2, exist above 21 km as no reliable balloon-borne technique has been developed and currently available cryogenic sampling techniques used on aircraft (INN et al., 1981; VEDDER et al., 1983) have not been used on balloons. However, ground-based and aircraft remote sensing of the SO_2 overburden indicate large enhancements following volcanic eruptions (EVANS and KERR, 1983).

(b) Condensation Nuclei

Figure 2, from HOFMANN and ROSEN (1983c), shows profiles of condensation nuclei ($r \geq 0.01$ μm) at Laramie (41°N) before and after the large increase at high altitude observed on January 28, 1983. These data were obtained with a balloon-borne condensation nuclei counter employing a growth chamber and optical particle counter. Typically, one sees high variable concentrations in the troposphere (below about 12 km in Figure 2), low stable concentrations in the 20 km region and the annual (wintertime) increases at about 30 km. The latter have

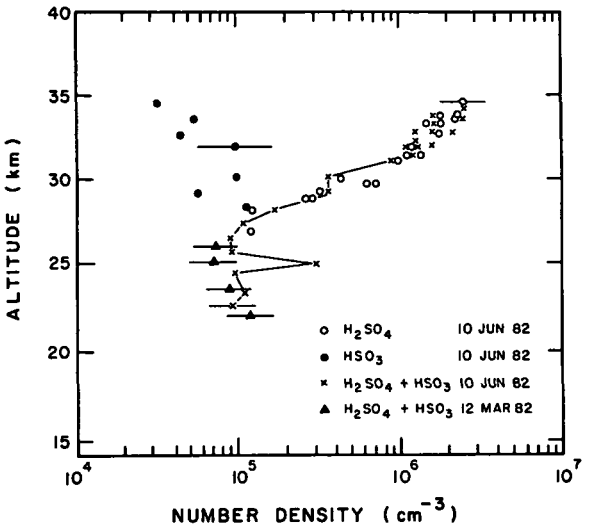

Figure 1. Concentration profiles of H_2SO_4 and HSO_3 vapor obtained by ion-mass spectrometers on balloons in southern France (from ARNOLD and BUHRKE, 1983).

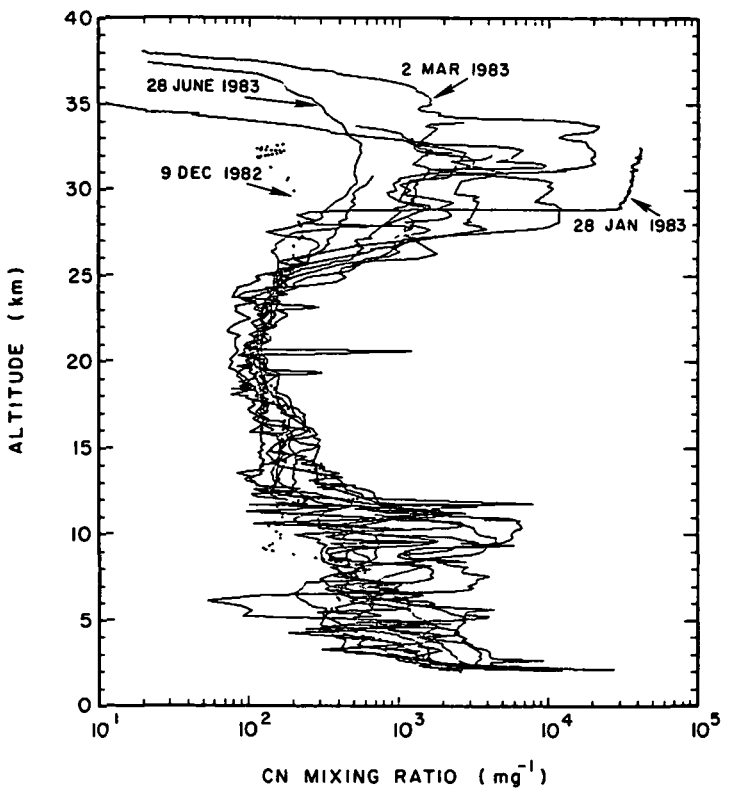

Figure 2. Profiles of condensation nuclei ($r \geq 0.01$ μ m) obtained with balloons at Laramie, Wyoming before (December 1982) and after the large increase at high altitude that began on January 28, 1983 (from HOFMANN and ROSEN, 1983c).

been observed every year since 1979 and are believed to be due to nucleation of new very small sulfuric acid droplets during stratospheric warming episodes in the polar region and subsequent transport to lower latitude during the incursion of arctic air at high altitude. It is possible that the high temperature associated with the warmings cause sulfuric acid aerosol to evaporate creating vapor which then recondenses due to cooling during transport.

Figure 3 shows the condensation nuclei mixing ratio versus time at Laramie in the region of the high altitude events (25-35 km) and in the stable 20 km region. The large increase at 20 km in 1982 was due to the nucleation of new aerosol following the eruption of El Chichon (HOFMANN and ROSEN, 1983a). The general increase in the background level at 25-35 km since 1980 is believed to be due to the increase in volcanic activity since this time, the latter supplying enhanced levels of both sulfuric acid aerosol and vapor which are transported to the polar regions during winter. Instruments launched by the University of Wyoming group in October 1983, on the largest balloon ever flown in Antarctica, revealed the presence of the El Chichon aerosol over McMurdo Station (78°S) and also indicated the presence of enhanced condensation nuclei at high altitude, presumably due to the Southern Hemisphere analog of the events observed in the Northern Hemisphere since 1979.

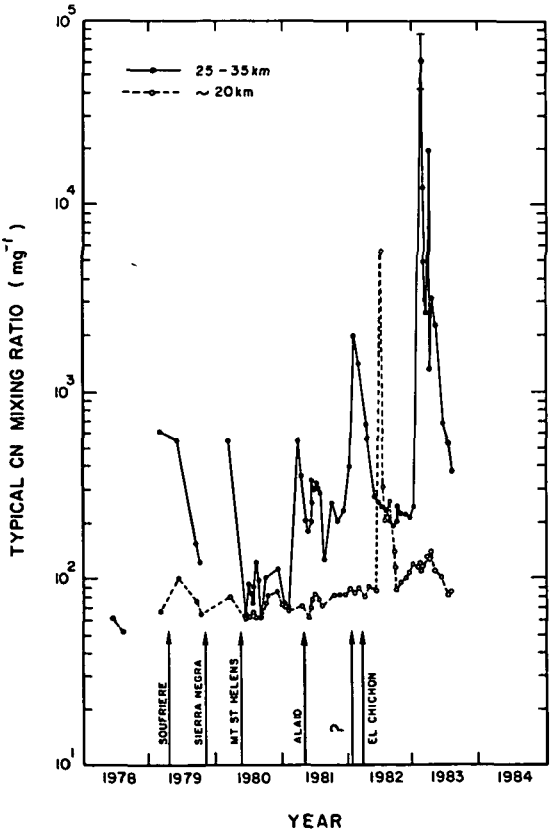

Figure 3. Condensation nuclei ($r \geq 0.01$ μ m) mixing ratios versus time in the region of the annual increases (25-35 km) and at 20 km as measured with balloons at Laramie, Wyoming. Times of major volcanic eruptions which perturbed the larger aerosol concentrations are indicated. An unidentified eruption in early 1982 is indicated by a question mark (from HOFMANN and ROSEN, 1983c).

(c) Total Sulfate

Figure 4, from LAZRUS and GANDRUD (1977), shows the average total sulfate ion mixing ratio and volume concentration profiles as determined from filter samples on balloon flights at 33°N during 1976. These measurements indicate that measurable amounts of sulfate are present to altitudes as high as 37 km. The advantage of balloon-borne measurements here are obvious as aircraft altitudes bring one barely beyond the maximum in the vertical distribution. Figure 5, from MROZ et al. (1983), shows the large increase in sulfate following the eruption of El Chichon in April 1982. These data were obtained from balloon-borne filter samples also at 33°N. Again, aircraft samples were ineffective in obtaining data on this eruption during the first six months since nearly all the enhanced sulfate remained above 21 km during this period.

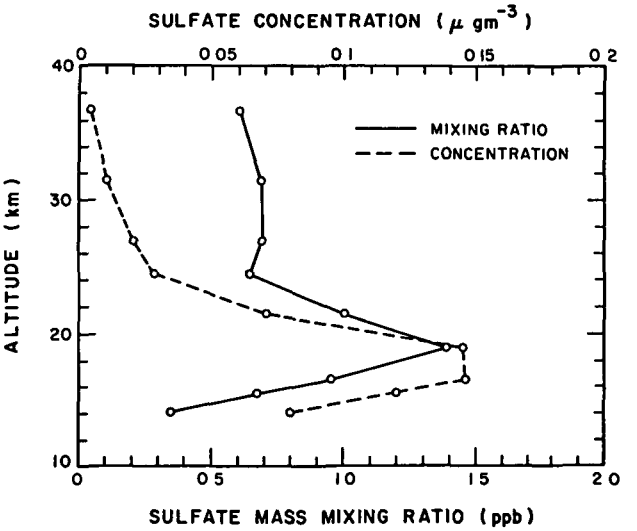

Figure 4. Average sulfate mixing ratio and concentration profiles measured by balloon-borne filter samplers at 33°N from four seasonal flights in 1976 (from LAZRUS and GANDRUD, 1977).

(d) Optically Active Aerosol

Figure 6, from HOFMANN and ROSEN (1983c), shows the aerosol mixing ratio of two size ranges versus time as measured at Laramie and in southern Texas with balloon-borne dustsondes. Times of major volcanic eruptions which perturbed the stratospheric aerosol at 41°N are indicated in the figure. The El Chichon eruption stands out as the most significant both because of the absolute magnitude of the increase and the large size of the aerosol which may be inferred from the relative magnitudes of the increase in the two size ranges in Figure 6.

Figure 7 shows aerosol profiles in six integral size ranges obtained from a complement of three balloon-borne particle counters at Laramie following the El Chichon eruption. Data such as in Figure 7 may be used to obtain the average radius of the aerosol which is plotted versus time after the El Chichon eruption in Figure 8. Two layers developed following this eruption with larger particles forming at higher altitude. The gradual merging of the two curves is due to gravitational settling of the particles in the upper layer thus decreasing their average size while increasing the average size in the lower layer. The particle

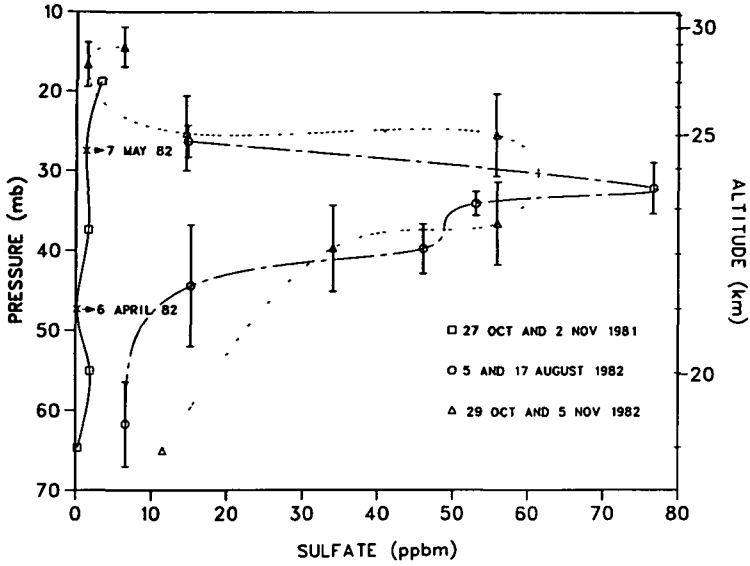

Figure 5. Sulfate concentration profiles obtained by balloon-borne filter samplers at 33°N before and after April 4, 1982 eruption of El Chichon (from) MROZ et al., 1983).

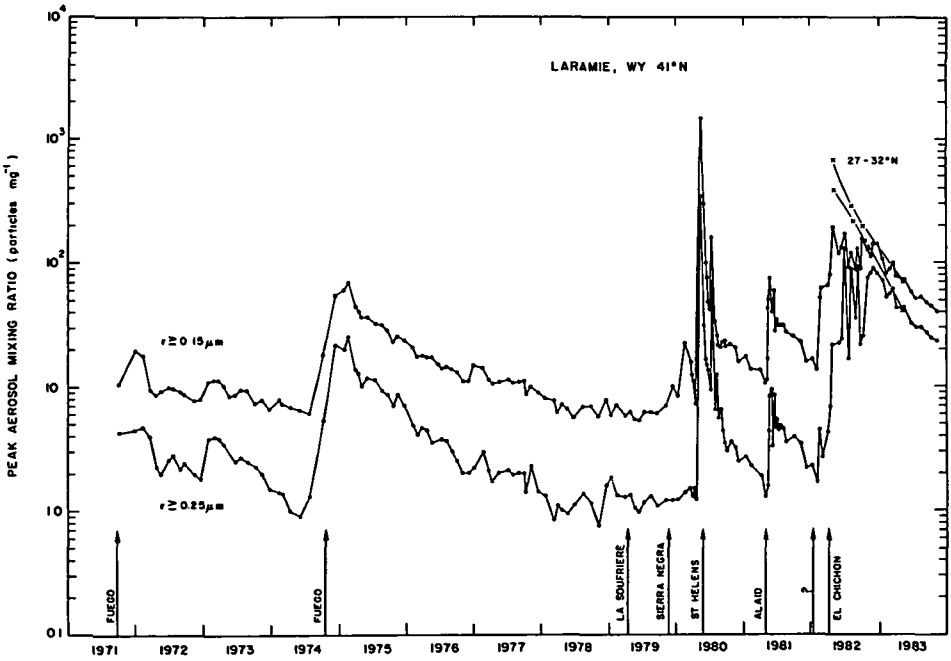

Figure 6. Maximum stratospheric aerosol mixing ratio for two size ranges measured by balloon-borne dustsondes as a function of time at Laramie, Wyoming and in southern Texas. Times of volcanic eruptions which caused stratospheric aerosol perturbations at Laramie are indicated (from HOFMANN and ROSEN, 1983c).

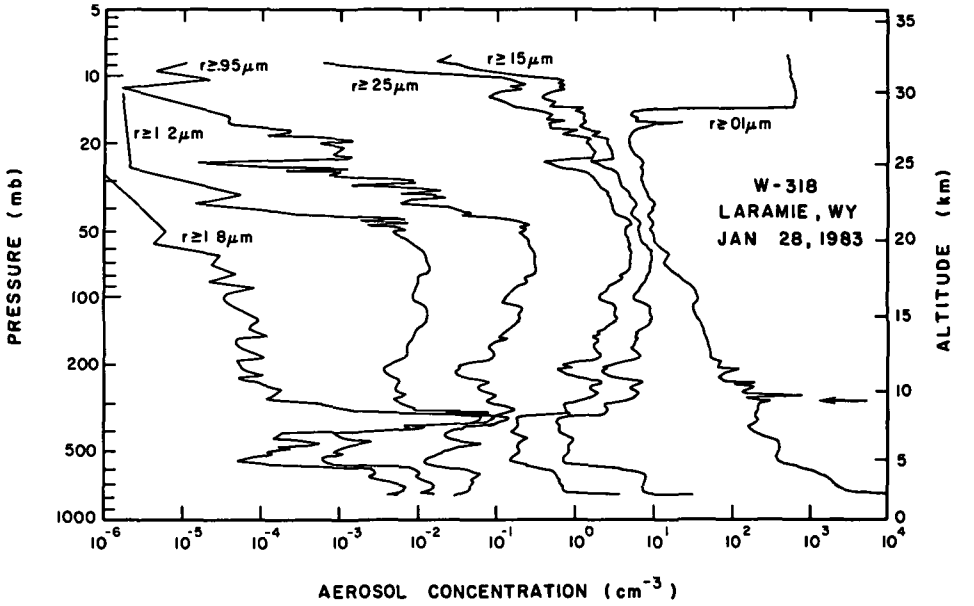

Figure 7. Aerosol concentration profiles for six size ranges as measured by three balloon-borne particle counters at Laramie, Wyoming on January 28, 1983. The arrow marks the position of the tropopause (from HOFMANN and ROSEN, 1983c).

size in the lower layer is typical of previous volcanic eruptions while that in the upper layer has never been observed before. These enhanced sizes are believed to be due to the large amount of sulfuric acid vapor which developed in the stratosphere following this eruption. The aerosol growth curves in Figure 8 are consistent with an H_2SO_4 concentration of about 10^7 molecules cm^{-3} and a lifetime of 25-50 days (HOFMANN and ROSEN, 1983b).

By heating the inlet to a particle counter during a slow balloon descent in southern Texas in October 1982, HOFMANN and ROSEN (1983a) were able to determine the vapor pressure curve of the aerosol. The results are given in Figure 9. These data suggest that the aerosol from the El Chichon eruption was composed of an 80% H_2SO_4, 20% H_2O solution in the upper layer at about 25 km and about 60-65% H_2SO_4 in the lower layer at about 18 km. More than 98% of the aerosol was volatile at 130°C. The distribution of the minute remaining non-volatile fraction could be resolved and indicated that it peaked at about 16 km, just above the tropopause indicating again that the silicate fraction of a volcanic eruption leaves the stratosphere very rapidly and is not important in determining any long term climate effect.

By constructing size distributions from data such as shown in Figure 7, and assuming a composition as suggested in Figure 9, the column mass above a given altitude may be determined (HOFMANN and ROSEN, 1983b). These data are shown plotted versus time in Figure 10 for balloon soundings at Laramie and in southern Texas following the eruption of El Chichon. The gradual increase observed at Laramie, which peaked in early 1983, is due to delayed meridional transport at 25 km which kept the upper layer of larger particles south of about 30°N until the fall of 1982. The total mass scale on the right in Figure 10 assumes longitudinal homogeneity and latitudinal extents as indicated on the mass scales. It may be used to estimate the global mass if one assumes that the measurements are representative of average conditions after approximate global

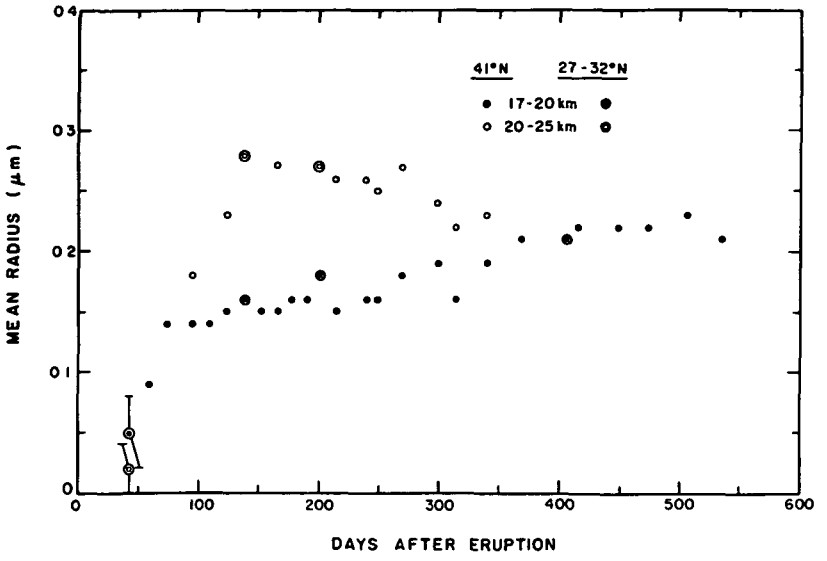

Figure 8. Aerosol mean radius versus time after the April 4, 1982 eruption of El Chichon in two altitude regions as obtained from balloon-borne particle counter data at Laramie, Wyoming and in southern Texas (from HOFMANN and ROSEN, 1983b).

equilibrium has been reached. While the latter condition probably never really prevails, the data are consistent with at least 10 Tg present in the stratosphere in early 1983.

(e) Large Particles

Evidence for growth of sulfuric acid aerosol to micrometer sizes was obtained by balloon-borne sensors after the eruptions of Mt. St. Helens and Alaid. These large droplets were found to be important in calculating expected lidar backscattering and in the total aerosol mass (HOFMANN and ROSEN, 1982; HOFMANN et al., 1983). Following the eruption of El Chichon, a bi-modal size distribution with a mode near 1 μm radius was a dominant feature of the stratospheric aerosol (HOFMANN and ROSEN, 1983a). These large droplets are thought to form, following major sulfur-rich eruptions, through growth of the preexisting aerosol which typically has a radius of about 0.1 μm (HOFMANN and ROSEN, 1983d).

Impactor samples collected by balloons have revealed the existence of aluminum oxide particles in the 3 to 8 μm diameter range during the period 1970-1976 (BROWNLEE et al., 1976). The total mass of these particles appears to be consistent with the burning of solid fuel by rockets. The latter use powdered aluminum as an additive and tests have shown that a byproduct of the burnt fuel is aluminum oxide spheres. This manmade aerosol dominates the 3-8 μm size range while sulfates dominate the submicrometer size range. Above 10 μm, the particles are mostly extraterrestrial in origin with a composition similar to that of primitive meteorites (BROWNLEE et al., 1976).

SUMMARY

While this review does not claim to be exhaustive as far as stratospheric aerosol measurements are concerned, it does indicate the considerable contribution made by balloon-borne sensors. This was especially true following the

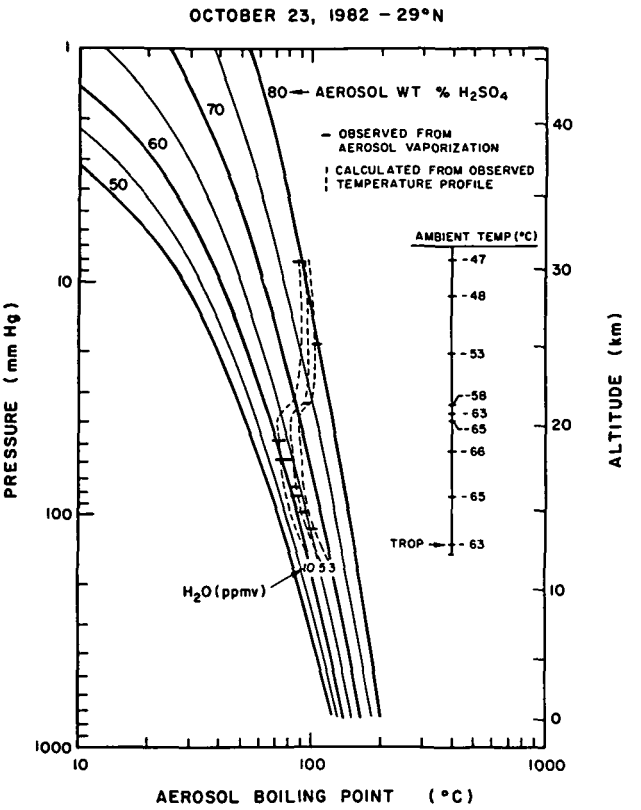

Figure 9. Aerosol boiling point temperature ranges (horizontal bars) as a function of altitude as obtained from a heated intake particle counter on a slowly descending balloon in southern Texas. The smooth curves are vapor pressure curves for various weight percentages of sulfuric acid and water. The ambient temperature, as measured during the balloon flight, is given and the theoretical sulfuric acid weight percentages, as dictated by the temperatures and by several representative ambient water vapor mixing ratios, are indicated by dashed lines (from HOFMANN and ROSEN, 1983a).

great eruption of El Chichon in 1982 when sulfuric acid aerosol formed at altitudes accessible only to balloon-borne sensors. In addition, the ability to obtain accurate vertical distributions is invaluable in assessing aerosol formation processes. Although the cost of large balloons is considerable, instruments such as the dustsonde, which weighs less than 20 kg, can be carried to 30 km by relatively inexpensive balloons which are easily launched under most conditions, thus facilitating numerous measurements at varied locations. It is clear that the balloon platform will see continued use in the study of the aerosol distribution and its gaseous precursors in the stratosphere.

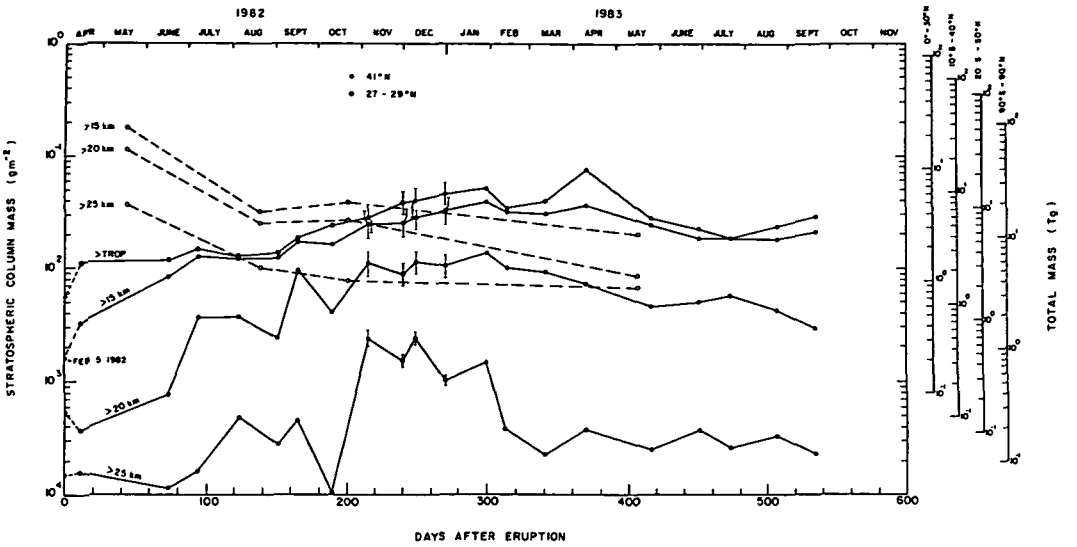

Figure 10. Stratospheric aerosol mass loadings above several altitudes as determined from balloon-borne particle counter measurements at Laramie, Wyoming and in southern Texas. The total mass scale on the right assumes longitudinal homogeneity and latitudinal extents as indicated (from HOFMANN and ROSEN, 1983b).

REFERENCES

Arijs, E., D. Nevejans, P. Frederick and J. Ingels (1981), Negative ion composition measurements in the stratosphere, Geophys. Res. Lett., 8, 121-124.

Arnold, F. and R. Fabian (1980), First measurements of gas phase sulphuric acid in the stratosphere, Nature, 283, 55-57.

Arnold, F. and Th. Buhrke (1983), New H_2SO_4 and HSO_3 vapour measurements in the stratosphere - evidence for a volcanic influence, Nature, 301, 293-295.

Bigg, E. K., A. Ono and W. J. Thompson (1970), Aerosols at altitudes between 20 and 37 km, Tellus, 22, 550-563.

Bigg, E. K. (1975), Stratospheric particles, J. Atmos. Sci., 32, 910-917.

Bigg, E. K. (1976), Size distributions of stratospheric aerosols and their variations with altitude and time, J. Atmos. Sci., 33, 1080-1086.

Brownlee, D. E., G. V. Ferry and D. Tomandl (1976), Stratospheric aluminum oxide, Science, 191, 1270-1272.

Castleman, A. W., Jr., H. R. Munkelwitz and B. Manowitz (1974), Isotopic studies of the sulfur component of the stratospheric aerosol layer, Tellus, 26, 222-234.

Evans, W. F. J. and J. B. Kerr (1983), Estimates of the amount of sulphur dioxide injected into the stratosphere by the explosive volcanic eruptions: El Chichon, mystery volcano, Mt. St. Helens, Geophys. Res. Lett., 10, 1049-1051.

Fiocco, G. and G. Grams (1964), Observations of the aerosol layer at 20 km by optical radar, J. Atmos. Sci., 21, 323-324.

Georgii, H.-W. and F. Meixner (1980), Measurements of tropospheric and stratospheric SO_2 distribution, J. Geophys. Res., 85, 7433-7438.

Gras, J. L. and J. E. Laby (1978), Southern hemisphere stratospheric aerosol measurements, 1. Simultaneous impactor and in situ single particle (light scater) detection, J. Geophys. Res., 83, 1869-1874.

Gras, J. L. and J. E. Laby (1981), Southern hemisphere stratospheric aerosol measurements, 3. Size distribution 1974-1979, J. Geophys. Res., 86, 9767-9775.

Heath, D. F., B. M. Schlesinger and H. Park (1983), Spectral changes in the ultraviolet absorption and scattering properties of the atmosphere associated with the eruption of El Chichon: Stratospheric SO_2 budget and decay (abstract), EOS Trans. AGU, 64, 197.

Hofmann, D. J. and J. M. Rosen (1981), On the background stratospheric aerosol layer, J. Atmos. Sci., 38, 168-181.

Hofmann, D. J. and J. M. Rosen (1982), Balloon-borne observations of stratospheric aerosol and condensation nuclei during the year following the Mt. St. Helens eruption, J. Geophys. Res., 87, 11,039-11,061.

Hofmann, D. J. and J. M. Rosen (1983a), Stratospheric sulfuric acid fraction and mass estimate for the 1982 volcanic eruption of El Chichon, Geophys. Res. Lett., 10, 313-316.

Hofmann, D. J. and J. M. Rosen (1983b), On the temporal variation of the stratospheric aerosol size and mass during the first 18 months following the 1982 eruptions of El Chichon, J. Geophys. Res. (in press).

Hofmann, D. J. and J. M. Rosen (1983c), Balloon-borne particle counter observations of the El Chichon aerosol layers in the 0.01-1.8 μm radius range, Geofisica Internacional (in press).

Hofmann, D. J. and J. M. Rosen (1983d), Sulfuric acid droplet formation and growth in the stratosphere after the 1982 eruption of El Chichon, Science, 222, 325-327.

Hofmann, D. J., J. M. Rosen, R. Reiter and H. Jager (1983), Lidar and balloon-borne particle counter comparisons following recent volcanic eruptions, J. Geophys. Res., 88, 3777-3782.

Inn, E. C. Y., J. F. Vedder and D. O'Hara (1981), Measurement of stratospheric sulfur constituent, Geophys. Res. Lett., 8, 5-8.

Jaeschke, W., R. Schmitt and H.-W. Georgii (1976), Preliminary results of stratospheric SO_2 measurements, Geophys. Res. Lett., 3, 517-519.

Junge, C. E., C. V. Chagnon and J. E. Manson (1961), Stratospheric aerosols, J. Meteorol., 18, 81-108.

Kaselau, K. H., P. Fabian and H. Rohrs (1974), Measurements of aerosol concentration up to a height of 27 km, Pure Appl. Geophys., 112, 877-885.

Lazrus, A. L., B. Gandrud and R. D. Cadle (1971), Chemical composition of air filtration samples of the stratospheric sulfate layer, J. Geophys. Res., 76, 8083-8088.

Lazrus, A. L. and B. W. Gandrud (1974), Stratospheric sulfate aerosol, J. Geophys. Res., 79, 3424-3431.

Lazrus, A. L. and B. W. Gandrud (1977), Stratospheric sulfate at high altitudes, Geophys. Res. Lett., 4, 521-522.

McCormick, M. P. and T. J. Swissler (1983), Stratospheric aerosol mass and latitudinal distribution of the El Chichon eruption cloud for October, 1982, Geophys. Res. Lett., 10, 877-880.

McKeen, S. A., S. C. Liu, S. Solomon and C. S. Kiang (1983), On the chemistry of stratospheric SO_2 from volcanic eruptions (abstract), EOS Trans. AGU, 64, 197.

Miranda, H. A., Jr. and R. Fenn (1974), Stratospheric aerosol sizes, Geophys. Res. Lett., 1, 201-203.

Mroz, E. J., A. S. Mason and W. A. Sedlacek (1983), Stratospheric sulfate from El Chichon and the mystery volcano, Geophys. Res. Lett., 10, 873-876.

Northam, G. B., J. M. Rosen, S. H. Melfi, T. J. Pepin, M. P. McCormick, D. J. Hofmann and W. H. Fuller (1974), Dustsonde and lidar measurements of stratospheric aerosols: A comparison, Appl. Opt., 13, 2416-2421.

Pepin, T. J. (1969), The use of extinction from high altitude balloons as a probe of the atmospheric aerosols, Atmos. Phys. Rep. No. AP-31, School of Phys. and Astron., Univ. of Minn., Mpls., Minn.

Pepin, T. J. (1970), Variability and scattering properties of the stratospheric aerosols, Atmos. Phys. Rep. No. AP-34, School of Phys. and Astron., Univ. of Minn., Mpls., Minn.

Pinnick, R. G., J. M. Rosen and D. J. Hofmann (1976), Stratospheric aerosol measurements III: Optical model calculations, J. Atmos. Sci., 33, 304-314.

Rosen, J. M. (1964), The vertical distribution of dust to 30 kilometers, J. Geophys. Res., 69, 4673-4676.

Rosen, J. M. (1971), The boiling point of stratospheric aerosols, J. Appl. Meteorol., 10, 1044-1046.

Rosen, J. M., D. J. Hofmann and J. Laby (1975), Stratospheric aerosol measurements II: The worldwide distribution, J. Atmos. Sci., 32, 1457-1462.

Rosen, J. M. and D. J. Hofmann (1977), Balloon-borne measurements of condensation nuclei, J. Appl. Meteorol., 16, 56-62.

Sedlacek, W. A., E. J. Mroz, A. L. Lazrus and B. W. Gandrud (1983), A decade of stratospheric sulfate measurements compared with observations of volcanic eruptions, J. Geophys. Res., 88, 3741-3776.

Swissler, T. J., P. Hamill, M. Osborn, P. B. Russell and M. P. McCormick (1982), A comparison of lidar and balloon-borne particle counter measurements of the stratospheric aerosol 1974-1980, J. Atmos. Sci., 39, 909-916.

Thompson, D. A. (1981), A model of atmospheric extinction based on atmospheric attenuation measurements for altitudes to 37 km and wavelengths of 350-1100 nm, Ph.D. Thesis, Dep. of Phys. and Astron., Univ. of Wyo., Laramie, Wyo.

Turco, R. P., P. Hamill, O. B. Toon, R. C. Whitten and C. S. Kiang (1979), A one-dimensional model describing aerosol formation and evolution in the stratosphere: I. Physical processes and mathematical analogs, J. Atmos. Sci., 36, 699-717.

Vedder, J. F., E. P. Condon, E. C. Y. Inn, K. D. Tabor and M. A. Kritz (1983), Measurements of stratospheric SO_2 after the El Chichon eruptions, Geophys. Res. Lett., 10, 1045-1048.

☆U S GOVERNMENT PRINTING OFFICE 1985 481 814 0

CUMULATIVE LISTING FOR THE MAP HANDBOOK

Volume	Contents	Date of Publication
1	National Plans, PMP-1 Report; PMP-2 Report, PMP-3 Report, MSG-4 Report, Approved MAP Projects	June 1981
2	Symposium on Middle Atmosphere Dynamics and Transport, (extended abstracts)	June 1981
3	PMP-5 Report, MSG-1 Report, MSG-2 Report, MSG-3 Report, Antarctic Middle Atmosphere Project (AMA), EXOS-C Scientific Observations, WMO Report No. 5, Updated Chapter 2 of MAP Planning Document, Condensed Minutes of MAPSC Meetings	November 1981
4	Proceedings of MAP Assembly held in Edinburgh, 14-15 August 1981, Condensed Minutes of MAP Steering Committee Meetings held in Edinburgh, Proceedings of MAP Open Meeting held in Hamburg, 19 August 1981	April 1982
5	A Catalogue of Dynamic Parameters Describing the Variability of the Middle Stratosphere during the Northern Winters	May 1982
6	MAP Directory	November 1982
7	Acronyms, Condensed Minutes of MAP Steering Committee Meetings, Ottawa, May 1982, MAP Project Reports, National Reports, Committee Reports, PMP and MSG Reports, Workshop Reports, Announcements and Corrigendum	December 1982
8	MAP Project Reports: DYNAMICS, GLOBUS, and SSIM, MSG-7 Report, National Reports: Czechoslovakia, USA	July 1983
9	Papers presented at the URSI/SCOSTEP Workshop on Aspects of MST Radar, May 23-27, 1983, Urbana	December 1983
10	Papers presented at the International Symposium on Ground-Based Studies of the Middle Atmosphere, May 9-13, 1983, Schwerin, German Democratic Republic	May 1984
11	Condensed Minutes of the MAP Steering Committee Meetings held in Hamburg 13-14 August 1983, Research Recommendations for Increased US Participation in the Middle Atmosphere Program, GRATMAP Project Report, MAP Study Group MSG-7 Report	June 1984
12	Coordinated Study of the Behavior of the Middle Atmosphere in Winter (PMP-1) Workshops	July 1984
13	Ground-Based Techniques	November 1984
14	Papers presented at the URSI/SCOSTEP Workshop on Technical Apsects of MST Radar, May 22-25, 1984	December 1984
15	Balloon Techniques	June 1985

BALLOON TECHNIQUES

TABLE OF CONTENTS